UNIVERSITY OF LIVERPOOL

Characterisation of *Plasmodium falciparum* NADPH-dependent diflavin reductase I (PfDFR1) and its role in primaquine mechanism of action

Thesis submitted in accordance with the requirement of the University of Liverpool for the degree of Doctor in Philosophy

By

Piyaporn Jirawatcharadech

October 2018

ACKNOWLEDGEMENTS

This PhD thesis represents a four-year journey for me in a new culture, new environment, and with new friendships. During my studies in the UK, I have received fantastic opportunities to broaden my intellectual horizon through collaboration and participation with some of the best scientists in the world. I am overwhelmed with happiness throughout my study here because of numerous acts of kindness from people. First, I would like to express my deep appreciation to my supervisors, Prof. Steve Ward and Prof. Giancarlo Biagini, for their valuable suggestions, advice, guidance, and all the opportunities given to me. Their kindly help and support are making me become a better scientist now.

I owe a huge thank you to my mentor, Dr. Grazia Camarda. I will always remember how much time and effort Grazia has spent to help me working in *"the gametocyte world"* as well as her valuable advice during my studies. My appreciation is also extended to my advisory panel members, Dr. Mark Paine and Prof. Lu-Yun Lain, for suggestions and constructive comments. I am grateful to Dr. Mark Paine and Dr. Cristina Yunta Yanes for their helping hands in protein expression and purification. I would also like to thank Prof. Andrew Munro and Dr. Kirsty McLean for their support in the CPR half-reaction experiments. I wish to thank Dr. Hanafy Ismail for his help in flavin determination. I thank Mrs Jill Davies and Mrs Alison Ardrey for helping hands in mouse bone marrow preparation.

The past and present of SAW/GB lab members (Jill, Alison, Ricky, Gavin, Matthew, Saif, Nham, Grazia, Wesam, Salwa, Dave, Paul, Shuan, Raman, Eva) deserve many thanks for creating a good lab environment and being good friends. I am grateful to Angela and Mary for their support. I thank Anfal and Shannon for being incredible friendship and making an enjoyable life in the school.

The life outside the school would be extremely drab if I had not joined the Liverpool Thai Society. I will remember every enjoyable moment with past and present members of the society. I wish to thank Kai and Bright for being incredible flatmates and friends. All good and bad times we have spent together are precious.

I am indebted for financial support during my study to the Royal Thai Government Scholarship. I also thank the Office of Educational Affairs staff for their help and support during the past years.

Finally, my deepest appreciation is extended to my mother and my family for their infinite love, concern, understanding and support. This work would not have succeeded without their encouragement.

ABSTRACT

Characterisation of *Plasmodium falciparum* NADPH-dependent diflavin reductase I (PfDFR1) and its role in primaquine mechanism of action

This thesis submitted to the University of Liverpool for the degree of Doctor of Philosophy (PhD) in the Liverpool School of Tropical Medicine by Piyaporn Jirawatcharadech, 2018.

Malaria is a major vector-born disease that affects populations in tropical and subtropical areas. The achievement in malaria elimination and control requires effective tools to block transmission and to prevent re-establishment of malaria. Primaquine is a currently available anti-malarial that has gametocytocidal activity against *P. falciparum* and the ability to kill liver stages, including hypnozoites in relapsing strains. In terms of the malaria elimination and control agenda, primaquine becomes one of the most important tools used alongside other anti-malarial drugs targeting asexual stages. However, primaquine cannot be given safely to all malaria patients because of haemolytic toxicity in patients who suffer from glucose-6-phosphate dehydrogenase deficiency. Despite over seventy years of investigation, the mechanism of action of primaquine remains poorly understood. It is hypothesised that the anti-malarial activity occurs via hydrogen peroxide, oxidative stress, and oxidative damage produced from the redox cycling of CYP 2D6-mediated primaquine metabolites. However, this still doesn't explain the unique susceptibility of malaria parasites to primaquine or it's metabolites. Here, for the first time we report on a novel and indispensable *P. falciparum* enzyme from the diflavin reductase family of enzymes, which we have called *P. falciparum* NADPH-dependent diflavin reductase I (PfDFR1), that is able to complete the redox cycling of primaquine metabolites. The gene was cloned and expressed in *E. coli*. The methodology of PfDFR1 characterisation involved spectrum analysis, HPLC-based flavin determination, pre-steady state kinetics, steady state kinetics, and enzyme inhibition profiling. The PfDFR1 shows similar properties to other enzymes in the diflavin reductase family in terms of spectral properties. Focussing on enzyme activity, PfDFR1 displays slow enzyme turnover rates compared to other CPRs. However, it could be comparable with the slow turnover of a number of diflavin reductase members, such as MSR and NR1. PfDFR1 was shown to be present in both sexual and asexual parasite stages. PfDFR1 was shown to be able to interact with hydroxylated metabolites of primaquine (OH-PQm), in a redox cycling mechanism that results in the formation of H_2O_2. Interestingly, in addition to PfDFR1, human CPR (hCPR) and liver and bone marrow extracts also displayed the ability to generate H_2O_2 from OH-PQm. These findings are discussed in the context of a new model for the mode of action of primaquine and an explanation of how this drug specifically displays efficacy against liver and gametocyte stages when used clinically. Collectively, the thesis data have contributed to the understanding of a novel and essential parasite enzyme, PfDFR1, whilst pharmacological findings have relevance towards the development of new and improved 8-aminoquinolines.

TABLE OF CONTENTS

LIST OF FIGURES

LIST OF TABLES

ABBREVIATIONS

2’5’-ADP	2’5’ adenine diphosphate
5-HPQ	5-hydroxypromaquine
5,6-DPQ	5,6-dihydroxyprimaquine
6OHPQQI	6-hydroxy-5-quinoneimine
aa	amino acid
ACT	artemisinin-based combination therapy
ART	artemisinin
ATQ	atovaquone
CaM	calmodulin binding region
CD	connecting domain
cDNA	complementary DNA
CPQ	carboxy primaquine
CQ	chloroquine
CYP	cytochrom p450
cyt c	cytochrome *c*
DNA	deoxyribonucleic acid
FAD	flavin adenine dinucleotide
Fld	flavodoxin
FMN	flavin mononucleotide
g	standard gravity
*g*DNA	genomic DNA
HPLC	high-performance liquid chromatography
IC_{50}	50% of maximal inhibitory concentration
IPTG	isopropyl β-D-1-thiogalactopyranoside
hCPR	human NADPH-cytochrome P450 reductase
H_2O_2	hydrogen peroxide
k	rate constant

k_{cat}	turnover number
kDa	kilodalton
K_m	Michaelis constant
LB	Luria-Bertani
MFQ	mefloquine
MSR	methionine synthase reductase
$NADP^+$	adenine dinucleotide phosphate reduced nicotinamide
NADPH	adenine dinucleotide phosphate
NOS	nitric oxide synthase
NR1	novel reductase 1
OD	optical density
P450 BM3	cytochrom P450 BM3
PCR	Polymerase chain reaction
PDB	protein data bank
PfDFR1	*Plasmodium falciparum* NADPH-dependent diflavin reductase I
PfCRT	*Plasmodium falciparum* chloroquine resistance transporter
PfFNR	*Plasmodium falciparum* ferredoxin-$NADP^+$ reductase
PfMDR1	*Plasmodium falciparum* multidrug resistance protein 1
PQ	primaquine
PQQI	5-quinoneimine
QN	quinine
SDS-PAGE	polyacrylamide gel electrophoresis
RNA	ribonucleic acid
SiR	sulphite reductase
TQ	tafenoquine
UV-Vis	ultraviolet-visible
wt	wild type

CHAPTER 1

INTRODUCTION

1.1 Malaria and malaria life cycle

Malaria is one of the major infectious diseases that affects humans [1-3]. The disease is caused by single-celled eukaryotic *Plasmodium* spp. in the phylum apicomplexa. There are five species of pathogens causing malaria in humans, including *P. falciparum, P. vivax, P. malariae, P. ovale,* and *P. knowlesi* [2, 4, 5].

Malaria spreads and affects throughout the resource-limited areas, including Africa, Asia, Central America, and South America (Figure 1.1). Although the malaria control policy successfully reduces malaria cases and malaria endemic areas over time [6], malaria still affects a heavy social development and human mortality in the endemic regions. The World Health Organization (WHO) estimated 216 million clinical cases and 445,000 deaths from malaria in 2016 [6]. Most of malaria cases are caused by *P. falciparum* and *P. vivax*. The majority of deaths and severe malaria cases are caused by *P. falciparum* that is found in tropical areas throughout the world. This species kills ~1,200 African children younger than 5 years of age each day [7]. Although *P. vivax* is less virulent than *P. falciparum,* it is the most widespread species. *P. vivax* also has a special characteristic in symptomatic relapses because the parasite can stay dormant in a liver hepatocyte for many years.

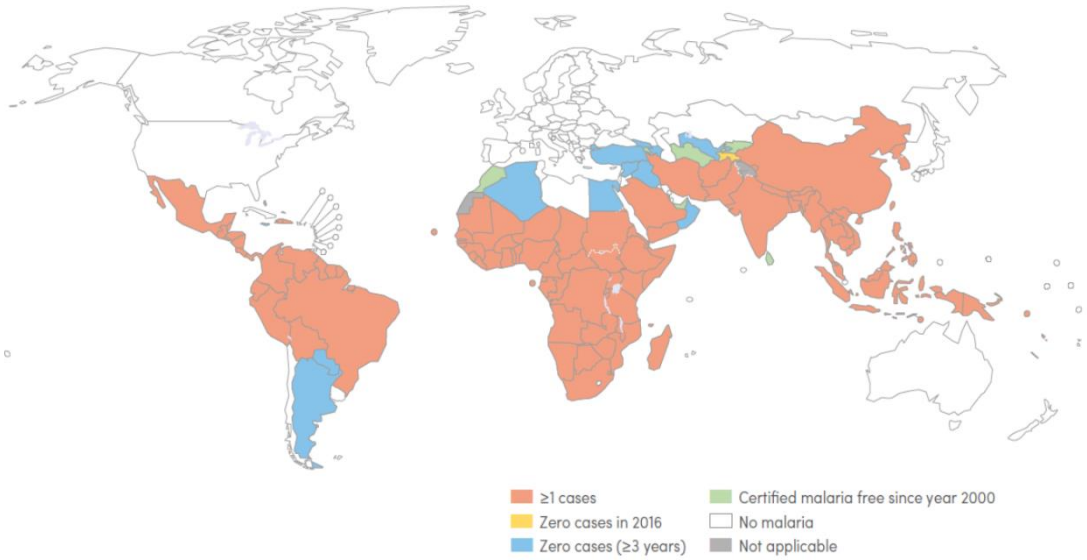

Figure 1.1 A map of malaria endemic areas in 2016. This map shows malaria status in 2016 of counties with indigenous cases in 2000. Malaria free areas are increase over time. The map was taken from the World malaria report 2017 [6].

Plasmodium has a complex life cycle that needs both vertebrate (human) and invertebrate (*Anopheles* spp. mosquitoes) hosts to complete the life cycle (Figure 1.2). The life cycle of human malaria parasites starts when sporozoites are transmitted into subcutaneous tissue by the bite of a *Plasmodium* spp.-infected mosquito. The parasites get into the blood circulation and migrate to the liver. The parasites infect hepatocytes where they remain for over a week and undergo asexual replication known as the exo-erythrocytic development. Hepatic-stage parasites mitotically divide into 10,000 to 30,000 of merozoites [8]. Then, the merozoites exit from the liver cells and invade red blood cells and enter the ~48 h of erythrocytic cycle (for *P. falciparum*, *P. vivax* and *P. ovale*), 72 h for *P. malariae*, and 24 h for *P. knowlesi*.

The parasites reproduce asexually through four different stages, commonly known as ring, trophozoite, schizont, and merozoite, during the erythrocytic cycle [9]. The first stage after red cell invasion is the ring stage; the name came from its hollow shape with dense purple spot on lineated mass (vesicle-like structure with the nucleus surrounded by elongated mitochondrion). Then, the parasites consume hemoglobin inside the red blood cell and grow into trophozoite (feeding) stages. During the trophozoite stage, the parasites need to process a lot of haemoglobin. However, the heme by-product and the free heme are toxic [10]. Therefore, the parasites pack heme into inert heme crystals called hemozoin [11]. Once the parasites are ready, nuclear division occurs without immediate cytoplasmic division. This kind of mitosis is called schizogony and this parasite stage is called schizont. Each mature schizont can release 8 to 32 merozoites that can invade new red blood cells to start a new erythrocytic cycle [12, 13]. Typically, a subset of the erythrocytic-stage parasites (<10% of erythrocytic parasites) become sexually-competent gametocytes.

After a female mosquito takes male and female gametocytes in its blood meal, they differentiate into male and female gametes that fertilize in the mosquito midgut to form zygotes. The zygote develops into a motile ookinete that transgresses through the gut lining and implants on the outer gut tissue as an oocyst. After several rounds of mitosis, the mature oocyst ruptures and releases thousands of sporozoites. Sporozoites migrate to the salivary gland and then ready to continue the life cycle in the human host [10].

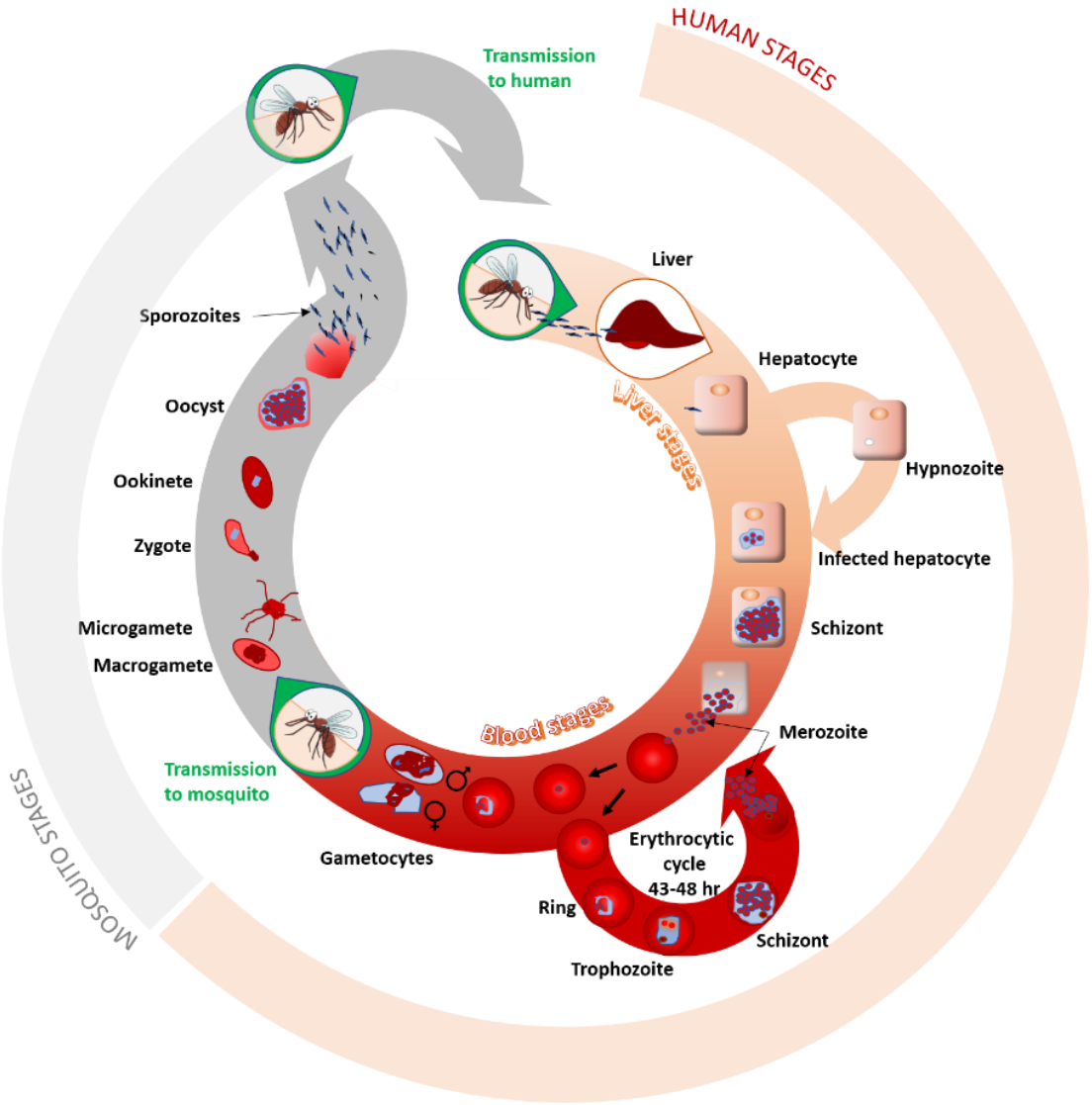

Figure 1.2 Life cycle of a human malaria parasite. The malaria life cycle (see review [8]) starts when an infected mosquito bites and injects sporozoites into a human host. The sporozoites migrate into the blood circulation and go to the liver. The parasites invade hepatocytes and undergo asexual replication for over a week. In *P. vivax* and *P. ovale*, parasites can stay as a dormant form in the hepatocyte cells called "hypnozoite". The merozoite progeny rapture from hepatocytes. They invade red blood cells and start ~48 hr cycle of asexual erythrocytic cycle. <10% of intra-erythrocytic parasites enter the sexual development for male and female gametocytes development (10-12 days for mature gametocyte development). The mosquito stages start when *Anopheles* mosquitoes take up their blood meal with mature gametocytes. In mosquito gut, gametocytes develop to micro and macro gametes before fertilising to zygote, forming ookinete and then oocyst. The mature oocyte raptures and releases sporozoites that migrate to salivary gland and ready for further human infection.

1.2 *Plasmodium falciparum* sexual blood stages (gametocytes)

The generation of gametocytes occurs in a small proportion (<10%) of the erythrocytic-stage parasites in both *in vivo* and *in vitro* [14, 15]. The parasite commitment to gametogenesis occurs before or during schizogony [15-17]. All merozoites in the schizont either commit to develop gametocytes or continue asexual proliferation. The molecular mechanism and the factors involved parasite commitment are not fully understood. Known factors associated with an increase in gametocyte commitment rate *in vitro* include high parasitaemia, conditioned medium, and drug treatment (such as chloroquine treatment) [15, 18-20]. However, high parasitaemia and drug treatment are not necessary for the increase in gametocyte commitment rate in natural infection [15, 21]. Recently, it was reported a new environmental signal called the host-derived lipid lysophosphatidylcholine (LysoPC) acts as a factor regulating differentiation by inhibiting gametocyte production [22, 23].

The genetic mechanisms in control of gametogenesis are not fully understood. Deletion of PF3D7_0935400 (now known as the gametocyte development protein 1 (GDV1)) coding region as well as mutations in the gene encoding the protein PF3D7_1222600 (now known as AP2-G) have been associated with gametocyte-deficient lines (see review [23]). The AP2-G was confirmed as a transcriptional master switch that initiates gametocytogenesis [24, 25]; in the absence of AP2-G, parasites do not produce gametocytes. The epigenetic silencing of the *ap2-g* locus is associated with heterochromatin protein 1 (HP1) [23]. Recent work suggests that GDV1 plays a role in the removal of HP1 from the *ap2-g* locus, resulting in de-repression of *ap2-g* allowing parasites to commit to gametogenesis [26]

After gametogenesis has been triggered, *P. falciparum* requires 10 to 12 days to reach maturity. In general, the gametocyte development can be divided into five stages based on light microscopy (Figure 1.3). Stage I gametocyte is the stage that is indistinguishable from the asexual trophozoite. In stage II (D shape), the parasite develops a subpellicular cytoskeleton and increases microtubule length. Therefore, the shape of stage II gametocyte becomes D shape. In stage III, the gametocyte elongates with slightly rounded ends and erythrocyte is slightly distorted. The subpellicular membrane complex and microtubule complex develop rapidly. At this stage, parasite usually has one curve side and one straight side. In stage IV (spindle shape), the gametocyte elongates with pointed ends and erythrocyte is distorted. The subpellicular membrane complex and microtubule complex surround the gametocyte. In females, the gametocyte shows an increase in endoplasmic reticulum and osmiophilic bodies. In stage V (crescent shape), the parasite in this stage will lose the microtubule complex. Therefore, the spindle shape develops to a characteristically crescent shape (the history of the "falciparum" name). Male and female gametocytes are easily distinguished in this stage. The female with dense pigment is more curved than male with scatter pigment.

Immature gametocytes, also known as early gametocytes (stage I to stage III), retain some of the same metabolic profiles as asexual blood stages. For example, both stages use the same source of amino acids from haemoglobin degradation. From the previous reports, activity against the early stage gametocytes was observed from a number of antimalarial drugs that target the metabolic pathways in asexual blood stages [27-29]. For example, chloroquine, a drug that interferes the heme digestion pathway, can inhibit immature gametocytes (stage I to stage III) [27, 30]. Another example is atovaquone. Atovaquone, a drug that acts on mitochondrial electron transport

(specifically the bc_1 complex), can inhibit immature gametocytes (stage I to stage II) [27, 31]. Mature gametocytes (stage IV to V) are known to have distinct metabolism compared to early gametocytes. Consequently, the majority of antimalarial drugs (except primaquine and tafenoquine) are not effective against mature gametocytes[27, 32].

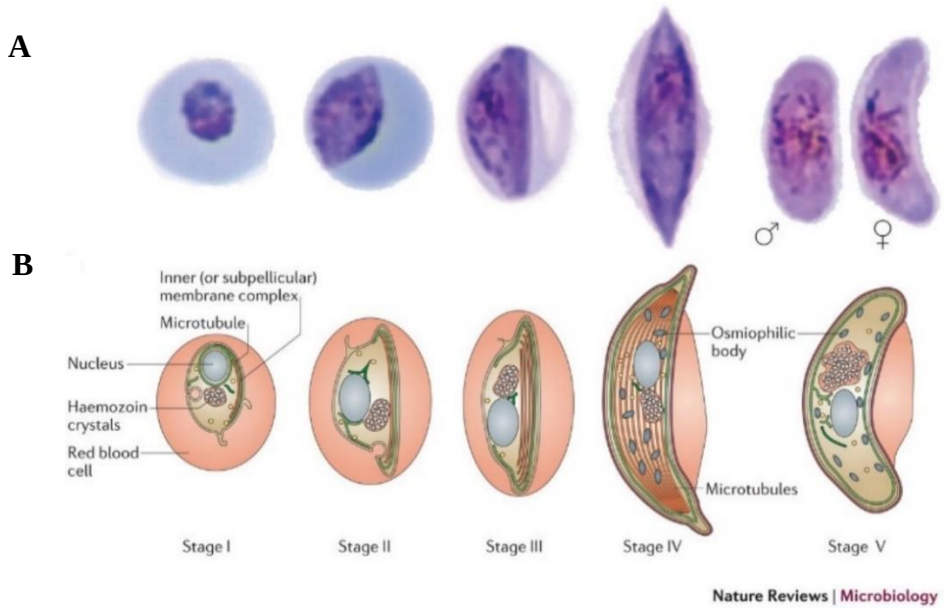

Figure 1.3 Five stages of gametocytogenesis based on light microscopy. A) photographs of Giemsa stain five stages of gametocytes. B) Schematics of five stages of gametocytes. This figure was adapted from [15] with the permission licence 4371380847933.

In *P. falciparum*, the gametocytes can be carried in peripheral blood by individual patients up to 3 to 6 weeks post asexual clearance [32, 33]. To avoid immune clearance in the spleen, gametocyte stage I to IV sequester in the human tissue such as bone morrow. Once the gametocytes develop to the mature stage V, they are released into the peripheral blood and are ready for taking up by mosquitoes. Recent work in the rodent malaria model shows that the mature gametocytes also display the vascular transmigration behaviour in the host bone marrow by entering and exiting in the intact

vascular barrier [34]. The importance of sequestration and transmigration behaviours in gametocytes on the primaquine mechanism of action is discussed in later chapters.

1.3 Malaria treatment and prevention strategies

The "world free of malaria" is a goal for World Health Organization (WHO) and the global malaria communities as described in the WHO's Global Technical Strategy for Malaria (GTS). The current tools and strategies that has been used for the malaria treatment and prevention are described.

1.3.1 Diagnosis

Since 2010, WHO has recommended to have parasitological confirmation of diagnostic in all suspected malaria patients prior to treatment. Early and accurate diagnosis is important for effective disease management and patient surveillance. The current diagnostic tools are microscopy and rapid diagnostic tests (RDTs). Microscopy (diagnostic from a blood smear) is the gold standard technique for the laboratory confirmation of malaria. However, the accuracy of this technique depends on the quality of reagent, the quality of microscope, and the experience of technician. The current RDTs (diagnostic from parasite specific antigens) are useful to diagnose malaria symptomatic patients who have high parasite densities. However, the RDTs have a limitation in the detection of the low parasite infection and the dormant stages [35]. The nucleic acid amplification tests (NAATs), including PCR and LAMP techniques, have been developed to detect low density malaria infections [35]. However, these techniques are not currently suitable for deployment in the field.

1.3.2 Treatment

Artemisinin-based combination therapies (ACTs) are the mainstay malaria treatment recommended by WHO [36]. By combining active artemisinin-based drug with other different mechanism of action drugs, ACTs are the most effective malaria treatment available today. There are 5 ACTs recommended from WHO, including artemether + lumefantrine, artesunate + amodiaquine, artesunate + mefloquine, dihydroartemisinin + piperaquine, and artesunate + sulfadoxin-pyrimethamine (SP).

1.3.3 Vaccines

Malaria vaccines is one of the essential tools required for achieving the malaria elimination goal. However, all of the current malaria vaccines strategies are at various stages of pre-clinical and clinical development (Figure 1.4). They are broadly three approaches to malaria vaccine development. The first approach involves pre-erythrocytic vaccines such as RTS,S that aim to eliminate parasites during early infection. The RTS,S is in the clinical trial phase IV development (post-registration) and will begin pilot studies in Ghana, Kenya, and Malawi in 2018 [37]. The second approach involves targeting the asexual blood stages such as PfRH5, with the aim to clear blood stage parasites and prevent disease. The PfRH5 and AMA1-RON2 vaccines are in clinical trial phase I and in preclinical development, respectively [37]. The third approach involves transmission-blocking vaccines, such as Pfs25 and Pfs230, that aim to interrupt malaria transmission. Both of these vaccines are in clinical phase I development [37].

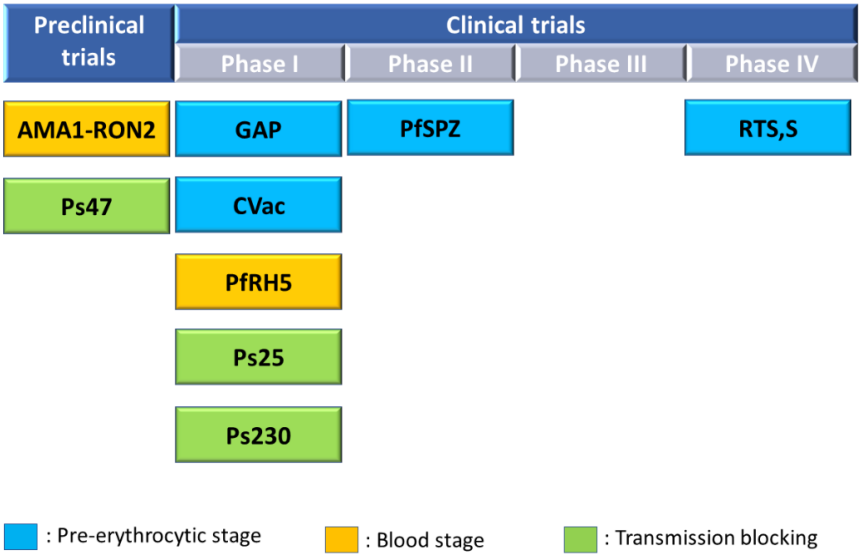

Figure 1.4 Current malaria vaccines under preclinical or clinical trials based on the information from [37].

1.3.4 Vector control

Vector control is one of the essential strategies in malaria prevention. The vector control targets mosquitoes that necessary for malaria transmission. Two core vector control strategies are insecticide-treated mosquito nets (ITNs) and indoor residual spraying (IRS). Using of ITNs to prevent the mosquito bites by sleeping inside the ITN has been shown the reduction of malaria case incident rate and malaria mortality rate in sub-Saharan Africa [6, 38]. Indoor residual spraying (IRS) such as spraying indoor with chlorfenapyr is another effective vector control method. Using ITNs and IRS has been considered as a major contribution in the reduction of malaria burden since 2010 [6, 39]. Larval control, environment modification, and modified mosquitoes are considered as alternative strategies in the vector control [6, 35].

1.3.5 Transmission blocking: Low-dose primaquine (PQ)

Artemisinin-based combination therapies (ACTs) are not successful in clearing mature gametocytes. Patients can carry gametocytes in blood circulation over 3 to 6 weeks after asexual clearance [32]. Low-dose PQ (0.25 mg/kg) shows ability to kill mature gametocytes. Therefore, in 2015 WHO recommended giving a single low dose of PQ with ACT to reduce the transmission of treated malaria infections [36]. PQ can cause hemolysis in G6PD-deficient patients. Recent reviews of PQ show that the single low dose PQ is safe in the G6PD-deficient patients [36, 40].

1.4 Antimalarial drugs against gametocytes

As described previously, antimalarial drugs with transmission-blocking activity (killing asexual stages malaria) are important for malaria elimination and control. However, antimalarial drugs with gametocytocidal activity are limited. Published antimalarial drugs with gametocytocidal activity (Figure 1.5) are grouped and reviewed in following subsections.

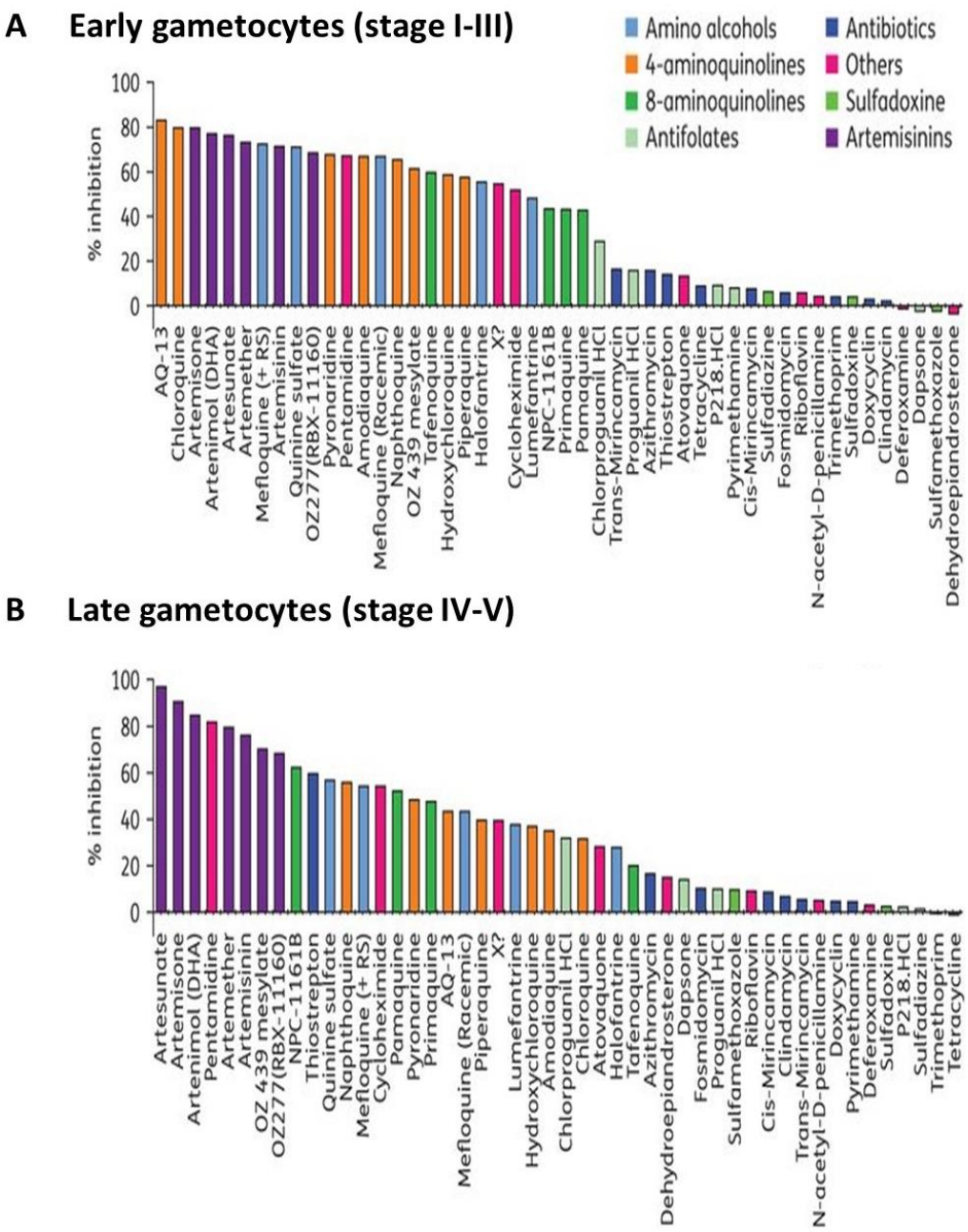

Figure 1.5 The inhibition of gametocyte viability from the treatment of compounds (5 µM) on early and late gametocytes. This figure was adapted from [41].

1.4.1 Artemisinin derivatives

Artemisinin (ART) was originally isolated from the plant *Artemisia annua* which has been used for centuries as a herbal crude extract in traditional Chinese medicine for fever illnesses treatment including malaria [42]. Isolation and identification of artemisinin from *Artemisia annua* was first discovered and reported in 1971 by Professor Youyou Tu, who was recently awarded the Nobel Prize in Physiology and Medicine in 2015 [43]. To improve solubility and drug efficacy, semi-synthetic artemisinin derivatives (Figure 1.6), including dihydroartemisinin (DHA), artemither, and artesunate, have been developed [44]. Artemisinin and its derivatives are generally safe and have been used in combination with other antimalarial drugs called artemisinin-based combination therapies (ACTs).

ART and its derivatives share a core 1,2,4-trioxane endoperoxide structure (Figure 1.6: red colour) which is essential for antimalaria activity [45]. The proposed artemisinin mechanism of action is shown in Figure 1.7. The ART is activated by reduced iron or heme to produce activated artemisinin [46]. The activated ART rapidly interacts with nucleophile-harbouring cellular components (i.e. proteins, unsaturated membrane lipid and heme) leading to parasite damage and death [47-49]. ART "resistant" parasites have been reported in Southeast Asia countries [50, 51]. The Kelch-like protein K13 gene has been identified as a molecular marker for ART resistance. The link between K13 mutation and ART resistant trait parasite is supported by data from the genome-wide association study (GWAS) on over 1,000 clinical cases [52]. The major mutations in K13 associated with ART resistance are C580Y, R539T, and I543T [8, 52]. Mutations in the K13 protein are believed to be associated with cell stress

response, unfolded protein response, ubiquitin/proteasome system, or production of phospholipid signalling molecule PI3P [8, 49].

ART and its derivatives are the effective drugs against asexual blood stages and sexual stage parasites [28, 53, 54]. At 12-120 nM, DHA has shown 50-75 % inhibition of immature gametocytes (stage I-III) *in vitro* [29, 30]. In mature stage V gametocytes, 10 µM artesunate have shown reduction of gametocyte viability by at least 50% *in vitro* [55]. Treatment of mature stage V gametocytes with artesunate has shown the transmission-blocking activity by the reduction of oocyst development in *Anopheles dirus* [56]. Although artemisinin derivatives show activity against gametocytes *in vitro,* the gametocytes were formed in patients who were negative for gametocytaemia before artesunate treatment [57].

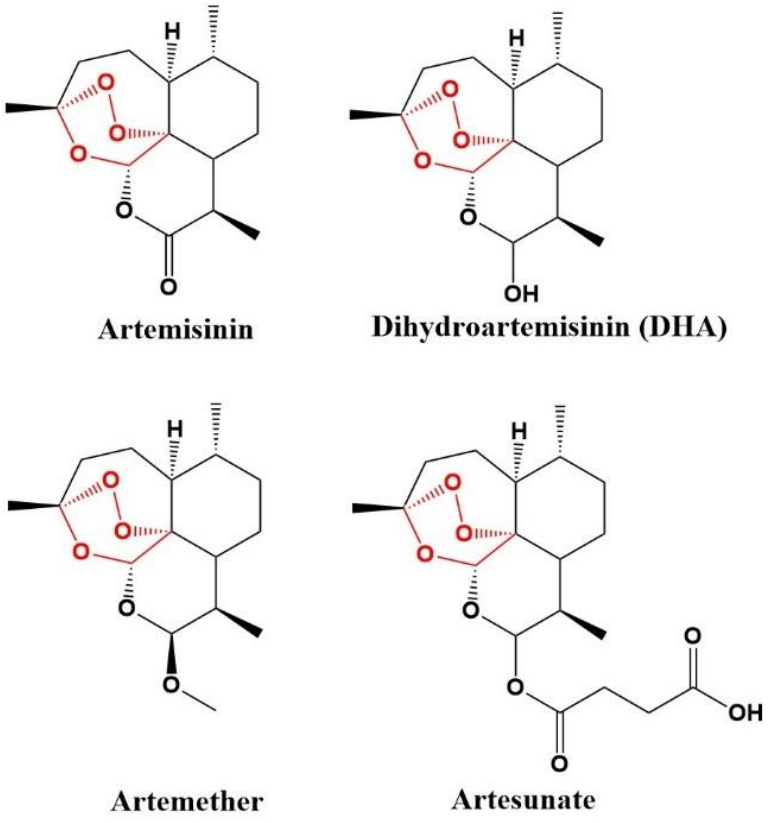

Figure 1.6 Chemical structures of artemisinin and artemisinin derivatives. 1,2,4-trioxane endoperoxide is shown in red.

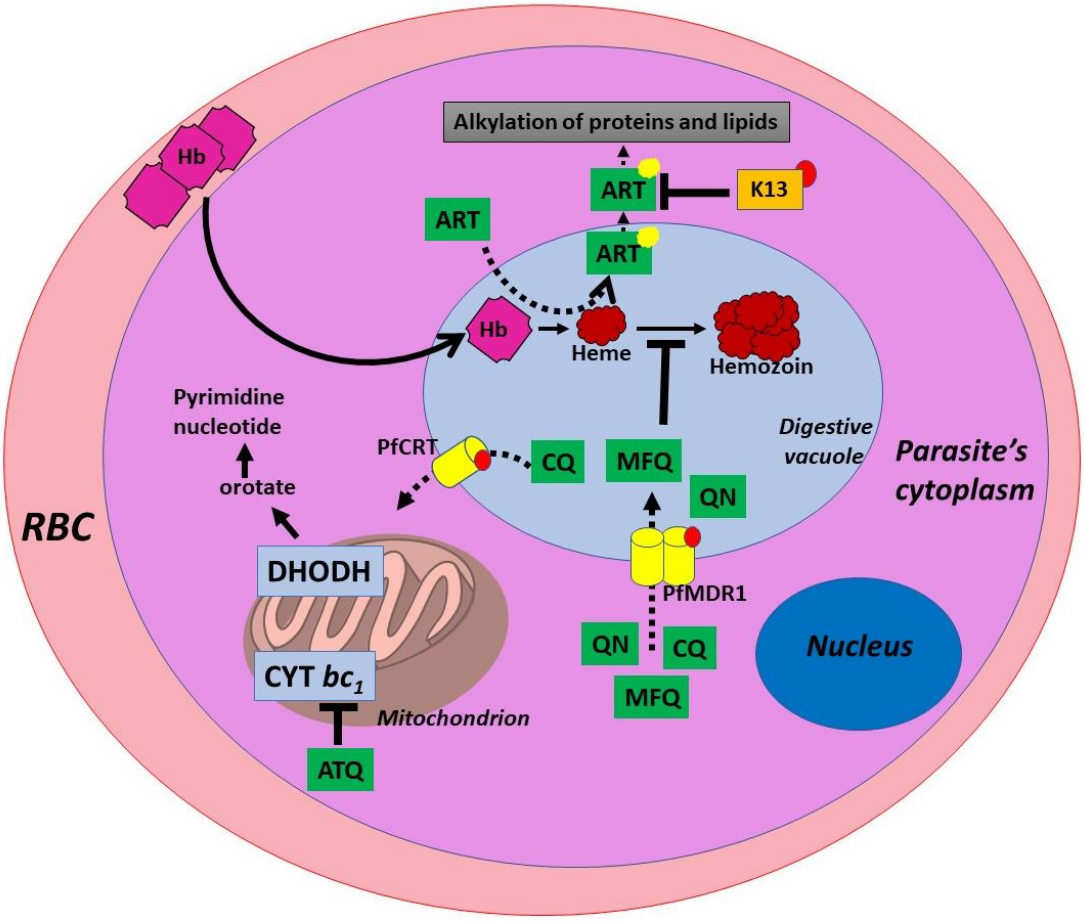

Figure 1.7 Proposed mechanism of action of antimalarial drugs. In the mechanism of action of artemisinin (ART), heme or ion (Fe^{2+}) from haemoglobin (Hb) degradation can activate ART and its derivatives by cleaving the endoperoxide bridge to generate the active ART (yellow star). The activated ART interacts with nucleophile-harbouring proteins and lipids resulting in cell damage and cell death. Mutations in K13 have been proposed to be involved in ART resistance. 4-aminoquinolines (i.e. chloroquine (CQ), amodiaquine (AQ), piperaquine (PPQ)) and arylamino alcohols (i.e. quinine (QN), mefloquine (MFQ)) are accumulated in the digestive vacuole and interfere heme detoxification. Mutations (red circle) in the PfMDR1 and PfCRT transporters are associated with the resistance to 4-aminoquinolines and arylamino alcohols. Atovaquone (ATQ) inhibits electron transport chain in the mitochondrion, which is a source of electrons for dihydroorotate dehydrogenase (DHODH). The DHODH is essential for *de novo* biosynthesis of pyrimidine nucleotides such as dTMP for DNA synthesis. Mutations in cytochrome b (subunit in the CYP bc_1 complex) can confer resistance to ATQ.

1.4.2 Quinoline-based antimalarial drugs

Quinoline-based antimalarial drugs have long been used to combat malaria, beginning with quinine. Drugs in this group contain a core quinoline ring which is a nitrogen containing heterocyclic aromatic structure (Figure 1.8). Current quinoline-containing antimalarial drugs can be classified into three classes including arylamino alcohols (i.e. quinine and mefloquine), 4-aminoquinolines (i.e. chloroquine, amadiaquine, and piperaquine), and 8-aminoquinolines (i.e. primaquine, tafenoquine, and bulaquine).

1.4.2.1 Arylamino alcohols

Arylamino alcohol (Figure 1.8) is one of the important antimalarial classes. Historical evidence exists that as far back as the 16th century, quinolines were used to treat malaria in the form of cinchona tree extracts. The active ingredient known as quinine (QN) was first isolated from cinchona tree in 1820 [58]. From the first discovery, QN has long been used in the malaria treatment. Although QN is recommended as a second-line option for malaria treatment, it is used to treat malaria during pregnancy in the first trimester and used to treat multidrug-resistant malaria [59, 60]. The mechanism of action of QN has not been fully elucidated. It is proposed to accumulate in the digestive vacuole and inhibit heme detoxification (Figure 1.7) [8, 59]. Mutations in the known parasite drug resistance transporters PfMDR1 and PfCRT, have been shown to be involved in the resistance to drugs in this group [8, 59]. Gametocytocidal activity in early gametocytes and transmission-blocking activities of QN have also been reported [56, 61].

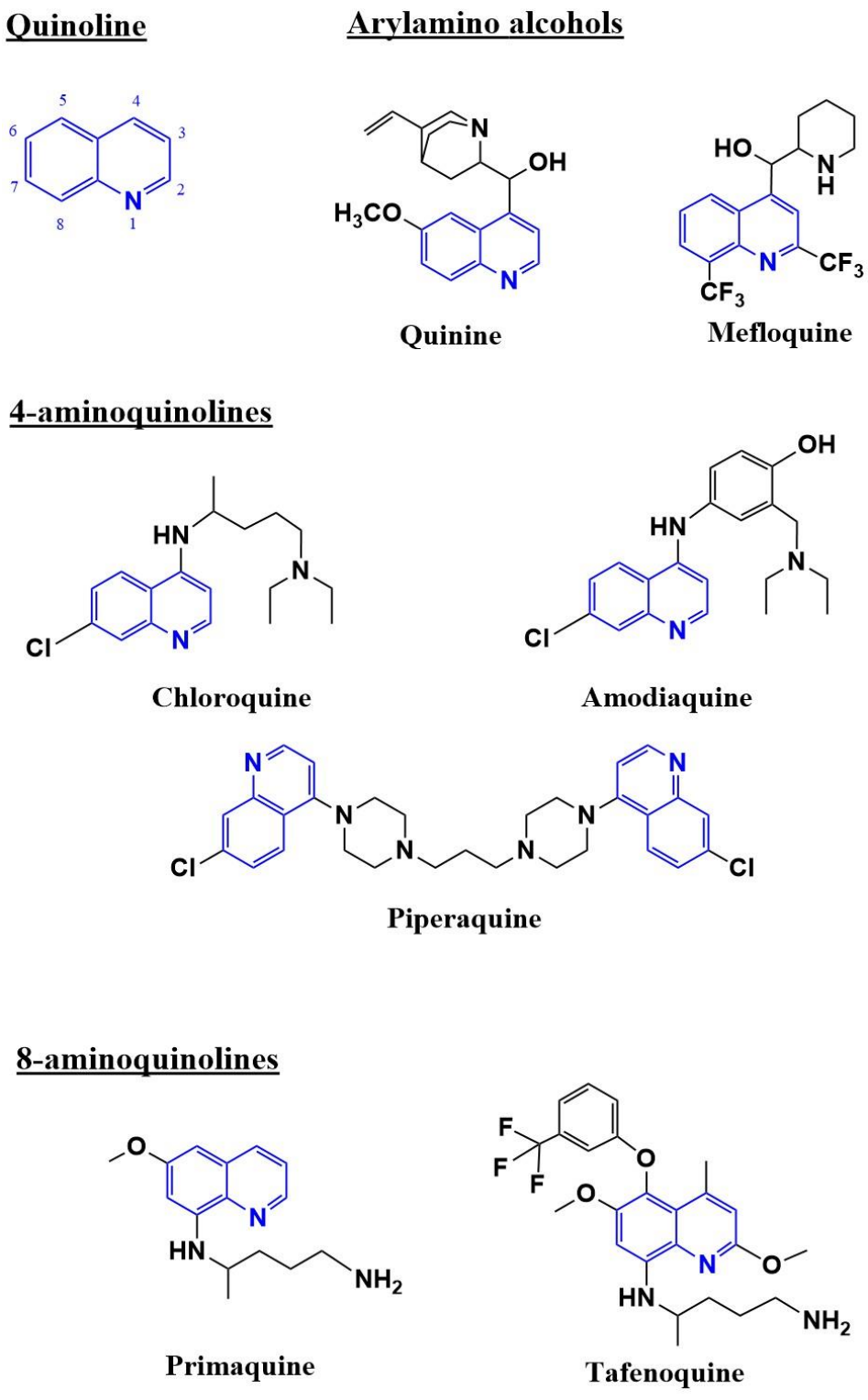

Figure 1.8 Chemical structures of quinoline-based antimalarial drugs.

Mefloquine (MFQ) is another drug having gametocytocidal activity in this class. MFQ is currently recommended to use in combination with artesunate in ACTs for non-severe malaria treatment and use in the chemoprophylaxis in countries with chloroquine resistance [6, 59]. MFQ is proposed to have the same mode of action as QN [59]. Recent studies have been reported that MFQ has activity against early gametocytes (IC_{50} 36-80 nM) [30] and mature gametocytes (IC_{50} >5 µM) [55] *in vitro* but there is little evidence of *in vivo* efficacy [62].

1.4.2.2 4-aminoquinolines

The 4-aminoquinoline class of antimalarial drugs contain a core quinoline ring(s) with an amine group at position 4 (Figure 1.8). There are three major antimalarial drugs in this group, including chloroquine (CQ), amadiaquine (AQ), and piperaquine (PPQ). All of these drugs exhibit activity against early-stage gametocytes but not late-stage gametocytes [27].

Chloroquine (CQ) was first introduced in 1946 [63]. Together with the introduction of the insecticide DDT, CQ was used in the Global Malaria Eradication campaign in 1955 to reduce transmission endemic areas [64]. Since the 1950s, CQ-resistant parasites developed and emerged after extensive use of drug [58]. Due to its potent efficacy, relative safety, and low cost, CQ is still used for the treatment of non-*falciparum* malaria as well as for malaria chemoprophylaxis [59]. The mechanism of action of CQ remains somewhat controversial, but it has been shown to accumulate in the digestive vacuole and inhibit heme detoxification (Figure 1.7) [8, 58, 59]. Mutations in PfMDR1 and PfCRT transporters are proposed to be involved in the resistance to

drugs in this group [8, 59]. CQ has activity against immature gametocytes *in vitro* [30], but it has no effect against mature gametocytes both *in vitro* and *in vivo* conditions [55, 65, 66].

Amodiaquine (AQ) was developed at the end of World War II [67]. Now, AQ is used in a combination with artesunate [6]. Like CQ, the mechanism of action of AQ is thought to inhibit heme detoxification [8, 58, 59, 68]. A recent study has revealed the activity of its active metabolite against early-stage gametocytes in vitro [29], however there is no reported efficacy against late stage (mature) gametocytes.

Piperaquine (PPQ) is a bisquinoline antimalarial drug, which consists of two quinoline moieties. PPQ was first synthesised in 1960s and used clinically for both the treatment and chemoprophylaxis of malaria in China [69]. PPQ has been shown to inhibit heme polymerization [70], suggesting that it has a similar mode of action to chloroquine. PPQ also shows activity against immature gametocytes [29]. The information on PPQ inhibitory activity against mature gametocytes is limited.

1.4.2.3 8-aminoquinolines

The 8-aminoquinolines are antimalarial drugs containing a quinoline core structure with an amine group at position 8 (Figure 1.8). Two members of this group, including PQ and tafenoquine (TQ), are the only two FDA licensed drugs with activity against mature gametocytes *in vivo*. PQ and its proposed mechanism of action is described in in more detail in the section 1.5.

Tafenoquine (TQ) is an 8-aminoquinoline analogue of PQ developed by the Walter Reed Army Institute of Research in 1978. TQ exhibits moderate activity against

asexual stages of *P. falciparum* [71] and activity against gametocytes, including mature late-stage forms [23, 69]. TQ also has improved pharmacokinetic properties, including a longer plasma half-life (12-16 days; 50 times over primaquine) [72, 73]. The mode of action of TQ is unknown but it has been proposed to be similar to that of PQ by virtue of its similar structure [27]. TQ was approved by the FDA for the radical cure of malaria in 2018. However, its deployment is expected to be limited due to concerns regarding hemolytic toxicity in patients who have G6PD deficiency.

1.4.3 Other antimalarial drugs

Atovaquone (ATQ) and methylene blue have also been shown to possess gametocytocidal activity. Atovaquone (ATQ) is a hydroxynapthoquinone (Figure 1.9) developed in 1980-90s [74, 75]. Now, it is used as a combination with proguanil (Malarone®) for non-severe malaria treatment and chemoprophylaxis for travellers [75-77]. The proposed mechanism of action of ATQ is shown in Figure 1.6. ATQ is a competitive inhibitor of ubiquinol, which directly inhibits the electron transport chain in the mitochondrion at the cytochrom bc_1 complex (ubiquinol-cytochrome *c* oxidoreductase) [78, 79]. Inhibition of the cytochrome bc_1 complex not only leads to the loss of mitochondria function [80, 81], but also affects the *de novo* synthesis of pyrimidine nucleotides through the mitochondrial dihydroorotate dehydrogenase (DHODH) [82, 83]. The mechanism of ATQ resistance involves mutations in cytochrome *b* subunit of the bc_1 complex [8, 75]. In terms of gametocytocidal activity, atovaquone is effective against immature gametocytes *in vitro* [29, 30]. However, it does not have activity against mature gametocytes [84, 85].

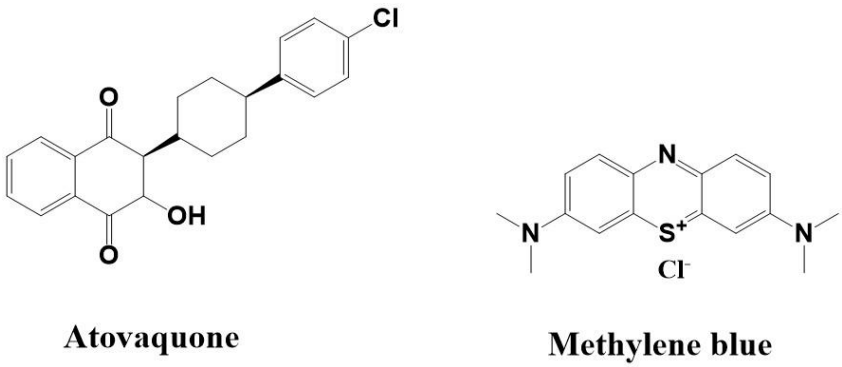

Figure 1.9 Chemical structures of atovaquone and methylene blue

Methylene blue was the first synthetic compound used in malaria treatment in 1891. Methylene blue was not widely used for malaria treatment because it causes discolouration of the skin and eyes. Work on methylene blue led to the development of chloroquine. The mechanism of action of methylene blue is not fully understood. Recent studies reveal the interaction between methylene blue and glutathione reductase (an antioxidant enzyme) that could affect the glutathione reductase level in parasite and produce the reactive oxygen species [86-88]. Currently, there is renewed interest in methylene blue due to its transmission-blocking activity against all gametocyte stages both *in vitro* and *in vivo* [27, 29, 89-91].

1.5 Primaquine and its mechanism of action

Primaquine (PQ) (Figure 1.8), a member of 8-aminoquinolines, was first synthesised in 1946. It was the only FDA-approved antimalarial drug to treat relapse malaria (caused by *Plasmodium vivax* and *Plasmodium ovale*) and to prevent the spread of malaria disease by blocking the transmission between humans and mosquito host until the approval of TQ in 2018. However, PQ has limited therapeutic utility because

of its hemolytic toxicity in glucose 6-phosphate dehydrogenase (G6PD) deficient population [92]. The exactly mechanism of action of PQ to eliminate hypnozoites and gametocytes is not fully understood.

1.5.1 Primaquine pharmacology

PQ is a pro-drug, which has been shown to be extensively metabolised in the liver. A number of PQ metabolites [93-96] (Fig. 1.10) and key metabolic enzymes (including cytochrome P450 2D6 (CYP 2D6), CYP 2C19, CYP 3A4, and monoamine oxidase A (MAO-A)) have been identified [95, 97]. The PQ metabolic pathways mediated by CYP2D6 and MAO-A are summarised in Figure 1.10. The MAO-A metabolic pathway plays a role in the metabolism of PQ aldehyde species which are converted to carboxy primaquine (CPQ). CPQ is the most abundant metabolite found in human plasma [95, 98], but this metabolite is not believed to have any antimalarial active and does not cause toxicity [99]. Primaquine CYP 2D6 mediated pathway has been shown in the production of hydroxylated metabolites (OH-PQms) which are redox active [95]. The dependence of PQ efficacy on CYP 2D6 is supported by a recent clinical study that shows the clinical failure of primaquine to eliminate *P. vivax* hypnozoites from CYP 2D6 poor metaboliser patients [100]. This argument is supported by another studied in an animal model showing the therapeutic failure of primaquine in CYP 2D knockout mice infected with *P. berghei*, however drug activity is restored in humanised CYP 2D knockout/ CYP 2D6 knock-in mice [97, 101]. Recent studies on PQ mode of action has mainly focused on the identification of the hemolytic effects of PQ in G6PD deficiency patients [93, 102, 103]. Earlier studies had investigated the

hemolytic potential of OH-PQms and oxidized products such as quinoneimine forms both *in vitro* and in *vivo* [93, 97, 104]. It is believed that CYP 2D6-mediated OH-PQms are involved in drug efficacy, which is supported by the decrease in OH-PQm level in CYP 2D knockout mice compared to wild type [105]. The most relevant species in this context are thought to be the hydroxyquinone forms carrying a hydroxyl group at the C5 position of the aminoquinoline ring (Fig. 1.10, 5-HPQ (5-hydroxy-primaquine) and 5,6-DPQ (5,6-dihydroxy-primaquine)). These species appear to be unstable, undergoing spontaneous oxidation and producing the corresponding stable quinoneimine forms (Fig. 1.10, PQQI (5-quinoneimine) and 6OHPQQI (6-hydroxy-5-quinoneimine)) [93]. In proof-of-concept studies using spinach ferrodoxin NADP-oxidoreductase FNR, quinoneimines can be enzymatically reduced with concomitant generation of H_2O_2 [93]. Despite intensive research efforts, the exact enzyme(s) and metabolic pathway(s) involved in the process remain to be fully elucidated (Fig. 1.11).

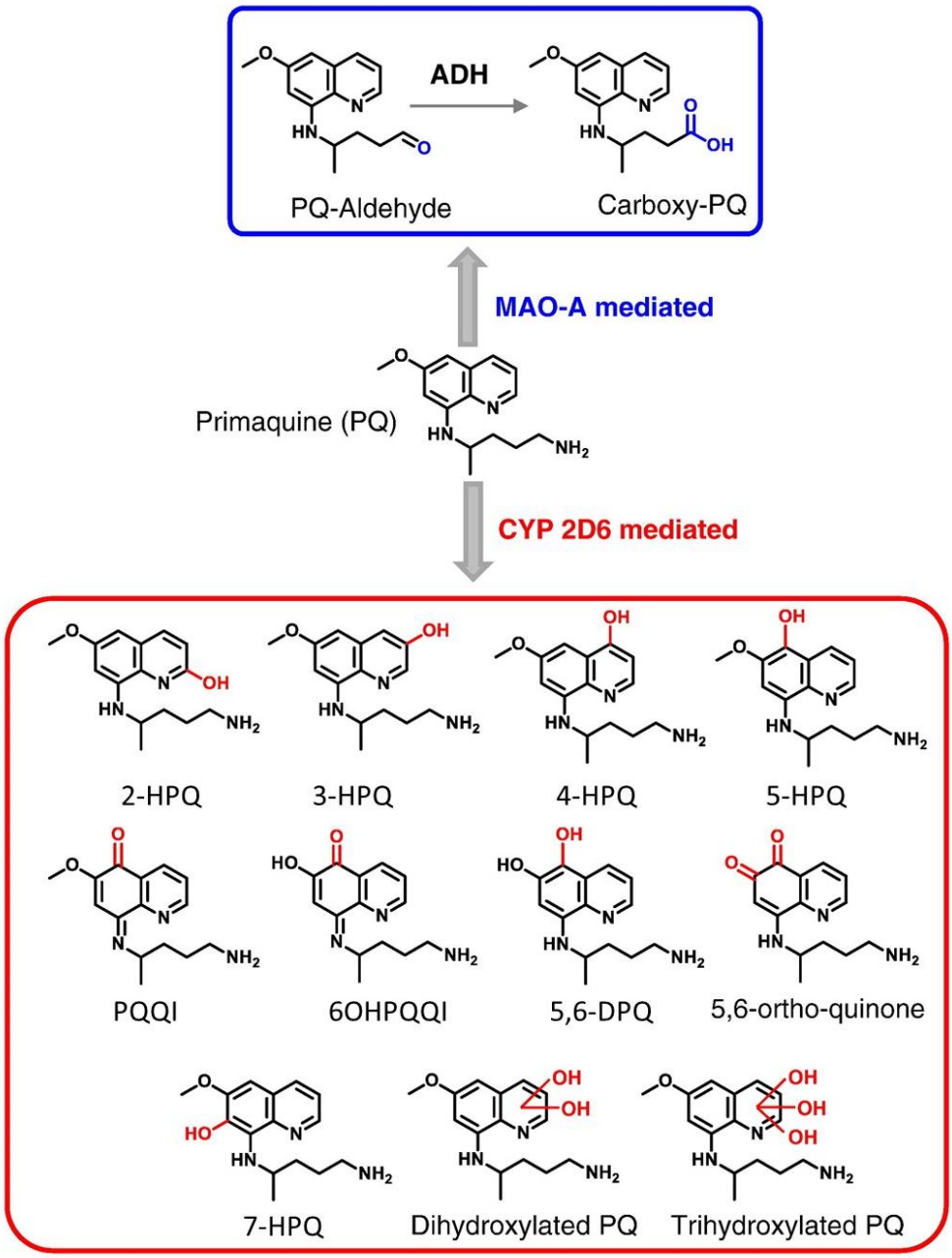

Figure 1.10 Identified primaquine metabolites mediated by CYP 2D6 and MAO-A. This figure is taken from [97] with modification.

1.5.2 Primaquine mechanism of action

The mechanism of action of primaquine against the malaria parasite is also largely unknown. A link between drug efficacy and metabolism through CYP2D6 is supported by recent animal and clinical studies referred to above [97, 100], including the association of the CYP2D6 poor metaboliser phenotype with primaquine failure in controlled human malaria infections with *P. vivax* [100]. The need for CYP2D6 metabolism to generate key OH-PQms supports a role for these metabolites in drug efficacy, however there has been no direct demonstration of the link between these metabolites and anti-parasitic activity. Any explanation of PQ action needs to address the apparent selectivity against dormant and active liver stage parasites and the ability of very low drug doses and subsequent low systemic exposures to kill gametocyte stages of *P. falciparum* clinically [106].

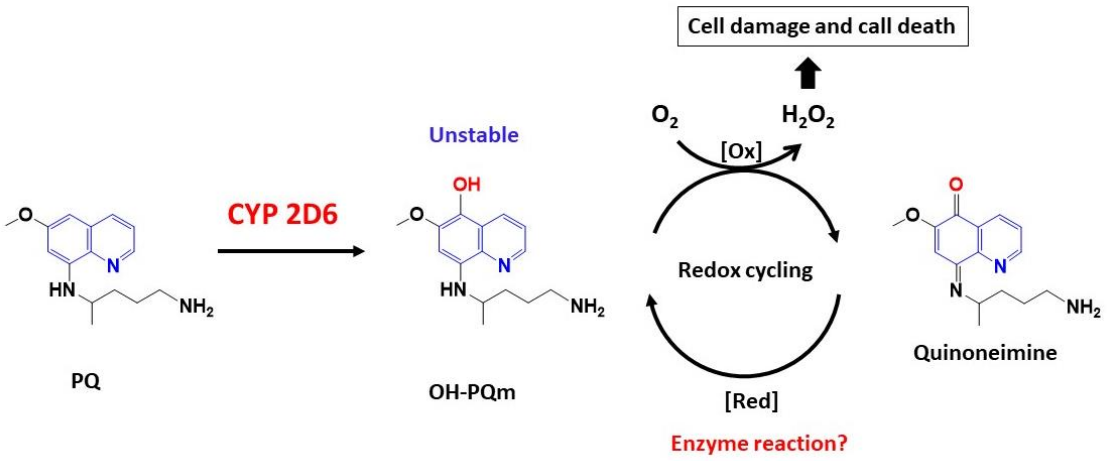

Figure 1.11 Proposed primaquine mechanism of action. PQ is metabolised in the liver via CYP 2D6 metabolism to generate redox-active OH-PQms. OH-PQms are spontaneously oxidised to quinoneimine with the concomitant production of H_2O_2. Currently, there is no direct evidence that OH-PQms are involved in parasite death and parasite or human enzymes capable of reducing quinoneimine-forms of metabolites have not been identified.

Further studies into primaquine pharmacodynamics have reported that the drug affects parasite mitochondria [107-109]. Mitochondrial swelling is reported following exposure of gametocyte-stage parasites to PQ [107]. The selectivity of PQ against liver and sexual stages of the parasite have been attributed to the differential presence/absence of parasite proteins/pathways in the different stages of development.

One of the hypotheses that forms the basis of this PhD thesis is that mitochondrial diflavin reductases present in the parasite, that are differentially expressed in sexual and asexual stages of development, may be responsible for the observed stage-dependent selectivity of the drug. The following sections will describe the diflavin reductase biochemistry and the major families found in the malaria parasite.

1.6 Diflavin reductase family

Enzymes in the diflavin reductase family contain one molecule of flavin mononucleotide (FMN) and flavin adenine dinucleotide (FAD) in a single polypeptide as a result of gene fusion of an ancestral flavodoxin (Fld)-like and a ferredoxin-$NADP^+$ reductase (FNR)-like. The members of this enzyme family in mammal are NADPH-cytochrome P450 reductase (CPR), isoforms of nitric oxide synthase (NOS) [110], novel oxidoreductase 1(NR1) [111], and methionine synthase reductase (MSR) [112]. In bacteria, the enzymes in this family include *Bacillus megaterium* flavocytochrome P450 (BM3) [113] and a flavoprotein subunit of sulphite reductase (SiR) [114]. In single-celled eukaryotes, the enzymes in this family include pyruvate: $NADP^+$ oxidoreductase from *Euglena gracilis* [115] and reductase Tah18 from yeast [116].

Amino acid sequence alignment and comparison of the three-dimensional structure of known diflavin reductases are clearly revealed that structures of reductase

part of proteins in this family are highly similar (Figure 1.12, 1.13). They have two main catalytic domains. One of them is the FMN-binding domain located in the N-terminal part of the protein. The second of which binds FAD and NADPH. The FAD/NADPH binding domain is located in the C-terminal part of the protein. Crystallographic structures of the diflavin reductase members (e.g. CPR [117, 118], NOS [119], and SiR [120]) have revealed that the FMN-binding domain is homologous to the structure of flavodoxin (Fld) and the FAD/NADPH-binding domain is homologous to the structure of ferredoxin-$NADP^+$ reductase (FNR). There is an additional domain called the connecting domain as well as the flexible hinge (~80 residues in MSR and 12 to 24 residues in the other members) that links the FMN-binding domain and the FAD/NADPH-binding domain [117, 121]. The role of the connecting domain has been proposed to control and modulate electron transfer between FAD and FMN cofactors by positioning of two catalytic domains [122, 123].

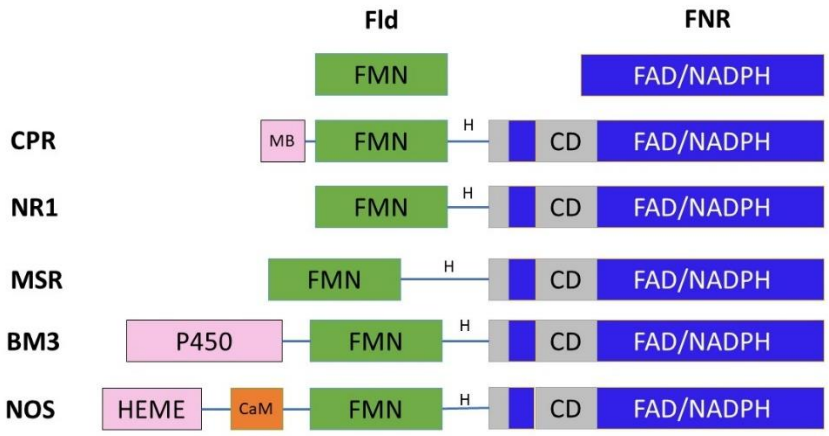

Figure 1.12 Domain organisation of members in the diflavin reductase family. Fld: flavodoxin; FNR: Ferredoxin-$NADP^+$ reductase; CD: connecting domain; CaM: calmodulin binding region; P450: cytochrome p450-like domain; HEME: heme binding domain; MB: membrane anchor part; H: the hinge loop.

The function of the diflavin reductase is to provide reducing equivalents from NADPH to their partners which carry out a variety of redox reactions. The main redox partners containing a heme domain for receiving electrons are cytochrome P450 [124], heme oxygenase [125], and NOS enzymes [126]. The diflavin reductase also involves non-heme dependent reactions such as the MSR-MS system [127]. The tight bound FMN and FAD cofactors are involved in the transfer of reducing equivalents from NADPH to the terminal electron acceptor. The series of electron transfer are similar among members of the diflavin reductase family. The selective removal of FMN by ionic strength buffer [128, 129] and site-directed inhibitor [130] in SiR reveals the sequence of electron transfer as described by the following scheme:

NADPH → FAD→ FMN→ electron acceptors

The separate roles of two flavin cofactors (FMN and FAD) and the sequence of electron transfer also confirmed by site-directed mutagenesis in diflavin reductases, including CPR [131, 132], P450BM3 [133], and NOS [134].

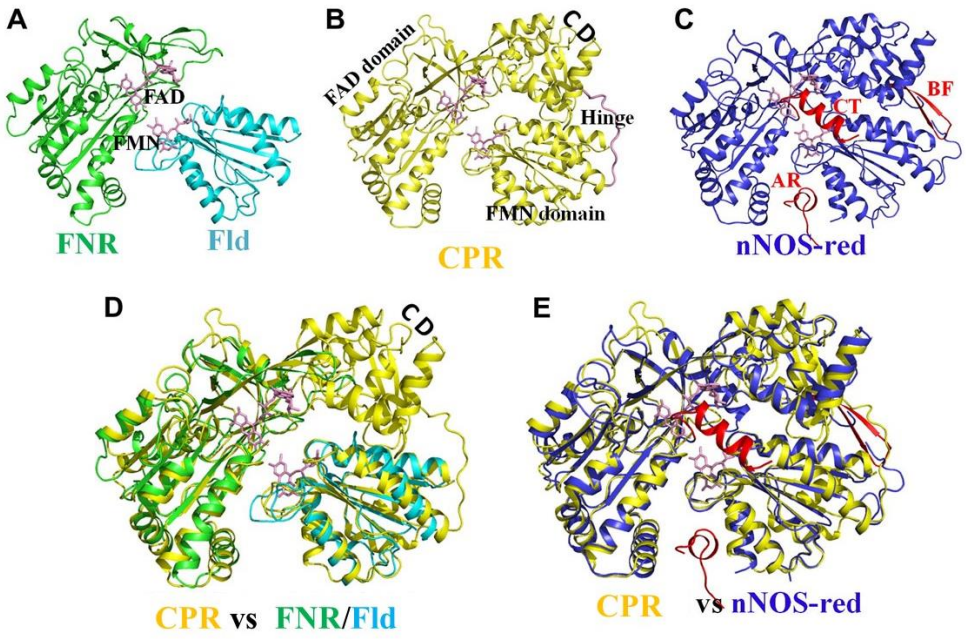

Figure 1.13 Evolutionary origins of the diflavin reductase structures. A) A model of flavodoxin (Fld) and ferredoxin-NADP$^+$ reductase (FNR). B) The rat CPR structure. C) The nNOS reductase domain structure. D) Overlay of CPR, Fld and FNR structures. E) Overlay of CPR and nNOS reductase domain. This figure was adapted from [135] with the permission licence 4386650000532.

1.7 Example of diflavin reductases

In this thesis, *P. falciparum* PF3D7_0923200 gene has been characterised. The PF3D7_0923200 has been predicted as a CPR putative and a NOS putative. The following sections review the state-of-art for these two enzymes.

1.7.1 Nitric oxide synthase (NOS)

Nitric oxide (NO), a smallest signalling molecule, plays a role in controlling neurotransmission, vasodilatation, gene transcription, mRNA translation, and protein post-translational modification (see review [136]). NO is produced by nitric oxide

synthase (NOS) which catalyses the production of nitric oxide from L-arginine, molecular oxygen, and NADPH. There are three kinds of NOS isoforms, including neuronal NOS (nNOS), inducible NOS (iNOS), and endothelial NOS (eNOS). All of them catalyse the same reaction. However, they are expressed from different genes, locate in different tissues, and have different downstream biological functions. The physiological roles, structure, and mechanism of NOS will be described in the following subsections.

1.7.1.1 Physiological roles of NOS

The physiological involvement of NOSs will be described based on their isotypes including nNOS, iNOS, eNOS (Figure 1.14).

Neuronal NOS (nNOS) is mainly expressed in central and peripheral neurons. In the central nervous system (CNS), nNOS plays a role in signalling and regulation of synaptic transmission such as long-term potentiation and long-term inhibition [137, 138]. These synaptic signalling events have been linked to an important physiological function including learning, memory, and neurogenesis [139]. Moreover, there is evidence that nitric oxide in the CNS also plays a role in the blood pressure control [140]. In the peripheral nervous system (PNS), nNOS plays a role in atypical neurotransmission, which mediates the relaxing of various smooth muscle types such as blood vessel (involves in vasodilation) [136] and corpus cavernoum (involves in erection) [141]. Abnormal production of nitric oxide from nNOS causes a variety of pathologies, such as stroke, Alzheimer's, Parkinson's, and multiple sclerosis [136, 142]. Overstimulation of nNOS by massive Ca^{2+} influx into neuronal cells leads to cell

damage which has been found in the N-methyl-D-aspartate (NMDA) receptor mediated neuronal death after stroke [143].

Inducible NOS (iNOS) can be found in almost any cell types, but it is not expressed under normal physiological conditions. The expression of iNOS is induced by infection with pathogens, inflammation, and stimulation of cytokines and other agents [136, 144-146]. Therefore, iNOS is important in terms of controlling intracellular pathogens and killing tumour cells. When iNOS is expressed at the wrong site, it is a harmful enzyme. Large amounts of nitric oxide production from iNOS are proposed to be a major contributor to various inflammatory diseases, atherosclerosis, and septic shock [147, 148].

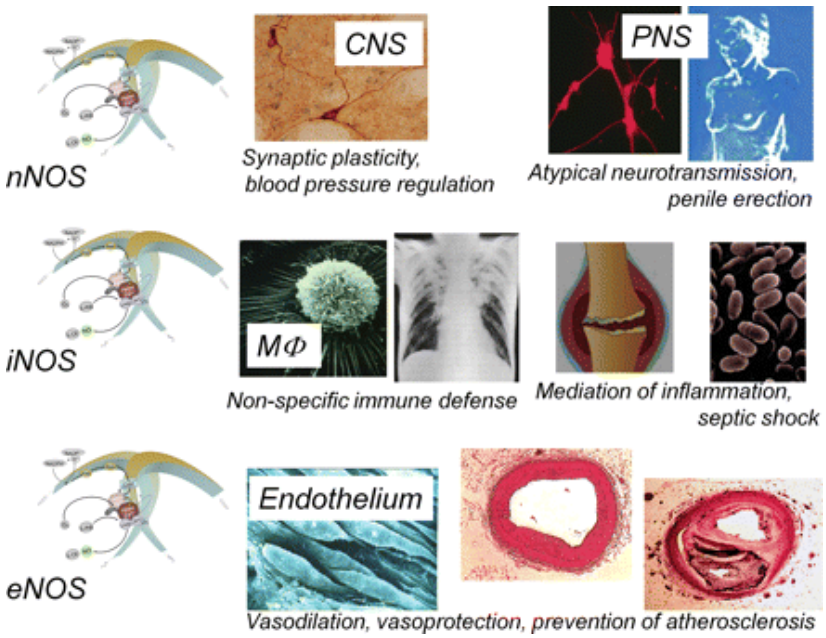

Figure 1.14 The physiological functions of three NOS isoforms. This figure was taken from [136].

Endothelial NOS (eNOS) is mainly expressed in endothelial cells and also found in other cells such as vascular smooth muscle cells and platelets. The eNOS-derived nitric oxide has been shown to regulate vasodilatation, inhibit platelet aggregation, suppress endothelial apoptosis, prevent atherosclerosis, control vascular smooth muscle proliferation, and stimulate angiogenesis (see review [136]). eNOS dysfunction (the enzyme lacks its ability to produce nitric oxide in adequate amounts) is found in patients who has risk factors for cardiovascular diseases, such as hypertension, diabetes mellitus, obesity, preeclampsia, etc. (see review [136]). The up-regulation of eNOS and NADPH oxidases found in cardiovascular diseases can cause oxidative damage to several biomolecules (including proteins, lipid, and DNA) because of the formation of peroxynitrite from the reaction of nitric oxide with superoxide anion (O_2^-) [136, 149, 150].

1.7.1.2 Structure and electron transfer of NOS

The size of monomeric NOS ranges from 130 kDa to 160 kDa, but the active enzyme is in the homodimeric form [151]. In general, the monomeric NOS comprises of two main parts including the oxygenase domain at the N-terminus and the reductase domain at the C-terminus. There is also a calmodulin (CaM) binding site that locates between the oxygenase domain and the reductase domain. The domain organisation of three NOS isotypes is shown in Figure 1.15A. The x-ray crystal structures have been reported for the oxygenase domains of all isoforms (see review [152, 153]). The example of rat nNOS oxygenase domain containing heme and tetrahydrobiopterin (H_4B) cofactors is shown in Figure 1.15B. There are published structures of the CaM-binding region of all isoforms (nNOS:PDB 2O60 (Figure 1.15C); iNOS: PDB 3GOF;

eNOS), and the reductase domains of nNOS (Figure 1.15D) [152, 153]. Structure of the NOS reductase domain is highly similar to CPR which contains four main domains including the FMN binding domain, the connecting domain, the FAD-binding domain, and the NADPH-binding domain (Figure 1.13E, Figure 1.15D) [135]. The additional parts found in NOS are an auto-regulatory region (AR) and a C-terminal tail (CT), which play a role in controlling conformational changes of NOS [152, 154-156]. The full-length crystal structure of NOS has not been reported, but the overall structure, architecture and structural dynamic of full-length NOS from cryo-EM data were recently published [157, 158]. A model of NOS architecture is shown in Figure 1.15E.

The mechanism of electron transfer and structural dynamic of NOS are shown in figure 1.16A and B, respectively. Summary of electron transfer and structural dynamic are recently published in reviews [152, 153, 159]. In general, electron transfer in NOS processes from NADPH through FAD and FMN cofactors to heme. After binding of NADPH, NOS undergoes 'Input state' that the FMN domain interacts with the FAD/NADPH domain allowing interdomain electron transfer from NADPH through flavin cofactors. The formation in this state is regulated by the interaction with the auto-regulatory loop (AR) and the C-terminal tail (CT) [154, 155, 160]. Then, the conformation is changed to the 'Output state' that the FMN domain interacts with the oxygenase domain allowing electron transfer from $FMNH_2$ to heme. CaM is proposed to be involved in conformational changes in both 'Input state' and 'Output state' [152, 153, 159]. When CaM binds with the NOS (stimulated by Ca^{2+} influx), it enhances the interdomain electron transfer from $FADH_2$ to FMN and triggers electron transfer from $FMNH_2$ to heme in the oxygenase domain of another subunit. Structural dynamic of NOS is another crucial factor involved in the NOS catalytic reaction.

The catalytic activity of NOS (both pre-steady state and steady state kinetics) has been extensive studied and used in NOS characterisation. The proposed reactive half-reaction of NOS is highly similar to other diflavin reductase members (see section 1.7.2.3 for more detail) [153, 159]. Rapid stopped-flow is a common technique used in the pre-steady state kinetic studies in NOS, which has been reported in the truncated reductase domain and full-length enzyme [161-164]. Steady-state kinetic studies of NOS have been performed in the truncated reductase domain, full-length enzyme, and mutated enzyme [165-168]. Not only the nitric oxide synthesis is measured in the NOS catalysis [165], but also the reduction of cytochrom *c* (receives electron from FMN) [166, 169] and ferricyanide (receives electron from FAD) [170] is commonly used in the measurement of different NOS modes of activities especially in the NOS reductase domain studies.

A

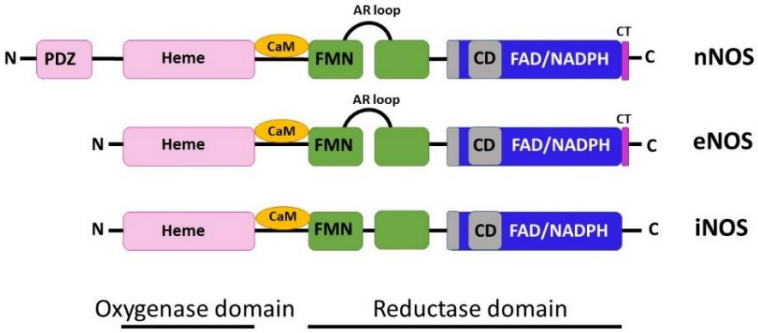

B **C** **D**

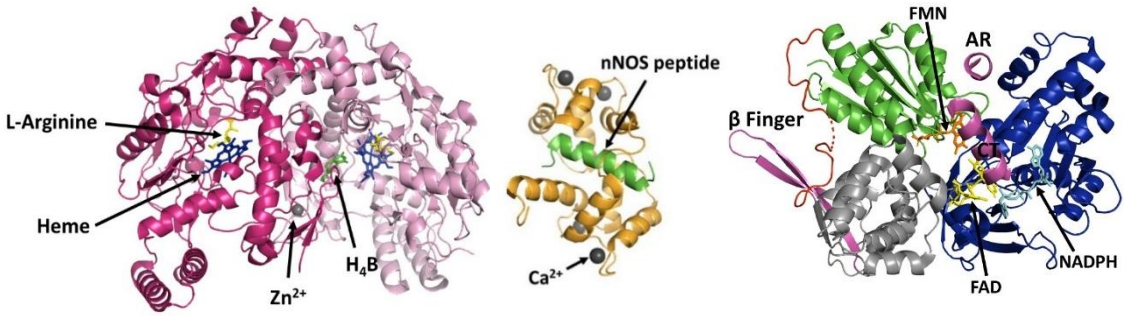

E

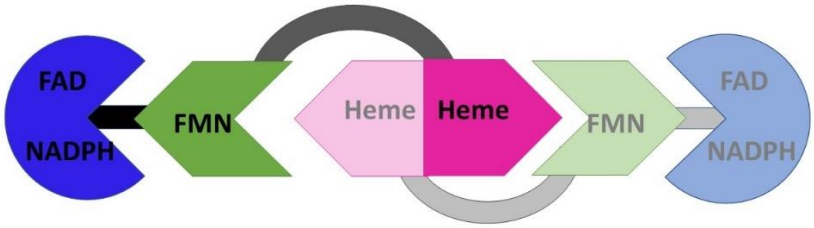

Figure 1.15 Domain organisation and structure of NOS. A) Domain organisation of neuronal NOS (nNOS), inducible NOS (iNOS), and endothelial NOS (eNOS). The heme domain, the CaM, the FMN domain, the connecting domain, the FAD/NADPH domain, and the C-terminus tail are shown in pink, orange, green, grey, blue, and magenta, respectively. B) The structure of rat nNOS oxygenase domain (PDB: 1MMV). Heme, L-arginine, H_4B, and Zn^{2+} are shown in blue, yellow, green, and grey, respectively. C) the structure of CaM bound nNOS peptide (PDB: 2O60). CaM, nNOS peptide, and Ca^{2+} ions are shown in orange, green, and grey. D) the structure of nNOS reductase domain (PDB: 1TLL). The FMN domain, the connecting domain, and the FAD/NADPH domain are shown in green, grey, and blue, respectively. Autoregulatory region (AR), C-terminus tail (CT), and beta-finger are shown in magenta. E) A model of molecular architecture of dimeric mammalian NOS.

A

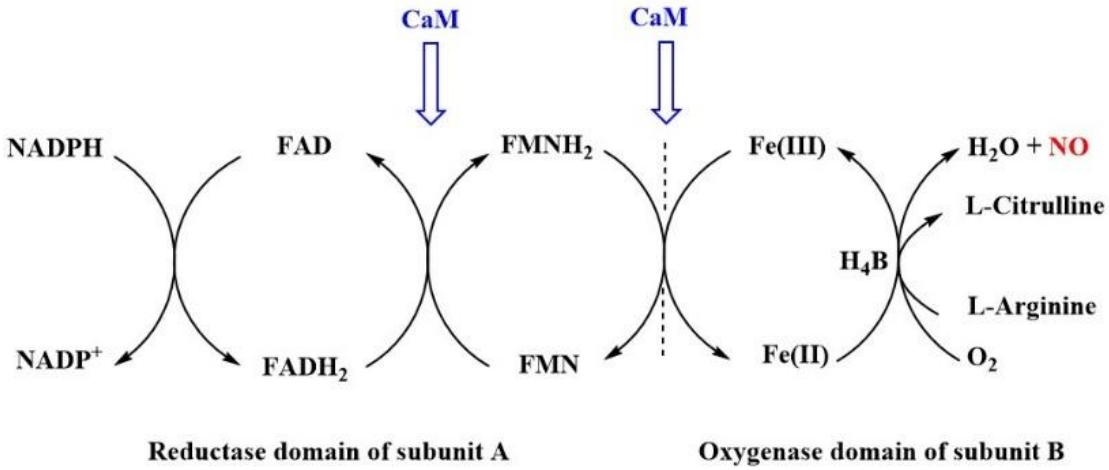

B

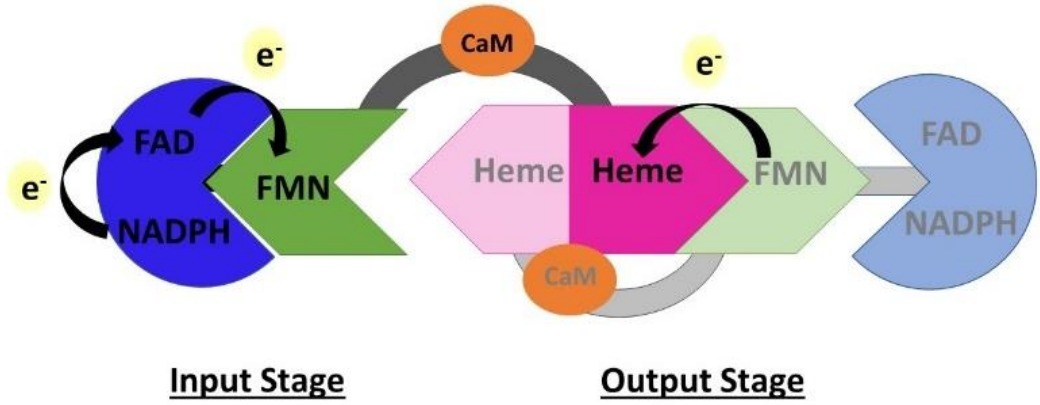

Figure 1.16 Electron transfer mechanism and structural dynamic of NOS. A) Proposed electron transfer mechanism of NOS. B) A model of structural change in the NOS to support the electron transfer.

1.7.2 NADPH-cytochrome P450 reductase (CPR)

CPR is the best characterised diflavin reductase. The size of monomeric CPR is 68 kDa to 85 kDa depending on the source [117, 171-174]. This enzyme acts as an electron donor for various electron acceptors (Figure 1.17) [175-177]. In mammal, the major physiological electron acceptors play an important role in multiple metabolic processes, including metabolism of drugs, xenobiotics, and steroids [175, 176]. Several non-physiological acceptors can interact and receive electrons from CPR, including cytochrome *c* [178], ferricyanide [179], dichlorophenolindophenol (DCPIP) [180], and menadione [181] (Figure 1.17). Non-physiological acceptors have been used in the measurement of different CPR modes of activity *in vitro*. For example, cytochrome *c* receives electrons from the FMN domain which can be used as a model for the CPR catalytic reaction with partner proteins, while ferricyanide receives electrons through the FAD domain which is useful in the study of electron transfer mechanism of CPR [118, 122, 182]. In this literature review, the physiological roles, structure and conformational variation of CPR, and electron transfer of CPR are discussed.

1.7.2.1 Physiological roles of CPR

An overview of the physiological involvement of CPR in various biochemical pathways can be described based on CPR's redox partners, including cytochrome P450 enzymes (CYPs) [175, 176, 183], cytochrome b_5 [184], heme oxygenase [185], squalene monooxygenase [186], and small molecules [187-189].

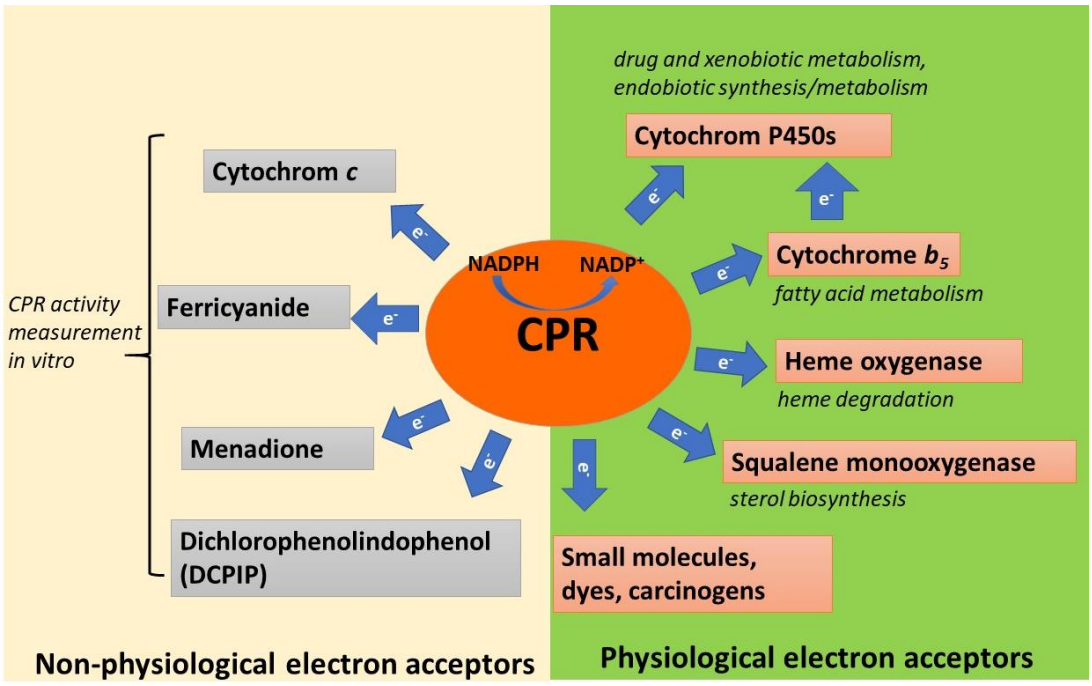

Figure 1.17 Electron accepting partners of CPR. The known physiological electron acceptors are shown in the green box. The non-physiological electron acceptors are shown in the light-yellow box.

Cytochrome P450 enzymes (CYPs) are one of the enzyme families that require electrons from CPR for their catalytic activities. There are two major classes of CYPs, including class I and class II. Class I enzymes are mitochondrial and bacterial CYPs. The CYPs in class I require two redox partners for their electron transfer processes. A flavin containing reductase (ferredoxin reductase or adrenodoxin reductase) receives electrons from NADPH then passing electrons through an ion-sulfur protein (ferredoxin or adrenodoxin) to CYPs [190, 191]. Class II enzymes are microsomal CYPs that receive electrons from CPR. In human, 57 CYPs have been identified. 50 of 57 CYPs are microsomal CYPs which involve in metabolism of xenobiotics (i.e. CYP1, CYP2, and CYP3 families), metabolism of fatty acid (CYP4 family), biosynthesis of steroids (i.e. CYP17, CYP19, and CYP21 families), and

biosynthesis of cholesterol (CYP46 and CYP51 families) [192-194]. 7 of 57 CYPs are mitochondrial CYPs which play an important role in the biosynthesis of steroids such as CYP11 family [192-194].

Cytochrome b_5, a 17 kDa haemoprotein, is one of CPR's partners. Cytochrome b_5 is involved in a number of cellular processes such as fatty acid metabolism by transferring electrons to fatty acid desaturase and fatty acid elongase [195]. In addition, cytochrome b_5 also plays a role in electron transfer to some microsomal CYPs that are involved in steroid biosynthesis/metabolism (i.e. CYP 17A1 [196] and CYP 3A4) and metabolism of xenobiotics (i.e. CYP 2B4, CYP 2D6, CYP 2E1) [197, 198].

The other two known CPR's partner proteins are heme oxygenase [185] and squalene monooxygenase [199]. Heme oxygenase plays a critical role in catabolism of heme and yields equimolar of biliverdin, iron, and carbon monoxide from the enzyme process that requires electrons from CPR for activity. Squalene monooxygenase receives electron from CPR to support sterol biosynthesis [177]. CPR is also directly responsible for the activation of small molecules, including mitomycin c, adriamycin, and tirapazamine [175]. The activation of small molecules such as mitomycin c leads to cell damage and cell death because of the generation of reactive oxygen species from its redox cycling mediating by CPR [175, 189].

The importance of CPR on a physiological function is shown by the phenotypes of CPR polymorphic variants [118, 175]. In general, the mutations causing CPR deficiency in patients are usually found in the cofactor binding sites of the protein (Figure 1.18). CPR deficiency causes disorders in steroidogenesis and cholesterol

biosynthesis with a broad phenotypic spectrum including disorders of sex development (DSD), cortisol deficiency, and skeletal malformations characteristic for Antley-Bixler syndrome (ABS) [175, 200]. Mutations found in patients and polymorphic variants found in healthy individuals have been identified and studied by numerous research groups to understand how does CPR work in a molecular level.

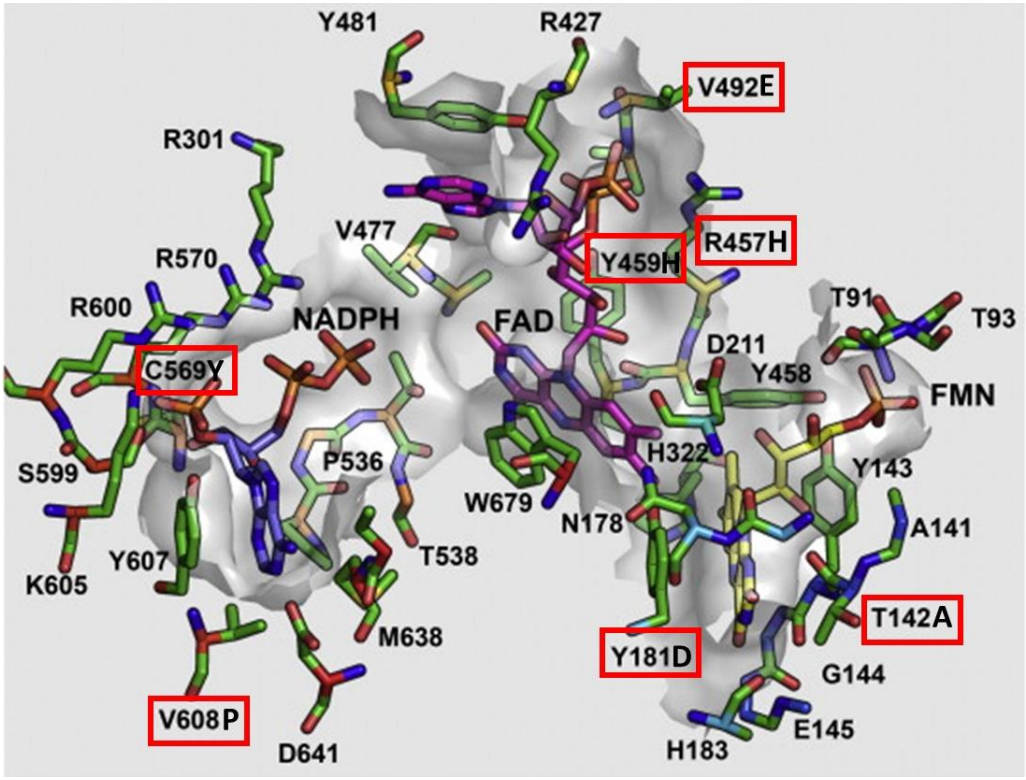

Figure 1.18 The cofactor binding sites of human CPR. The mutations causing CPR deficiency found in patient are shown in red boxes. This figure was adapted from [175].

1.7.2.2 Structure and conformational variation of CPR

In mammal, CPR contains two parts including a soluble catalytic part (~72 kDa) and a membrane anchor part (~6 kDa) [117]. Since 1997, CPR crystallographic structures of a soluble catalytic part from numerous organisms have been reported [117, 118, 122, 123, 201]. Based on their three-dimensional structures, CPRs consist of four structural domains, including the FMN-binding domain, the connecting domain, the FAD-binding domain, and the NADPH-binding domain (Figure 1.19 A). The binding pockets for both flavin cofactors are hydrophobic. The flexible hinge between the FMN-binding domain and the connecting domain that involves in the conformational variation is missing from the structures [117].

The published CPR structures, that are available in both 'closed'[117, 118] and 'open' [122, 201, 202] forms, support the conformational variation of CPR. The mammalian wild type CPR structures are usually shown in the 'closed' form. In this form, FMN isoalloxazine and FAD isoalloxazine are in close contact around 3.5 angstroms (Figure 1.19 A) [117]. Electrons are able to transfer from FAD to FMN in this proximity of two flavin cofactors. Evidence from the disulfide cross-liked 147CC514 mutant (locked to 'closed' form) kinetic and structure studies shows that the interflavin electron transfer is partially maintained in this mutant. However, the electron transfer from the mutant CPR to CYP redox partner is impaired [123].

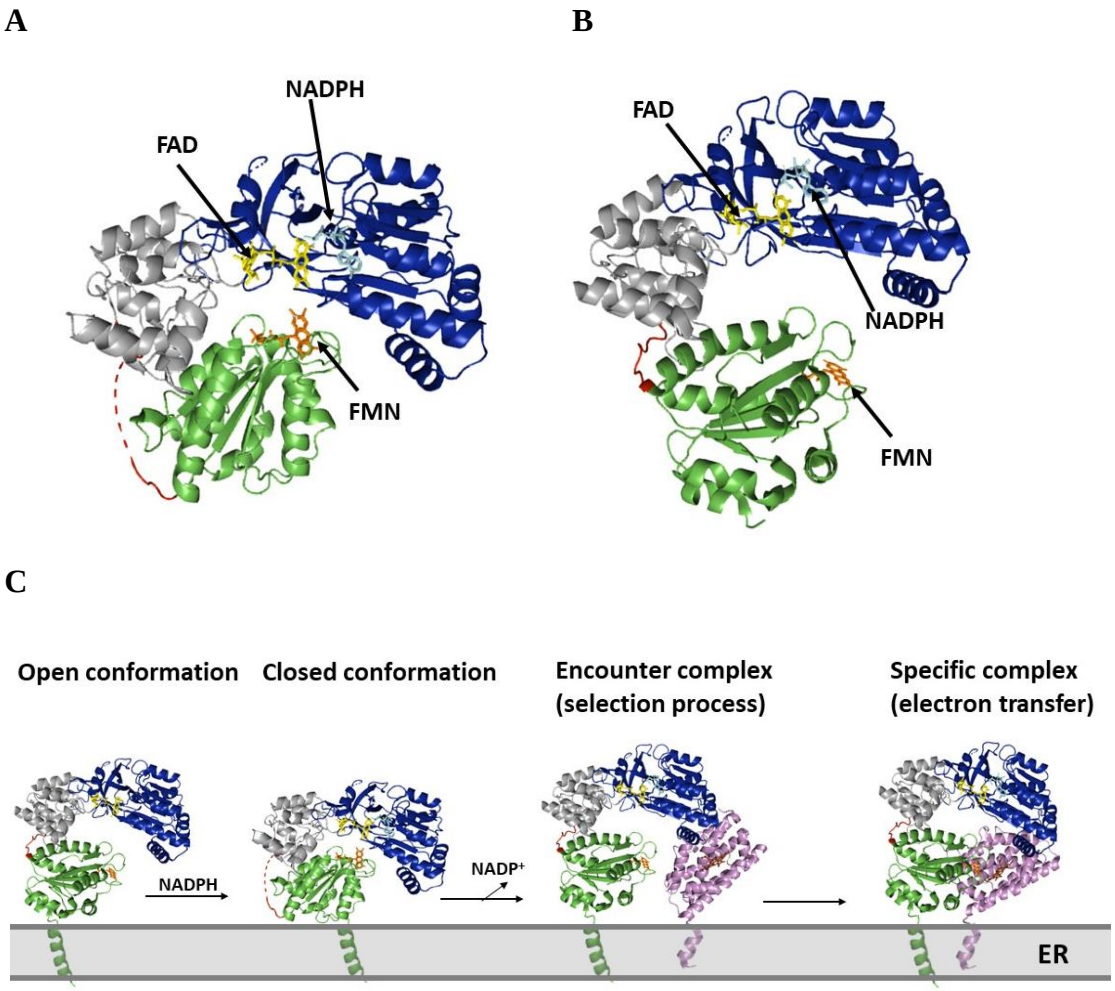

Figure 1.19 Structures of 'closed' and 'open' forms of rat CPR. A) Closed conformation of wild- type rat CPR (PDB: 1AMO). B) Open conformation of rat CPR with ΔTGEE in the hinge loop between FMN domain and the rest part of protein (PDB: 3ES9). C) A model of CPR and P450 complex formation in the endoplasmic reticulum (ER) membrane. When NADPH binds to the 'open' form CPR, resulting in the conformational change to the 'closed' form. In the 'closed' form, the hydride transfer and interflavin electron transfer, and release of $NADP^+$ occur, resulting in the change of conformation to open form. Then, the 'open' form interacts with the CPR partner (i.e. heme oxygenase) called encounter complex. After the conformational adjustment, they form the specific complex, which have optimal conformation for electron transfer from FMN to heme. The FMN domain, the hinge loop, the connecting domain, and the FAD/NADPH domain are shown in green, red, grey, and blue, respectively. The heme oxygenase is shown in violet. The FMN, FAD, NAP, and heme are shown in orange, yellow, cyan, and brown, respectively.

In the ‘open’ form (Figure 1.19 B), the distance between isoalloxazines of FMN and FAD increases to ~30 to 60 angstroms which impairs the interflavin electron transfer [123]. However, this ‘open’ form has been proposed as a suitable form for electron transfer from CPR to partner proteins. There is strong evidence supporting this hypothesis from the complex structure between ΔTGEE of rat CPR (‘open’ form) and heme oxygenase which has a close contact (6 angstrom) between the FMN of CPR and the heme of heme oxygenase [201]. Kinetic analysis of mutated CPR demonstrated that the ‘open’ form, which had slow interflavin electron transfer, is able to interact and support catalysis of the CYP partner [122].

Taken together, the kinetic and structural analysis suggest that conformational changes are essential for catalysis and CPR’s partner protein electron transfer. A model representing the current hypotheses of a productive CPR-CPR’s partner electron transfer complex is shown in Figure 1.19 C.

1.7.2.3 Electron transfer and enzyme kinetics measurement in CPR

CPR function in electron transfer depends on the ability of tight-bound flavin cofactors (FMN and FAD) to engage in both one- and two-electron redox chemistry. The flavin cofactors can exist as the oxidised (ox), one-electron reduced semiquinone (sq), and two-electron fully reduced (red) forms (Figure 1.20). The free semiquinone and fully reduced forms in solution can exist in both neutral and anionic forms with pKa 8.5 and 6.5, respectively [135]. However, the pKa values of protein bound flavins has not been determined. In CPR, the semiquinone usually present in the blue neutral within the pH range 6.5-8.5 [203]. The special oxidation and protonation states of flavins can be visualised by their characteristic absorption spectra [173, 204].

The oxidised forms have broad absorption maxima at 380 and 450 nm. Their blue neutral semiquinone forms have a broad band in between 500-700 nm with maxima in the region 580-600 nm.

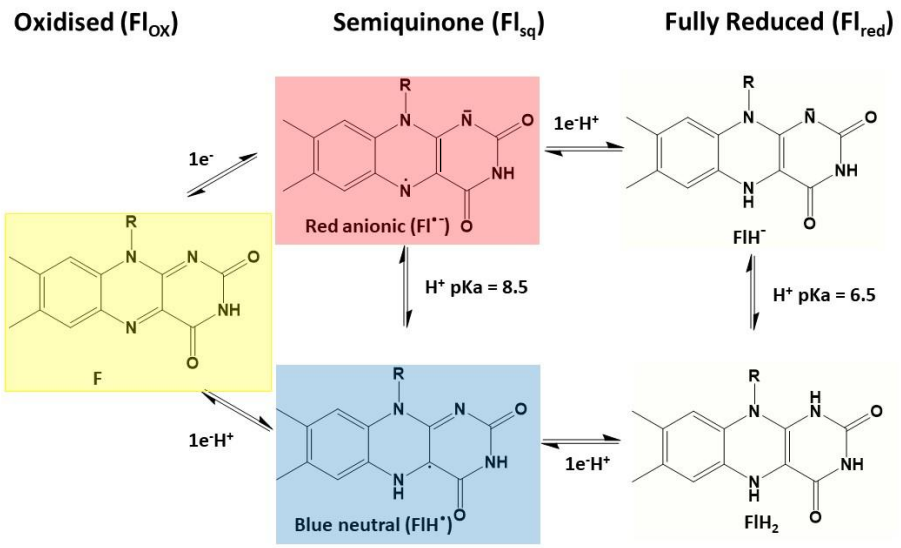

Figure 1.20 Various redox states of isoalloxazine ring of FMN and FAD. The visible spectrum of each redox state is shown in the background colour box.

To investigate the electron transfer in CPR, stopped-flow spectroscopy is the widely used technique in the pre-steady stage kinetic study of the reductive half-reaction of CPR [203, 204]. The pre-steady state kinetic parameters have been studied in truncated CPR, mutated CPR, and wild type CPR. The proposed reductive half-reaction of CPR summarised from Gutierrez *et al* [204] and Brenner *et al* [203] is shown in Figure 1.21. Pre-steady state data has been obtained by rapid mixing of oxidised CPR with excess NADPH in a stopped-flow instrument. Pseudo-first-order kinetic is then tracked by following the flavin reduction at 450 nm or the formation of semiquinone signal at 600 nm. After curve fitting to standard double exponential expression, there

are two main rate constants corresponding to two-electron reduced enzyme species (k_1 in Figure 1.21) and four-electron reduced enzyme species (k_2 in Figure 1.21).

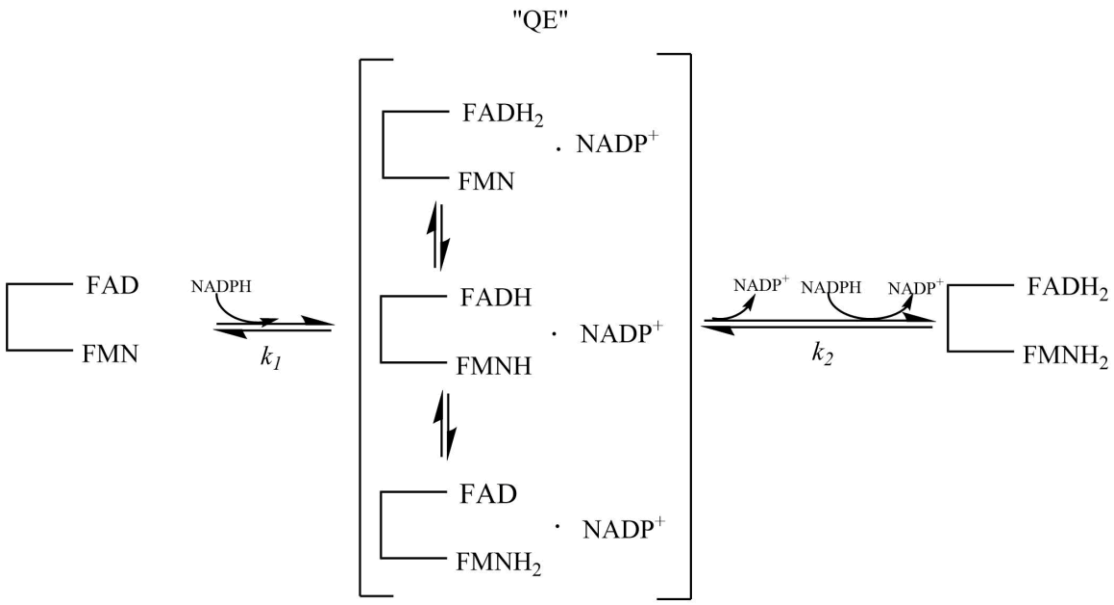

Figure 1. 21 The proposed kinetic scheme of the reductive half-reaction of CPR.

It is proposed that the mechanism of electron transfer starts from hydride transfer from NADPH to the FAD cofactor yield the two-electron reduced FAD species called a FAD hydroquinone ($FADH_2$). Electrons are then passed onto the FMN cofactor yield the formation of intermediates called di-semiquinone (FMNH, FADH) and the formation of a FMN hydroquinone ($FMNH_2$). During the reaction, it is proposed that the thermodynamic equilibrium of all FMN and FAD redox states ($FADH_2$, FMN; FADH, FMNH; FAD, $FMNH_2$) called a quasi-equilibrium ("QE") occurs. $NADP^+$ then dissociates and another NADPH binds to the CPR. The second hydride is transferred

from NADPH to the CPR and leads to the four-electron reduced enzyme species ($FADH_2$, $FMNH_2$).

Steady state kinetics have been extensively studied in both truncated CPR, mutated CPR, and wild type CPR [122, 131, 182]. Due to the lack of the ability to transfer electrons to the physiological partners in the N-terminus truncated CPR (soluble CPR), the non-physiological partners (such as cytochrome *c* [131, 178, 182] and ferricyanide [118, 182]) have been used in the catalytic activity measurement using UV-vis spectroscopy. Cytochrome *c* (receives electrons from the FMN domain) and ferricyanide (receives electrons from the FAD domain) are widely used in the measurement of different CPR modes of activities.

Taken together, pre-steady state kinetic, steady-state kinetic, spectroscopic, and structure analyses are required for further understanding and characterisation of unidentified CPR including mechanism of electron transfer, residues involved in electron transfer, residues involved in cofactor binding sites, and conformational variation.

1.8 *P. falciparum* NADPH-cytochrome P450 reductase putative

NADPH-cytochrome P450 reductase (CPR, putative) has been identified in several malaria parasites including *P. falciparum* [205], *P. vivax* [206], and *P. berghei* [207]. However, the knowledge of CPR-like in *Plasmodium* spp. is limited to bioinformatics prediction of their structure and function. The experimental characterisation and functional role have not been described.

In *P. falciparum*, there are two gene sequences (Gene ID: PF3D7_0923200 and PF3D7_11450300) that have been predicted to function as CPR. Recent genetic validation experiments also predict both PF3D7_0923200 and PF3D7_11450300 to be an indispensable gene [208]. There is less information in both genes in terms of experimental characterisation. PF3D7_0923200 has been predicted as a NOS candidate by Ostera *et al* [209]. The Ostera's group did not report the gene expression in trophozoites from the immunofluorescence data but did report PfDFR1 mRNA from trophozoite stages [209]. Due to the reactivity problem of their anti-PF3D7_0923200 monoclonal antibody, the immunofluorescence data could not confirm the expression of PF3D7_0923200 at the protein level. For PF3D7_11450300, Fan *et al* [205] reported a bioinformatics analysis of this gene. To date, the experimental expression and characterization of PF3D7_0923200 and PF3D7_11450300 have not been reported.

Sequence alignment of predicted *P. falciparum* CPR candidates and known diflavin reductase members is shown in Figure 1.22 and the amino acid identity is shown in Table 1.1. In PF3D7_0923200, the alignment shows sequence similarity of 26.0 % with hCPR, 23.3% with PF3D7_11450300, and ranging from 18.6% to 22.8% in other diflavin reductase members. In PF3D7_11450300, the alignment shows sequence similarity of 23.3 % with PF3D7_0923200, 21.2% with hNR1, and ranging from 16.8% to 18.8% in other diflavin reductase members. However, PF3D7_0923200 shows higher sequence similarity than PF3D7_11450300 in the FMN, FAD, and NADPH binding domains.

Due to the presence of a predicted mitochondrion targeting sequence, PF3D7_0923200 has been predicted to localise in mitochondrion. Unlike PF3D7_0923200, PF3D7_11450300 has been predicted to be located in nucleus [205]. PF3D7_11450300 (103.1 kDa) is larger than PF3D7_0923200 (92.1 kDa), but both of them are bigger in size than published CPRs (68 kDa to 85 kDa) [117, 171-174]. In addition, PF3D7_11450300 lacks an important feature of CPRs, which is a membrane anchor in the N-terminal part of the protein. Both have not yet been characterised and their biological role(s) have not been reported. Due to the lack of sequence conservation for cytochrome P450 in *Plasmodium* genome, the biological role(s) and the partner proteins are unknown.

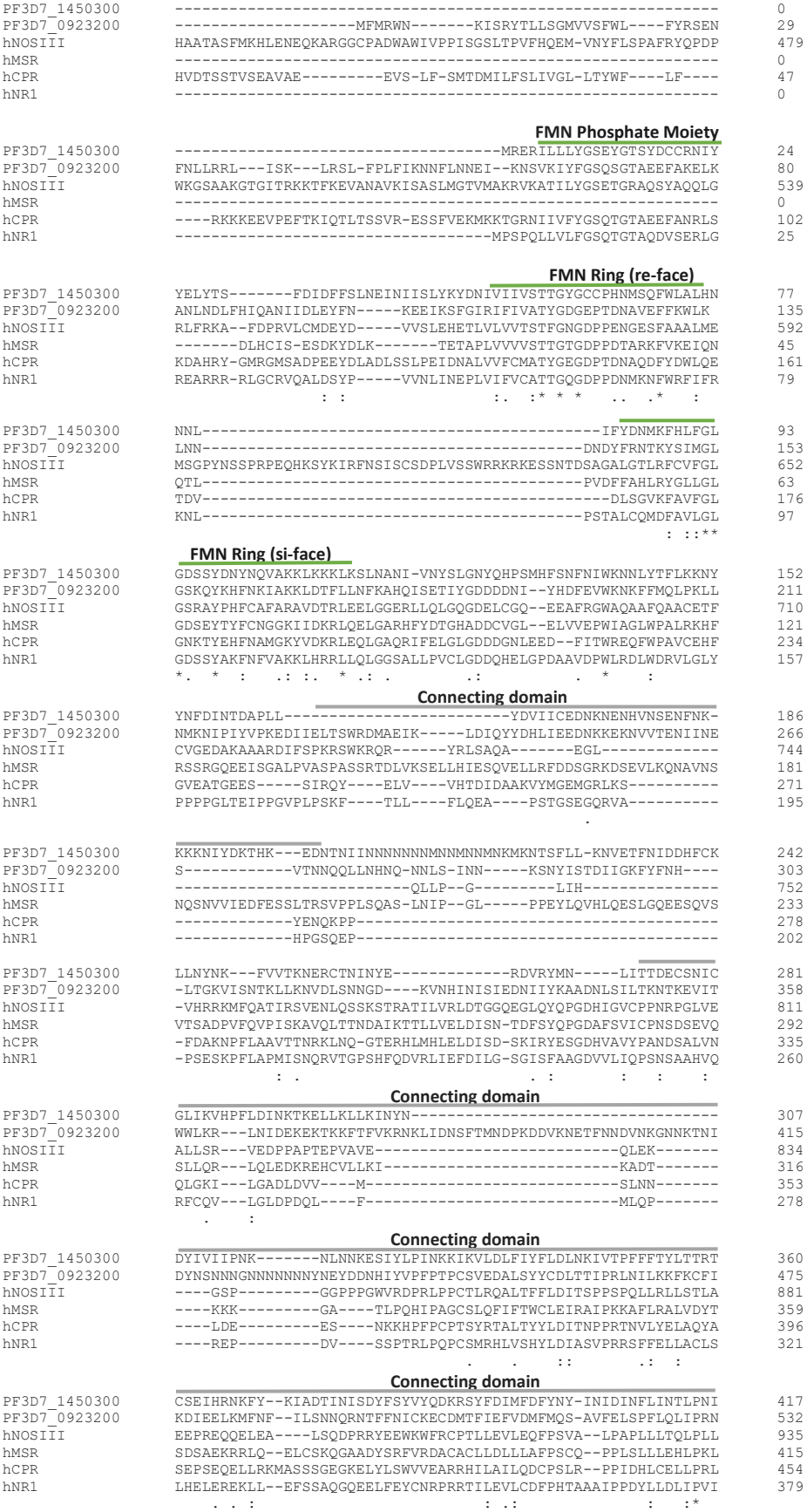
FMN Phosphate Moiety
FMN Ring (re-face)
FMN Ring (si-face)
Connecting domain
Connecting domain
Connecting domain
Connecting domain

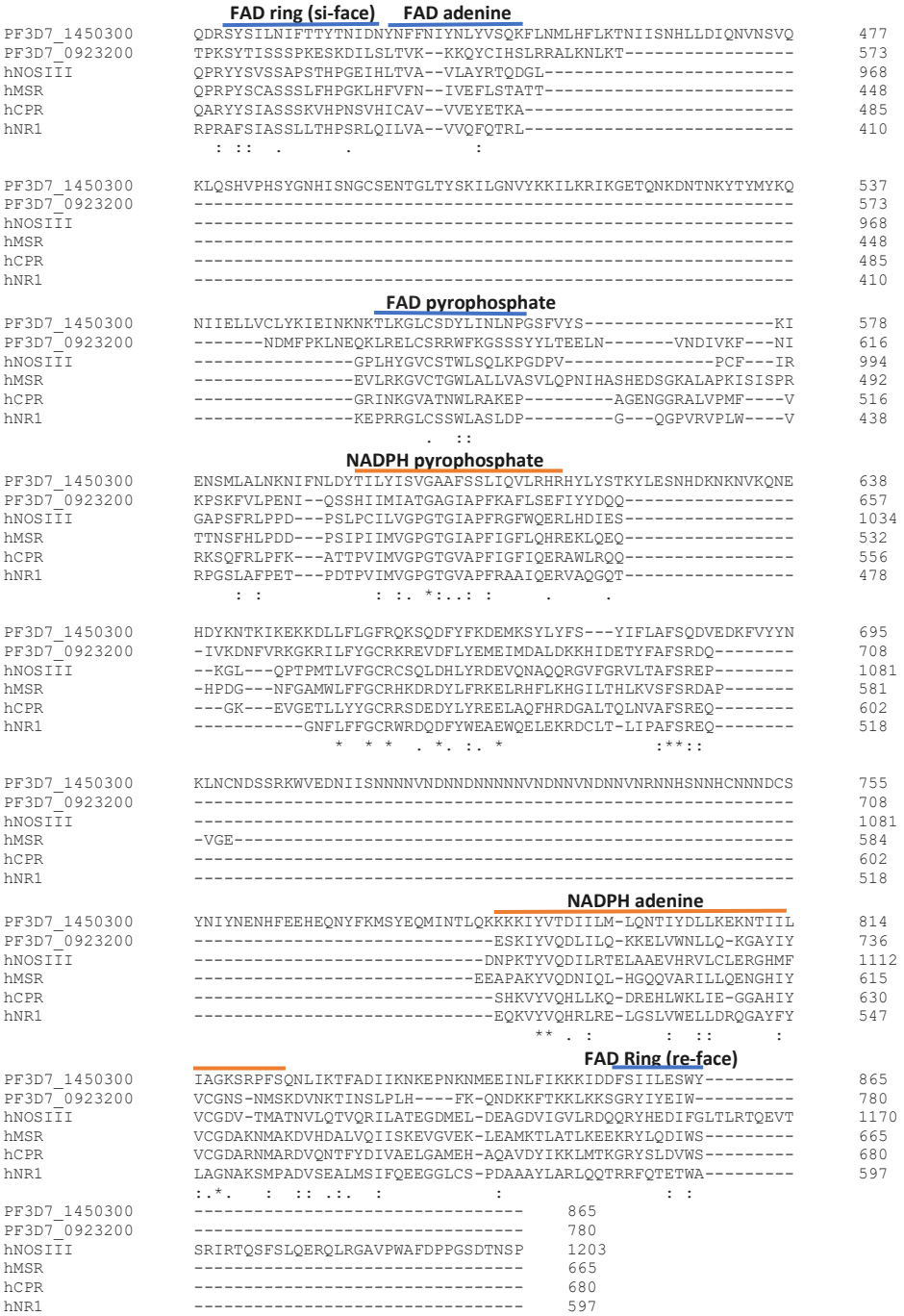

Figure 1.22 Alignment of PF3D7_1450300 and PF3D7_0923200 with other members of diflavin reductase. Sequences shown are; hCPR: human CPR (NP_000932.3); hNOSIII: human endothelial nitric oxide synthase (NP_000594.2); hMSR: human methionine synthase reductase (Q9UBK8); hNR1: human novel oxidoreductase 1 (Q9UHB4). The sequences were aligned by Clustal Omega. Cofactor binding sites are defined based on CPR by Wang *et al* [117]. FMN binding regions are shown with green lines. FAD and NADPH binding regions are represented by blue lines and orange lines, respectively. The connecting domain is shown with grey lines.

Table 1.1 Amino acid identity between PfDFR1 candidates and known diflavin reductases

NADPH-cytochrome P450 reductase	% Identity with PF3D7_1450300	% Identity with PF3D7_0923200
PF3D7_1450300	100.00	23.30
PF3D7_0923200	23.30	100.00
hNOSIII	16.76	18.63
hMSR	18.48	21.41
hCPR	18.84	26.09
hNR1	21.20	22.78

In this thesis, PF3D7_0923200 has been characterised. We have called the enzyme *P. falciparum* NADPH-dependent diflavin reductase I (PfDFR1) for two reasons. First, *P. falciparum* lacks a sequence-conserved cytochrome P450. Therefore, PF3D7_0923200 is not a real CPR protein. Second, the PF3D7_0923200 lacks the important characters of NOS including the CaM binding region and the oxygenase domain.

1.9 Thesis aims

PQ was the first licensed drug by the FDA capable of eliminating the vivax hypnozoites, liver stage schizonts, and mature gametocytes. For the safe use of PQ, testing for G6PD deficiency is required due to PQ-induced hemolytic anemia in patients suffering from G6PD deficiency. Despite over 70 years of use, the mode of action of

primaquine is not understood, limiting efforts to develop improved second-generation drugs. A working hypothesis of this thesis is that the antiparasitic efficacy of primaquine is a result of hydroxylated primaquine metabolites (OH-PQms) undergoing spontaneous oxidation, generating toxic intermediates (e.g. H_2O_2) and the corresponding stable quinoneimine forms. It is further hypothesised that the stable quinoneimine metabolites are reduced to the OH-PQm via the action of diflavin reductase(s), including those of the parasite.

The PfDFR1 (gene ID: PF3D7_0923200), which has a predicated mitochondrion targeting sequence, a predicted transmembrane helix at the N-terminus, and which has been shown to be upregulated in gametocyte stages, is hypothesised here to be a candidate enzyme involved in primaquine activity. As this PfDFR1 has not yet been studied, characterisation and understanding of its biological role(s) and of its potential role in the mode of action of PQ, are seen as an important research question. Towards this aim, the specific objectives of the thesis are;

a) Generation of recombinant PfDFR1 in an *E. coli* expression system. Optimisation of the expression conditions for efficient production of functional recombinant PfDFR1.
b) Characterisation of spectral properties of PfDFR1. Comparison of flavin contents between PfDFR1 and human CPR using HPLC analysis. Determination of pre-steady state kinetic of PfDFR1 half-reaction. Investigation of the pH and temperature effects on PfDFR1 activity.

c) Comparative characterisation of PfDFR1 and human CPR in terms of enzymatic properties (i.e. kinetic parameters and IC_{50} of known inhibitors) in cytochrome *c* and ferricyanide assays.

d) Comparative characterisation of PfDFR1 and human CPR and elucidation of their potential role in the mechanism of action of primaquine.

e) Determination of PfDFR1 expression and localisation in *P. falciparum* asexual and sexual stages.

CHAPTER 2

GENERAL MATERIALS AND METHODS

2.1 Materials

2.1.1 General reagents

Chemicals and reagents were obtained from commercial sources in either analytical or molecular grade. Acetic acid, agarose, ammonium persulfate, ampicillin, bovine serum albumin (BSA), chloramphenicol, cytochrome *c*, hydrochloric acid, imidazole, magnesium chloride hexahydrate, dithiothreitol (DTT), ethanol, ethylenediaminetetraacetic acid (EDTA), kanamycin, glycine, sodium chloride, sodium dodecyl sulfate (SDS), tris[hydroxymethyl]aminomethane (Tris), and urea were purchased from Sigma. Isopropylthio-β-galactoside (IPTG) was purchased from MERCK. Glycerol was purchased from Fisher. NADPH, NAD, $NADP^+$, and NADH were purchased from Melford Laboratories Ltd. FMN and FAD were purchased from Tokyo Chemical Industry UK Ltd. LB Broth (Miller) powder was purchased from Sigma and Formedium™.

2.1.2 Bacteria strains and plasmid

Escherichia coli strain TOP10 [F- *mcrA* Δ(*mrr-hsd*RMS-*mcr*BC) Φ80*lac*ZΔM15 Δ *lac*X74 *rec*A1 *ara*D139 Δ(*araleu*)7697 *gal*U *gal*K *rps*L (StrR) *end*A1 *nup*G] was used for DNA cloning.

Escherichia coli strain BL21 (DE3) [F– dcm ompT hsdS(rB– mB–) gal λ(DE3)] was used for recombinant protein expression.

pETM-11 plasmid (Figure 2.1) was used for the construction of the codon optimised PfDFR1 expression system. The pETM-11 expression vector carries the N-terminal and C-terminal His•Tag sequences. The expression of the recombinant protein is under control of the T7 promoter. This plasmid contains the kanamycin resistance gene.

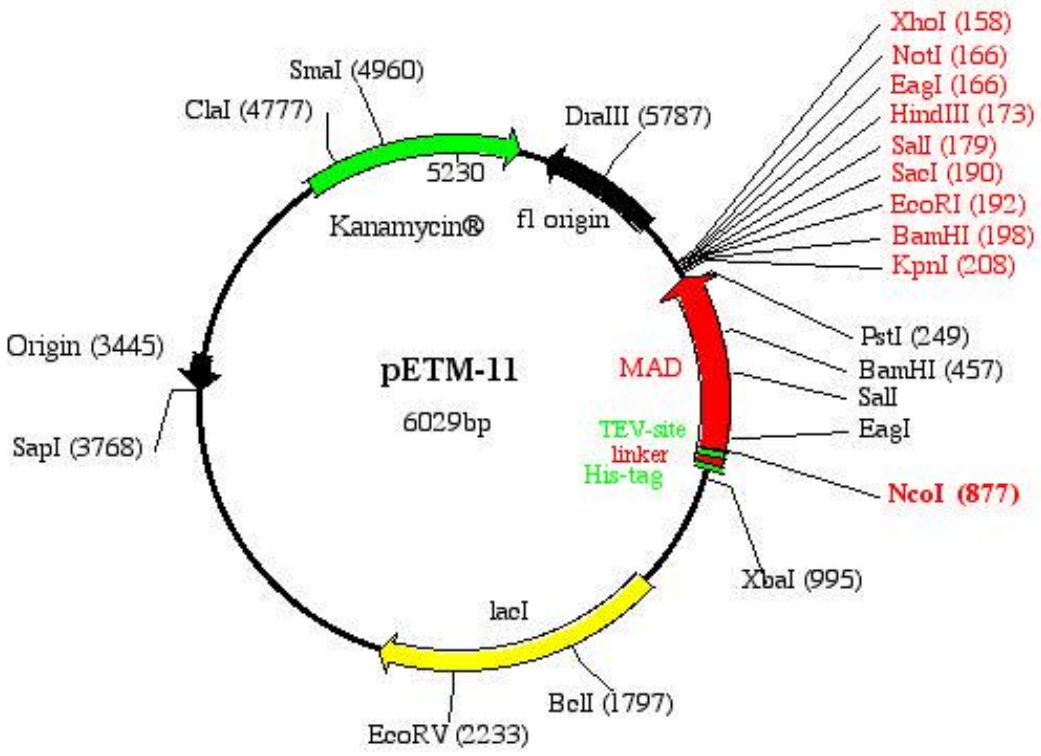

Figure 2.1 pETM-11 plasmid map taken from The European Molecular Biology Laboratory (EMBL).

2.1.3 Primers

The sequences of oligonucleotides used for DNA sequencing (Table 2.1) were designed to read the section of the *PfDFR1* gene away from the T7-promoter and T7-terminater primers. Real-time PCR primers (Table 2.2) were designed and purchased from Sigma. The sequences of 60S ribo L18 primers were obtained from a reference [210].

Table 2.1 DNA sequencing primers

Name	**Length (bp)**	**Tm (˚C)**	**%GC**	**Sequence (5'-3')**
PfDFR1 Left primer	21	55.4	52.4	GACATCTTGGAGAGACATGGC
PfDFR1 Right primer	22	53.4	45.5	GATCCCTTAAACCATCTTCTGC

Table 2.2 Real-time PCR primers

Primer name	**Length (bp)**	**Tm (˚C)**	**%GC**	**Sequence (5′-3′)**
PfDFR1_F_qPCR	20	54.3	50	GGACAGCAGAAGAATTTGCC
PfDFR1_R_qPCR	19	54.4	52.6	CGTTGGTTCTCCATCTCCA
60S ribo L18 F	21	53.1	42.9	ATTATCACATGGCCAATCACC
60S ribo L18 R	22	45.5	27.3	CAATCTCTTATCATCTGTTATT

2.2 Methods

2.2.1 Plasmid construction

2.2.1.1 Preparation of plasmid harbouring target DNA

A set of *E. coli* strain TOP10 harbouring pBluescript PfDFR1_FMN (aa28-aa260), pBluescript PfDFR1_FAD/NADPH (aa258-aa780), and pBluescript PfDFR1_FMN/FAD/NADPH (aa28-aa780) were obtained from Dr. Grazia Camarda. A small aliquot (~ 5 µl) of each glycerol stock was streaked on LB-agar plat containing 100 µg/ml ampicillin and incubated at 37 ˚C overnight. A single colony of each construct was pre-cultured in 5 ml LB broth containing 50 µg/ml ampicillin overnight at 37 ℃. The plasmid DNA was extracted from 5 ml of bacteria culture by QIAprep® Spin Miniprep Kit (QIAGEN).

2.2.1.2 Restriction enzyme digestion

The DNA was digested with appropriate restriction enzymes. The 40 µl reaction contained the appropriate amount plasmids (see restriction enzyme manuals), 1X CutSmart (NEB), 20 U of each restriction enzyme and deionized water up to 40 µl. The reaction was incubated at 37˚C for at least 2 h. The DNA fragments were separated by agarose gel-electrophoresis. The DNA bands without UV exposure were cut and purified from the gel by QIAquick Gel Extraction kit (QIAGEN).

2.2.1.3 Alkaline phosphatase treatment

To prevent recircularization during ligation, alkaline phosphatase (Promega or Fermentas) was used to dephosphorylate 5´-phosphate group from linearlised DNA. The digested vector was treated with 1 U of alkaline phosphatase at 37˚C for 15 min. The reaction was stopped by adding 1/6 volume of 6x Gel Loading Dye (NEB or Thermo Scientific) and immediately ran on the agarose gel.

2.2.1.4 Agarose gel electrophoresis

1% agarose gel was prepared by dissolving 1 g of agarose in 100 ml of 1x Tris-Borate EDTA buffer (89 mM Tris, 89 mM Boric acid, 2 mM EDTA, pH 8.3). The mixture was heated until the agarose completely dissolved. After the mixture became warm, 10 µl of 10,000x SYBR^{TM} Safe DNA gel strain (Invitrogen) was added into the mixture. The mixture was mixed thoroughly and poured into the gel casting tray. The gel comb was put immediately to the gel tray to set the loading wells. The gel was allowed to set at room temperature for 20 min. Then, the comb was removed. The samples were mixed with 6x Gel Loading Dye (NEB or Thermo Scientific). The samples and Gene Ruler 1 kb Plus DNA Ladder (Thermo Scientific) were loaded to the gel. The gel was run at 100 V in 1x Tris-Borate EDTA buffer for 45-60 min. The DNA fragments were visualised under UV light from the UV box or Gel Doc Imager (Bio-Rad).

2.2.1.5 Ligation of vector and insert fragments

T4 DNA ligase was used to ligate two DNA fragments together. The ligation reaction was performed in 20 µl containing the digested insert and vector in an appropriate molar ratio, 3 U of T4 DNA ligase (Fermentas), 1 µl of 10X Ligase Buffer, and water. In this study, the 3:1 ratio of insert to vector was used. Reactions of vector alone with and without ligase were used as control reactions. The reactions were incubated at 22˚C for 30 min before transformed into *E. coli* TOP10 strain.

2.2.1.6 Preparation of competent cells

A few microliters from the commercial stock of *E. coli* TOP10 strain was added to 5 ml of LB broth. The culture was grown overnight at 37˚C with shaking at 220 rpm. The overnight culture (0.5 ml) was inoculated in 50 ml fresh LB broth. The culture was grown at 37˚C with shaking at 220 rpm until the OD_{600} nm was reached 0.4. The culture was transferred to a new 50 ml tube and placed on ice for 20 min. The cells were harvested by centrifugation at 1,349x*g* for 10 min at 4˚C The packed cells were resuspended in 30 ml of ice-cold 0.1 M $CaCl_2$ and incubated on iced for 30 min. The cells were again harvested by centrifugation at 1,349x*g* for 10 min at 4˚C The cell pellet was resuspended in 2 ml ice-cold 0.1 M $CaCl_2$ with 15% glycerol. The cell suspension was divided into 50 µl aliquots and kept at -80˚C. All reagents used in the competent cell preparation were sterilized using 0.2 µm membrane filters.

2.2.1.7 Transformation of *E. coli* competent cells

An appropriated amount of ligation reaction (< 5 µl) or plasmid (<5 µl, 10pg – 100 ng) was mixed gently with 50 µl of the *E. coli* competent cells. The reaction was incubated on ice for 30 min. The reaction was heat shocked at 42°C for 90 s. Subsequently, the reaction tube was immediately chilled on ice for 2 min before adding 950 µl of LB broth. The transformation reaction was incubated at 37˚C with shaking at 220 rpm for 60 min. The cells were spread on the LB-Agar plate with selected antibiotic (50 µg/ml kanamycin for pETM-11 series, 20 µg/ml chloramphenicol for chaperone plasmids from TAKARA, 50 µg/ml ampicillin for pET15b series). Finally, the plate was incubated at 37˚C overnight.

2.2.1.8 Selection of positive clone and DNA sequencing

The positive clones were selected from colonies grown on LB-Agar plate with selected antibiotic/s. The plasmids were purified from the positive clone and the insertion of expected DNA fragment was confirmed by double digestion with restriction enzymes using in the plasmid construction. Then, the plasmids were sent for sequencing (Eurofins Scientific) to confirm that the sequence was correctly inserted. The PfDFR1 sequencing primers (Table 2.1) were used for the sequencing of the middle part of PfDFR1 gene. Finally, the plasmids with correct insertion sequence were transformed into *E. coli* strain BL21 (DE3) for the recombinant protein expression.

2.2.2 Expression of recombinant protein

The protein expression host (BL21(DE3)) containing each plasmid construct was pre-cultured in LB-broth containing selected antibiotic (50 μg/ml kanamycin for pETM-11 harbouring codon optimised PfDFR1 or 50 μg/ml ampicillin for pET15b harbouring PfDFR1). The pre-culture was incubated overnight at 37˚C with shaking at 220 rpm. Then, the pre-culture was inoculated to get 1% (v/v) of pre-culture in sterilised LB-broth with selected antibiotic. The culture was incubated at 37˚C with shaking at 220 rpm until the OD at 600 nm was reached 0.4-0.6.

For the induced expression of pETM-11 harbouring codon optimised PfDFR1 fragment, 1 M IPTG was added into the culture flask to get the chosen concentration (0.5 mM IPTG). The induced cells were incubated at 16˚C with shaking at 160 rpm overnight. The induced cells were harvested by centrifugation at 8,000x*g* for 10 min at 4 ˚C (BECKMAN Avanti^{TM} J-25). The induced cell pellet was transferred into the 50 ml tube before storing at -80˚C.

For leaking expression of pET15b harbouring PfDFR1 fragment, the IPTG inducer was not added to the culture. Riboflavin (Sigma), the source of FMN and FAD cofactors, was added to the culture flask in 5 mg/L. The cells were grown at 16˚C with shaking at 160 rpm for 24 h. Then, the cells were harvested and kept at -80˚C using the same method as above.

2.2.3 Purification of recombinant protein

2.2.3.1 Preparation of cell lysate

The cell pellet kept at -80˚C was thawed on ice and resuspended in the lysis buffer (100 mM Tris-HCl pH 7.0, 200 mM NaCl, 20 mM Imidazole, 10% glycerol) containing the cOmplete protease inhibitor (Roche). Sonication was carried out at 70% amplitude with the total time for 2 min using pulse on for 10 s and pulse off for 10 s. Sonication was finished when the suspension was clear. Whole cell extract was centrifuged at 34,750x*g* for 30 min at 4˚C (BECKMAN Avanti^{TM} J-25). The supernatant was collected for the next step of protein purification.

2.2.3.2 Ni-NTA affinity chromatography

The Ni-NTA media was resuspended to get the homogenous suspension. The slurry media was poured into a column in a single continuous motion to pack bead. The column was rinsed with 10 column volumes of DW followed by 10 column volumes of the lysis buffer (100 mM Tris-HCl pH 7.0, 200 mM NaCl, 20 mM Imidazole, 5 mM CHAPS, 10% glycerol) containing the cOmplete protease inhibitor (Roche). The cell lysate was prepared as described (section 2.2.3.1). The supernatant was loaded into a Ni-NTA column. Then, the column was washed with 40 column volumes of the wash buffer (100 mM Tris-HCl pH 7.0, 150 mM NaCl, 50 mM Imidazole, 10% glycerol). The protein was eluted by elution buffer (100 mM Tris-HCl pH 7.0, 25 mM NaCl, 300 mM Imidazole, 5 mM CHAPS, 10% glycerol).

2.2.3.3 Ion-exchanger chromatography

The SP-sepharose media was resuspended to get the homogenous suspension. The slurry media was poured into a column. The column was washed with 10 column volumes of DW followed by 10 column volumes of the start buffer (100 mM Tris-HCl pH 7.0, and 10% glycerol). The partial purified PfDFR1 from the Ni-NTA column was loaded into the SP-sepharose column. The column was washed with 20 column volumes of the start buffer, 15 column volumes of the wash buffer A (100 mM Tris-HCl pH 7.0, 100 mM NaCl, and 10% glycerol), 15 column volumes of the wash buffer B (100 mM Tris-HCl pH 7.0, 200 mM NaCl, and 10% glycerol), and 15 column volumes of the wash buffer C (100 mM Tris-HCl pH 7.0, 250 mM NaCl, and 10% glycerol), respectively. Then, the column was eluted with 5 column volumes of the elution buffer (100 mM Tris-HCl pH 7.0, 400 mM NaCl, 5 mM CHAPS, and 10% glycerol).

2.2.3.4 Histidine tag removal using thrombin protease

Eluted fractions from the SP-sepharose were pooled and measured protein concentration. Thrombin protease (GE-healthcare 27-0846-01) was added to the pooled PfDFR1 as a ratio of one unit to cleave 0.1 mg of PfDFR1 sample. The tube was incubated at 4 ˚C for over 16 h. Then, the thrombin treated sample was loaded into a Ni-NTA column. The flow through was collected and the column was washed with 5 column volumes of the lysis buffer. The flow through and wash fractions were pooled. Thrombin was removed from the pooled sample by incubating the sample with *p*-aminobenzamidine agarose resin at room temperature for 30 min. After incubation, the

sample was loaded into an entry column. The flow through was collected as histidine tag cleaved off PfDFR1.

2.2.3.5 Desalting of sample using PD10 column

Histidine tag cleaved off PfDFR1 was incubated with excess FMN and FAD for 30 min. Buffer exchange was performed by PD10 column with the exchange buffer containing 50 mM Tris-HCl pH 7.0, 100 mM NaCl, 5 mM CHAPS, and 10% glycerol. The PD10 column was equilibrated with 5 column volumes of the exchange buffer. Then, 2.5 ml of the protein sample was loaded into the column and the flow through was discarded. The column was eluted with 3.5 ml of the exchange buffer.

2.2.3.6 Concentration of the purified protein

The purified PfDFR1 was concentrated using Amicon Ultra Centrifugal Filter Unites (Millipore). The chosen molecular weight cut-off was depended on the protein size. The concentrator with 3 kDa cut-off was used for the partial purified PfDFR1_FMN. The partial purified PfDFR1_FAD/NADPH and PfDFR1 wt were concentrated using the concentrator with 30 kDa cut-off. After protein concentration, glycerol was added to the concentrated protein to get 40% glycerol. The purified protein was stored at -80˚C. Protein calculation was determined by Bradford assay.

2.2.4 Sodium dodecyl sulfate polyacrylamide gel electrophoresis (SDS-PAGE)

The SDS-PAGE gels were prepared. There are two parts of the SDS-PAGE gel, including the resolving gel and the stacking gel.

For two (8 cm x 12 cm x 0.75 mm) gels, 10 ml of 10% resolving gel solution was made using the reagents described in Table 2.3. Then, 50 µl of fresh 10% ammonium persulfate (APS) and 10 µl of TEMED were added to polymerise the resolving gel solution. The solution was immediately poured up to 2.5 cm below the top between the glass plates of the gel cassettes. The isopropanol or DW was gently added on the top to make the gel flat. The resolving gel was allowed to set at room temperature for 45 min. Then, the isopropanol was removed and washed out using distilled water.

The striking gel solution was prepared using the reagents described in Table 2.3. Then, 25 µl of fresh 10% APS and 10 µl of TEMED were added to polymerise the stacking gel solution. The isopropanol or DW was removed, and the stacking gel solution was poured on the top of the resolving gel. The gel comb was put immediately to the top of the gel cassettes to set the loading wells. The gel was left to set at room temperature for 30 min.

The gels were clamped into apparatus, and combs were removed. The chamber was filled with the 1X SDS-PAGE running buffer (25 mM Tris, 192 mM Glycine and 0.1% (w/v) SDS). The samples were prepared by mixing the protein sample with 2X Laemmli buffer. Then, the sample tubes were boiled at 95˚C for 10 min to denature the protein samples. The protein samples and protein marker were pipetted in to each well. For the 10-well gel, up to 25 µl of the denatured sample can be loaded into each well. For the 15-well gel, up to 10 µl of the denatured sample can be loaded into

each well. The gel running set was run at 80 V until the dry front moved to the resolving gel. Then, the voltage was increased to 150 V until the dry front run to the bottom of the gel.

Table 2.3 SDS-PAGE gel ingredients for two gels with 0.75 mm thickness

10% resolving gel (10 ml)		stacking gel	
Ingredient	Volume (ml)	Ingredient	Volume (ml)
30% Acrylamide bis	3.3	30% Acrylamide bis	0.45
1.5 M Tris-HCl pH 8.8	2.5	0.5 M Tris-HCl pH 6.8	0.85
H_2O	4.1	H_2O	2.05
10% SDS	0.1	10% SDS	0.035

2.2.5 Quantitation of protein concentration

The protein concentration was determined using the Bradford method. The working solution of protein assay reagent was prepared from Protein Assay Dry Reagent Concentrate (Bio-Rad) by diluting one part of concentrated reagent with four parts of distilled deionised (DDI) water. The bovine serum albumin (BSA) was used as a standard protein in the assay. Five dilutions of the BSA protein standard were prepared in that range 0.1 - 1 mg/ml. The assay was performed in a 96-well plate. 5 µl of each protein standard and sample solution was added into three separate wells. Then, 250 µl of the working solution of protein assay reagent was added into each well. The reagent and sample were mixed thoroughly by pipetting or using a plate mixer. The plate was incubated at room temperature for 5 min. Then, the absorbance at 595 nm was read

using a microplate reader. The standard curve was generated by plotting absorbance against protein concertation. The sample concentration was calculated using the equation from the standard curve in mg/ml unit.

2.2.6 Western blot analysis

The protein bands in the SDS-PAGE gel were transferred to a nitrocellulose membrane (Hybond ECL, GE-healthcare) at 350 mA for 75 min. The membrane was blocked for 1 hour in phosphate buffer saline (PBS) containing 5% non-fat dry milk. The membrane was washed three times with excess PBST (PBS containing 0.05% Tween 20) in 5 min each. Then, the membrane was incubated with optimal dilution of primary antibody in PBST for 2 h at room temperature. The membrane was washed three times for 5 min each with PBST before incubated with optimal dilution of secondary antibody for 1 h at room temperature. The membrane was again washed three times with PBST. The reactive bands were developed by ECL Western blotting substrate (Thermo Scientific); then, the membrane was blotted on a film.

2.2.7 Flavin content determination of PfDFR1 and hCPR

The protein samples were diluted to 0.1 mg/ml in the sample buffer (50 mM Tris pH 7, 100 mM NaCl, 5 mM CHAPS, and 10% glycerol). The protein samples were boiled for 5 min before centrifugation at 20,000x*g* for 5 min. 50 µl of supernatant was mixed with 150 µl of the sample buffer. Then, 50 µl of each protein sample was loaded into a mobile phase of 50 mM ammonium acetate; pH 4.5 with 15 % (v/v) acetonitrile

for separation on a 250 mm C18 column (Acclaim®120, Dionex) at 23 °C. The flavins were determined by measuring absorption and fluorescence (Ex: 450 nm, Em: 525 nm) of flow-through for 7 min. The measurements of FMN (Tokyo Chemical Industry) and FAD (Tokyo Chemical Industry) standard samples in the range 0 nM – 2,000 nM were performed as the same as the sample preparation method. Quantification of flavin content was determined by comparison of integration of the fluorescence peaks with standard FMN and FAD.

2.2.8 Diflavin reductase activity assay with cytochrome *c*

Diflavin reductase activity was determined by measuring the reduction rate of cytochrome *c* using a Cary 300 UV-Visible spectrophotometer at room temperature. The activity assay mixture contains protein sample, 50 μM NADPH, 50 μM cytochrome *c,* 0.3 M potassium phosphate buffer pH 7.7 in a total volume of 500 μl. The reaction was initiated by addition of NADPH. The absorbance change at 550 nm was measured for 2 min. Reduced cytochrome *c* amount was calculated using 21 $mM^{-1}cm^{-1}$ as an extinction coefficient.

2.2.9 Diflavin reductase activity assay with potassium ferricyanide

Diflavin reductase activity was measured based on the reduction of potassium ferricyanide. The change in absorbance at 420 nm was measured using a Cary 300 UV-Visible spectrophotometer at room temperature. The assay reaction contains protein sample, 50 mM NADPH, 1 mM potassium ferricyanide, 0.3 M potassium phosphate buffer pH 7.7 in a total volume of 500 μl. The reaction was initiated by adding

NADPH. The change in absorbance at 420 nm was measured for 2 min. The activity of enzyme was calculated using the extinction coefficient (1.02 $mM^{-1}cm^{-1}$) of reduced potassium ferricyanide.

2.2.10 Malaria parasite culture

The *P. falciparum* CBG and NF54 were cultured in RPMI 1640 medium supplemented with 25 mM HEPES, 50 μg/ml hypoxanthine, 0.25 mM $NaHCO_3$ and 28.5 μg/ml gentamicin and 10% heat-inactivated human serum. The culture was diluted to 0.5% mixed stages asexual parasites at 5% haematocrit in complete media. The culture flask was gassed with the gas mixed composed of 4% CO_2, 3% O_2, 93% N_2 to create microaerophilic environment. Then, the culture flask was transferred to a 37˚C incubator. Gimsa-stained thin blood smear of each culture flask was prepared every day to monitor the parasitaemia and parasite stages of the culture.

2.2.11 RNA extraction and cDNA synthesis

Total RNA was isolated from the parasite pellet using RNeasy Mini Kit (QIAGEN), following the manufacture's instruction. cDNA synthesis from RNA was performed using QuantiTect Reverse Transcription Kit (QIAGEN), following the manufacture's instruction.

2.2.12 Real-time PCR

The real-time PCR samples were run using the QuantiTech SYBR Green PCR Kit (QIAGEN) according to the manufacturer's instruction. Primer sequence and PCR condition were summarized in Table 2.4. The initial denaturation was performed at 95˚C for 15 min, followed by 50 cycles of 95˚C for 15 s, 57˚C for 30 s, and 72˚C for 30 s. The melting temperature of *PfDFR1* and the *60s* control were measured. The C_q was determined and used in double delta C_q method to compare the amount of *PfDFR1* in each parasite stage.

Table 2.4: Real-time PCR primers and conditions

PCR conditions	Primer name	Sequence
-95˚C 15 min -50 cycles of 94˚C 15 s, 57˚C 30 s, 72˚C 30 s	PfDFR1_F_qPCR	GGACAGCAGAAGAATTTGCC
	PfDFR1_R_qPCR	CGTTGGTTCTCCATCTCCA
-95˚C 15 min -50 cycles of 94˚C 15 s, 57˚C 30 s, 72˚C 30 s	60S ribo L18 F	ATTATCACATGGCCAATCACC
	60S ribo L18 R	CAATCTCTTATCATCTGTTATT

CHAPTER 3

CONSTRUCTION, EXPRESSION, AND PURIFICATION OF *PLASMODIUM FALCIPARUM* NADPH-DEPENDENT DIFLAVIN REDUCTASE I

3.1 Introduction

In 1950, NADPH-cytochrome P450 reductase (CPR) was initially identified as NADPH-cytochrome *c* reductase from pig liver [178]. Over the next six decades, CPR has been identified from many organisms, including *Rattus norvegicus* (rat) [211, 212], *Mus musculus* (mouse) [213], *Anopheles gambiae* [171], *Drosophila melanogaster* [214], *Arabidopsis thaliana* [215], *Saccharomyces cerevisiae* [216], and *Homo sapiens* (human) [182]. Human and rat CPRs are the most well characterised in terms of their biochemical and biophysical properties. However, little is known about CPR in *Plasmodium* species. Structure and function of *Plasmodium* CPR putative sequences have been described based on bioinformatics analysis. In *P. falciparum*, the PF3D7_0923200 has been predicted as a CPR candidate. Due to the lack of sequence-conserved cytochrome P450, we have called the PF3D7_0923200 as *Plasmodium falciparum* NADPH-dependent diflavin reductase I (PfDFR1) in this thesis. To date, experimental characterization of PfDFR1 have not been reported.

In early studies, the soluble CPR was prepared via protease treatment to remove the membrane anchor. The complete deletion of the N-terminus sequence loses the P450 reductase activity in the mammalian CPR, but the soluble CPR still has ability

to reduce cytochrome *c* [217, 218]. Then, solubilisation of microsomes using detergent was used to improve the CPR preparation. The detergent purified CPR is able to transfer electron to P450s [217, 219]. Since the heterologous expression system was developed in 1980s, a number of CPRs have been characterised. The expression systems are based on yeast, bacteria, insect, and mammalian cells [215, 220-223].

The heterologous expression of target proteins in bacteria remains the preferred method due to the high yield and low cost. Successfully cloned, expressed and purified of CPRs in the *Escherichia coli* expression system have been extensively described in several publications [171, 182, 221]. CPRs can be expressed in both the full-length CPR, or the N-terminus transmembrane truncated CPR in the *E. coli* expression system.

To achieve the goal of PfDFR1 characterisation, production of the functional PfDFR1 protein is the key factor. The primary aim of this chapter is to construct the expression vector for PfDFR1 heterologous expression in the *E. coli* system. The second aim is to produce the functional PfDFR1 protein to allow onward biochemical characterisation.

3.2 Methods

3.2.1 Plasmid construction

3.2.1.1 Codon optimised PfDFR1

A set of PfDFR1 expression plasmids was designed to express three different parts of PfDFR1 protein, including the FMN domain (PfDFR1_FMN; aa28-

aa260), the FAD/NADPH domains (PfDFR1_FAD/NADPH; aa258-aa780), and the FMN/FAD/NADPH domains (PfDFR1_FMN/FAD/NADPH; aa28-aa780). The PfDFR1 DNA sequence was modified with the optimal codon bias for protein expression in *E. coli*. The codon optimised PfDFR1 fragments that are available in our laboratory were amplified by PCR and inserted into pBluescript plasmids. The pBluescript plasmids carrying a series of codon optimised PfDFR1 genes were obtained from Dr. Grazia Camarda (LSTM) and used as templates for the PfDFR1 expression plasmid construction. A series of codon optimised PfDFR1 expression plasmids were inserted into pETM-11 between *Nco*I and *Xho*I restriction sites. The recombinant protein expressed from pETM-11 should have 6xHis tag and a TEV protease cleavage site at the N-terminus. The insertion was checked by double digestion with *Nco*I and *Xho*I restriction enzymes. The DNA sequence was confirmed by direct sequencing.

3.2.1.2 Transmembrane truncated PfDFR1

A pET15b harbouring the PfDFR1 DNA coding sequence amplified from *P. falciparum g*DNA (pET15b PfDFR1; aa48-aa780) was obtained from our collaborator. The sequencing result showed a non-synonymous mutation (D436G) in a non-conserved region between the FMN and FAD domains. From a pET15b PfDFR1 (D436G) map (Figure 3.1), the non-synonymous mutation occurs at position 1,358 changing GAT (Aspartic acid (D) codon) to GGT (Glycine (G) codon). Suitable restriction sites (*PstI* (1,642) and *NsiI* (1,315) sites) were identified to remove the mutated fragment. Wild-type fragment (synthesised by GenScript Company) was inserted into the same positions. Colony PCR was used to determine the presence or

absence of the synthesised fragment insertion in plasmid constructs. Correction orientation of the inserted fragment was confirmed by diagnostic digestion with *Pst*I and *Nsi*I and DNA sequencing.

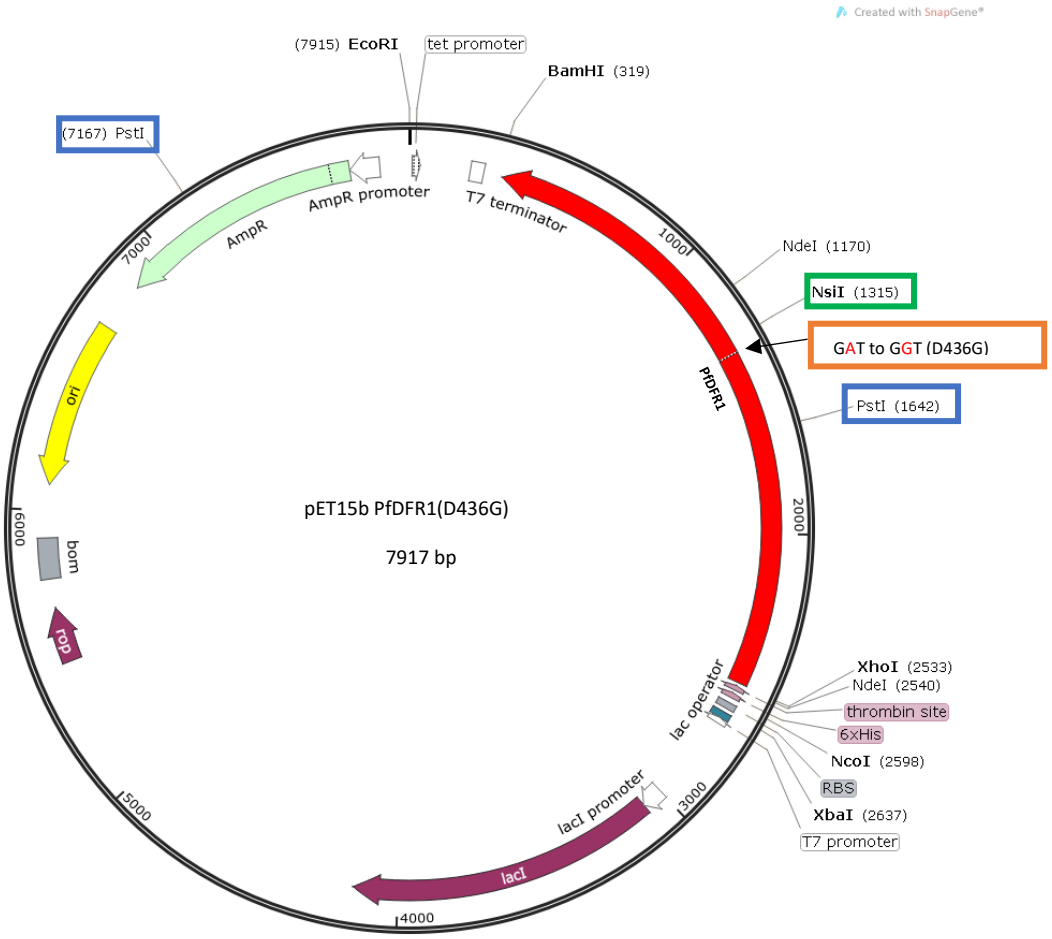

Figure 3.1. The pET15b PfCPR (D436G) map. The plasmid map was created by SnapGene Viewer software (GSL Biotech, available at snapgene.com). A non-synonymous (D436G) from GAT to GGT is shown in an orange box with black arrow. *PstI* restriction sites are highlighted in blue boxes. *NsiI* restriction site is in a green box.

3.2.2 Expression of PfDFR1 protein

Competent BL21(DE3) cells were transformed with pETM-11 PfDFR1_FMN, pETM-11 PfDFR1_FAD/NADPH, pETM-11 PfDFR1 FMN/FAD/NADPH, or pET15b PfDFR1 wt plasmids. The colonies were selected and grown as described in the general materials and methods (2.2.1.8). BL21(DE3) pETM-11 PfDFR1 series were cultured in LB broth containing 50 μg/ml kanamycin, and LB broth with 50 μg/ml ampicillin was used for BL21(DE3) pET15b PfDFR1 wt. The general protein expression was described in the general materials and methods (2.2.2).

3.2.3 Optimisation of PfDFR1 expression

3.2.3.1 Codon optimised PfDFR1

3.2.3.1.1 Co-expression with molecular chaperones

A set of chaperone plasmids from TAKARA (Figure 3.2, Table 3.1) were co-expressed with PfDFR1. The BL21(DE3) expression host was transformed with one of the molecular chaperone plasmids. The transformants were selected from LB agar plates containing 20 μg/ml chloramphenicol. The transformants with the chaperone plasmid were cultured in LB broth containing 20 μg/ml chloramphenicol and competent cells were prepared using the calcium chloride method. The competent cells were re-transformed with pETM-11 PfDFR1_FMN, pETM-11 PfDFR1_FAD/NADPH, or pETM-11 PfDFR1_FMN/FAD/ NADPH. The transformants were plated on LB-agar containing 20 μg/ml chloramphenicol and 50 μg/ml kanamycin.

The co-expression of the BL21(DE3) cells harbouring 2 kinds of plasmids were cultured in LB-broth containing 20 μg/ml chloramphenicol and 50 μg/ml kanamycin for plasmid selection and 0.5 mg/ml L-arabinose and/or 5 ng/ml tetracycline for chaperone expression. When the culture optical density (OD) at 600 nm reached 0.4 -0.6, IPTG was added at a final concentration of 1 mM. The induced expression bacteria were cultured at 37˚C for 3 h. The bacterial cells were harvested by centrifugation 8,000x*g* for 10 min at 4 ˚C (BECKMAN Avanti^{TM} J-25), and the packed cells were stored at -80˚C.

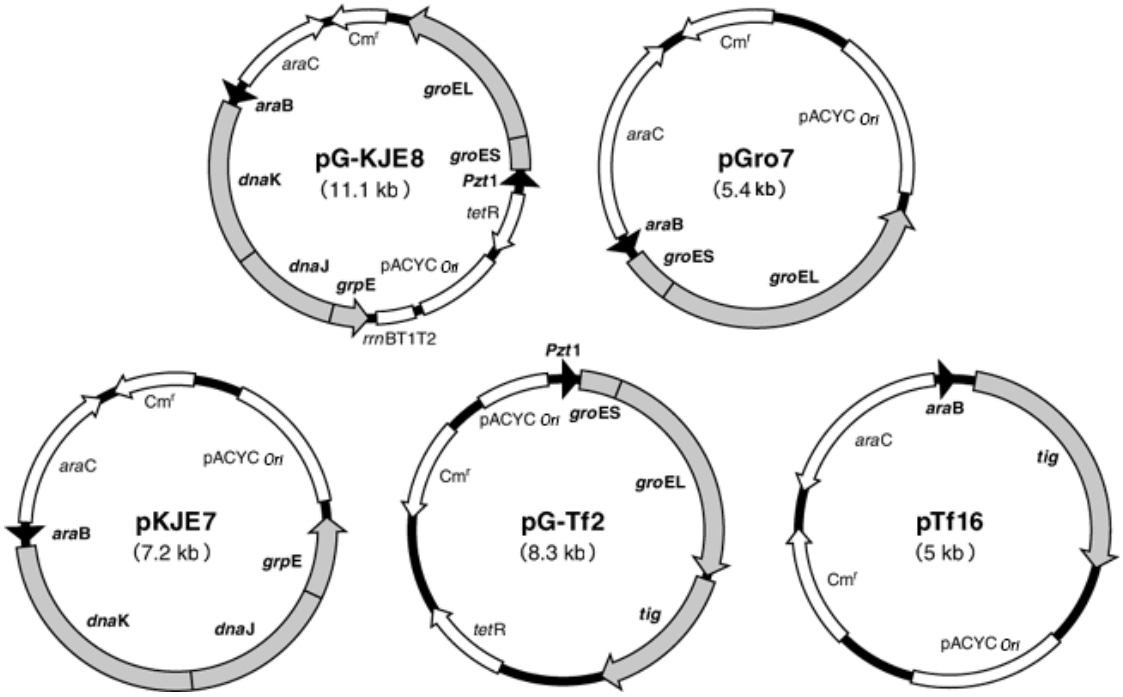

Figure 3.2 Molecular chaperone plasmid maps taken from TAKARA.

Table 3.1. Molecular chaperone plasmids

Plasmid	Inducer	Chaperone
pG-KJE8	L-arabinose Tetracycline	dnaK-dnaJ-grpE groES-groEL
pGro7	L-arabinose	groES-groEL
pKJE7	L-arabinose	dnaK-dnaJ-grpE
pG-Tf2	Tetracycline	groES-groEL tig
pTf16	L-arabinose	tig

Chaperone	Size (kDa)
GroEL	60
GroES	10
DnaK	70
DnaJ	40
Tf	56
GrpE	22

3.2.3.2 Truncated PfDFR1 protein

3.2.3.2.1 Optimisation of expression temperature

For temperature optimisation, protein expression was induced using 1 mM IPTG at a range of different temperatures. Protein expression was performed at 16˚C, 25˚C, and 37˚C for 24 h, 18 h, and 2 h, respectively. Bacterial cells were harvested and stored at -80˚C as described in 3.2.3.1.1.

3.2.3.2.2 Optimisation of inducer concentration

The expression temperature was fixed at 16˚C and various IPTG concentrations were tested. Five concentrations of IPTG (0.01 mM, 0.05 mM, 0.1 mM,

0.5 mM, and 1 mM) were used in the experiment with an uninduced control. After induced expression for 24 h, the bacteria cells were harvested and stored at -80˚C as described in 3.2.3.1.1.

3.2.3.2.3 Optimisation of culture media

The BL21(DE3) harbouring pET15b PfDFR1 wt sequence was cultured in 6 kinds of bacteria culture media. The liquid media used in this experiment were LB broth, 2YT broth, terrific broth, auto-induction LB broth, auto-induction 2YT broth, and auto-induction terrific broth. The bacteria were cultured in each kind of medium containing 50 μg/ml ampicillin. When the OD at 600 nm was 0.4 - 0.6, 5 mg/L riboflavin (a source of flavin cofactors) was added to the culture. The protein was expressed at 16˚C for 24 h. Then, the cells were harvested and kept at -80˚C as described in 3.2.3.1.1.

3.2.4 Preparation of cell lysate and protein solubility analysis

The cell lysate was prepared as described in the general methods section 2.2.3.1. The supernatants containing soluble proteins were collected. Aliquots of soluble proteins were electrophoresed in a 10% (w/v) sodium-dodecyl-sulphate (SDS) polyacrylamide gel. Protein bands were visualised by staining the SDS-PAGE gel with InstantBlue™ (Expedeon) for 15 min.

The Western blot with anti-6xHis antibody was performed as described in the general materials and methods section 2.2.6. The primary antibody (monoclonal mouse anti-6X His tag antibody from Thermo Scientific) recognising the 6xHis-tag was

prepared at 1:3,000 dilution in PBST. The secondary antibody (anti-mouse IgG-peroxidase from Sigma) was used at 1:10,000 dilution. The signals were developed as described in the general methods section 2.2.6.

3.2.5 Optimization of lysis buffer for PfDFR1 solubility

The lysis buffers used in this experiment are shown in Table 3.2. Bacteria cells were cultured, and expression induced as described. Cell lysates were prepared as described in different lysis buffers. After protein gel electrophoresis, the SDS-PAGE gel was stained with InstantBlue^{TM} (Expedeon) for 15 min. Then, the protein bands were analysed.

3.2.6 Purification of PfDFR1 protein

The PfDFR1 protein was purified as described in the general materials and methods section (2.2.3). In brief, the PfDFR1 protein was purified using a Ni-NTA affinity column (QIAGEN) followed by a SP-FF cation exchanger column (GE healthcare). The His-tag was removed from the protein by thrombin cleavage (see section 2.2.3.4). Then protein samples were incubated with excess FMN and FAD. Finally, buffer exchange was performed using PD-10 (50 mM Tris pH 7.0, 100 mM NaCl, 5 mM CHAPS, and 10% glycerol).

Table 3.2 The solubility screening buffers

Number	Buffer
1	100 mM Tris pH 7.5, 200 mM NaCl, 1 mM DTT, 1 mM PMSF, 10% glycerol
2	100 mM Tris pH 7.5, 200 mM NaCl, 5 mM EDTA, 0.1% Triton X-100, 1 mM DTT, 1 mM PMSF, 10% glycerol
3	100 mM Tris pH 7.5, 200 mM NaCl, 1% CHAPS, 1 mM EDTA, 1 mM DTT, 1 mM PMSF, 10% glycerol
4	100 mM Tris pH 7.5, 200 mM NaCl, 8 M urea, 1 mM DTT, 1 mM PMSF, 10% glycerol
5	100 mM Tris pH 7.5, 200 mM NaCl, 5 mM EDTA, 1% Triton X-100, 1 mM DTT, 1 mM PMSF, 10% glycerol
6	100 mM Tris pH 7.5, 200 mM NaCl, 2.5% CHAPS, 1 mM EDTA, 1 mM DTT, 1 mM PMSF, 10% glycerol
7	100 mM Tris pH 7.5, 200 mM NaCl, 1M urea, 1 mM DTT, 1 mM PMSF, 10% glycerol
8	100 mM Tris pH 7.5, 200 mM NaCl, 4 M urea, 1 mM DTT, 1 mM PMSF, 10% glycerol
9	100 mM HEPES pH 7.5, 200 mM NaCl, 1 mM DTT, 1 mM PMSF, 10% glycerol
10	100 mM HEPES pH 7.5, 200 mM NaCl, 2.5% CHAPS, 1 mM EDTA, 1 mM DTT, 1 mM PMSF, 10% glycerol
11	100 mM sodium phosphate pH 7.5, 200 mM NaCl, 1 mM DTT, 1 mM PMSF, 10% glycerol
12	100 mM sodium phosphate pH 7.5, 200 mM NaCl, 2.5% CHAPS, 1 mM EDTA, 1 mM DTT, 1 mM PMSF, 10% glycerol
13	100 mM Tris pH 7.5, 200 mM NaCl, 5 M urea, 1 mM DTT, 1 mM PMSF, 10% glycerol
14	100 mM Tris pH 7.5, 200 mM NaCl, 6 M urea, 1 mM DTT, 1 mM PMSF, 10% glycerol
15	100 mM Tris pH 7.5, 200 mM NaCl, 7 M urea, 1 mM DTT, 1 mM PMSF, 10% glycerol

3.2.7 PfDFR1 activity assay

PfDFR1 activity was determined by measuring the production of reduced cytochrome *c* at 550 nm using a Cary 300 UV-Visible spectrophotometer as described in the methods section 2.2.8. 30 pmol of purified PfDFR1 protein was used in the assay reaction while the cytochrome *c* and NADPH were fixed at 50 µM.

3.3 Results

3.3.1 Sequence analysis of the PfDFR1 gene

In 2014, two sequences were annotated as *Plasmodium falciparum* NADPH-cytochrome P450 reductase (CPR) putative sequences form different databases (PlasmoDB and NCBI). The first one is Gene ID PF3D7_0923200 in PlasmDB. The second is Gene ID 812060 in the NCBI database (PF3D7_1450300 in PlasmoDB). Both have a function prediction as NADPH—hemoprotein reductase. PF3D7_0923200 (previously ID PFI1140W) is now annotated as a putative nitric oxide synthase (NOS) in PlasmoDB. However, its function was predicted as an NADPH-cytochrome P450 reductase in the past 3 years. PF3D7_1450300 is now called NADPH-cytochrome P450 reductase putative in PlasmoDB. Both PF3D7_0923200 and PF3D7_1450300 are upregulated in mature gametocyte stage [224] and are reported as an essential gene in *P. falciparum* [208].

The alignment results show that PF3D7_0923200 has higher percent identity to known CPR proteins than PF3D7_1450300 (Figure 3.3, Table 3.3). PF3D7_0923200 also has more conserved key residues (Figure 3.3 highlight in yellow) for FMN, FAD, and NADPH binding than PF3D7_1450300. The alignment results with known NOSs show that PF3D7_0923200 has higher percent identity to known NOS proteins than PF3D7_1450300 (Appendix 3.1, Table 3.4). The percent identity of PF3D7_0923200 to known CPR protein is higher than the percent identity to known NOS proteins. Predicted three-dimensional modelling of the candidates using Phyre^2 server shows that both candidate sequences are homologous with yeast CPR (PEB;

2BPO) with 100 % confidence (Figure 3.4). However, the percent coverage of PF3D7_0923200 (80%) is better than PF3D7_1450300 coverage (68%).

After searching for a mitochondrial targeting peptide and subcellular localisation using TargetP 1.1 server [225] and WoLF PSORT Prediction server [226], only PF3D7_0923200 was predicted to locate in mitochondria (Table 3.5 and 3.6). That prediction agrees with previous reports on the target organelle of antimalarial primaquine. Taken together, PF3D7_0923200 sequence was chosen for recombinant protein production and biochemical characterisation.

Table 3.3 Amino acid identity between PfCPR candidates and known NADPH-cytochrome P450 reductase

NADPH-cytochrome P450 reductase	% Identity with PF3D7_0923200	% Identity with PF3D7_1450300
PF3D7_0923200	100.00	23.60
PF3D7_1450300	23.60	100.00
S. cerevisiae	23.25	16.69
R. norvegicus	27.49	17.84
H. sapiens	27.65	17.64
A. gambiae	26.34	17.01
D. melanogaster	28.16	16.70

Table 3.4 Amino acid identity between PfCPR candidates and known nitric oxide synthases

NADPH-cytochrome P450 reductase	% Identity with PF3D7_0923200	% Identity with PF3D7_1450300
PF3D7_0923200	100.00	23.60
PF3D7_1450300	23.60	100.00
***M. musculus* iNOS**	21.86	16.06
***R. norvegicus* eNOS**	19.22	15.87
***H. sapiens* eNOS**	19.22	15.87
***A. stephensi* NOS**	21.58	18.43
***D. melanogaster* NOS**	23.14	16.72

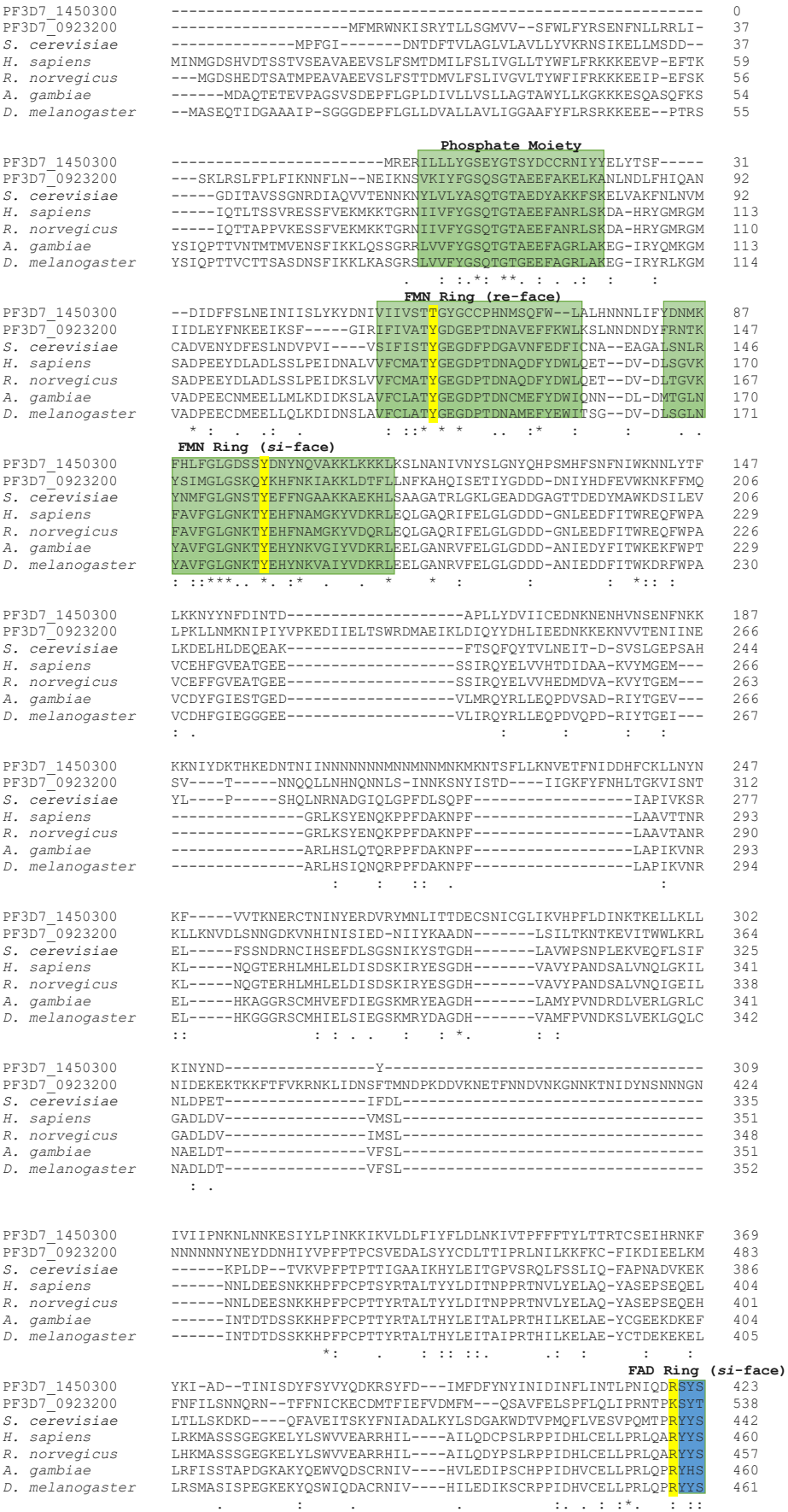
Phosphate Moiety
FMN Ring (re-face)
FMN Ring (si-face)
FAD Ring (si-face)

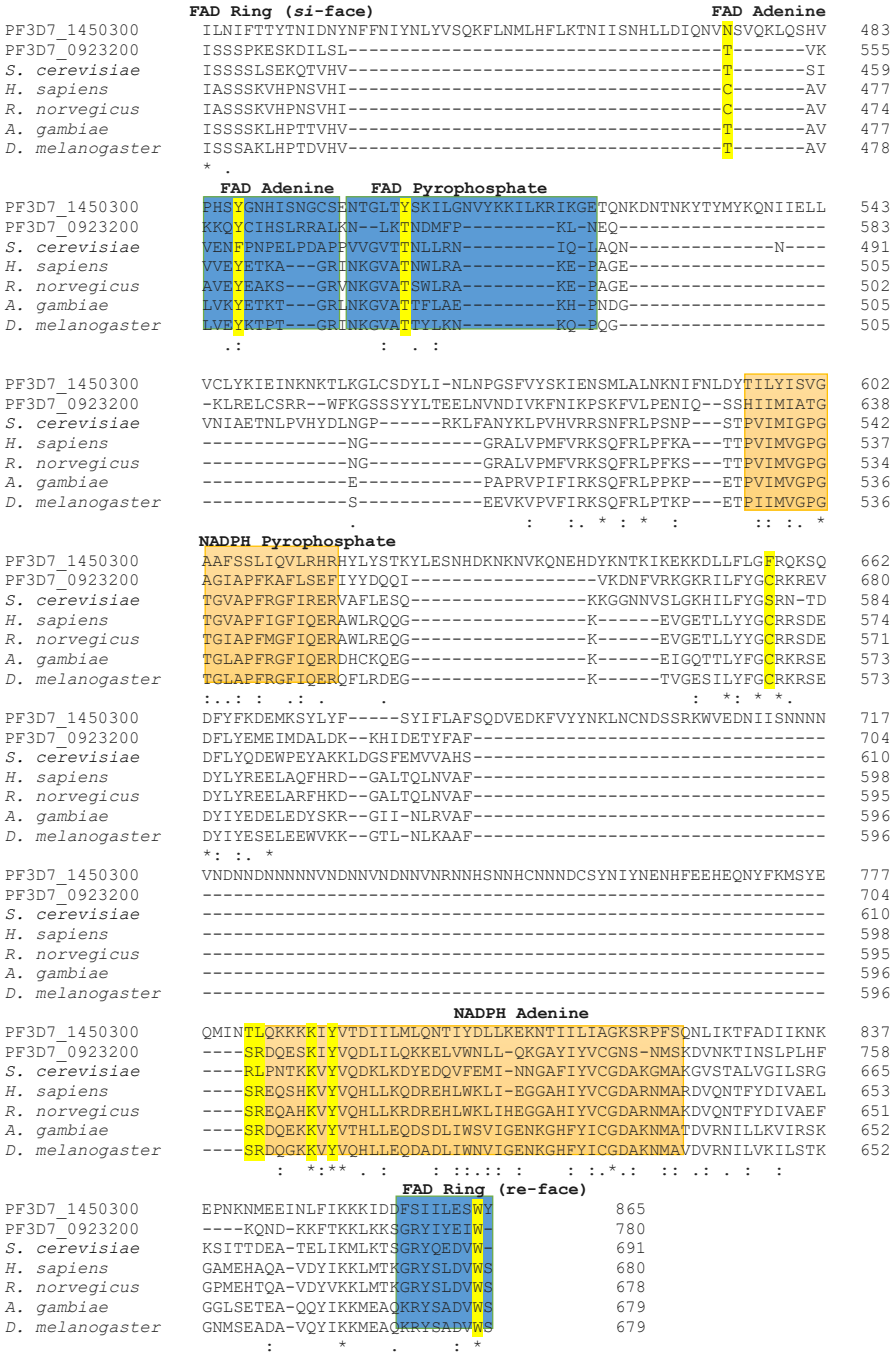

Figure 3.3. CPR amino acid sequence alignment. *P. falciparum* PF3D7_1450300, *P. falciparum* PF3D7_0923200, *S. cerevisiae* (ONH80480.1), *R. norvegicus* (NP_113764.1), *H. sapiens* (NP_000932.3), *A. gambiae* (AAO24765.1) and *D. melanogaster* (NP_477158.1). Th sequences were aligned by Clustal Omega. Cofactor binding sites are defined by Wang *et al*. FMN binding regions are shown in green boxes. FAD and NADPH binding regions are represented by blue boxes and orange boxes, respectively. The key residues for FMN, FAD, and NADPH binding are highlight in yellow.

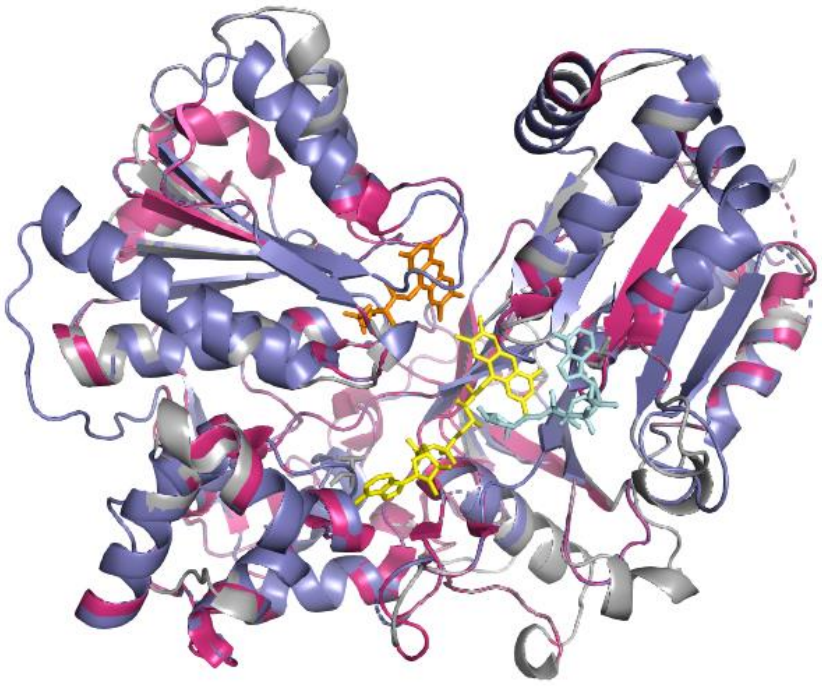

Figure 3.4 Three-dimensional models of predicted *P. falciparum* CPR candidates aligned with yeast CPR. *P. falciparum* PF3D7_1450300 model is shown in slate. *P. falciparum* PF3D7_0923200 model is shown in grey. Yeast CPR (PEB; 2BPO) is shown in pink. FMN, FAD, and NAP are shown in orange, yellow, and cyan, respectively. The 3D models of *P. falciparum* CPR candidates were predicted using Phyre[2].

Table 3.5 Prediction of mitochondrial targeting peptide of predicted *P. falciparum* CPR putative sequences using TargetP 1.1

Name	Length	mTP	SP	other	Loc
PF3D7_0923200	780	0.796	0.328	0.014	M
PF3D7_1450300	865	0.085	0.162	0.835	_

C : Chloroplast, i.e. the sequence contains **cTP**, a chloroplast transit peptide

M: Mitochondrion, i.e. the sequence contains **mTP**, a mitochondrial targeting peptide

S : Secretory pathway, i.e. the sequence contains **SP**, a signal peptide

_ : Any other location.

Table 3.6 Prediction of subcellular localisation of predicted *P. falciparum* CPR putative sequences using WoLF PSORT Prediction

WoLF PSORT converts a protein's amino acid sequences into numerical localization features; based on sorting signals, amino acid composition and functional motifs. The prediction is predicted from a k-nearest neighbour classifier after conversion.

Name	Length	Mito	Nucl	Nucl-Cyto	Cyto	Pero
PF3D7_0923200	780	12	7	-	5	2
PF3D7_1450300	865	2	17.5	10.5	2.5	-

Mito: mitochondrial

Nucl: Nuclear

Nucl-Cyto: Nuclear and cytoplasmic

Cyo: Cytoplasmic

Pero: Peroxisome

3.3.2 Cloning of codon optimised PfDFR1

To construct the codon optimised PfDFR1 expression plasmids, a series of codon optimised PfDFR1 fragments were subcloned into the pETM-11 expression vector. The plasmid maps are shown in figure 3.5 A. The insertion of target DNA was checked by double digestion with *Nco*I and *Xho*I (Figure 3.5 B). The DNA sequence was confirmed by direct sequencing.

3.3.3 Expression of codon optimized PfDFR1

E. coli BL21(DE3) harbouring the expression plasmid (pETM-11 PfDFR1_FMN, pETM-11 PfDFR1_FAD/NADPH, or pETM-11 PfDFR1_ FMN/FAD/NADPH) was cultured and induced expression was initiated by 1 mM IPTG for 24 h at 16˚C. The resulting protein overexpression was analysed by SDS-PAGE (Figure 3.6 A). Western Blot analysis was performed with a mouse anti-His antibody to confirm the expression of recombinant proteins with 6xHis tag (Figure 3.6 B). The result showed overexpression of the expected PfDFR1_FMN, PfDFR1_FAD/NADPH and PfDFR1_FMN/FAD/NADPH at 31 kDa, 64 kDa, and 92 kDa, respectively. Most of PfDFR1 proteins were expressed in insoluble form. Protein truncation bands of all PfDFR1 constructs appear in the blotting film.

A

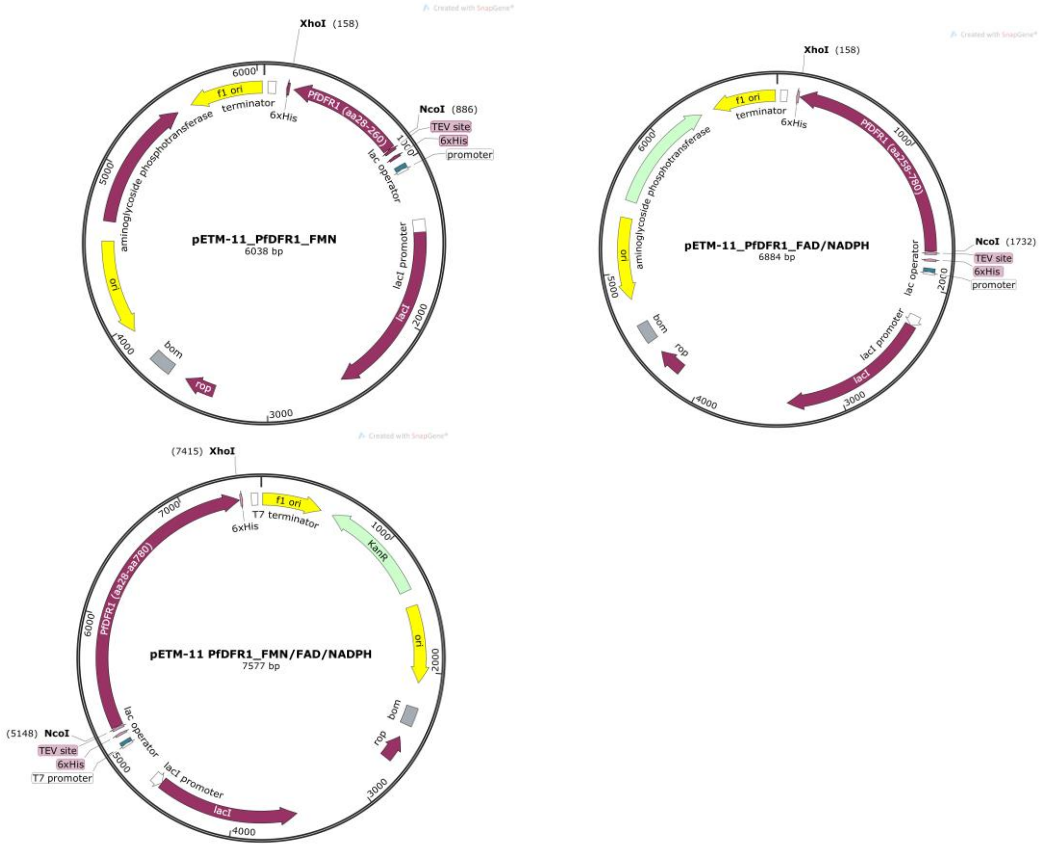

B

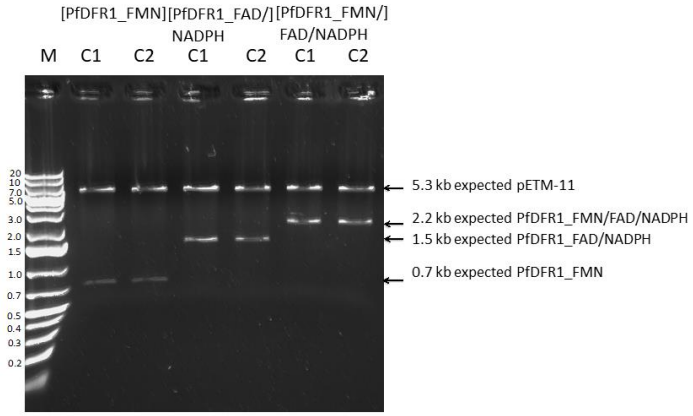

Figure 3.5 PfDFR1 plasmid construction and digestion analysis of pETM-11 containing PfDFR1. A) Plasmid maps for codon optimised PfDFR1 plasmid construction. B) The insertion of each *PfDFR1* fragment in 2 random colonies was checked by restriction enzyme digestion with *Nco*I and *Xho*I. Lane M is 100 ng/µL DNA ladder. C1 and C2 are colony 1 and 2, respectively. Samples were run on 0.8% agarose gel in 0.5x TBS buffer at 90 volts for 40 min.

A **B**

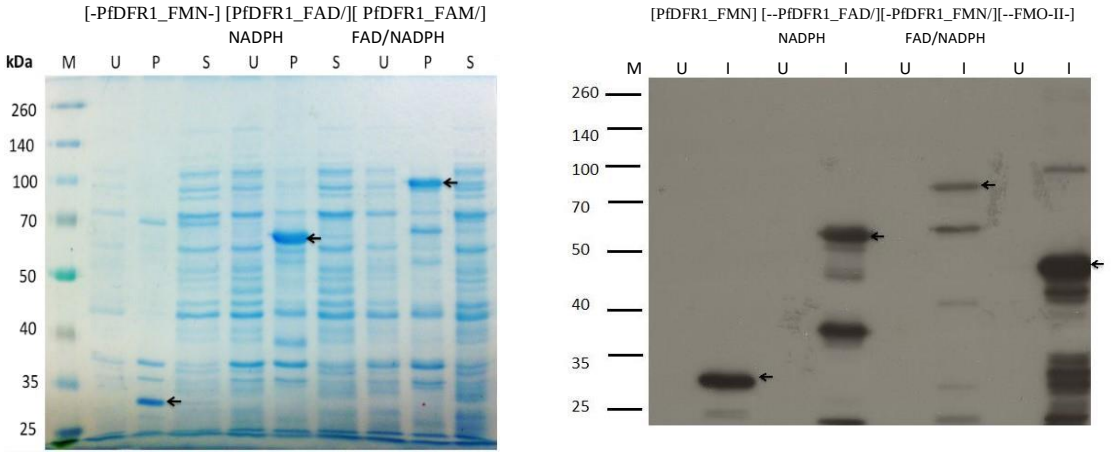

Figure 3.6 Expression and Western Blot with anti-His antibody of PfDFR1 constructs. A) SDS-PAGE of the PfDFR1 expression at 16˚C. B) Western Blot film of PfDFR1 and positive control FMO-2. M: protein marker; U: uninduced; I: induced; P: induced pellet; S: induced supernatant. Black arrow: bands corresponding to the expected size of each recombinant protein band.

3.3.4 Improving the solubility of codon optimised PfCPR

3.3.4.1 Buffer optimisation for PfDFR1 solubility

To solve the solubility problem, we screened different buffers. As predicted the pI of PfDFR1_FMN, PfDFR1_FAD/NADPH, and PfDFR1_FMN/FAD/NADPH are 6.1, 9.0, and 8.8, respectively, therefore pH 7.5 was selected for the preparation of the three PfDFR1 recombinant proteins to avoid precipitation. The solubility of PfDFR1_FMN/FAD/NADPH was tested in 15 different buffers and additives (Table 3.2) for the best buffer selection. The PfDFR1 was soluble in the buffers containing more than 6 M urea, namely buffers 4, 14, and 15 (Figure 3.7).

A

PfDFR1_FMN/FAD/NADPH

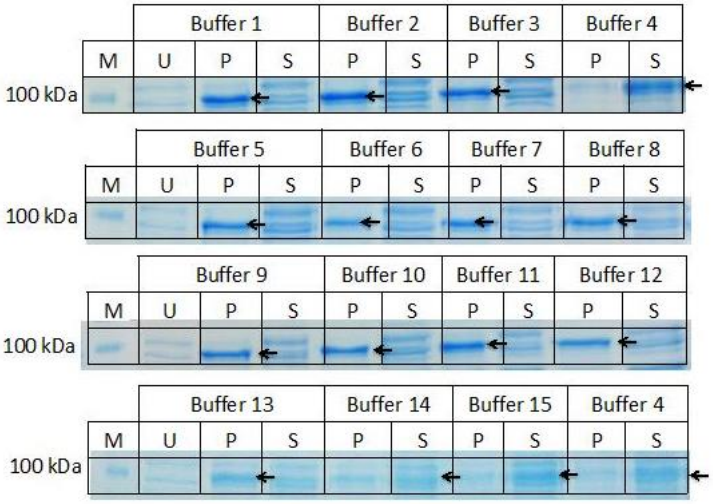

B

PfDFR1_FMN

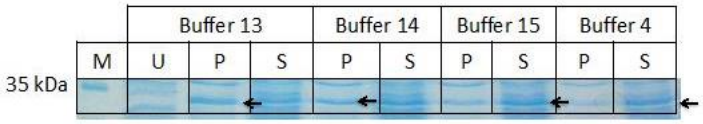

PfDFR1_FAD/NADPH

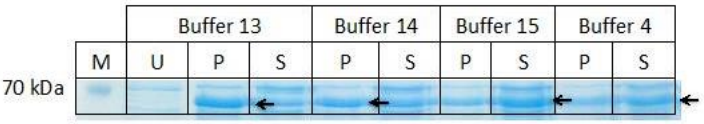

Figure 3.7 PfDFR1 solubility screening in 15 buffer conditions. InstantBlue™ staining of protein fractions from bacterial cultures after SDS-PAGE. M: Protein marker; U: uninduced; P: induced pellet; S: induced supernatant. A) PfDFR1_FMN/FAD/NADPH (92 kDa) in 15 different lysis buffers. B) PfDFR1_FMN (31 kDa) and PfDFR1_FAD/NADPH (64 kDa) in lysis buffers containing 5 to 8 M urea. Black arrow: bands corresponding to the expected size of each recombinant protein band.

3.3.4.2 Co-expression of PfDFR1 with molecular chaperones

Five molecular chaperone plasmids (Table 3.1) were co-expressed with PfDFR1. The InstantBlue staining of SDS-PAGE gels shows that the solubility of PfDFR1_FMN and PfDFR1_FMN/FAD/NADPH increased in co-expression with pG-KJE8, pKJE7, and pTF16 (Figure 3.8A, 3.8C). The pKJE7 chaperones tested improved the soluble expression of PfDFR1_FAD/NADPH (Figure 3.8B). The western blot result confirmed that pG-KGE8 and pKJE7 improved the production of PfDFR1_FMN and PfDFR1_FAD/NADPH soluble proteins, while leaving unaffected PfDFR1_FMN/ FAD/NADPH solubility (Figure 3.9).

A

PfDFR1_FMN

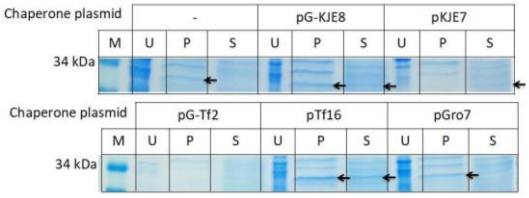

B

PfDFR1_FAD/NADPH

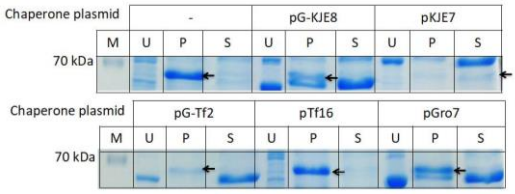

C

PfDFR1_FMN/FAD/NADPH

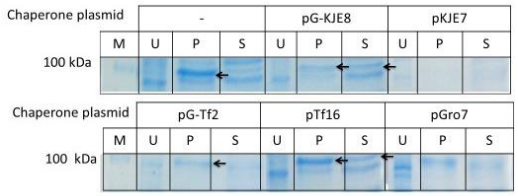

Figure 3.8 Co-expression of PfDFR1 with molecular chaperones. A) PfDFR1_FMN co-expression with five molecular chaperone plasmids. B) PfDFR1_FAD/NADPH co-expression with five molecular chaperone plasmids. C) PfDFR1_FMN/FAD/NADPH co-expression with five molecular chaperone plasmids. M: Protein marker; U: uninduced; P: induced pellet; S: induced supernatant; Black arrow: bands corresponding to the expected size of each recombinant protein band.

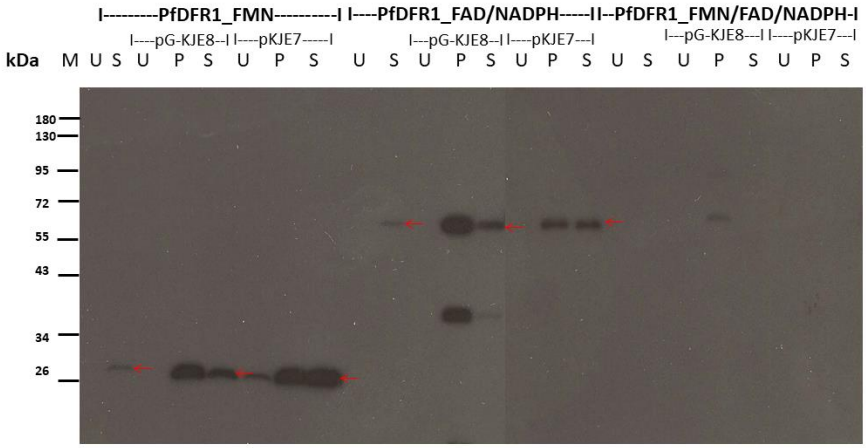

Figure 3.9 Western blot analysis of PfDFR1 co-expression with pG-KJE8 and pKJE7 molecular chaperone plasmids. M: Protein marker; U: uninduced; P: induced pellet; S: induced supernatant; Red arrow: bands corresponding to the expected size of each recombinant protein band.

3.3.5 Purification of codon optimised PfDFR1

3.3.5.1 Purification of codon optimised PfDFR1 in native conditions

PfDFR1_FMN and PfDFR1_FAD/NADPH co-expressed with pKJE7 were scaled up. Proteins were purified via a Ni-NTA column under native conditions (Figure 3.10). PfDFR1_FMN (31 kDa) and PfDFR1_FAD/NADPH (64 kDa) were eluted in the elution fractions. However, molecular chaperones (DnaK (70 kDa) and DnaJ (40 kDa)) were clearly detected as contaminants (Figure 3.10).

Because substrate binding and release in chaperones are related to their ATPase activity, 5 mM Mg-ATP was added in the wash buffer to eliminate contaminant chaperones. Although the Ni-NTA resin bound with the PfDFR1_FMN was washed

with over 80 column volumes of wash buffer containing 5 Mg-ATP, the contaminant chaperones were not removed from the elution fractions (Figure 3.11).

3.3.5.2 Purification of codon optimised PfDFR1 in denaturing condition

Based on the contaminant problem of partially purified PfDFR1_FMN and PfDFR1_FAD/NADPH from co-expression with molecular chaperones, the proteins were purified under denaturing condition and used for polyclonal antibody production. Lysis buffer containing 8 M urea and wash buffer containing 4 M urea were used in the protein purification via a Ni-NTA column. The purification results are shown in Figure 3.12. From the band intensity calculation, PfDFR1_FMN and PfDFR1_FAD/NADPH had 50% and 30% purity, respectively. The partially purified protein was run on SDS-PAGE gel in a large single well. The expected bands of PfDFR1_FMN and PfDFR1_FAD/NADPH were cut and sent to the Metabolomics & Proteomics Lab (Department of Biology, University of York, UK) for mass spectrometry-based protein identification. The protein identification results confirmed that all sample bands were PfDFR1 (Gene ID: PF3D7_0923200) with correct matching domain regions (Appendix 3.2 and 3.3). The partial purified protein was run on SDS-PAGE gel in a large single well. The expected bands of PfDFR1_FMN and PfDFR1_FAD/NADPH were cut and sent Davids Biotechnologie for antibody production.

A

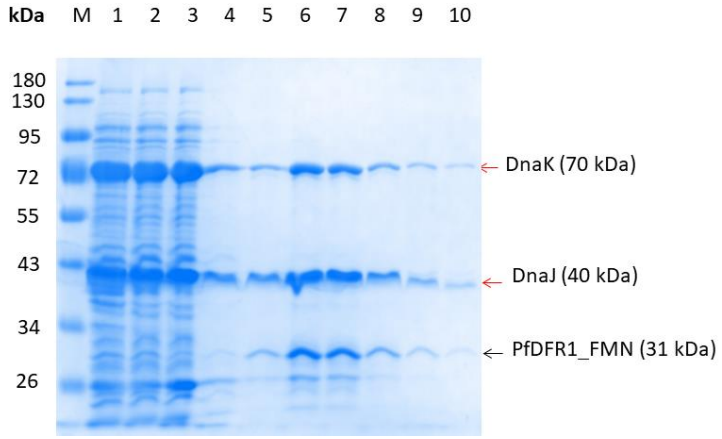

B

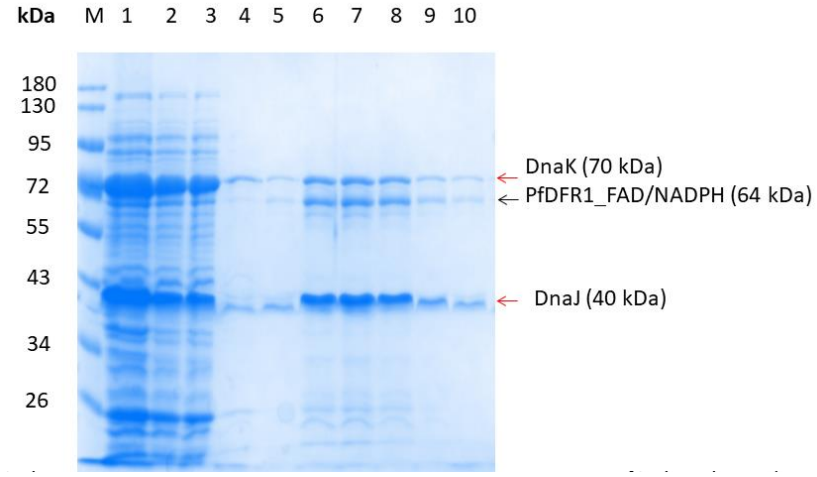

Figure 3.10 PfDFR1_FMN and PfDFR1_FAD/NADPH purification under native condition. A) SDS-PAGE gel of PfDFR1_FMN purification. B) SDS-PAGE gel of PfDFR1_FAD/NADPH purification. M: Protein marker; 1: whole cell lysate; 2: supernatant; 3: Flow-through: 4: wash fraction; 5-10: elution fractions; Black arrow: PfDFR1_FAD/NADPH; Red arrow: chaperone bands.

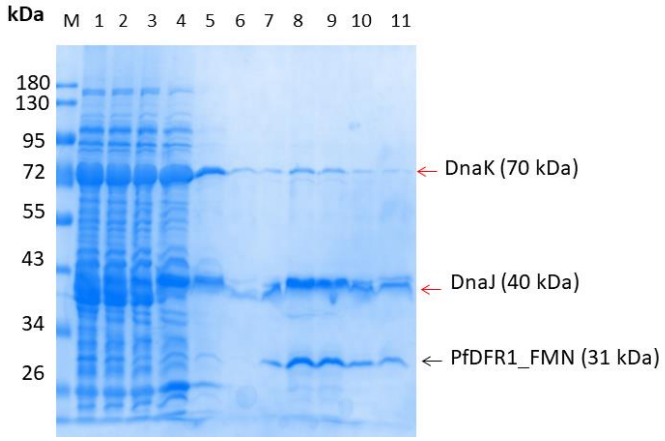

Figure 3.11 PfDFR1_FMN purification under native condition with 5 mM Mg-ATP in wash buffer. M: protein marker; 1: whole cell lysate; 2: supernatant; 3: Flow-through; 4-5: wash fractions with 10 column volumes wash buffer with 5 mM Mg-ATP; 6; wash fraction with 60 column volumes wash buffer with 5 mM Mg-ATP; 7-11: elution fractions; Black arrow: PfDFR1_FMN; Red arrow: chaperone bands.

A **B**

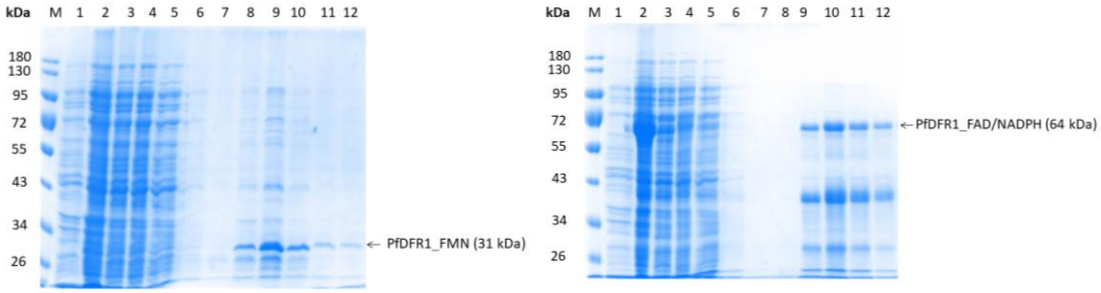

Figure 3.12 PfDFR1_FMN and PfDFR1_FAD/NADPH purification under denaturing condition. A) SDS-PAGE gel of PfDFR1_FMN purification. B) SDS-PAGE gel of PfDFR1_FAD/NADPH purification. M: Protein marker; 1: uninduced; 2: whole cell lysate; 3: supernatant; 4: Flow-through; 5-7: wash fractions; 8-12: elution fractions; Black arrow: PfDFR1.

3.3.6 Molecular cloning of PfDFR1 wt

Based on an expression problem of PfDFR1_FMN/FAD/NADPH, we tried an alternative way to produce functional PfDFR1. pET15b harbouring PfDFR1 coding sequence (originally cloned from *P. falciparum g*DNA) was generated. A non-synonymous mutation (D436G) was found later in a non-conserved region between FMN and FAD domains. To fix the error, a PfDFR1 wt DNA sequence was designed to replace the *Pst*I - *Nsi*I (333 bp) fragment containing the mutation (Figure 3.1).

There are two *Pst*I restriction sites and the completely digest both *Pst*I makes the cloning challenging. Therefore, the double-digested plasmids (Figure 3.13) were prepared by *Nsi*I (NEB: R0127S) digestion (10 units/50 µl reaction) at 37˚C for 45 min. Then, the partial digestion of *Pst*I was performed by digesting *Nsi*I-digested plasmid with 6 units of *Pst*I (NEB: R0140S) on ice for 3 min. The double-digested plasmid with partial *Pst*I digestion in size 7.6 kb was used in the PfDFR1 wt plasmid construction.

However, the overhang sequences after digestion with *Pst*I and *Nsi*I are the same (Figure 3.14A). Double digestion with these enzymes allows self-ligation of digested plasmid. Synthesized fragments can ligate together and lead to more than one copy of synthesized fragment in the ligated plasmid (Figure 3.14B). We screened a number of positive colonies by colony PCR (Figure 3.14C). Self-ligation occurred in colonies C1, C2, and C8. Colonies C3, C4, C6, and C7 had a single insertion of the synthesized fragment. Plasmids harbouring one copy of insert fragment were digested with *Pst*I and *Nsi*I to determine insert orientation (Figure 3.14D). As shown in Figure 3.14B, plasmids with the wrong insertion direction cannot cleave with *Pst*I and *Nsi*I at

the insertion site. Only plasmids extracted from the colony C4 have correct insertion direction. The plasmid with correct insertion direction was confirmed by direct sequencing. The DNA sequences were translated in silico using ExPASy Translate software and the protein sequence obtained compared with PF3D7_0923200 using Clustal Omega (Figure 3.15).

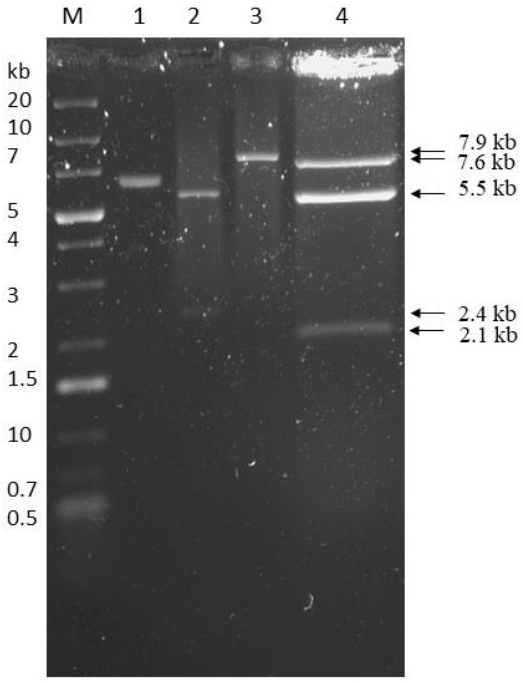

Figure 3.13 Preparation of double-digested destination plasmid for PfDFR1 wt construction. 1: uncut plasmid; 2: *Pst*I digested plasmid (has two fragments in size 5.5 kb and 2.4 kb); 3: *Nsi*I digested plasmid (has one fragment in size 7.9 kb); 4: *Pst*I and *Nsi*I double-digested plasmid. The double-digested plasmid with partial *Pst*I digestion is 7.6 kb fragment. The completely double-digested plasmid has 3 fragments in size 5.5 kb, 2.1 kb and 0.3 kb.

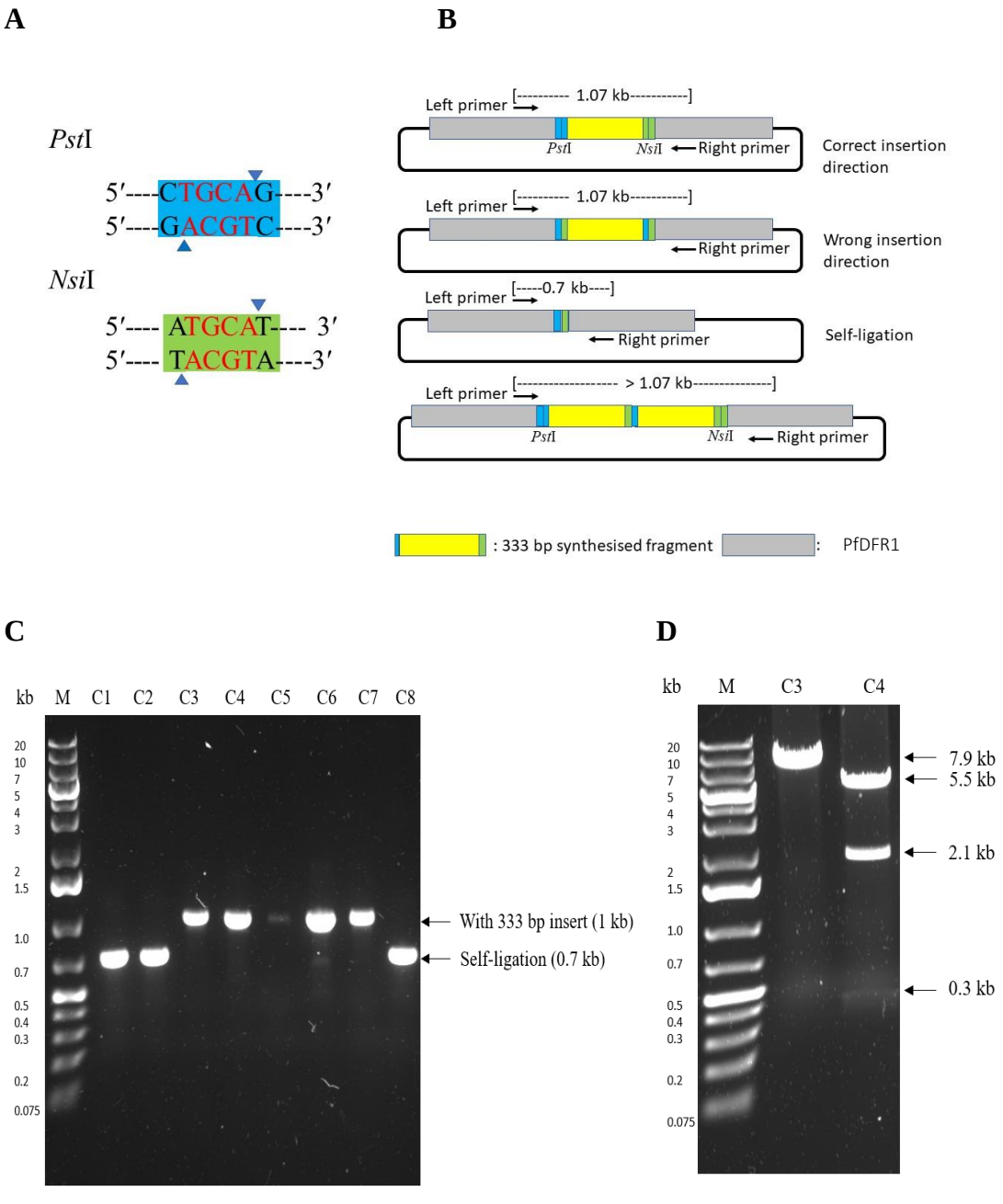

Figure 3.14 Screening of transformed colonies by PCR. A) *Pst*I and *Nsi*I recognition sequences. B) Three expected PCR amplification results. The plasmid harbouring one synthesized fragment insertion (both correct and wrong insertion directions) has 1 kb amplified fragment. The plasmid resulting from self-ligation has 0.7 kb amplified fragment. The plasmid harbouring two or more synthesized copies has more than 1 kb amplified fragment. C) PCR screening from 8 selected colonies. D) The insertion direction of synthesised 333 bp of *PfDFR1* fragment in colonies C3 and C4 were checked by double digestion with *PstI* and *NsiI*. Correct clone could have three expected fragments (0.3 kb, 2.1 kb, and 5.5 kb).

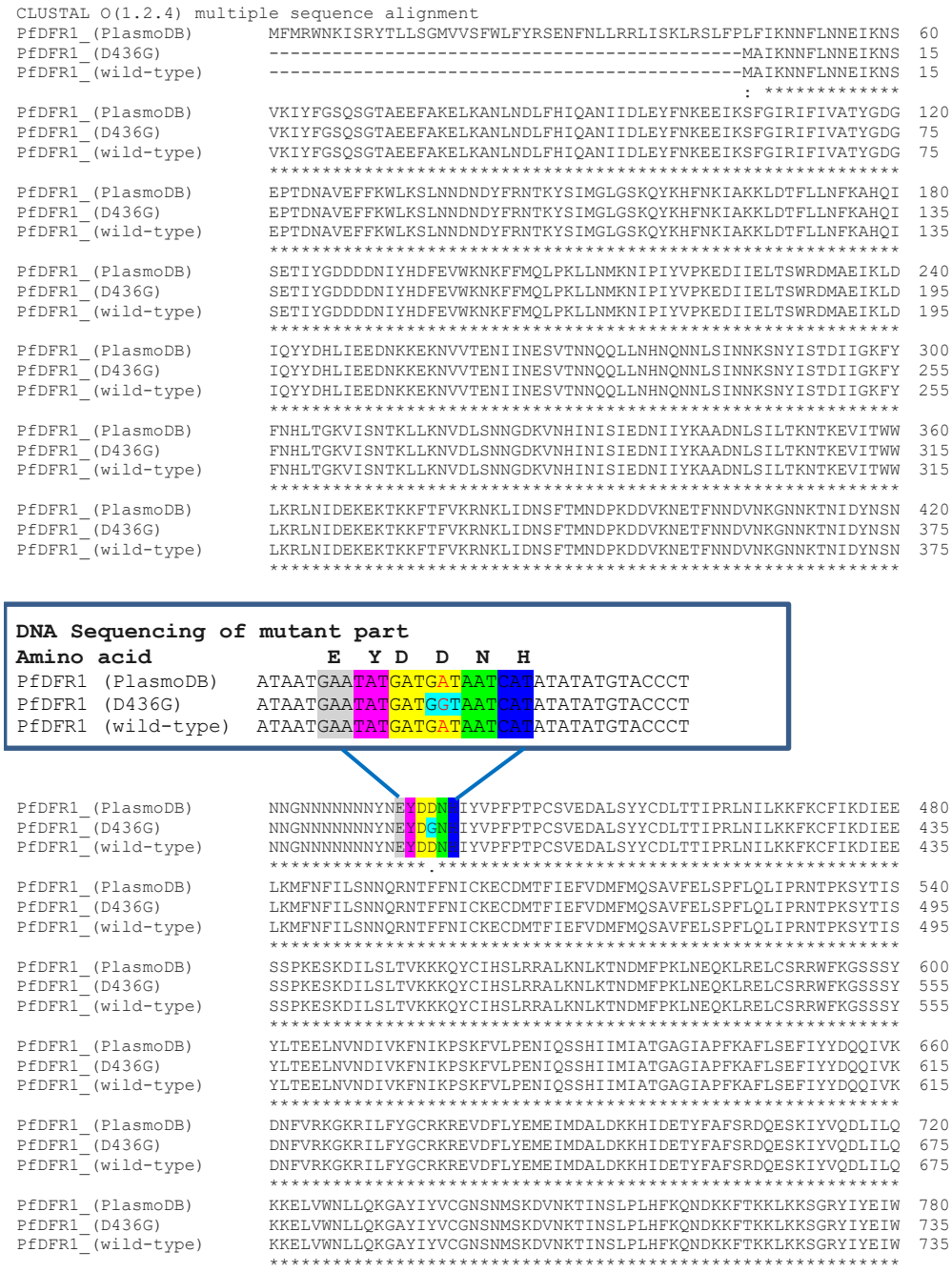

Figure 3.15 Protein sequence alignment of PfDFR1 constructs. The reference protein sequence in the alignment is *Plasmodium falciparum* strain 3D7 NADPH-cytochrome P450 reductase (accession number PF3D7_0923200). The DNA sequences were translated to protein sequences and compared with the reference sequence by Clustal Omega multiple sequence alignment.

3.3.7 Expression of PfDFR1 wt

To express PfDFR1 wt, pET15b PfDFR1 wt was transformed into expression host BL21(DE3). A pilot experiment to explore the best conditions for expression revealed the presence of the protein in the soluble fraction when growth was performed at low temperature, suggesting leaky expression from the T7 promoter (Figure 3.16).

To optimise the expression of PfDFR1 wt, induced expression with IPTG inducer was performed at 16˚C with a range of IPTG concentrations (Figure 3.17). The amount of soluble protein dramatically decreased when the IPTG concentration was increased. Leaking expression of PfDFR1 wt or induced expression with 0.01 mM IPTG at 16˚C was selected as appropriate ways for the protein production.

The effect of cofactors on protein folding and protein activity has been reported in the heterologous expression system [227, 228]. Insufficient flavin cofactors during protein expression could affect PfDFR1 folding and lead to the formation of inclusion bodies. Therefore, riboflavin was added in the late exponential growth phase. Supplementation of PfDFR1 cofactors during the protein production improved the production of soluble PfDFR1 wt (Figure 3.18). Extra nutrient did not improve the soluble PfDFR1 wt production compared with the regular LB broth medium. The PfDFR1 wt expression with riboflavin supplementation was also performed in the auto-induction media, including AIM LB-broth, AIM 2xTY, and AIM Terrific broth (Figure 3.19). Bacteria cultured in auto-induction media did not show higher soluble PfDFR1 expression as compared to cultures in LB broth. Therefore, LB broth with riboflavin supplementation was chosen for the PfDFR1 wt production.

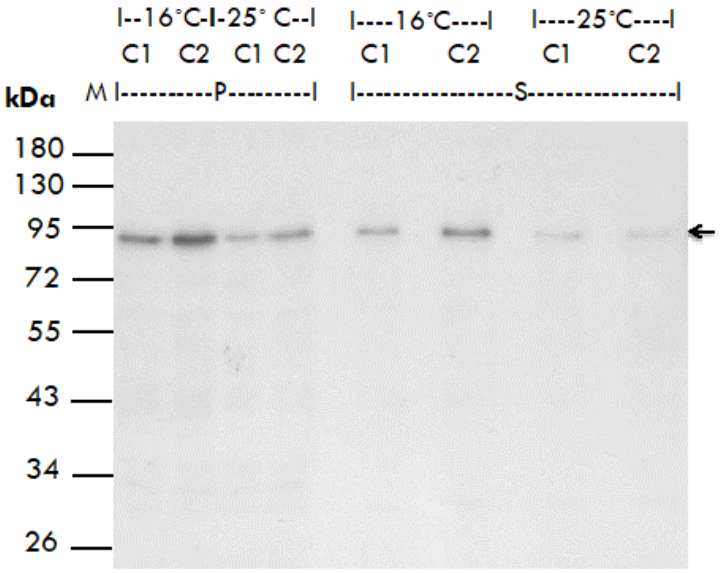

Figure 3.16 Western Blot with anti-His antibody of the PfDFR1 wt. Western Blot film of PfDFR1 wt leaking expression at 16˚C and 25˚C. Two transformants (C1 and C2) were selected for the expression test. M: protein marker; P: pellet; S: supernatant; Black arrow: band corresponding to the expected size of the recombinant protein band.

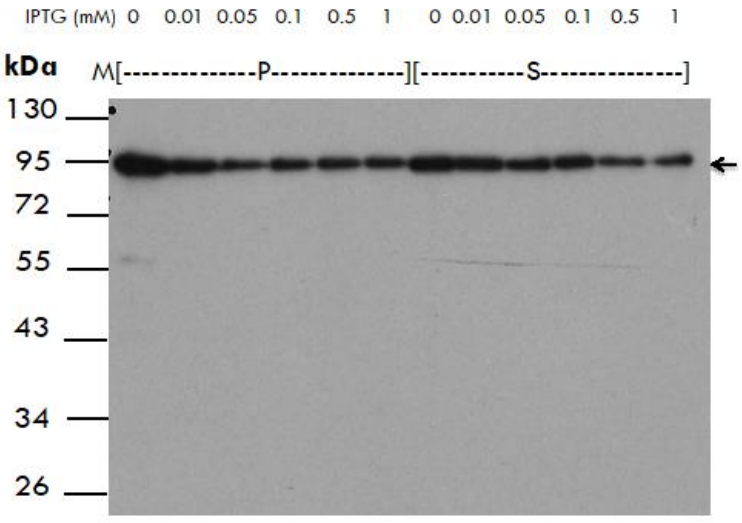

Figure 3.17 Western Blot with anti-His antibody of the PfDFR1 wt with various IPTG concentrations. M: protein marker; P: pellet; S: supernatant; Black arrow: band corresponding to the expected size of the recombinant protein band.

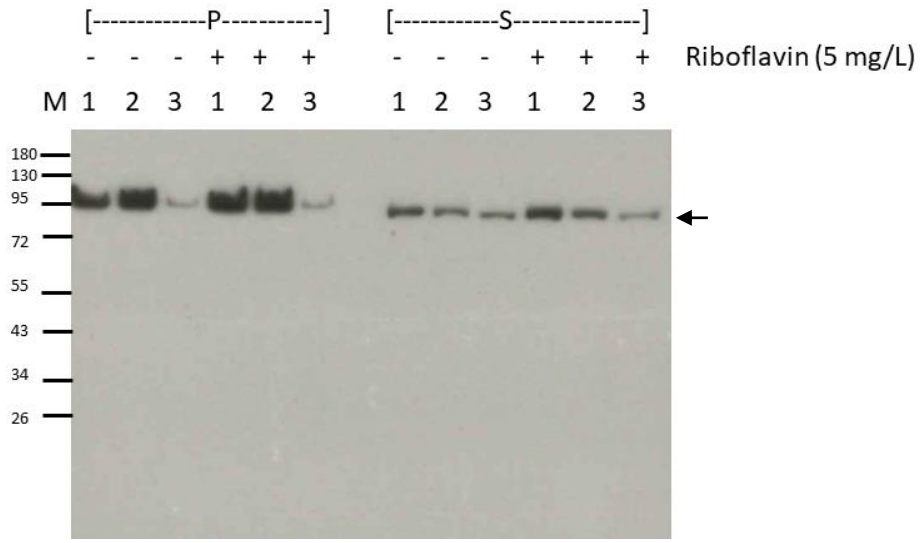

Figure 3.18 Western Blot with anti-His antibody of the PfDFR1 wt cultured with various culture media. The effect of riboflavin addition on PfDFR1 wt protein solubility was assessed on cultures grown at 16˚C for 24 h. The cell lysate was normalised and loaded 3 µg/well. M: protein marker; P: pellet; S: supernatant; 1: LB-broth; 2: 2xYT; 3: Terrific broth; (-): without adding riboflavin; (+): with 5 mg/L riboflavin addition in culture media; Black arrow; band corresponding to the expected size of recombinant protein band.

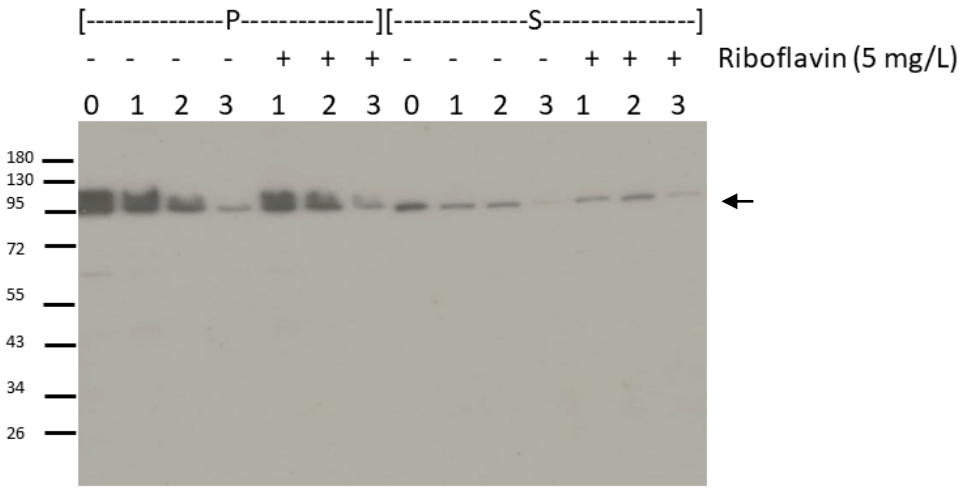

Figure 3.19 Western Blot with anti-His antibody of the PfDFR1 wt culture with various auto-induction media. The effect of riboflavin addition on PfDFR1 wt protein solubility was assessed on auto-induction media at 16˚C for 24 h. The cell lysate was normalised and loaded 3 µg/well. M: protein marker; P: pellet; S: supernatant; 0: LB-broth; 1: AIM BL-broth; 2: AIM 2xYT; 3: AIM Terrific broth; (-): without adding riboflavin; (+): with 5 mg/L riboflavin addition in culture media; Black arrow; band corresponding to the expected size of recombinant protein band.

3.3.8 Purification of PfDFR1 wt

PfDFR1 wt was purified via a Ni-NTA affinity column and analysed by SDS-PAGE (Figure 3.20, Lane 3). The result demonstrated the expected PfDFR1 wt at 87 kDa. However, two major contaminants were found at 72 kDa and 60 kDa.

To improve protein purity, the partially purified PfDFR1 was further purified using ion exchanger chromatography. The partially purified PfDFR1 wt was processed with both anion and cation exchanger chromatography columns. The strong cation exchanger chromatography column (SP-sepharose FF) showed the ability to separate the major contaminants from the PfDFR1 (Figure 3.20, Lanes 4-5).

Thrombin was used to remove the histidine tag from the PfDFR1 and to improve overall protein purity. The histidine tag cleaved off PfDFR1 was analysed by SDS-PAGE (Figure 3.20, Lane 6). The expected PfDFR1 was generated with a few minor contaminants after treatment with thrombin. The protein purity analysed from the band intensity was increased to over 85 percent. After purification, the yield of pure protein was 1 mg per litre of cell culture.

The expected band of PfDFR1 wt was cut and sent to the Metabolomics & Proteomics Lab (Department of Biology, University of York, UK) for the mass spectrometry-based protein identification. The protein identification results confirmed that PfDFR1 wt was PfDFR1 (Gene ID: PF3D7_0923200) with peptides matching throughout protein sequence (Appendix 3.4).

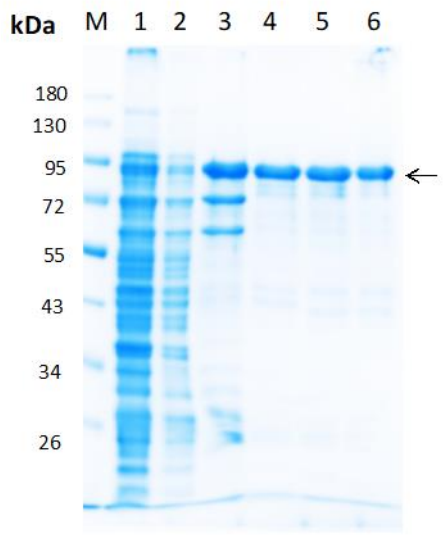

Figure 3.20 Purification profile of PfDFR1 wt. SDS-polyacrylamide gel electrophoresis of PfDFR1 sequentially purified by Ni-NTA affinity chromatography, SP sepharose ion exchanger chromatography, and histidine tag cleavage. M: protein marker; 1: whole cell lysate; 2: supernatant; 3: partial purified PfDFR1 from the Ni-NTA column; 4-5: further purified PfDFR1 via the SP-sepharose column (the same sample); 6: thrombin treated PfDFR1; Black arrow: PfDFR1 wt band.

3.3.9 Biochemical activity with PfDFR1 wt

To confirm that the PfDFR1 was catalytically active, the ability to transfer electrons from NADPH to the electron accepter cytochrome *c* was measured by determining the change in reduced cytochrome *c* absorbance at 550 nm. As shown in Figure 3.21, the increase in absorbance 550 nm related to the successful acceptance of an electron of cytochrome *c* from PfDFR1 wt catalytic reaction occurred in the reaction with NADPH as substrate. This indicates that the PfDFR1 wt is an active enzyme. Therefore, the purified PfDFR1 wt could be further used in biochemical assays.

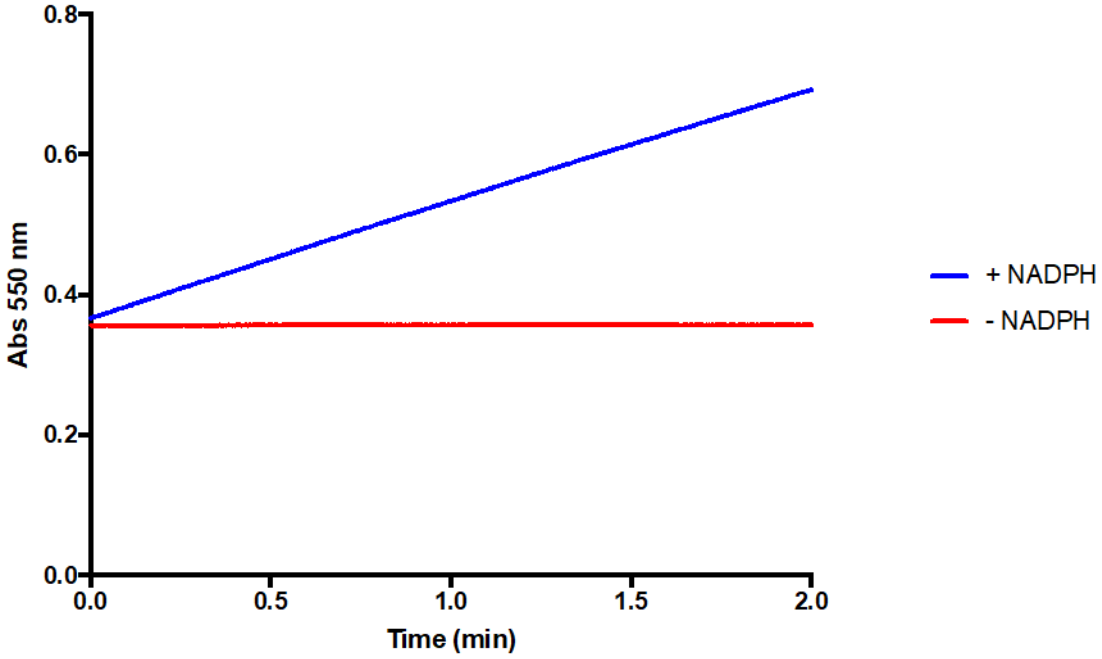

Figure 3.21 Measurement of reduced cytochrome c of PfDFR1 activity assay. Each assay reaction was performed with 30 pmol PfDFR1, 50 μM cytochrome *c*, with or without 50 μM NADPH. Absorbance at wavelength 550 nm was measured for 2 min. A representative experiment out of three performed is shown.

3.4 Discussion

This chapter describes the construction, expression and purification of PfDFR1 protein. PF3D7_0923200 was chosen to study as the most probable PfDFR1 protein based on careful consideration of sequence and structure data (Table 3.3-3.5, Figure 3.3-3.4). The structural analysis and transmembrane prediction (TMpred sever) confirmed that PfDFR1 has possible transmembrane helices at the N-terminus (aa8 to aa27). A series of pETM-11 containing different catalytic domains of codon optimised PfDFR1 protein were successfully constructed but without predicted transmembrane helices (first 27 aa). However, soluble proteins were not successfully produced from any of the pETM-11 PfDFR1 constructs using IPTG induced expression.

It is hypothesised that the attempted deletion of predicted transmembrane helices may not have been completely successful and that further transmembrane-spanning residues remained. Partial transmembrane residues in the truncated PfDFR1 protein might have had an impact on protein folding and solubility. Known soluble recombinant CPRs are typically constructed by truncating at least 10 amino acids in addition to the predicted transmembrane helices [118, 171, 182, 229, 230]. To overcome this issue, various strategies, including modified lysis buffers, additives, and co-expression with chaperones, were investigated to improve protein solubility and folding (Figure 3.7-3.8).

The use of molecular chaperones to improve protein folding and proteostasis has been reported extensively [231-233] and shown to be effective in generating soluble recombinant protein expression [234, 235]. However, in this instance, chaperones (DnaK and DnaJ) were shown to be co-eluted with the PfDFR1

proteins. Washing the column with ATP is an approach developed to remove DnaK [236, 237], but this approach is not consistently effective [238, 239]. In the PfDFR1 purification, DnaK presence was not abolished (Figure 3.11) using the ATP approach. Further purification steps might be needed to remove chaperones.

Instead of using codon optimised PfDFR1 sequence, the original PfDFR1 sequence was used in plasmid construction with 47 amino acids deleted at the N-terminus. Protein misfolding occurred on induced expression. Leaking expression, low recombinant protein expression during the bacteria growth prior to induction, has been reported in the T7 system [240, 241]. This phenomenon can be an advantage for the production of membrane and secretory proteins without induction [241], probably because the low expression does not saturate the Sec-translocon capacity [241]. Using this strategy, the soluble PfDFR1 protein with catalytic activity was successfully produced from the leaky expression at low temperatures. The availability of cofactors is known to affect protein folding [227, 228] and enzyme maturation [242]. Supplementation of riboflavin, a source for FMN and FAD, has been reported to improve the production of recombinant CPRs [243, 244]. A similar finding was observed in this study, with PfDFR1 protein expression shown to be enhanced following supplementation with riboflavin (Fig. 3.18)

The non-synonymous mutation at D436G found in the plasmid construction from *g*DNA was unexpected. From the dataset of 3,488 clinical malaria samples generated by the MalariaGEN *Plasmodium falciparum* Community Project, 183 single nucleotide polymorphisms (SNPs) were found in the gene coding for PfDFR1 protein [245]. 120 SNPs were non-synonymous SNPs. At position 436, a SNP changing from

aspartic acid (D) to asparagine (N) was reported from Variant Catalogue tool (Figure 3.22). Adjacent amino acids also have SNPs, such as D435H and N437D. SNPs at the same position can occur with different amino acids changing, such as I439T and I439M. Experiments from the original *g*DNA and bioinformatics are needed for further analysis to prove the D436G SNP finding.

Sequence alignment and predicted 3D-modelling of the PfDFR1 protein indicate that D436G is likely to be in the connecting domain of the protein (Figure 3.23). The flexible connecting domain plays an important role in the relative positioning of the two catalytic domains for electron transfer [123, 246]. Changing from aspartic acid to glycine could increase the loop flexibility because the hydrogen bonds formed with the aspartic acid side chain are reduced. The effect of D436G on enzyme catalytic activity was studied (Appendix 3.5). Our results demonstrate that mutation at D436G does not significantly alter the PfDFR1 activity.

In conclusion, the active recombinant PfDFR1 protein was successfully generated from *E. coli*, taking advantage of "leaky" expression at low temperatures. Because of the difficulty and limitations in protein purification, biochemical characterisation of each PfDFR1 catalytic domain (codon optimised PfDFR1_FMN and PfDFR1_FAD/NADPH) was not possible in this study. Based on the similar catalytic activity between PfDFR1 wt and PfDFR1 D436G, only PfDFR1 wt was used for the biochemical characterisation described in chapters 4, 5 and 6.

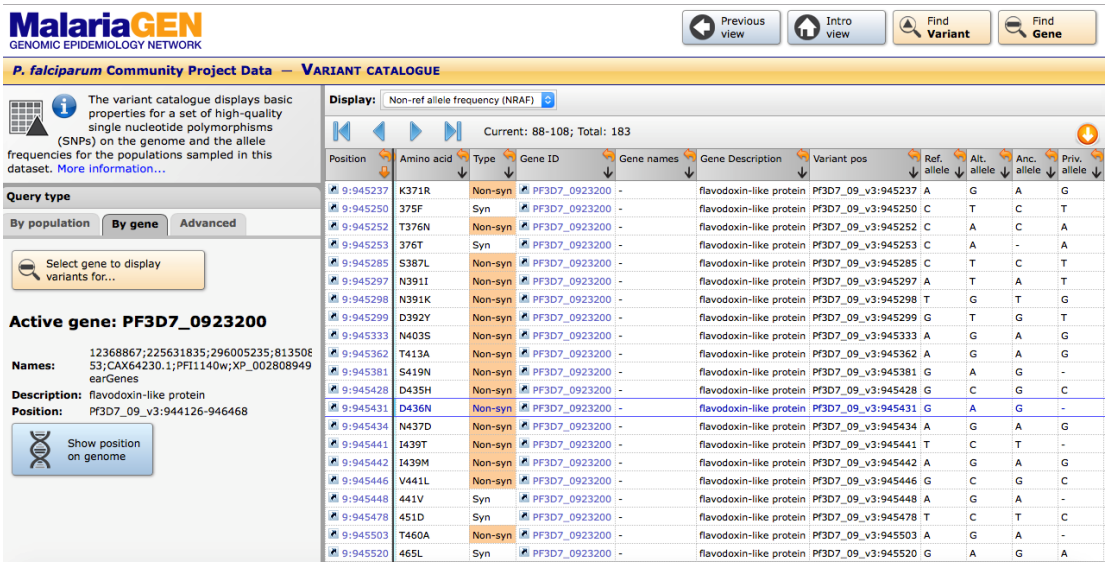

Figure 3.22 Variant catalogue of PfDFR1 (PF3D7_0923200). Variant Catalogue from MalariaGEN *Plasmodium falciparum* Community Project website (https://www.malariagen.net/apps/pf/4.0/) showed SNPs of PfDFR1 at the region close to position 436.

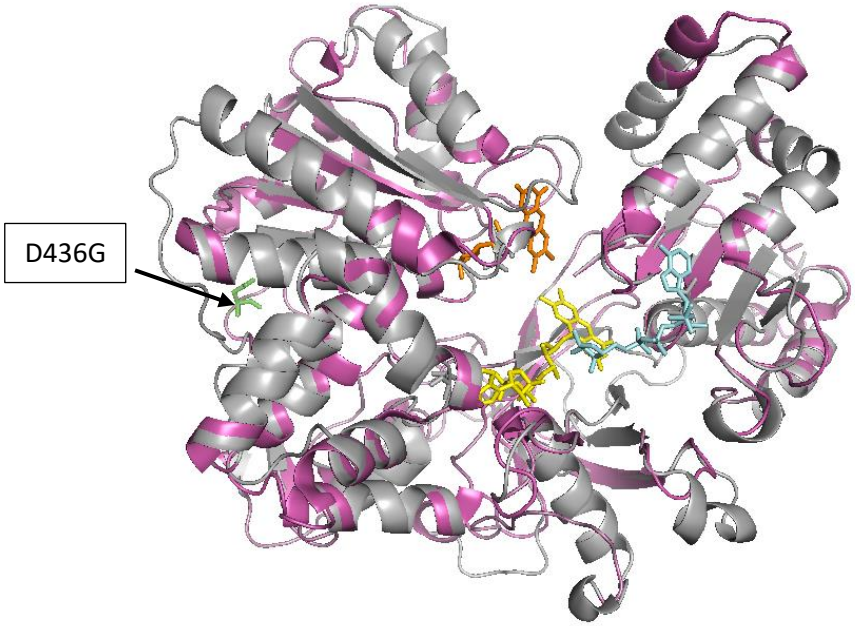

Figure 3.23 Predicted D436G position. *P. falciparum* PF3D7_0923200 model is shown in grey. Yeast CPR (PEB; 2BPO) is shown in pink. FMN, FAD, and NAP are shown in orange, yellow, and cyan, respectively. D436 is shown is green.

CHAPTER 4

CHARACTERISATION OF *PLASMODIUM FALCIPARUM* NADPH-DEPENDENT DIFLAVIN REDUCTASE I

4.1 Introduction

Over 50 years, numerous diflavin reductases, such as CPRs and NOSs, have been identified and characterised from various organisms. The most well characterised CPR's and NOS's are those from human and rat. However, little is known about *Plasmodium falciparum* diflavin reductases, including the putative NADPH-dependent diflavin reductase I (PfDFR1) cloned and expressed in Chapter 3.

As discussed in Chapter 1, a feature of diflavin reductase members is the presence of a FMN and a FAD co-factor in each monomeric subunit of the protein. The flavin cofactors play an important role in the electron transfer from NADPH to partner proteins. The flavin cofactors can exist in three forms including the oxidised (ox), one-electron reduced semiquinone (sq), and two-electron fully reduced (red) forms (Figure 4.1). The oxidised forms have maxima absorption peaks at 380 and 450 nm. The blue neutral semiquinone form has a broad absorption band between 500-700 nm, with maxima in the region 580-600 nm [135]. In CPR, the semiquinone is usually found in the blue neutral region within the physiological pH range 6.5-8.5 [203]. The spectroscopic properties of each flavin form has been used to aid the analysis of

semiquinone stability and interflavin electron transfer of the diflavin reductases [179, 182, 204, 247].

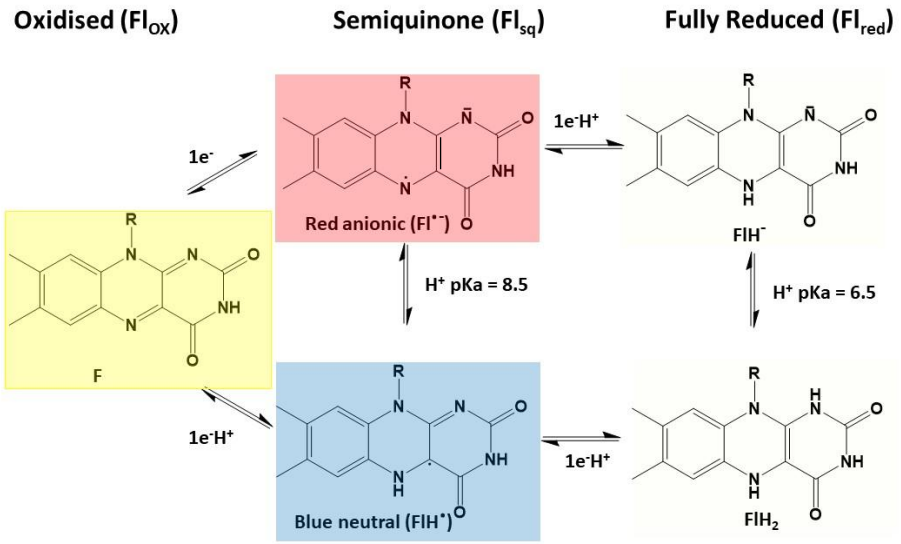

Figure 4.1 Various redox states of flavin isoalloxazine ring. The visible spectrum of each redox state is shown in the background colour box.

In this chapter, the spectroscopic characterisation of the PfDFR1 protein is described. The spectral characteristic of the N-terminus truncated PfDFR1 protein (first 47 amino acids deletion) were studied using UV-Vis spectroscopy. The flavin contents of the recombinant PfDFR1 protein and human CPR (hCPR) were determined by HPLC analysis. The half-reaction of the PfDFR1 protein was studied using stopped-flow spectroscopy. Finally, the pH and temperature optima of the PfDFR1 protein were determined to explore the factors that affect PfDFR1 protein catalytic activity.

4.2 Methods

4.2.1 Spectral analysis of PfDFR1

As described in the introduction, different flavin cofactor redox states possess unique absorption spectra signatures. The oxidised PfDFR1 was prepared in 0.3 M potassium phosphate buffer pH 7.7. The absorption spectrum of 10 µM oxidised PfDFR1 (500 µl) was scanned using a UV-VIS spectrophotometer from 700 nm – 300 nm in a 0.7 ml quartz cuvette. The spectrum of the PfDFR1 semiquinone form was scanned after addition of NADPH (100 µM). The fully reduced PfDFR1 was prepared by addition sodium dithionite.

For air oxidation of NADPH-reduced PfDFR1, 10 µM of the oxidised PfDFR1 was prepared in the same buffer as above and placed in a 0.7 ml quartz cuvette. The spectrum was scanned using a UV-VIS spectrophotometer from 700 nm – 300 nm. Then, NADPH was added into the assay cuvette to the final concentration 100 µM and the spectra were recorded at 30 min, 1 h, 2 h, 4.5 h, and 9.5 h.

For air re-oxidation fully-reduced PfDFR1, 10 µM of the oxidised PfDFR1 was prepared in the same buffer as above and placed in a 0.7 ml quartz cuvette. The absorbance was scanned using a UV-VIS spectrophotometer from 700 nm – 300 nm. Sodium dithionite was added to make the fully reduced PfDFR1. Then, the fully oxidised PfDFR1 was allowed to oxidise with air. The change of spectrum was monitored every 10 min until the protein was fully oxidised.

4.2.2 Flavin content determination of PfDFR1 and hCPR

The PfDFR1 and hCPR (obtained from Dr. Mark Paine, LSTM) were diluted to 0.1 mg/ml in the sample buffer (50 mM Tris pH 7, 100 mM NaCl, 5 mM CHAPS, and 10% glycerol). The protein samples, standard FMN and standard FAD were prepared and analysed as described in the section 2.2.7. Quantification of flavin content was determined by comparison of integration of the fluorescence peaks with standard FMN and FAD.

4.2.3 Single-wavelength analysis of the PfDFR1 half reaction

The pre-steady state studies of PfDFR1 were performed using an Apply Photophysics SX.17 MV stopped-flow spectrophotometer. The assay conditions were carried out at 25˚C in 0.3 M potassium phosphate buffer pH 7.7 with 10 µM of PfDFR1. All experiments were performed under anaerobic conditions using a Belle Technology anaerobic glove box. In the single wavelength study, the reduction of PfDFR1 by NADPH was observed at 455 nm. The rate constants of hydride transfers were obtained by fitting the graph to the double exponential expression (equation 4.1).

$$A=C_1e^{-k_{obs1}t} + C_2e^{-k_{ob21}t} + b$$

Equation 4.1

Where k_{obs1} and k_{obs2} are the observe rate constants of the faster phase and the slower phase. C_1 and C_2 are their relative amplitude values, and b is the final absorbance.

4.2.4 Substrate specificity of PfDFR1 on nicotinamide-based compounds

The substrate specificity of PfDFR1 was determined from the change of reduced cytochrome *c* absorbance at 550 nm. The reaction was performed in a total reaction volume of 500 µl carried out at room temperature (18˚C to 20˚C), with the absorbance determined using a Cary 300 UV-Visible spectrophotometer. The PfDFR1 (30 pmol PfDFR1) was incubated with 50 µM cytochrome *c* prepared in 0.3 M potassium phosphate buffer pH 7.7 for 2 min. There are four different nicotinamide-based compounds including NADPH, $NADP^+$, NADH, and NAD. First, the reaction was initiated by the addition of NADPH to a final concentration of 50 µM. The absorbance at 550 nm was measured for 2 min. The experiment was repeated using other nicotinamide-based compounds ($NADP^+$, NADH, and NAD). The reduction was calculated from triplicate measurements.

4.2.5 PfDFR1 optimal pH determination

The optimal pH determination experiment was performed in a total reaction volume of 300 µl at 25˚C in a 96-well plate. Each reaction mixture (18 pmol PfDFR1, 0.3 M potassium phosphate buffer, 50 µM cytochrome *c*, 50 µM NADPH) was plated into a well of a 96-well plate. Potassium phosphate (0.3 M) buffer solutions were added with the final pH ranging from 5.8 to 8.2. The experiment at each pH was performed in four wells including three experimental wells and one control well (using the sample buffer instead of NADPH). The reaction was initiated by the addition of NADPH. The absorbance at 550 nm was monitored every 5 s for 2 min using a Varioskan® plate reader (Thermo Scientific).

4.2.6 PfDFR1 optimal temperature determination

The optimal temperature determination experiment was performed in a total reaction volume of 300 µl in a 96-well plate. Each reaction mixture (18 pmol PfDFR1, 0.3 M potassium phosphate buffer pH 7.7, 50 µM cytochrome *c*, 50 µM NADPH) was plated into a well of a 96-well plate. The tested temperature range was from 22.5˚C to 42.5˚C. First, the plate reader was set up at 22.5˚C. The plate containing four assay wells including three experimental wells and one control well (using the assay buffer instead of NADPH) was incubated in the plate reader for 5 min to allow the plate to reach the correct temperature. The reaction was initiated by the addition of NADPH. The absorbance at 550 nm was monitored every 5 s for 2 min. The experiment was repeated with additional temperatures (25˚C, 30˚C, 32.5˚C, 35˚C, 37.5˚C, 40˚C, and 42.5˚C).

4.3 Results

4.3.1 Spectral properties of PfDFR1

The oxidised diflavin reductase harbouring the tight bound FMN and FAD cofactors has unique characteristic absorption peaks at 380 nm and 450 nm. Like other diflavin reductase members, the fully-oxidised PfDFR1 was found to have two absorbance peaks at 382 nm and 455 nm (Figure 4.2: blue line). The ability to form the semiquinone of PfDFR1 was established after the addition of NADPH. The changing spectra (Figure 4.2: red line) with decreasing absorbance in the 382 nm and 455 nm peaks and increasing absorbance in the 500-700 nm region was observed, that representing the characteristics of the air-stable neutral flavin semiquinone. In the fully-reduced PfDFR1, the protein loses all peaks in 382 nm, 455 nm, and the 500-700 region (Figure 4.2: green line).

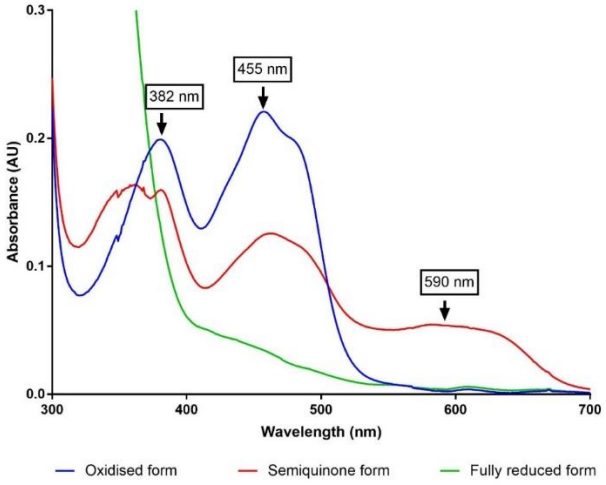

Figure 4.2 A spectral characterisation of Purified PfDFR1 (10 μM PfDFR1 in 0.3 M potassium phosphate buffer pH 7.7) under aerobic conditions. Spectrum of oxidised form of PfDFR1 (blue). Spectrum of semiquinone form (red) was prepared by addition of NADPH to a final concentration of 100 μM. The spectrum was recorded at 30 second after the addition of NADPH. Few grains of sodium dithionite were added to make a completely reduced form (green).

4.3.2 Air oxidation of NADPH-reduced PfDFR1

After the oxidised PfDFR1 (Figure 4.3: Spectrum A) was reduced by the addition of NADPH, the air-stable semiquinone was immediately observed under aerobic conditions (Figure 4.3: Spectrum B). The spectra recorded over 9 h indicated that the semiquinone was further oxidized by oxygen in air and recovered to 80% of oxidised form based on the comparison of the absorbance 455 nm between the initial oxidised enzyme and the air oxidised enzyme after 9h.

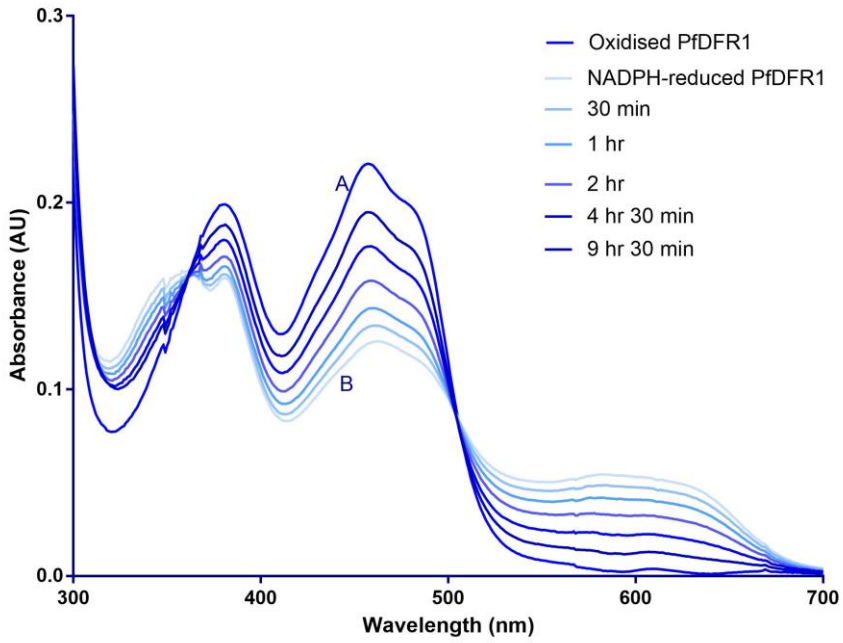

Figure 4.3 Air oxidation of NADPH-reduced PfDFR1. Spectrum A is the oxidised PfDFR1 (10 µM PfDFR1 in 0.3 M potassium phosphate buffer pH 7.7). PfDFR1 was reduced by the addition of 100 µM NADPH under aerobic condition (Spectrum B). The other spectra were recorded at the indicated time points after the addition of NADPH.

4.3.3 Air reoxidation of fully reduced PfDFR1

Oxidation of the fully reduced PfDFR1 by oxygen at air-saturation as a function of time is shown in Figure 4.4. the oxidation proceeded rapidly from the fully reduced PfDFR1 (Figure 4.4: blue dash line) to the semiquinone form (Figure 4.4: red dash line), while the oxidation proceeded slowly from the semiquinone form to the oxidised form (Figure 4.4: black dash line). The change occurring at 455 nm (oxidised flavins), 590 nm (semiquinone), and 503 nm (isosbestic point) is shown in the inset of Figure 4.4.

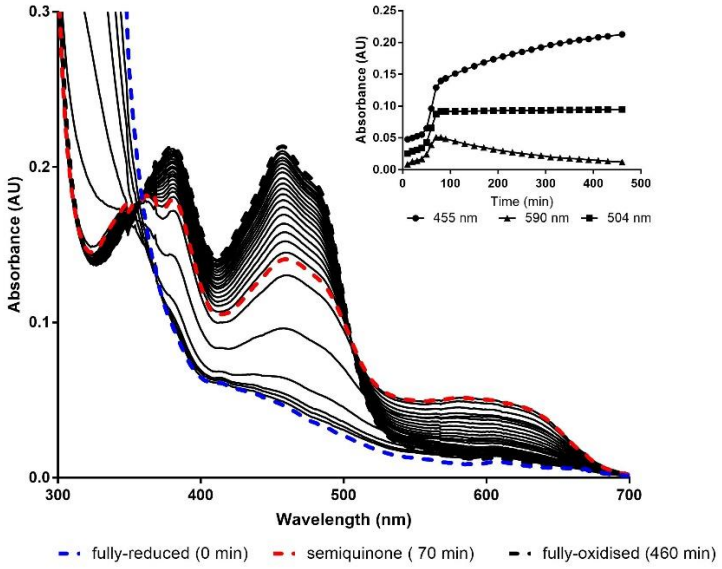

Figure 4.4 Air oxidation of the fully-reduced PfDFR1. The oxidised PfDFR1 (10 µM PfDFR1 in 0.3 M potassium phosphate buffer pH 7.7) was fully reduced by addition of sodium dithionite (blue dash line). The absorption spectra of PfDFR1 undergoing oxidise by air were monitored over 460 min. The semiquinone form of PfDFR1 is shown in a red dash line. The oxidised form of PfDFR1 is shown in a black dash line. Black lines are intermediates measured every 10 min from the fully reduced form to the oxidised form of PfDFR1. The inset shows the change occurring at 455 nm, 504 nm, and 590 nm.

4.3.4 Flavin content determination

Flavin cofactors (FMN and FAD) are necessary for the diflavin reductase function. In general, the ratio of each flavin to protein usually in 1:1. The most common method used in the separation of FMN and FAD is the HPLC method. The results from HPLC analysis showed a good separation of FMN and FAD standards with the elution time of 5.3 min for FMN and 4.5 min for FAD (Figure 4.5A and B). After flavins were isolated from the PfDFR1 and hCPR, FMN was separated from FAD using the HPLC method (Figure 4.5C and D). The peak areas of FMN and FAD from the enzyme samples were compared to the FMN and FAD standard peak areas to calculate the concentration of flavin loaded onto the column. The ratios of each flavin concentration to each protein concentration (calculated by Bradford assay) are shown in the table 4.1. Both PfDFR1 and hCPR show close to a 1:1 in the FMN to protein concentration ratio. However, the FAD to protein ratio of PfDFR1 (0.77± 0.2 : 1) is lower than hCPR (1.0±0.02 : 1). Taken together, the hCPR is fully saturated with flavins, but the PfDFR1 looks FAD deficient.

A) FMN **B) FAD**

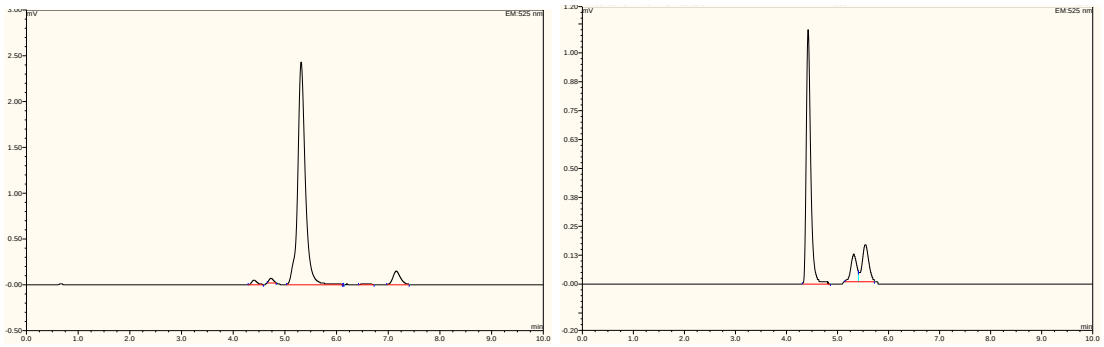

C) PfDFR1 **D) hCPR**

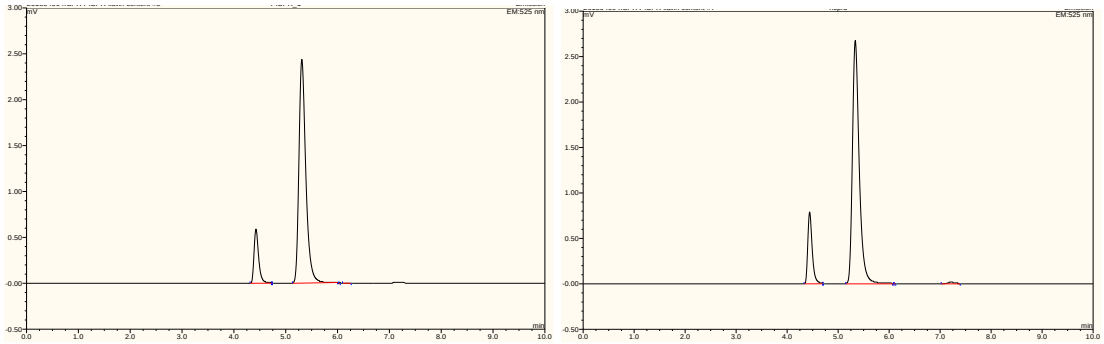

Figure 4. 5 HPLC analysis of PfDFR1 and hCPR flavin content. A) the elution peak of standard FMN. B) the elution peak of standard FAD. C) Elution peaks of PfDFR1. D) Elution peaks of hCPR. the HPLC was carried out on a 250 mm C18 column (Acclaim®120, Dionex) at room temperature (23 °C). The mobile phase is 50 mM ammonium acetate; pH 4.5 with 15 % (v/v) acetonitrile. The fluorescent emission of flavins was measured at 525 nm.

Table 4.1 The comparison of flavin contents between PfDFR1 and hCPR

Recombinant CPR	**Flavin content**	
	[FMN]/ [protein]	[FAD]/[protein]
PfDFR1	1.14 ±0.15	0.77 ± 0.20
hCPR	1.17 ±0.02	1.00 ± 0.02

4.3.5 Single-wavelength analysis of PfDFR1 half reaction

The reduction of PfDFR1 by NADPH was monitored using a stopped flow spectrophotometer. After the rapid mixing of the NADPH and the PfDFR1, the transient observed at 455 nm (Figure 4.6) was fitted using a double exponential expression (equation 4.1) yielding the rate constants k_{obs1} (the fast phase: rate of the first hydride transfer) and k_{obs2} (the slow phase: rate of the second hydride transfer). The detail of interflavin electron transfer is described in the introduction (section 1.7.2.3). The dependence of the NADPH concentrations on the observed rates was studied as shown in Figure 4.7. At the same NADPH concentration, the observed rate of the first hydride transfer in the PfDFR1 (Figure 4.7A) is faster than the rate of the second hydride transfer (Figure 4.7B). At low NADPH concentrations (below 50 µM NADPH), the observed rates for both first and second hydride transfers were found to be increased. This phenomenon was also reported in the hCPR [204]. In the pseudo-first-order regime, the hydride transfer rates were found to be independent of the NADPH concentration. The rate constants k_{obs1} and k_{obs2} under pseudo-first-order conditions are ~2 s^{-1} and ~0.25 s^{-1}, respectively.

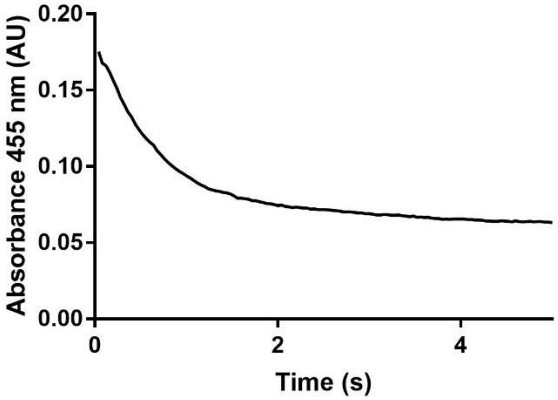

Figure 4.6 Example of single-wavelength absorption transient for the reduction of PfDFR1 by NADPH. The experiment (0.3 M potassium phosphate buffer pH 7.7, 10 µM PfDFR1, 160 µM NADPH) was performed at 25˚C. Transient was observed at 455 nm. The double exponential expression (equation 4.1) was used to describe the transient data.

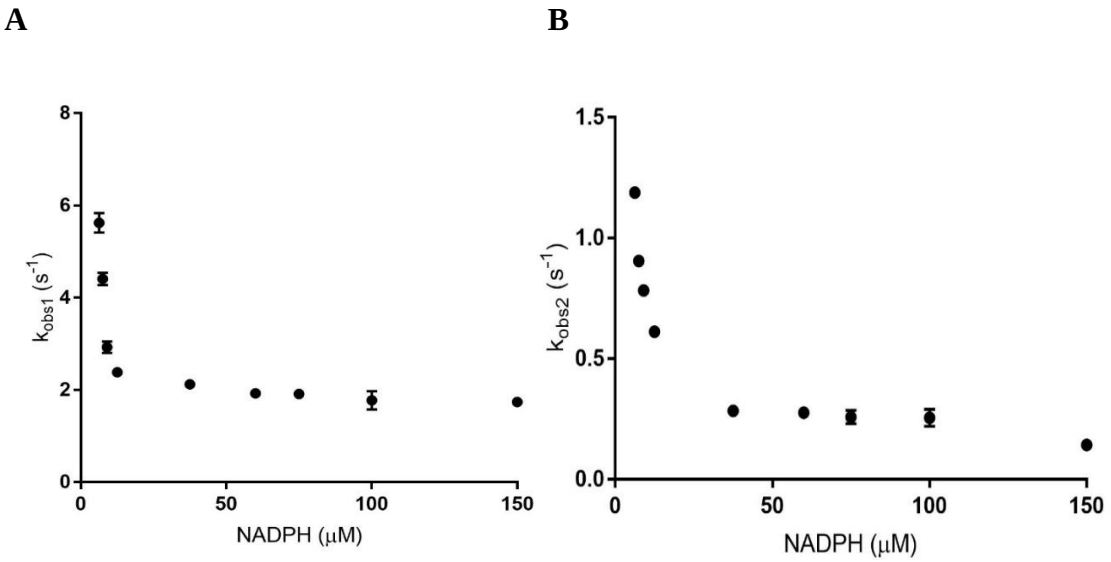

Figure 4.7 Dependence of the observed rates of PfDFR1 on NADPH concentrations monitored by a single wavelength stopped-flow spectrophotometer. 10 µM PfDFR1 was used in the experiment. (A) Observed rates of fast phase measured at 455 nm. (B) Observed rates of slow phase measure at 445 nm. The values were calculated from three measurements.

4.3.6 Substrate specificity of PfDFR1

The PfDFR1 assay with cytochrome *c* was repeated with various nicotinamide-based compounds to examine the ability to donate electron to PfDFR1. Four kinds of nicotinamide-based compounds, including NADPH, $NADP^+$, NADH, and NAD, were tested in this experiment. Under these assay conditions (30 pmol PfDFR1, 50 µM cytochrome *c*, 0.3 M potassium phosphate buffer pH 7.7, and 50 µM tested compound), NADPH was the only affective substrate yielding formation of the reduced cytochrome *c* (Figure 4.8). The results demonstrated that PfDFR1 has only substrate specificity to NADPH.

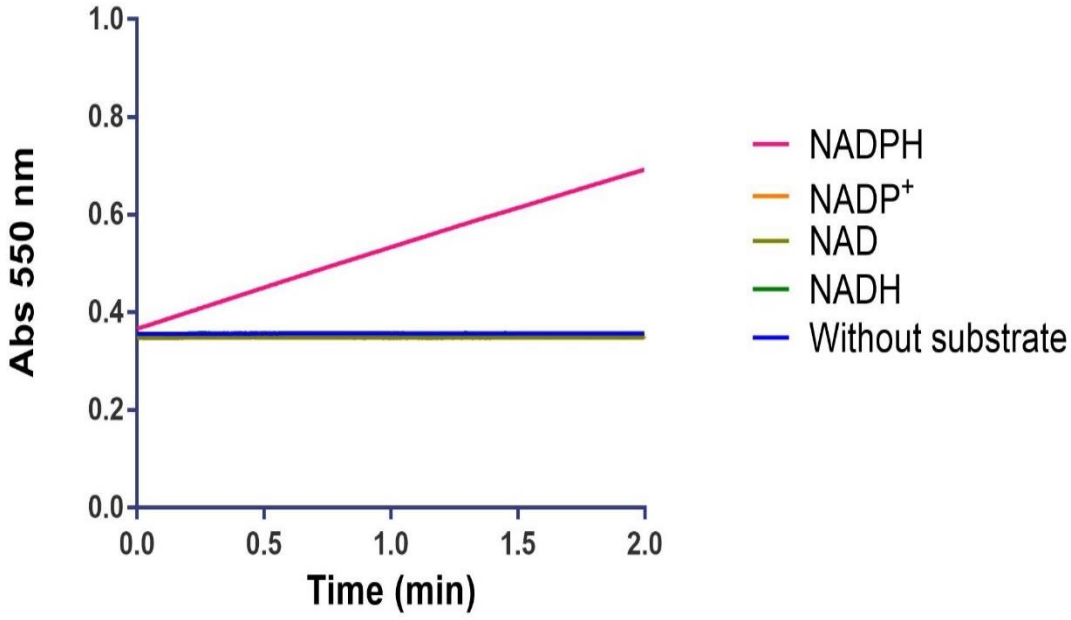

Figure 4.8 Substrate specific of PfDFR1. PfDFR1 activity was measured in 0.5 ml reaction. 50 µM cytochrome *c* in 0.3 M potassium phosphate buffer pH 7.7, and 30 pmol PfDFR1 were mixed. The reactions were initiated by addition of (50 µM for all) NADPH (pink line), $NADP^+$, NADH (dark green line), NAD (light green line) or buffer (blue line). The absorbance 550 nm was measured using a Cary 300 UV-Visible spectrophotometer.

4.3.7 Effect of pH of PfDFR1 activity

The PfDFR1 assay with cytochrome *c* was repeated at a range of pHs from pH 5.8 to pH 8.2 in order to examine the effect of pH on PfDFR1 activity. The results are shown in Figure 4.9. The PfDFR1 shows the highest activity at pH 7.8, significantly different from activities at other pHs (Tukey's multiple comparison test with $P<0.001$, see Appendix 4.1).

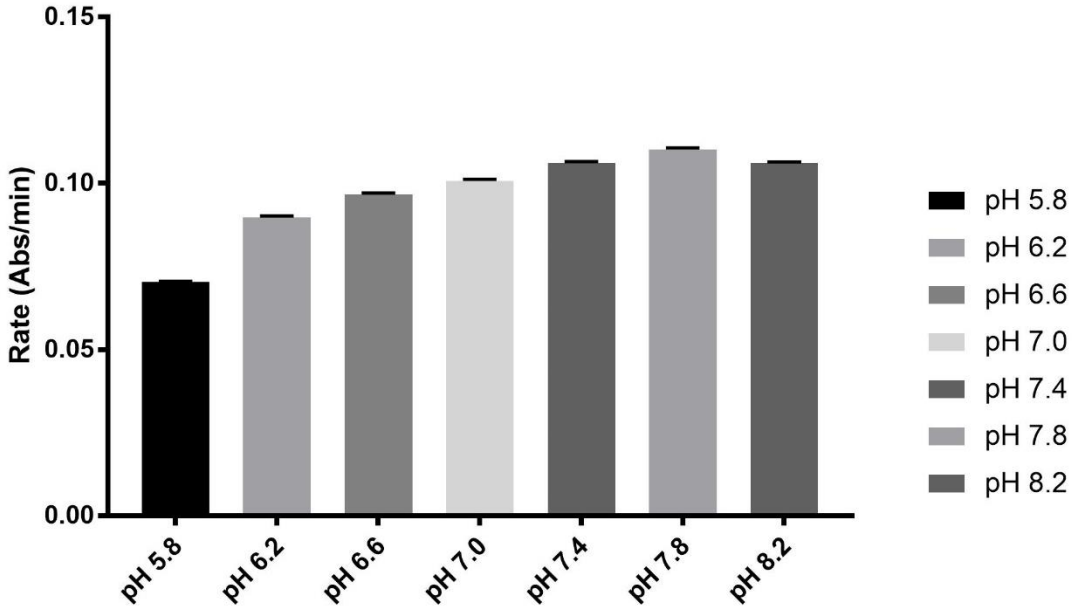

Figure 4.9 Effect of pH on PfDFR1 activity. Enzyme activity was determined using cytochrome *c* in 0.3 ml reaction. 50 µM cytochrome *c* in 0.3 M potassium phosphate buffer in various pH, and 18 pmol PfDFR1 were mixed and incubated for 5 min at 25˚C. 50 µM NADPH was added to initiate the reaction. The absorbance 550 nm was measured using a pate reader (VARIOSKAN, Thermo Scientific). Rates of PfDFR1 were means of three independent purifications.

4.3.8 Effect of temperature on PfDFR1 activity

The PfDFR1 assay with cytochrome *c* was repeated with various temperatures from 22.5˚C to 42.5˚C to examine the effect of temperature on PfDFR1 activity. The results are shown in Figure 4.10. The PfDFR1 shows the highest activity at 40˚C with significantly different from other temperatures (Tukey's multiple comparison test with P<0.001, see Appendix 4.2).

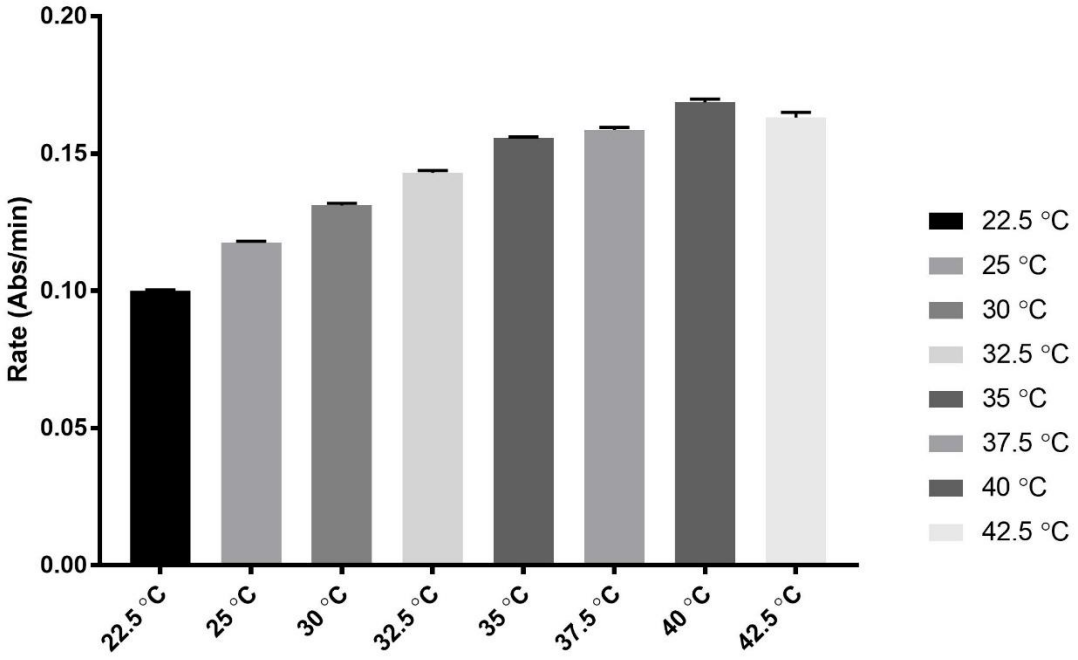

Figure 4.10 Effect of temperature on PfDFR1 activity. Enzyme activity was determined using cytochrome *c* in 0.3 ml reaction. 50 µM cytochrome *c* in 0.3 M potassium phosphate buffer pH 7.7, and 18 pmol PfDFR1 were mixed and incubated for 5 min at the assay temperature. 50 µM NADPH was added to start the reaction. The absorbance 550 nm was measured using a pate reader (VARIOSKAN, Thermo Scientific). Rates of PfDFR1 were means of three independent purifications.

4.4 Discussion

In mammalian systems, NADPH-cytochrome P450 reductase (CPR) acts as an electron donor for several partners involved in a number of biocatalytic processes. However, little is known about the PfDFR1. This chapter represents the first time that the PfDFR1 has been isolated and initially characterised *in vitro*. The spectral properties of PfDFR1 confirmed that PfDFR1 is a member of the diflavin reductase family. There are similarities in spectral peak maxima and spectral patterns between PfDFR1 and the reductase domain of other diflavin reductases (such as CPR [171, 173], NOS [248], MSR [127], and NR1[249]) in their oxidised and semiquinone forms. However, these spectral characteristics could not definitely confirm the type of PfDFR1 enzyme family.

Interestingly, the PfDFR1 semiquinone generated from reduction of the enzyme with excess NADPH under aerobic condition was unstable and reoxidised by over 50% within 4 h (Figure 4.3), while the semiquinone from human CPR (hCPR) was stable over 16 h [181, 182]. The previous reported providing evidence of rapid reoxidation by air in hCPR occurred because of flavin depletion [179] and mutations in NADPH-binding site [182]. HPLC analysis of PfDFR1 and human CPR revealed a slight difference in the protein:FAD ratios of the human and parasite enzymes, (1:1 in human and 1:0.77 in PfDFR1). The depletion of flavin cofactors in PfDFR1 may be a factor in the observed air reoxidation rate of PfDFR1 compared to hCPR.

Although PfDFR1 is structurally related to the reductase domain of other diflavin reductase members, the rate constants of PfDFR1 half reaction reveal striking difference between PfDFR1 and other family members. Under the pseudo-first -order condition, the rate constant of the first hydride transfer (fast phase) of PfDFR1 (2 s^{-1}) is slower than the rates in hCPR (20 s^{-1}) [204], rabbit CPR (28 s^{-1}) [247], rat CPR (55 s^{-1})

[250], *Artemisia annua* CPR (48 s^{-1}) [251], human MSR (24.9 s^{-1}) [252], rat nNOS (200 s^{-1}) [161], but comparable with the human NR1 (1 s^{-1}) [253]. The rate constant of second hydride transfer (slow phase) in the PfDFR1 (0.25 s^{-1}) is also slower than other diflavin reductases (3 s^{-1} in hCPR [204] and 5 s^{-1} in rabbit CPR [247]), but close to human NR1 (0.2 s^{-1}) [253] and human MSR (0.17 s^{-1}) [252].

After searching for the basis for the reduced rates of hydride transfer in PfDFR1 protein, the mutagenesis and structural studies in rat CPR have demonstrated a role for residues S457, D675, and C630 in hydride transfer from NADPH to FAD [250, 254]. Mutation in these three residues results in decreased hydride transfer rates [250]. In the PfDFR1 protein, the equivalent residues of S457 and D675 in rat CPR are T538 and E778, respectively (Figure 3.3). The absence of two of the three residues is found in the NR1 at the residue corresponding to the C630 and D675 in the rat CPR. The equivalent residues in the NR1 are A549 and E594 [111]. We believe that the lack of these key residues could explain the slow hydride transfer rates in the PfDFR1 as found in the NR1.

The optimal pH and temperature parameters of PfDFR1 obtained from this study are consistent with the physical context of the protein. Although the PfDFR1 has the highest activity at pH 7.8, the enzyme is highly active in the pH rang 6.6-8.2. Recent studies reported that the malaria parasite has a cytosolic pH around 7.15-7.3 and digestive vacuole pH around 5.18 [255, 256]. If the parasite mitochondrion pH is similar to mammalian mitochondria, which has pH 6.68-7.8 [257], localisation of PfDFR1 in this organelle would also allow for optimal activity. The temperature optimum of PfDFR1 is 40˚C corresponding to the body temperature of patients with malaria symptom (body temperature ≥ 38˚C) [258, 259] and would be consistent with a

functional role during human stages of the parasite life cycle, from normal resting temperatures up into temperatures associated with fever.

In conclusion, data from the spectral properties and HPLC analysis of the flavin content confirms that the PfDFR1 is a protein in the diflavin reductase family. PPfDFR1 pre-steady state kinetic and initial enzymatic characterisation of the protein indicate that this parasite diflavin reductase has some unique features which warrant further investigation. To this end, the next chapter will investigate PfDFR1 steady-state kinetics and inhibitor profiles for this enzyme.

CHAPTER 5

ENZYMATIC PROPERTIES OF PLASMODIUM FALCIPARUM NADPH-DEPENDENT DIFLAVIN REDUCTASE I

5.1 Introduction

NADPH-cytochrome P450 reductase (CPR) acts as an electron donor for a number of partners, including cytochrome P450 (CYPs), cytochrome *b*5, heme oxygenase and squalene monooxygenase [177]. Previous work in rat-liver microsomal fractions demonstrated the presence of CPR in both smooth and rough membranes [260, 261]. Therefore, CPR is widely used as a marker for the endoplasmic reticulum since the 1980s [260-263]. Due to the involvement of CPR in xenobiotic and antioxidant mechanisms via P450 systems, CPR is used as a biomarker for ecological pollution, especially in aquatic organisms [264, 265].

Three-dimensional structural analysis studies show that CPR is composed of four structural domains, including the FMN-binding domain, the FAD-binding domain, the NADPH-binding domain, and a "connecting" domain [117]. The general electron transfer from CPR to physiological partners occurs via the following pathway:

NADPH → FAD → FMN → Partner proteins

The connecting domain, the domain between the FMN-binding domain and the FAD/NADPH-binding domain, plays a role in positioning of two catalytic domains resulting in the optimal arrangement for electron transfer.

Elucidation of enzymatic properties is a critical aspect in CPR characterisation. Several dyes and electron accepters have traditionally been used for enzymatic characterisation purposes, including cytochrome *c*, potassium ferricyanide, tetrazolium and dichlorophenol indophenol [179, 266-268]. Cytochrome *c* and potassium ferricyanide are popular electron accepters used in the CPR activity assays owing to their distinct spectroscopic signatures.

Cytochrome *c* binds and receives electron from the FMN catalytic domain representing the diflavin reductase activity of CPR. Unlike cytochrome *c*, potassium ferricyanide accepts electron directly from the FAD/NADPH catalytic domain. Comparison of steady-state kinetic parameters from two electron acceptors bound at different CPR catalytic domains was used to explain the effect of domain modification on the enzyme activity [118, 122, 182].

PfDFR1, which have cloned and characterised in Chapter 3 and 4, has been predicted as CPR putative. In the enzymatic studies, the comparison between PFDFR1 and the well characterised enzyme such as hCPR could help us understand the special properties of the PfDFR1 enzyme.

The aim of this chapter is to undertake comparative analyses of PfDFR1 and hCPR using the described spectroscopic approaches. Specific activity and steady-state kinetic parameters of PfDFR1 and hCPR were determined using cytochrome *c* and potassium ferricyanide. The inhibition studies of both proteins with known inhibitors (2’5-ADP, NADP+, and diphenyliodonium chloride) were performed using cytochrome *c* as an electron acceptor.

5.2 Methods

5.2.1 Specific activity measurement

5.2.1.1 Cytochrome *c* – linked spectroscopic analysis

Specific activities of PfDFR1 and hCPR were measured from the change of reduced cytochrome *c* absorbance at 550 nm. The enzyme activity assay was performed in a total reaction volume of 500 µl at room temperature (18˚C to 20˚C) and the absorbance was determined using a Cary 300 UV-Visible spectrophotometer. The CPR (30 pmol PfDFR1 or 1.5 pmol hCPR) was incubated with 50 µM cytochrome *c* prepared in 0.3 M potassium phosphate buffer, pH 7.7 for 2 min. The reaction was initiated by the addition of NADPH to a final concentration of 50 µM. The absorbance at 550 nm was measured for 2 min. The activity was calculated from triplicate measurements using an extinction coefficient 21 $mM^{-1}cm^{-1}$.

Flavin cofactors (FMN and FAD) were added into the assay reaction to confirm that CPR were saturated with flavin cofactors. The CPR was incubated with FMN or FAD in 5X CPR concentration for 2 min. Then, the specific activity was measured as described above.

5.2.1.2 Potassium ferricyanide-linked spectroscopic analysis

The change of potassium ferricyanide absorbance at 420 nm was measured in a total reaction volume of 500 µl using a Cary 300 UV-Visible spectrophotometer. The CPR (30 pmol PfDFR1 or 1.5 pmol hCPR) was incubated with 1 mM potassium ferricyanide (dissolved in 0.3 M potassium phosphate buffer pH 7.7) for 2 min at room

temperature. To initiate the reaction, NADPH was added to a final concentration of 100 µM. The absorbance at 420 nm was measured over 2 min. The activity was calculated from triplicate measurements using an extinction coefficient 1.02 $mM^{-1}cm^{-1}$.

5.2.2 Steady-state kinetics

5.2.2.1 Cytochrome *c* – linked steady state analysis

The rate of change of reduced cytochrome *c* absorbance was measured as described above. For NADPH kinetics, the CPR (30 pmol PfDFR1 or 1.5 pmol hCPR) was pre-incubated with 50 µM cytochrome *c* (dissolve in 0.3 M potassium phosphate buffer pH 7.7) for 2 min at room temperature. The reaction was initiated with 0 to 100 µM NADPH for PfDFR1 or 0-150 µM NADPH for hCPR. The absorbance at 550 nm was measured as described using a Cary 300 UV-Visible spectrophotometer. The experiment was performed in triplicate. For cytochrome *c* kinetics, the NADPH concentration was kept at 50 µM. The cytochrome *c* concentrations were varied from 0 to 100 µM for PfDFR1 or 0 to 150 µM for hCPR. The basic kinetic parameters were calculated.

5.2.2.2 Potassium ferricyanide- linked steady state analysis

The rate of change in potassium ferricyanide absorbance at 420 nm was detected as described above. For NADPH kinetics, the CPR (30 pmol PfDFR1 or 1.5 pmol hCPR) was pre-incubated with 200 µM potassium cyanide for 2 min at room temperature. The reactions were initiated with different concentrations of NADPH (0 to

100 µM). The absorbance at 420 nm was measured over 2 min using a Cary 300 UV-Visible spectrophotometer at room temperature. Assay reactions were performed in triplicate for each NADPH concentration. For potassium ferricyanide kinetics, the NADPH concentration was fixed at 100 µM. The potassium ferricyanide was varied from 0 to 200 µM.

5.2.3 Inhibition measurement

The inhibition profile of PfCPR was undertaken using cytochrome *c* as an electron acceptor as described above. The compounds used in the inhibition studies are shown in Figure 5.1. A PfDFR1ssay reactions contained 30 pmol of PfDFR1, 50 µM cytochrome *c*, 0.3 M potassium phosphate buffer pH 7.7, and 2'5-ADP, NADP+, diphenyliodonium chloride, NADH, or methylene blue added at a range of concentrations and pre-incubated at room temperature for 2 min. The assay reaction was initiated by addition of 5 µM NADPH (K_m of PfDFR1). For hCPR, the protein amount used in the assay reaction was 1.5 pmol. The assay reaction was initiated by addition of 10 µM NADPH (K_m of hCPR). The experiments were performed in triplicate. The IC_{50} of each compound was calculated.

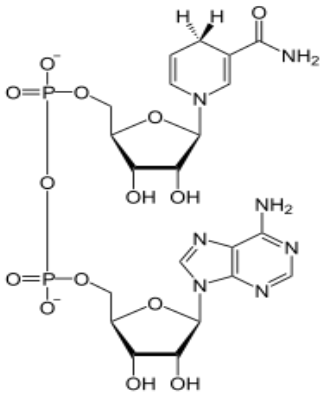

NADH

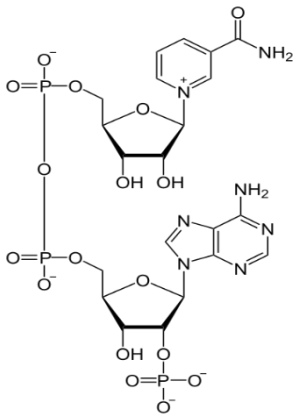

$NADP^+$

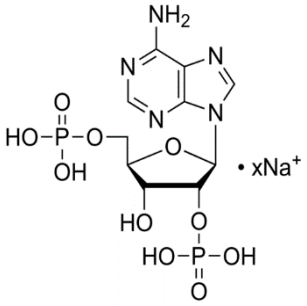

2′,5′-ADP

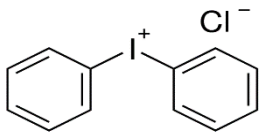

Diphenyliodonium chloride

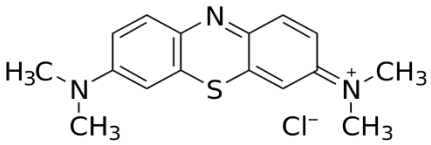

Methylene blue

Figure 5.1 Structures of compounds used in the inhibition study.

5.3 Results

5.3.1 Specific activities of PfDFR1 and hCPR

The specific activities of PfDFR1 and hCPR were measured under an optimal potassium phosphate buffer for hCPR. Using cytochrome *c* as an electron acceptor, a typical trace of reduced cytochrome *c* production measured at 550 nm is shown in Figure 5.2. The cytochrome *c* extinction coefficient (21 $mM^{-1}cm^{-1}$) was used in the enzyme activity calculation. A typical trace of a potassium ferricyanide-linked assay is shown in Figure 5.3. The enzyme activity was calculated based on the potassium ferricyanide extinction coefficient (1.02 $mM^{-1}cm^{-1}$).

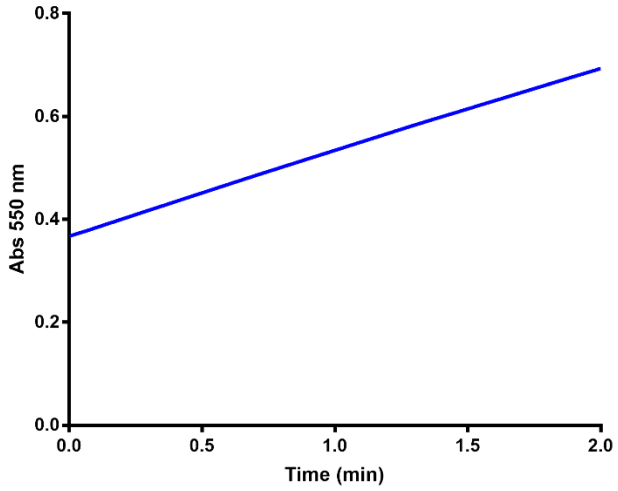

Figure 5.2. A typical trace of cytochrome *c* production from CPR catalytic reaction. In this example graph, the reaction was contained 50 µM cytochrome *c*, 30 pmol PfDFR1, 0.3 M potassium phosphate buffer pH 7.7. The reaction was initiated by adding NADPH to 50 µM. The change in absorbance at 550 nm was monitored for 2 min using a Cary 300 UV-Visible spectrophotometer at room temperature.

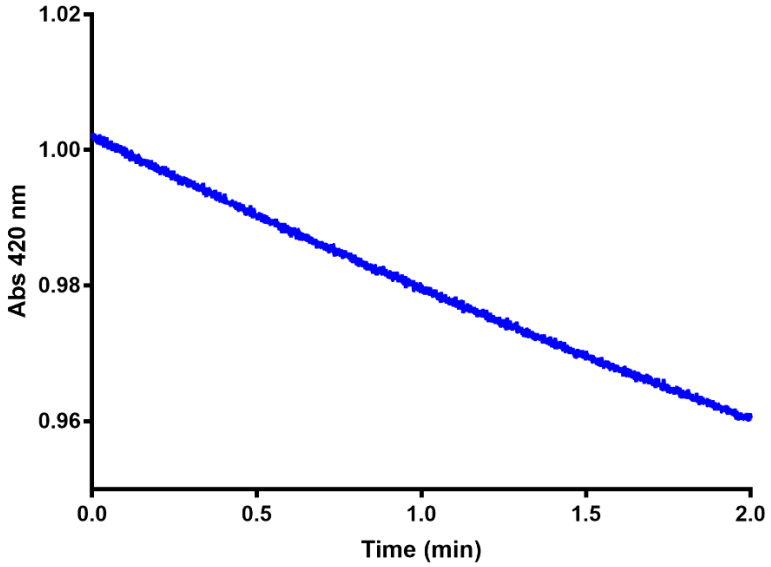

Figure 5.3. A typical trace of a potassium ferricyanide-linked CPR catalytic reaction. In this example graph, the reaction was contained 1 mM potassium ferricyanide, 30 pmol PfDFR1, 0.3 M potassium phosphate buffer pH 7.7. The reaction was initiated by adding NADPH to 100 µM. The change in absorbance at 420 nm was monitored for 2 min using a Cary 300 UV-Visible spectrophotometer at room temperature.

Specific activities of PfDFR1 and hCPR from the cytochrome *c* assay are summarised in Table 5.1. PfDFR1 and hCPR specific activities were 1.46 µmol $min^{-1}mg^{-1}$ and 34.08 µmol $min^{-1}mg^{-1}$, respectively. Although specific activity of PfDFR1 was seen to be in the range (1 to 60 µmol $min^{-1}mg^{-1}$) of identified CPRs, PfDFR1 specific activity displayed a 24-fold lower value than the value from hCPR.

The assay reactions with additional FAD and FMN were performed to confirm both CPRs were saturated with flavin cofactors. The specific activities with or without additional flavin cofactors were determined as shown in Table 5.1. In the case of PfDFR1, specific activities of PfDFR1 with 5-fold excess flavin were not significantly different from the normal reaction. Again, hCPR specific activities were not improved with additional flavin cofactors.

The fold change in specific activities determined from potassium ferricyanide and cytochrome *c* could be used for the prediction of domain affecting CPR activity. Therefore, the specific activities of PfDFR1 and hCPR using potassium ferricyanide were measured (Table 5.2). The specific activity of potassium ferricyanide reduction for PfDFR1 was 3.74 µmol $min^{-1}mg^{-1}$ while the specific activity for hCPR was 83.30 µmol $min^{-1}mg^{-1}$. The specific activity from potassium ferricyanide reduction in PfDFR1 displayed a 2.7-fold higher value than the specific activity measured from reduced cytochrome *c*. In the case of hCPR, a 2.4-fold increase in specific activity measured from potassium ferricyanide was seen. The same fold change occurred in both PfDFR1 and hCPR suggesting that the low enzyme activity of PfDFR1 is a result of the FAD/NADPH catalytic domain reaction kinetics.

Table 5.1. Specific activities of PfDFR1 and hCPR based on cytochrome *c* assay

Recombinant CPR	**Specific activity (µmol $min^{-1}mg^{-1}$)**		
	Without additional FAD and FMN	+FAD	+FMN
PfDFR1[a]	1.46 ± 0.01	1.52 ± 0.14	1.48 ± 0.11
hCPR[b]	34.08 ± 0.80	34.16 ± 1.06	35.56 ±0.58

Specific activities of each protein were determined with or without FAD ([FAD]= 5x[protein]) or FMN ([FMN]=5x[protein]). 50 µM cytochrome *c* in 0.3 M potassium phosphate buffer pH 7.7 was reduced by 30 pmol PfDFR1 or 1.5 pmol hCPR. 50 µM NADPH was added to start the reaction. The absorbance 550 nm was measured using a Cary 300 UV-Visible spectrophotometer at room temperature.

[a] Specific activities from PfDFR1 were means of three independent purifications.

[b] Specific activities from hCPR were means of three measurements from one preparation.

Table 5.2. Specific activities of PfDFR1 and hCPR based on potassium ferricyanide assay

Recombinant CPR	Specific activity (μmol $min^{-1}mg^{-1}$)
PfDFR1	3.74 ± 0.08
hCPR	83.30 ± 0.79

Specific activities of PfDFR1 and hCPR were determined using potassium ferricyanide as described in the method section and were means of three measurements. 1 mM potassium ferricyanide in 0.3 M potassium phosphate buffer pH 7.7 was reduced by 30 pmol PfDFR1 or 1.5 pmol hCPR. 100 μM NADPH was added to start the reaction. The absorbance 420 nm was measured using a Cary 300 UV-Visible spectrophotometer at room temperature.

5.3.2 Steady-state kinetics

To investigate the difference in basic enzymatic properties between PfDFR1 and hCPR, steady-state kinetics were carried out with cytochrome *c* and potassium ferricyanide.

5.3.2.1 Cytochrome *c*

Both PfDFR1 and hCPR exhibited Michaelis–Menten behaviour with respect to the dependence of the initial cytochrome *c* reduction rate on the concentration of NADPH (NADPH kinetics) and cytochrome *c* (cytochrome c kinetics). The K_m and k_{cat} values are shown in Figure 5.4 for PfDFR1 and Figure 5.5 for hCPR. Flavin content and steady-state kinetic parameters are shown in Table 5.3. The k_{cat} for PfDFR1 with respect to NADPH (130.10 ± 1.66 min^{-1}) and cytochrome *c* (133.10 ± 3.80 min^{-1}) were approximately 25- and 26-fold lower than the k_{cat} values for hCPR. The apparent

K_m^{NADPH} (5.72 ± 0.27 µM) and $K_m^{cyt\ c}$ (4.58 ± 0.51 µM) values for PfDFR1 were around 2- and 5-fold lower than hCPR K_m values, respectively.

A

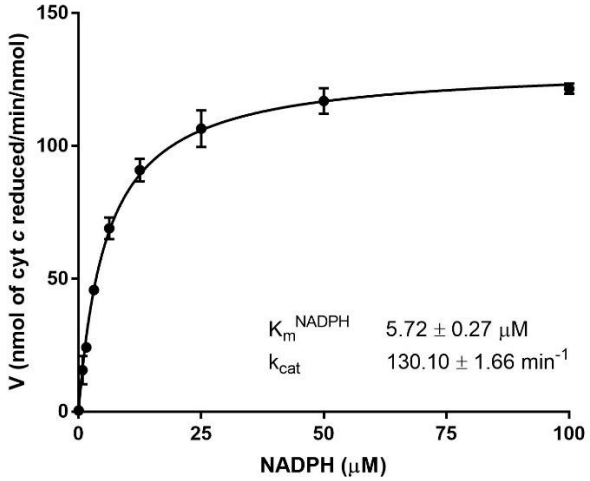

B

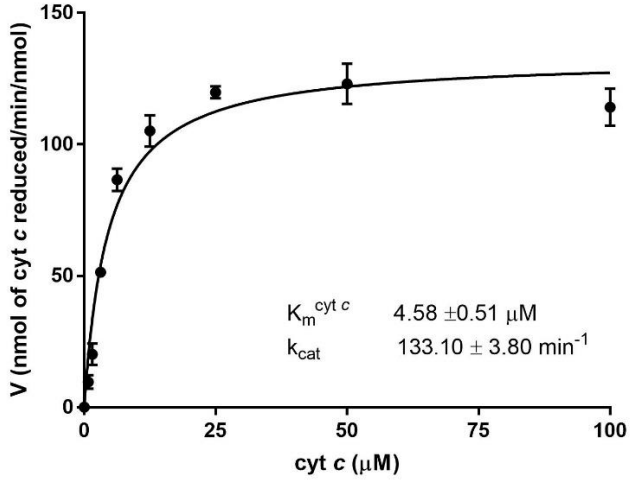

Figure 5.4 Kinetic analysis of PfDFR1 from the cytochrome *c* assay. A) NADPH kinetics. NADPH was test in the range 0 - 100 µM while cytochrome *c* was kept at 50 µM. B) Cytochrome *c* kinetics. Cytochrome *c* was varied in the range 0 - 100 µM while NADPH was kept at 50 µM. The reaction was performed in 0.3 M potassium phosphate buffer pH 7.7 at room temperature. 30 pmol PfDFR1 was used in the assay. Rates were means of four measurements from two independent purifications.

A

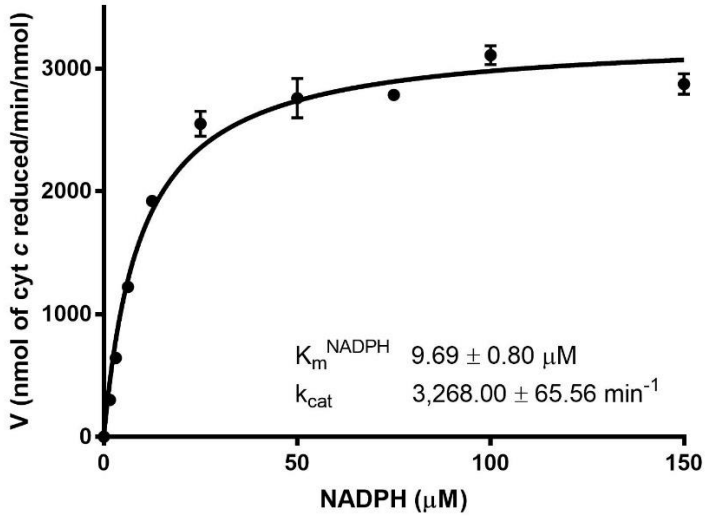

B

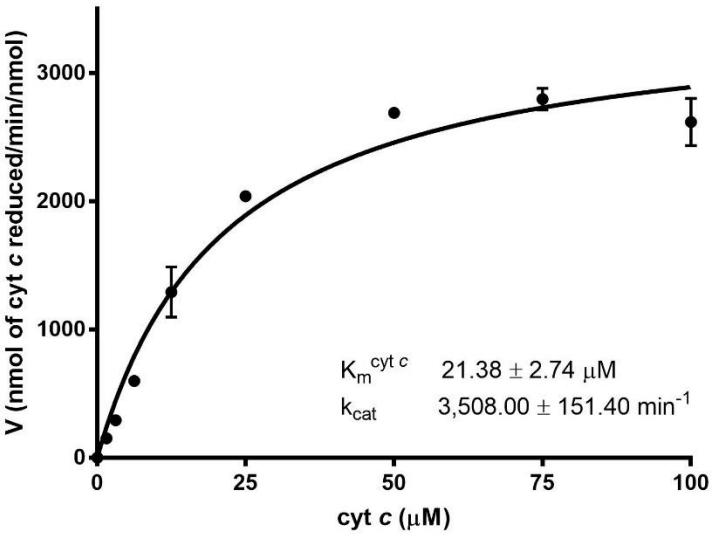

Figure 5.5 Kinetic analysis of hCPR from the cytochrome *c* assay. A) NADPH kinetics. NADPH was varied from 0 - 150 μM while cytochrome *c* was kept at 50 μM. B) Cytochrome *c* kinetics. Cytochrome *c* was varied in the range 0 - 100 μM. NADPH was kept constant at 50 μM. The reaction took place in 0.3 M potassium phosphate buffer pH 7.7 with 1.5 pmol hCPR at room temperature. Rates were means of three measurements.

Table 5.3 Steady-state kinetic parameters of PfDFR1 and hCPR from the cytochrome *c* assay

Recombinant CPR	Flavin content		K_m (µM)		k_{cat} (min^{-1})	
	[FMN]/ [protein]	[FAD]/ [protein]	NADPH	Cyt *c*	NADPH	Cyt *c*
PfDFR1	1.14 ±0.15	0.77 ± 0.20	5.72 ± 0.27	4.58 ± 0.51	130.10 ± 1.62	133.10 ± 3.80
hCPR	1.17 ±0.02	1.00 ± 0.02	9.69 ± 0.80	21.38 ± 2.74	3,268.00 ± 65.56	3,508.00 ± 151.40

5.3.2.2 Potassium ferricyanide

PfDFR1 and hCPR also exhibited Michaelis–Menten behaviour for the dependence of the potassium ferricyanide reduction with respect to the concentration of NADPH (NADPH kinetics) and potassium ferricyanide (potassium ferricyanide kinetics). The K_m and k_{cat} for PfDFR1 and hCPR are shown in Figure 5.6 and Figure 5.7, respectively. Kinetic parameters and flavin content are summarised in Table 5.4. PfDFR1 displayed a lower k_{cat} than hCPR, with an approximately 15- and 13-fold reduction measured with NADPH and potassium ferricyanide, respectively. The K_m^{NADPH} for PfDFR1 (13.19 ±1.17 µM) was slightly higher than the K_m^{NADPH} for hCPR (11.55 ±1.15 µM), this was not statistically significantly different between the two CPRs. The $K_m^{ferricyanide}$ for PfDFR1 showed a 2-fold higher value than the $K_m^{ferricyanide}$ value for hCPR.

A

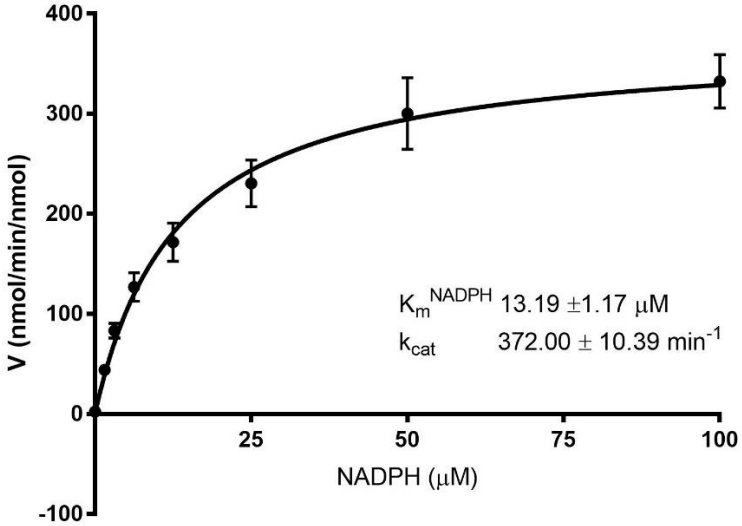

B

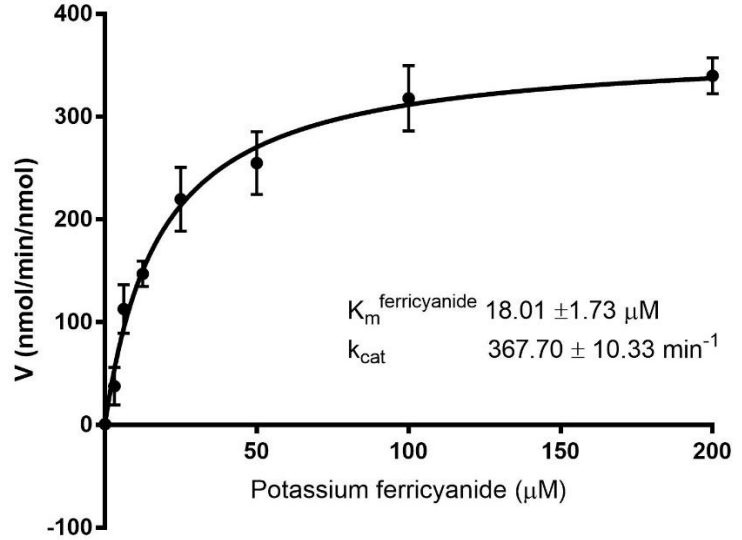

Figure 5.6 Kinetic analysis of PfDFR1 from the potassium ferricyanide assay. A) NADPH kinetics. NADPH was test in the range 0 - 100 μM. Potassium ferricyanide was kept constant at 200 μM. B) Potassium ferricyanide kinetics. Potassium ferricyanide was in various concentrations from 0 - 200 μM. NADPH was kept at 100 μM. The reaction was done at room temperature in 0.3 M potassium phosphate buffer pH 7.7. 30 pmol PfDFR1 was used in the assay. Rates were means of six measurements from two independent purifications.

A

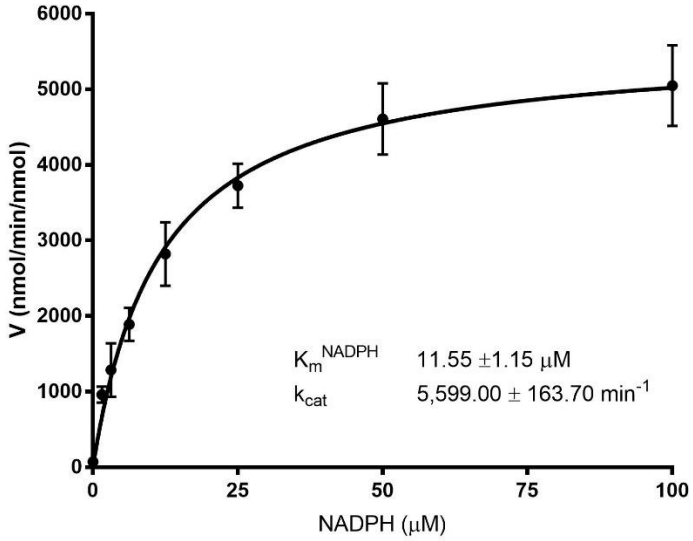

B

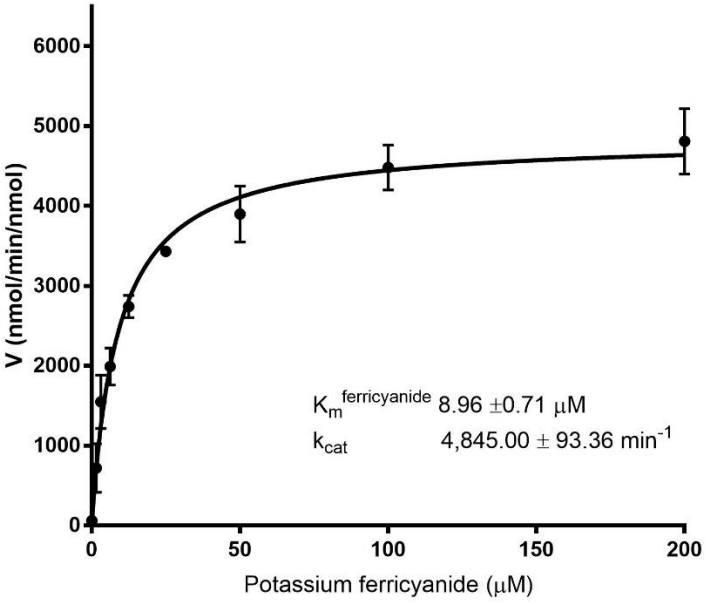

Figure 5.7 Kinetic analysis of hCPR from the potassium ferricyanide assay. A) NADPH kinetics. NADPH was varied from 0 - 100 μM, and potassium ferricyanide was kept constant at 200 μM. B) potassium ferricyanide kinetics. Potassium ferricyanide was varied in the range 0 - 200 μM while NADPH was kept at 100 μM. The reaction was performed with 0.3 M potassium phosphate buffer pH 7.7 and 1.5 pmol hCPR. Rates were means of six measurements from two independent experiments.

Table 5.4 Steady-state kinetic parameters of PfDFR1 and hCPR from the potassium ferricyanide assay

Recombinant CPR	Flavin content		K_m (μM)		k_{cat} (min^{-1})	
	[FMN]/ [protein]	[FAD]/ [protein]	NADPH	Potassium ferricyanide	NADPH	Potassium ferricyanide
PfDFR1	1.14 ± 0.15	0.77 ± 0.20	13.19 ±1.17	18.01 ±1.73	372.00 ± 10.39	367.70 ± 10.33
hCPR	1.17 ± 0.02	1.00 ± 0.02	11.55 ±1.15	8.96 ± 0.71	5,599.00 ± 163.70	4,845.00 ± 93.36

Flavin cofactors (FMN and FAD) are important for electron transfer in CPRs. Losing flavin cofactors leads to a loss of CPR catalytic activity (Table 5.3 to 5.4). Flavin contents of PfDFR1 and hCPR were determined. The deficiency of FAD in PfDFR1 was observed, with approximately 23% of FAD lost when compared to hCPR. The kinetic parameters were re-calculated using the FAD amount instead of the CPR amount (Table 5.5). When the reduced FAD cofactor is considered, there is a slight change in PfDFR1 kinetic parameters. The K_m values were the same as the K_m calculated from the CPR values. However, the k_{cat} values of PfDFR1 in both cytochrome *c* and potassium ferricyanide assays were increase by around 30% compared with the k_{cat} calculated from the total protein amount. The fold change in k_{cat} between PfDFR1 and hCPR was improved. From the cytochrome *c* assay, the k_{cat} values for PfDFR1 were improved from around 25-fold to 20-fold lower than the k_{cat} in hCPR. For the potassium ferricyanide assay, the k_{cat} values for PfDFR1 were improved from around 15-fold to 10-fold lower than the k_{cat} in hCPR.

Table 5.5 Steady-state kinetic parameters of PfDFR1 and hCPR calculated relative to FAD content.

Recombinant CPR	Flavin content		k_{cat} (min^{-1})			
			Cytochrome *c*		Potassium ferricyanide	
	[FMN]/ [protein]	[FAD]/ [protein]	NADPH	Cyt *c*	NADPH	Potassium ferricyanide
PfDFR1	1.14 ±0.15	0.77 ± 0.20	169.09 ± 1.1	172.85 ± 6.98	483.11± 17.35	476.68 ± 20.47
hCPR	1.17 ±0.02	1.00 ± 0.02	3,268.00 ± 65.56	3.508.00 ± 151.40	5,599.00 ± 163.70	4,845.00 ± 93.36

5.3.3 Inhibition studies

To investigate the different inhibition sensitivities between PfDFR1 and hCPR, three known CPR inhibitors ($NADP^+$, 2′,5′-ADP, and diphenyliodonium chloride) were used in the inhibition study. The structures of the inhibitor compounds are shown in Figure 5.1. $NADP^+$ and 2′,5′-ADP are nucleotide analogues of NADPH. $NADP^+$ and 2′,5′-ADP can compete with NADPH to bind to the NADPH binding site. Diphenyliodonium chloride is a CPR irreversible inhibitor. Diphenyliodonium chloride was proposed to inhibit CPR via the covalent modification of FMN [269, 270]

The inhibition potential of the three inhibitors for PfDFR1 and hCPR are shown in Figure 5.8 and Figure 5.9, respectively. The concentration of each test compound which inhibit 50% of enzyme activity (IC_{50}) was calculated as shown in Table 5.6.

2′,5′-ADP is the most effective inhibitor for both PfDFR1 and hCPR. The IC_{50} values of 2′,5′-ADP for PfDFR1 and hCPR were 1.9 $\pm$ 0.2 µM and 21.3 $\pm$ 2.4 µM,

respectively. Compared between two CPRs, PfDFR1 was more sensitive to 2′,5′-ADP than hCPR based with a 10-fold difference in their IC_{50} values.

$NADP^+$ is another inhibitor that inhibits both CPRs. The IC_{50} values of $NADP^+$ were 34.7 $\pm$ 5.5 μM for PfDFR1 and 51.1 $\pm$ 6.0 μM for hCPR. Again, PfDFR1 also displayed more sensitivity to $NADP^+$ than hCPR, with a 2.5-fold lower IC_{50} than hCPR.

Diphenyliodonium chloride was previously reported as the least potent inhibitor among the three compounds (2′,5′-ADP, 2′,5′-ADP, and diphenyliodonium chloride) in hCPR [171]. The same trend was observed in this study. Interestingly, the PfDFR1 had a difference in the diphenyliodonium chloride inhibition trend compared with hCPR. Up to 5 mM of diphenyliodonium chloride was used in the inhibition assay, but no reduction in the PfDFR1 activity was observed.

NADH was also included in the inhibition study. The IC_{50} curves for PfDFR1 and hCPR are shown in Figure 5.8 and Figure 5.9. Both PfDFR1 and hCPR were not inhibited by NADH, although up to 10 mM and 5mM NADH were tested in hCPR and PfCPR inhibition studies, respectively.

Methylene blue was another compound tested in the PfDFR1 inhibition study. The IC_{50} curve for PfDFR1 is shown in Figure 5.8. The results demonstrate that methylene blue does not inhibit the cytochrome *c* reduction via PfDFR1 at concentrations lower than 100 μM.

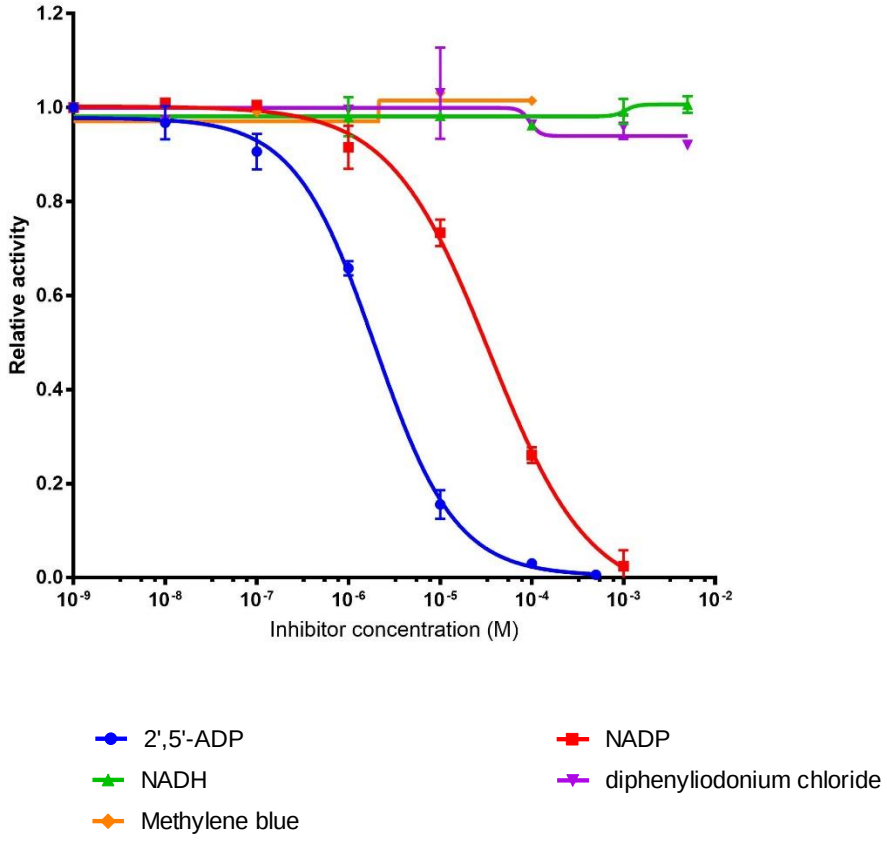

Figure 5.8 IC_{50} curve of PfDFR1 with test compounds. The inhibition study was done as described in the method section. The assay was done with 30 pmol of PfDFR1, 50 µM cytochrome *c*, and 0.3 M potassium phosphate pH 7.7 buffer. The concentration of NADPH was kept at the K_m^{NADPH} value (5 µM). Rates from assays with test compounds were normalised to rates without additional compounds. Six measurements from two independent preparations were used in the calculation.

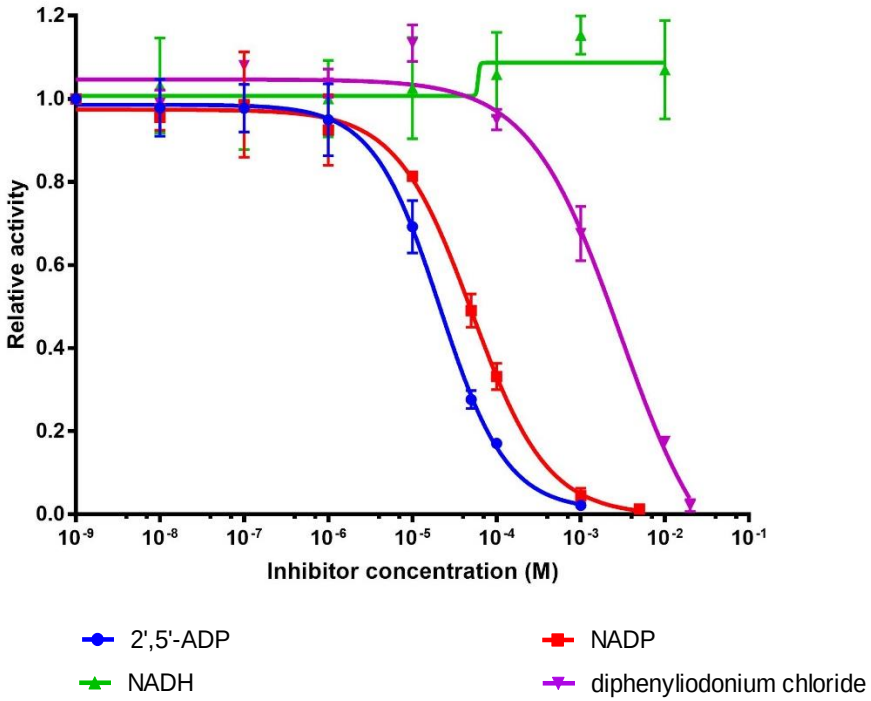

Figure 5.9 IC_{50} curve of hCPR with test compounds. The inhibition study was done as described in the method section. The assay was done with 1.5 pmol of hCPR, 50 µM cytochrome *c*, and 0.3 M potassium phosphate pH 7.7 buffer. 10 µM NADPH which corresponded to hCPR K_m^{NADPH} value were used in the assay. Rates were means from three measurements and were normalised to rates without additional compounds.

Table 5.6 Inhibition of the cytochrome c reduction by nucleotide analogues and diphenyliodonium chloride (DPIC)

Compound	IC_{50} (µM)	
	PfDFR1	hCPR
2′,5′-ADP	1.9 ± 0.2	21.3 ± 2.4
$NADP^+$	34.7 ± 5.5	51.1 ± 6.0
NADH	N/A[a]	N/A
Diphenyliodonium chloride	N/A	2,917 ± 1,787
Methylene blue	N/A	N/D[b]

[b] N/A is not applicable.

[a] N/D is not done.

5.4 Discussion

NADPH-cytochrome P450 reductase (CPR), a member of the diflavin reductase family, plays a crucial role in several organisms by providing electrons to partner proteins such as P450s. P450s are the major enzymes involved in detoxification of the toxic compounds. Therefore, P450s were proposed to be involved in drug and insecticide resistance [271, 272]. With the critical function, as P450s partner, CPR has been considered as a novel target for synergist development [273, 274]

Unlike other organisms, cytochrome P450s have not been identified in the malaria parasite. The exact role and enzymatic properties of PfDFR1 has not been reported, but PfDFR1 is reported as an essential gene in both *P. berghei* [275] and *P. falciparum* [208]. Characterisation of the malaria CPR-like and comparative analyses with other diflavin reductases such as hCPR is an important first step in elucidating the biological function of this enzyme and it's potential as a drug target. This chapter describes steady state analysis of PfDFR1 and hCPR reporting on measured PfDFR1specific substrate activities and inhibition profiles.

The direct comparison of enzymes in the diflavin reductase family (Table 5.7) reveal the variation in the enzymatic activity of this enzyme family (based on cytochrome *c* reduction). The activity of PfDFR1 is 5 to 100-fold lower than published wild-type or N-terminus truncated CPRs. The PfDFR1 activity is close to the rat neuronal NOS and also compares closely to the slow turnover of a number of enzymes including MSR [127] and NR1 [111]. However, the cytochrome *c* reduction should not be regarded as a real turnover number with its physiological electron acceptor. The commercial cytochrome *c* is usually prepared from equine heart mitochondria which is

a physiological electron acceptor for endoplasmic reticulum or bacteria diflavin reductases.

Table 5.7 Comparison of k_{cat} from the diflavin reductases in the cytochrome *c* reduction

Organism	Protein	k_{cat} (min^{-1})	Reference
P. falciparum	CPR-like	133	This study
Human	CPR	3,508	This study
Rat	CPR wt CPR S596D CPR R597M CPR K602W CPR W677A CPR R597M/K602W CPR R597M/W677A CPR K602W/W677A	3,280 140 2,980 1,110 38 2,830 468 77	[131]
Human	CPR CPR W679H CPR W679A	4,082 453 10	[182]
Human	CPR CPR R457H CPR V492E	2,385 748 13	[118]
A. gambiae	CPR	6,300	[171]
M. domestica	CPR	3,024	[276]
C. annuum	CPR	2,740	[277]
A. thaliana	CPR (ART1) CPR (ART2)	12,780 840	[278]
Yeast	CPR	12,000	[278]
S. typhimurium	SiR (sulphite reductase)	9,200	[114]
E. coli	SiR	3,000	[279]
B. megaterium	P450BM3	3,531	[280]
B. megaterium	P450BM3	2,628	[281]
Mouse	NOS	3,100	[282]
Human	iNOS CaM^- (deleted CaM binding domain) iNOS CaM^+	3,000 3,000	[166]
Nouse	iNOS CaM^- iNOS CaM^+	2,800 1,200	[166]
Rat	nNOS CaM^- nNOS CaM^+	360 210	[166]
Human	MSR	34	[127]
Human	NR1	78	[111]

Interestingly, the results here show that hCPR is much more active (over 20-fold) than PfDFR1 with both cytochrome *c* and potassium ferricyanide assays. The flavin content of PfDFR1 and hCPR were determined (Table 5.3). The protein:FMN:FAD contents were 1:1.4:0.77 for the PfDFR1 compared to 1:1.17:1 for the hCPR. However, the addition of flavin cofactors (FMN and FAD) did not restore the PfDFR1 activity (Table 5.1). One possibility could be the short incubation time that were insufficient to allow flavin cofactors to bind adequately to their binding pocket.

Key residues in the catalytic domains could be another factor affecting the enzyme catalytic activity. Focussing on the FAD/NADPH domain, key residues involved in NADPH binding are conserved between PfDFR1 and hCPR (Table 5.8: highlighted in orange). Mutation in the hCPR NADPH binding domain (W679H and W679A) significantly decreased its catalytic activity [182]. A decrease in enzyme catalytic activity was also observed in the rat CPR with mutation in the FAD/NADPH domain (S596D, R597M, K602W, W677A) [131].

In the FAD-binding domain, some residues that have an impact on FAD binding are not conserved in PfDFR1 (Table 5.8: highlighted in green). In hCPR, R457 and V492 are important for FAD binding. The effect of mutations in these residues (R457H and V492E) were reported in hCPR [118]. Mutated hCPR proteins were reported to have lost their FAD: protein content (over 65% in R457H and over 95% in V492E) and their enzymatic activities (over 60% in R475H and over 99% in V492E). However, both residues are not conserved in PfDFR1. Other residues (including R427, S460, I474, V477, and A493 in hCPR) are also not conserved in the PfDFR1 protein compared with that in other organisms. The docking results (Fig. 5.10) show that FAD

is not docked in the same position as the FAD in the hCPR structure. This could be a possible reason that explains the low enzymatic activity of the PfDFR1 protein compared with hCPR.

Table 5.8 Comparison of key residues involved in FAD (green colour) and NADPH (yellow colour) interaction

hCPR	AgCPR	sCPR	rCPR	PfDFR1
R427	R427	F406	R424	M505
R457	R457	R439	R454	K535
Y459	H459	Y441	Y456	Y537
S460	S460	S442	S457	T538
C475	T475	T457	C472	T553
V477	V477	I459	V474	K555
Y481	Y481	F463	Y478	Y559
V492	V492	V477	V489	L571
A493	A493	T478	A490	K572
S599	S597	R611	S596	S705
R600	R598	L612	R597	R706
K605	K603	K617	K602	K711
Y607	Y605	Y619	Y604	Y713
W679	W679	W691	W677	W780

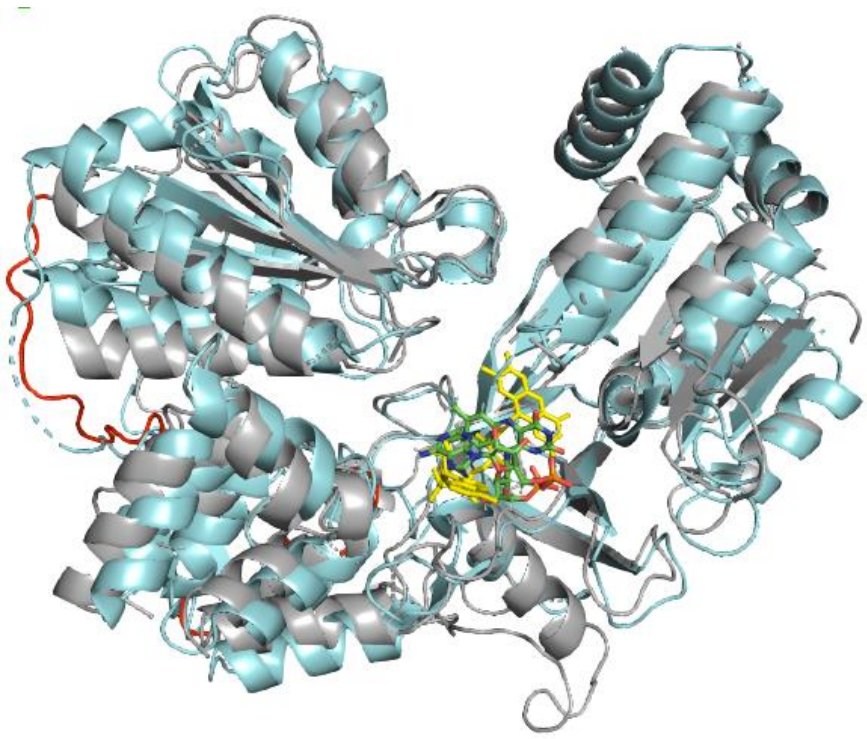

Figure 5.10 Docking of FAD in the predicted PfDFR1 model. The predicted PfDFR1 model (grey colour) was done by Phyre[2]. The PDB of wild-type hCPR structure (cyan colour) is 3qe2. FAD docking in PfDFR1 was done by Swiss Dock. FAD in the hCPR structure is shown in yellow. Docking of FAD in PfDFR1 is shown in green (Energy: 43.2, Full Fitness: -5820.5) The predicted linker loop in PfDFR1 is shown in red.

The effect of the hinge loop (linking the FAM catalytic domain to the FAD/NADPH domain) on the rate of electron transfer in the CPR and NOS has been reported [122, 283-285]. Both lengthening the hinge loop and mutations in the hinge loop affect CPR and NOS activity [122, 284, 285]. The alignment indicates that the 12 amino acid residues in the hinge loop (G232 to R243 in rat protein) of CPR are highly conserved in mammals and insects (Figure 5.11). However, the hinge loop in PfDFR1 (Figure 5.11 and red colour in Figure 5.10) is not conserved with other CPRs with the parasite enzyme having a longer hinge loop (with 19 amino acids plus) than hCPR. In NOS enzymes, the hinge loop (23 to 25 amino acids) has a varied sequence composition

among isoforms (Figure 5.12) [285]. Compared with NOSs, it is 6 to 8 amino acids longer in PfDFR1 and the sequence is not conserved to any NOS isoforms. In hNR1, the hinge loop is 31 amino acids predicted from a 3D-modelling done by Phyre[2]. Compared with hNR1, there are similar in length between PfDFR1 and hNR1 hinge loops, but the sequences are not conserved (Figure 5.13). The hinge loop in PfDFR1 is also unique when compared with the hinge loop of other diflavin reductases such as the MRS hinge loop (80 amino acids) [121]. It is reasonable to think that the unique linker loop in PfCPR could affect the conformational behaviour of the enzyme which in turn may have an impact on electron transfer and catalysis PfDFR1.

```
PF3D7_0923200(PfDFR1)     LPKLLNMKNIPIYVPKEDIIELTSWRDMAEIKLDIQYYDHLIEEDNKKEKNVVTENIINE 266
S. cerevisiae              LKDELHLDEQEAK-------------------FTSQFQYTVLNEIT-D-SVSLGEPSAH 244
H. sapiens                 VCEHFGVEATGEE-------------------SSIRQYELVVHTDIDAA-KVYMGEM--- 266
R. norvegicus              VCEFFGVEATGEE-------------------SSIRQYELVVHEDMDVA-KVYTGEM--- 263
A. gambiae                 VCDYFGIESTGED-------------------VLMRQYRLLEQPDVSAD-RIYTGEV--- 266
D. melanogaster            VCDHFGIEGGGEE-------------------VLIRQYRLLEQPDVQPD-RIYTGEI--- 267
```

Figure 5.11 Alignment of the hinge loop with known CPR enzymes. *P. falciparum* PF3D7_0923200, *S. cerevisiae* (ONH80480.1), *R. norvegicus* (NP_113764.1), *H. sapiens* (NP_000932.3), *A. gambiae* (AAO24765.1) and *D. melanogaster* (NP_477158.1). The linker loop of each organism is highlight in yellow based on *R. norvegicus* (rat) protein.

```
PF3D7_0923200(PfDFR1)     NIYHDFEVWKNKFFMQLPKLLNMKNIPIY-V-PKEDIIELTSWRDMAEIKLDIQYYDHLI        248
Mouse-iNOS                GQEDAFRSWAVQTFRAACETFDVRSKHHIQ--IPKRFTSNATWEPQQ---YRLIQ-----        594
Rat-nNOS                  GQEEAFRTWAKKVFKAACDVFCVGDDVNIEKANNSLISNDRSWKRNK---FRLTY-----       1007
Human-eNOS                GQEEAFRGWAQAAFQAACETFCVGEDAKA--AARDIFSPKRSWKRQR---YRLSA-----        739
Rat-eNOS                  GQEEAFRGWAQAAFQAACETFCVGEDAKA--AARDIFSPKRSWKRQR---YRLST-----        738
                          .  . *. *    *    . : : .         . :    :*.       :
```

Figure 5.12 Alignment of the hinge loop with known NOS enzymes. *P. falciparum* PF3D7_0923200, *M. musculus* iNOS (NP_001300850.1), *R. norvegicus* nNOS (NP_434686.1), *H. sapiens* eNOS (NP_000594.2), and *R. norvegicus* eNOS (NP_068610.1). The linker loop of each organism is highlight in yellow based on *R. norvegicus* (rat nNOS) protein.

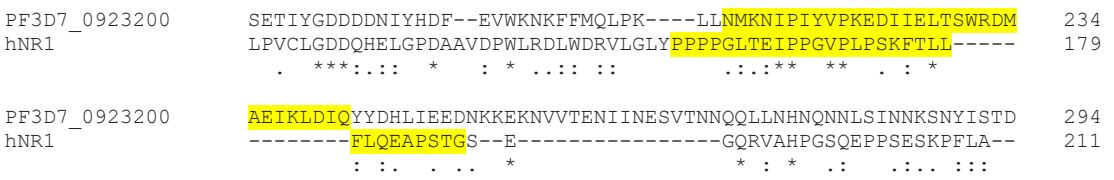

Figure 5.13 Alignment of the hinge loop with human NR1. *P. falciparum* PF3D7_0923200 and human NR1 (Q9UHB4). The linker loop of each organism is highlight in yellow based on predicted 3D models.

Differences between the parasite enzyme and human CPRs also extends to the inhibition profile. PfDFR1 is more sensitive to $NADP^+$ (1.5-fold) and 2′,5′-ADP (10-fold) than hCPR. Diphenyliodonium chloride (up to 5 mM) cannot inhibit PfDFR1, while it can inhibit hCPR. Based on the diphenyliodonium chloride mode of action, it could be due to different protein structures between both enzymes especially in the FMN binding pocket. The difference in PfDFR1 could prevent the interaction between diphenyliodonium chloride and FMN leading to the blocking of FMN covalent modification via diphenyliodonium chloride. Clearly a three-dimension crystal structure of PfDFR1 will be important for a deeper understanding of the mechanisms underpinning these functional differences.

In conclusion, steady-state kinetic analyses including substrate and inhibitor profiles were determined for the *P. falciparum* essential diflavin reductase PfDFR1. The measured data reported herein, reveal key differences between the malaria parasite and human enzymes. Analyses of primary sequence data and of homology structure-based models point to differences in the hinge-loop region of the enzyme – directing future site-directed mutagenesis and structural studies to confirm the impact of manipulations in this region of the enzyme PfDFR1.

CHAPTER 6

A ROLE FOR NADPH-CYTOCHROME P450 REDUCTASE IN THE MECHANISM OF ACTION OF PRIMAQUINE

6.1 Introduction

Primaquine (PQ) is one of the two antimalarial drugs approved by the FDA for the treatment of relapse malaria on account of efficacy against the dormant hypnozoites stages of *P. vivax* and *P. ovale.* Another important therapeutic effect of PQ is the ability to kill mature gametocytes. On account of its gametocidal activity, PQ has been recommended by the WHO for use as a single low dose PQ (25 mg/ml) for malaria transmission blocking [36].

PQ is an 8-aminoquinoline member which has a methoxy group and the amino sidechain at position 6 and 8, respectively. PQ itself is a pro-drug that needs biotransformation to active metabolites. The proposed mechanism of action of PQ is shown in Figure 6.1. The core structure and properties of PQ allow them to be metabolically activated by cytochrome P450 enzymes (CYPs) in the human liver to species active against hypnozoites [95, 97]. A link between drug efficacy and metabolism through CYPs, specifically CYP2D6, is supported by recent animal and clinical studies, including the association of CYP2D6 poor metaboliser phenotype status with primaquine failure in human malaria infections with *P. vivax* [100].

Other than the requirement of CYP2D6 metabolism, the exact mechanism of action of PQ is not known. Several research groups have investigated and studied the oxidative and haemolytic potential from hydroxylated PQ metabolites (OH-PQms) [93, 94]. The result from these studies, including those using proof-of-concept enzymes such as spinach ferrodoxin oxidoreductase, show that H_2O_2 can be released by the redox cycling of OH-PQm. However, the identity of parasite or host enzymes that could be involved in these reactions in malaria infected patients is unknown [93, 97].

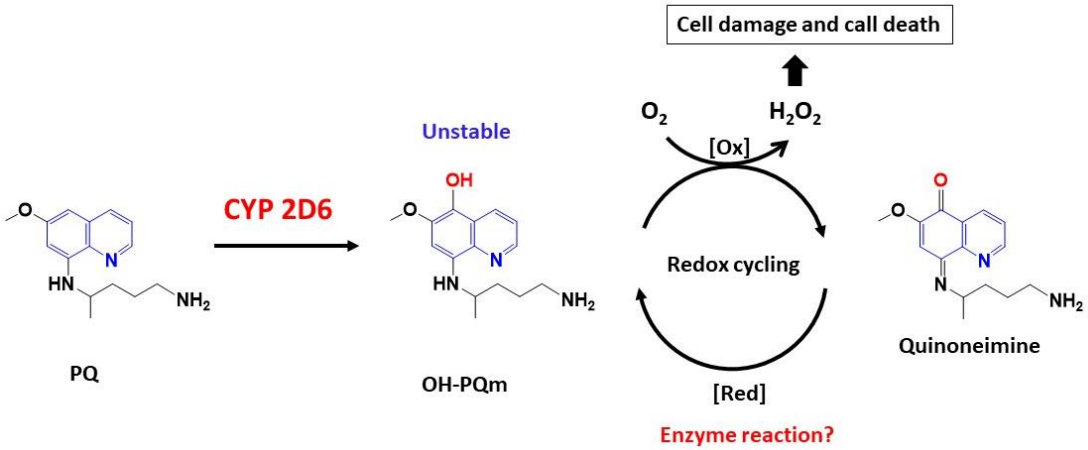

Figure 6.1 The proposed mechanism of action of PQ.

Furthermore, the factors that drive the stage-specificity of PQ also remain unknown. Circulating OH-PQm levels after low single dose treatments are in the low nM level yet the drug displays exquisite potency against gametocytes, why?

The focus of this chapter is to investigate the ability of recombinant CPRs (PfDFR1 and hCPR) to complete the redox cycling of key PQ derivatives (5-HPQ, 5,6-DPQ, PQQI, 6OHPQQI, CPQ, and PQ) and related 8-aminoquinoline compounds (SL-6-41, SL-6-46, SL-6-56, and TQ). The steady-state reaction kinetics of each compound with PfDFR1 and hCPR were studied. The production of H_2O_2 from CPR-mediated redox cycling of PQ derivatives was determined. In addition, the ability of PQ derivatives to generate H_2O_2 in bone marrow cells was studied and compared with red blood cells to address the research question regarding the potent efficacy and selectivity against specific parasite stages.

6.2 Materials and methods

6.2.1 PQ derivatives

Structure and molecular weight of PQ derivatives and the related 8-aminoquinolines used in this experiment are shown in Table 6.1 and Figure 6.2. The PQ metabolites (5-HPQ, 5,6-DPQ, PQQI, 6OHPQQI) and 8-aminoquinolines (SL-6-41, SL-6-46, SL-6-56) were synthesised in the Chemistry Department by Prof Paul O'Nell group, University of Liverpool, UK.

Table 6.1 PQ derivatives and 8-aminoquinolines used in the experiments

Compound name	Molecular weight (g/mol)	Solvent
PQ diphosphate (PQ)	455.3	50% MeOH
5-HPQ	275.35	50% MeOH
5,6-DPQ	261.33	50% MeOH
PQQI	273.33	50% MeOH
6OHPQQI	259.30	50% MeOH
Carboxy PQ (CPQ)	274.32	DMSO
SL-6-41	275.35	DMSO
SL-6-46	261.33	DMSO
SL6-56	273.35	DMSO
Tafenoquine (TQ)	581.58	50% MeOH

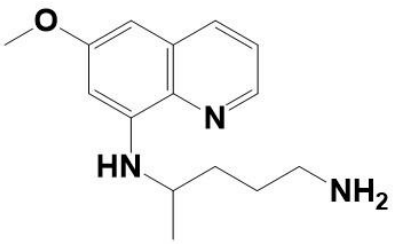

PQ (PQ)

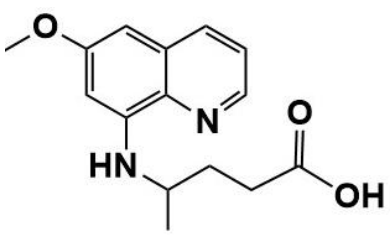

Carboxy PQ (CPQ)

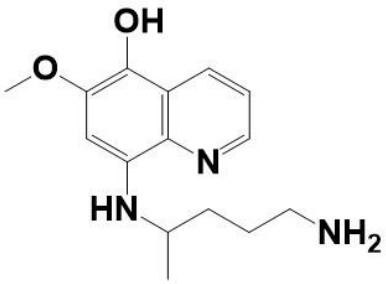

5-hydroxy-PQ (5-HPQ)

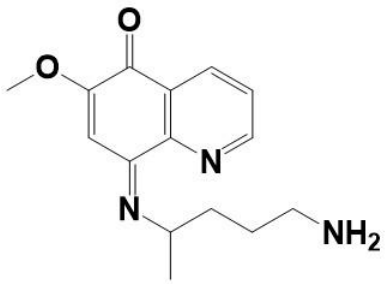

5-quinoneimine (PQQI)

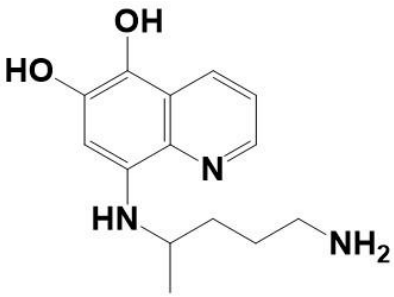

5,6-dihydroxy-PQ (5,6-DPQ)

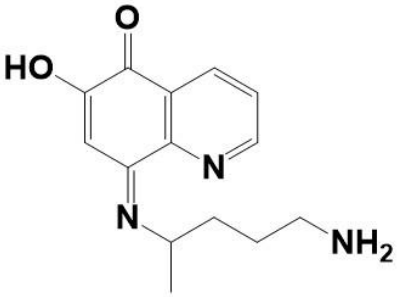

6-hydroxy-5-quinoneimine (6OHPQQI)

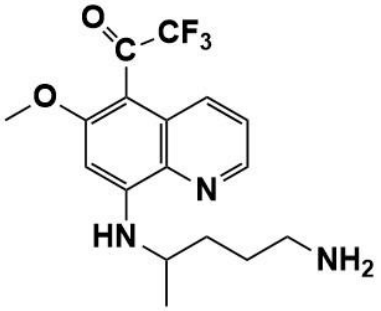

SL-6-41

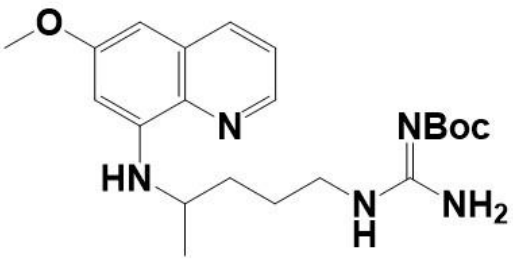

SL-6-46

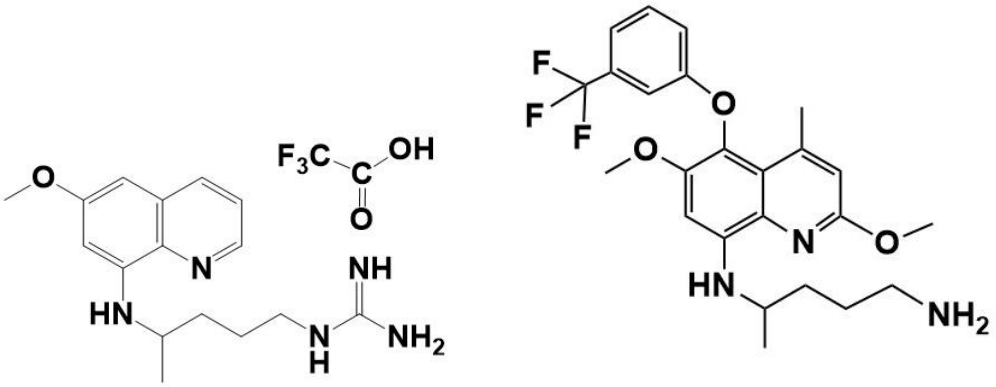

SL-6-56 **Tafenoquine (TQ)**

Figure 6.2 PQ derivatives and 8-aminoquinolines chemical structures.

6.2.2 Steady-state kinetics of PfDFR1 and hCPR

Recombinant CPR mediated-consumption of NADPH was determined by monitoring the change in absorbance at 340 nm on a microplate spectrophotometer (Thermo Electron Varioskan). The purified PfDFR1 was prepared as described in section 3.2.6 and the purified hCPR was obtained from Dr. Mark Paine (LSTM).

For PfDFR1, the assay comprised of 0.3 ml contained 0.3 M potassium phosphate (pH 7.7), 200 nM PfDFR1, 100 µM NADPH, and a range of concentrations of the PQ derivatives and analogues (0 to 100 µM 5-HPQ, 0 to 25 µM 5,6-DPQ, 0 to 25 µM 6OHPQQI, 0 to 200 µM SL-6-41, 0 to 200 µM SL-6-56, 0 to 35 µM TQ, 0 to 1,000 µM CPQ, or 0 to 1,000 µM PQ). Each compound was studies at a range of concentrations performed in triplicate with two controls (using the sample buffer instead of PfDFR1 and test compound) on a 96 well plate format. Reactions were initiated by adding NADPH to a final concentration of 100 µM after equilibrating the assay mixture

with all other components at 25 °C for 2 min. Data were recorded every 5 s over 4 min. The Michaelis–Menten equation was used to determined K_m and k_{cat} values.

For hCPR, the activity assay comprised of 0.3 ml contained 0.3 M potassium phosphate (pH 7.7), 25 nM for hCPR, 100 µM NADPH, and various concentrations of PQ derivatives (0 to 200 µM 5-HPQ, 0 to 100 µM 5,6-DPQ, 0 to 150 µM PQQI, 0 to 150 µM 6OHPQQI, 0 to 400 µM SL-6-41, 0 to 600 µM SL-6-56, or 0 to 1,000 µM PQ). Reactions were performed and initiated as described in the PfDFR1 assay. The absorbance 340 nm was monitored every 5 s over 4 min. K_m and k_{cat} values were calculated based on the Michaelis–Menten equation.

6.2.3 Determination of O_2 consumption and H_2O_2 production

6.2.3.1 Calibration of the oxytherm system

Measurement of O_2 consumption and H_2O_2 production was performed using the Oxytherm system and O_2 View software v.2.06 (Hansatech Instruments Ltd). The Oxytherm system was calibrated using O_2-saturated distilled water under normal atmospheric pressure and 37˚C temperature. The reducing agent sodium dithionite was used to deplete O_2 in the chamber for the zero oxygen line.

6.2.3.2 Recombinant CPRs experiments

A compound's propensity to generate H_2O_2 from the reaction assay was determined using the Oxytherm system and O_2 View software v.2.06 (Hansatech Instruments Ltd) by measuring the catalase-mediated O_2 release (scheme 6.1).

$$2H_2O_2 \xrightarrow{\text{catalase}} 2H_2O + O_2$$

scheme 6.1

PfDFR1 reactions (containing 0.3 M potassium phosphate (pH 7.7), 200 nM PfDFR1, 30 µM compound, 100 µM NADPH) were performed at 37°C in 0.5 ml. The assay mixture without PfDFR1 was pre-incubated in the Oxytherm's chamber at 37˚C while recording O_2 content. The reaction was initiated by addition of PfDFR1. When the rate of O_2 consumption reached zero (the reaction has run out of NADPH substrate), catalase (from bovine sources, prepared in 50 mM potassium phosphate buffer pH 7.0) was added to a final concentration 10 µg/ml. Then, O_2 generation was monitored (nmol/ml) over 5 min. Control reactions, including reactions without PfDFR1, reactions with methanol, and reactions with DMSO, were also performed in parallel. For ease of visual comparison of individual traces, the x-axis and the y-axis were normalised by defining the addition of catalase as t=0 and the corresponding O_2 concentration as 0 nmol/ml.

For hCPR, the hCPR reactions (containing 0.3 M potassium phosphate (pH 7.7), 200 nM hCPR, 30 µM compound, 100 µM NADPH) were performed at 37°C in 0.5 ml. The assay mixture without hCPR was pre-incubated in the Oxytherm's chamber at 37˚C while recording O_2 concentration. The reaction was initiated by the addition hCPR. When the kinetic trace reached a clear plateau, catalase (from bovine sources, prepared in 50 mM potassium phosphate buffer pH 7.0) was added to a final concentration 10 µg/ml to release O_2 from H_2O_2. The data was recorded and analyzed as described above.

6.2.3.3 Bone marrow and red blood cell experiments

Bone marrow extracts were prepared from mice femurs by flushing out with cold Ringer's solution pH 7.4 (125 mM NaCl, 1.5 mM $CaCl_2$, 5 mM KCl, 0.8 mM Na_2HPO_4) using a 2 ml syringe connect with a 25GA needle. The bone marrow cells were washed twice and resuspended with cold Ringer's solution. Washed bone marrow cells were lysed by sonication. The protein concentration of crude extracts was measured by Bradford assay (section 2.2.5). O_2 measurements were performed at 37˚C in 0.4 ml samples containing Ringer's solution pH7.4, 8.5 mg/ml bone marrow extracts, 1X regeneration system (Thermo scientific), 30 µM test compound, 30 µM $NADP^+$. The assay mixture without $NADP^+$ was pre-incubated in the Oxytherm's chamber at 37˚C while recording O_2 content. The reaction was initiated by addition of $NADP^+$. After addition of $NADP^+$ for 30 min, catalase (from bovine sources, prepared in 50 mM potassium phosphate buffer pH 7.0) was added to release O_2 from H_2O_2. Experiments with human red blood cells were performed as described above with same amount of protein extract. The data was recorded and analyzed as described in the assay of recombinant CPR.

6.2.3.4 H_2O_2 determination from 5-HPQ incubation with hCPR in the NADPH regeneration system.

The assay reactions (containing 0.3 M potassium phosphate (pH 7.7), 200 nM hCPR, 0-30 µM compound, 1X regeneration system (Thermo scientific), 30 µM test compound, 30 µM $NADP^+$) were performed at 37°C in 0.5 ml. First, the regeneration system was pre-incubated with test compound in the Oxytherm's chamber at 37˚C while recording O_2 concentration. Then, hCPR was added into the chamber to

record the O_2 level of hCPR with test compound. The reaction was initiated by the addition $NADP^+$ and incubated proceeded for 30 min. Then, catalase (bovine, prepared in 50 mM potassium phosphate buffer pH 7.0) was added to the final concentration 10 µg/ml to release O_2 from H_2O_2. The data was recorded and analyzed as described above. For the assay reaction with 1 nM 5-HPQ, the assay reactions were performed as described above with an extended 4h incubation.

6.3 Results

6.3.1 Steady-state kinetics of PfDFR1 and hCPR with PQ derivatives

The ability of recombinant CPRs to redox cycle OH-PQm and PQ-derivatives was measured by monitoring NADPH consumption. Steady-state kinetics of the recombinant CPRs (PfDFR1 and hCPR) with various PQ derivatives and 8-aminoquinolines were determined.

6.3.1.1 PfDFR1

To investigate the difference in specificities of test compounds to PfDFR1, kinetic analyses were carried out with PQ derivatives (5-HPQ, 5,6-DPQ, 6OHPQQI, CPQ, PQ) and 8-aminoquinolines (SL-6-41, SL-6-56, TQ) with saturated NADPH substrate concentrations. Kinetic traces of PfDFR1 with test compounds (with the exception of TQ) exhibited Michaelis–Menten behaviour in terms of the NADPH initial consumption rate against a range of test compound concentrations (Figure 6.3 and 6.4). The resultant apparent K_m and k_{cat} values are summarised in Table 6.2. The k_{cat} values for all PQ derivatives were in the range 48 ± 7 to 58 ± 3 min^{-1}, while analogue 8-aminoquinolines (62 ±6 to 72 ± 6 min^{-1}) had higher k_{cat} values than PQ metabolites. The OH-PQms (5,6-DPQ and 6OHPQQI) showed the highest affinity to PfDFR1 based on their lowest K_m (~ 0.7 µM); K_m ranking was 5,6-DPQ≈6OHPQQI<5-HPQ<SL-6-56< SL-6-41≤PQ<CPQ. The fold-difference between K_m of 5,6-DPQ and other test compounds was 6-fold lower than 5-HPQ, 30-fold lower than SL-6-56, and over 170-fold lover than SL-6-41, CPQ, and PQ.

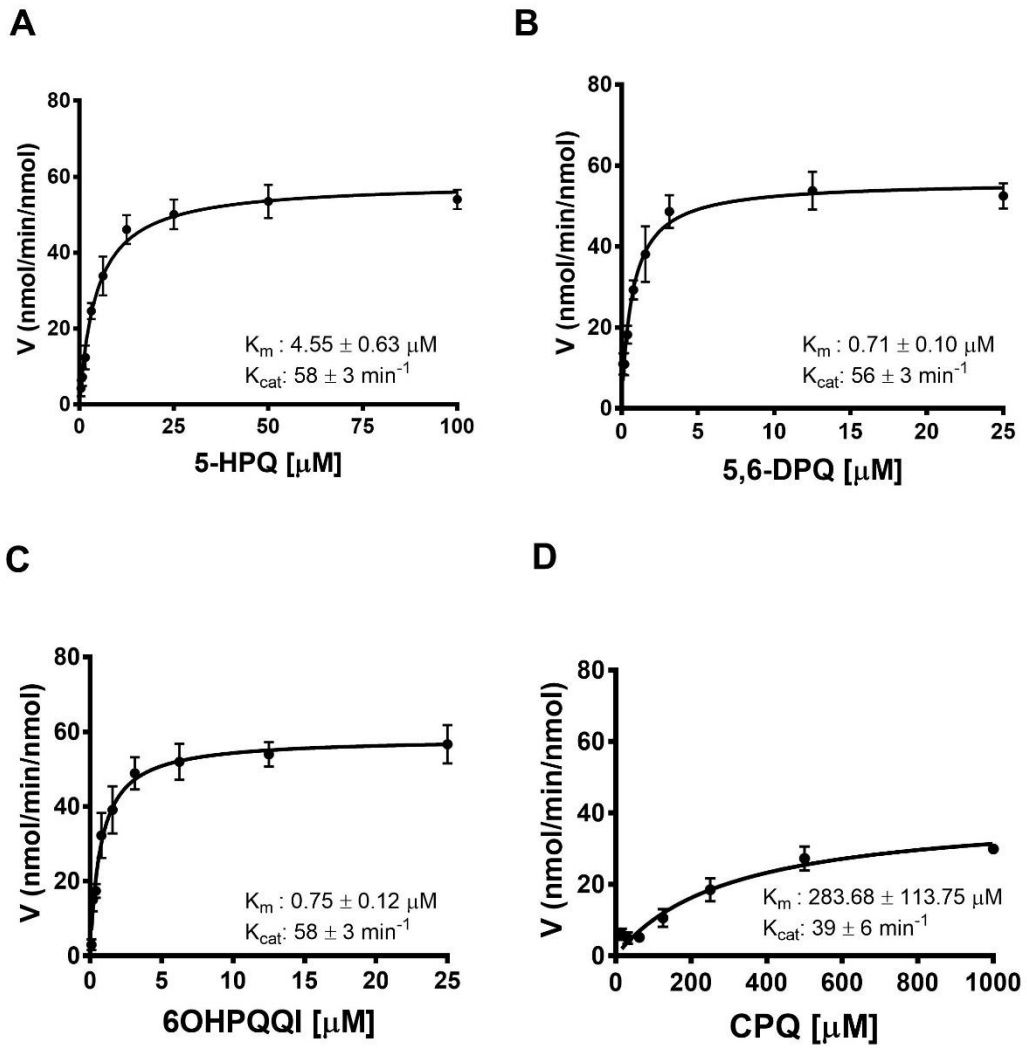

Figure 6.3 Initial reaction rates for PfDFR1 with different PQ derivatives and 8-aminoquinolines. NADPH consumption was measured at 340 nm with 200 nM PfDFR1, 100 μM NADPH, and various PQ derivatives. Initial reaction rates were obtained from two independent experiments with at least five determinations. The solid lines represent the Michealis-Menten curve fits using GraphPad Prism 7. A: 5-HPQ; B: 5,6-DPQ; C: 6OHPQQI; D: CPQ.

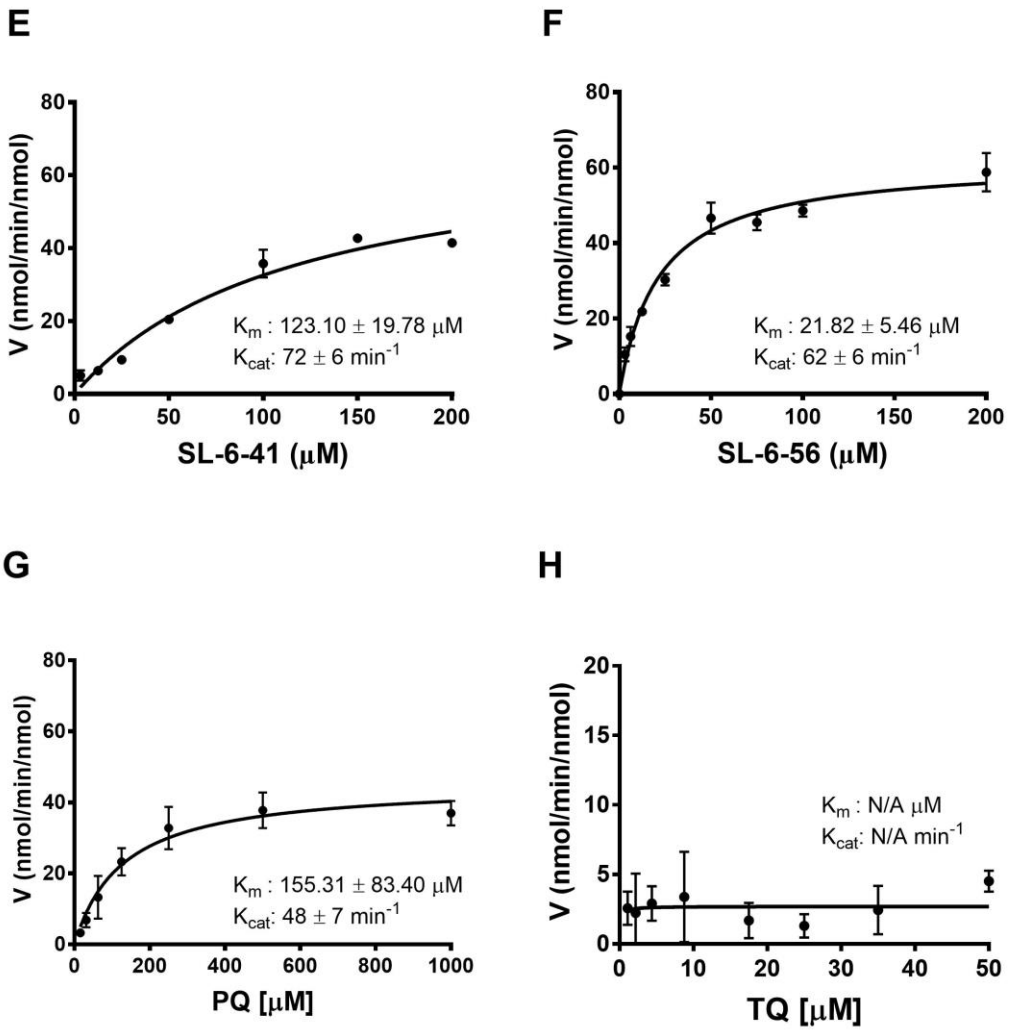

Figure 6.4 Initial reaction rates for PfDFR1 with different PQ derivatives and 8-aminoquinolines (continue). NADPH consumption was measured at 340 nm with 200 nM PfDFR1, 100 μM NADPH, and various PQ derivatives. Initial reaction rates were obtained from two independent experiments with at least five determinations. The solid lines represent the Michealis-Menten curve fits using GraphPad Prism 7. E: SL-6-41; F: SL-6-56; G: PQ; H: TQ.

6.3.1.2 hCPR

To investigate for differences in specificities of the test compounds for hCPR, kinetic analysis was carried out with PQ derivatives (5-HPQ, 5,6-DPQ, PQQI, 6OHPQQI, PQ) and analogue 8-aminoquinolines (SL-6-41, SL-6-56) in the presence of saturated NADPH substrate. Kinetic traces of hCPR with the test compounds exhibited Michaelis–Menten behaviour (Figure 6.5 and 6.6). The apparent K_m and k_{cat} values are summarised in Table 6.2. For PQ, due to the (absorbance) interference from the drug at high concentrations, the K_m and k_{cat} values of PQ were estimated from fitting Michaelis–Menten curves. The k_{cat} values for all test compounds were in the range 1,051 ± 60 (SL-6-41) to 1,574 ± 465 min^{-1} (PQ). The 5,6-DPQ showed the highest affinity to hCPR based on its lowest K_m (~19 µM), while 6OHPQQI, PQQI, and 5-HPQ had similar K_m values in the range 51 to 61 µM. K_m ranking was 5,6-DPQ< 6OHPQQI≤PQQI≤5-HPQ<SL-6-41≤SL-6-56<PQ. The overall results revealed a strong preference of PfDFR1 on PQ derivatives (5,6-DPQ, 6OHPQQI, PQQI, and 5-HPQ) rather than 8-aminoquinolines and PQ.

The results demonstrated that both PfDFR1 and hCPR have the ability to transfer electrons from NADPH to PQ derivatives and related 8-aminoquinolines. The PfDFR1 and hCPR showed a preference for OH-PQms compared to other compounds (Table 6.2). Although the catalytic reactions of hCPR showed a higher catalytic turnover than the PfDFR1 reactions for all PQ derivatives, PfDFR1 compensated its slow catalytic rates with low K_m values as seen in the comparison of k_{cat}/K_m between both enzymes (Table 6.2). Interestingly, PfDFR1 and hCPR showed different trends with respect to the 8-aminoquinoline derivatives, SL-6-41 and SL-6-56. In hCPR, SL-6-41

and SL-6-56 did not show significantly different kinetic parameters. In PfDFR1, SL-6-56 showed a 6-fold lower K_m than SL-6-41, while k_{cat} values were not significantly different.

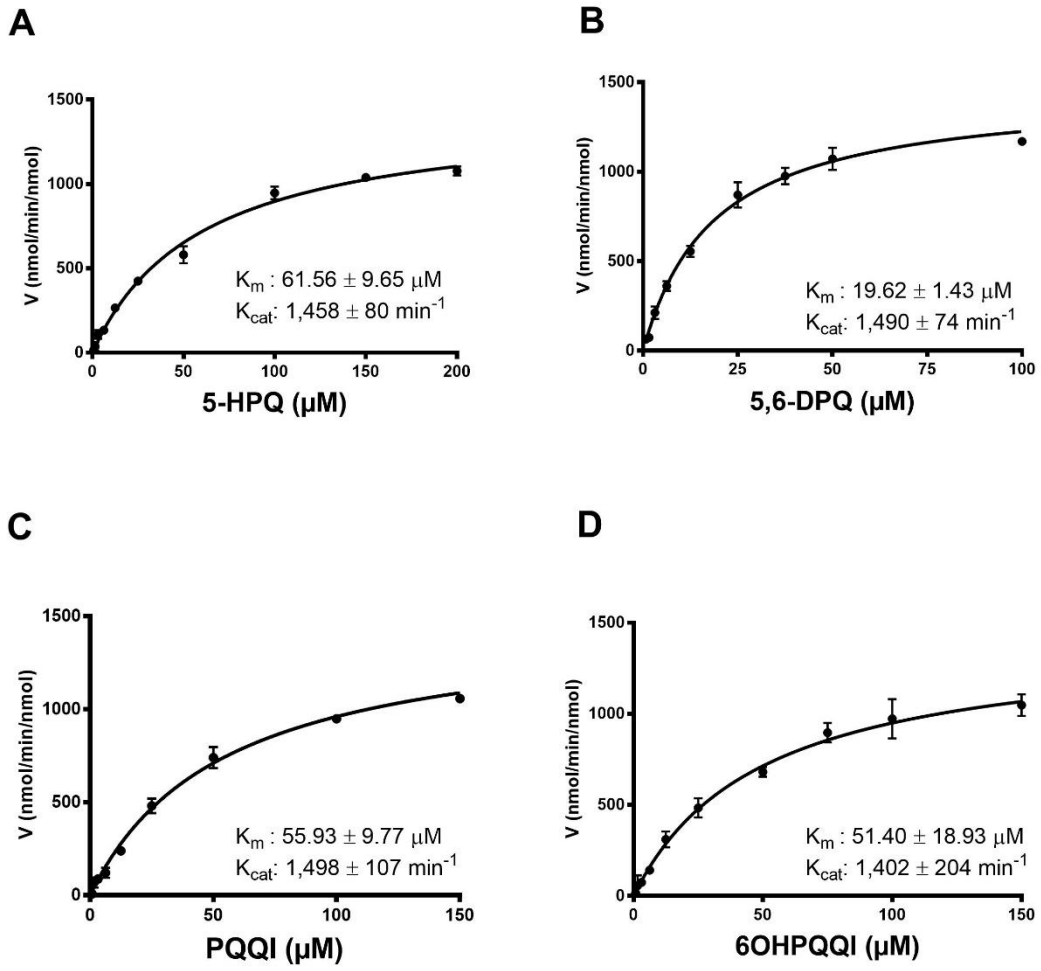

Figure 6.5 Initial reaction rates for hCPR with different PQ derivatives and 8-aminoquinolines. NADPH consumption was measured at 340 nm with 25 nM hCPR, 100 µM NADPH, and various PQ derivatives. Initial reaction rates were obtained from two independent experiments with at least five determinations. The solid lines represent the Michealis-Menten curve fits using GraphPad Prism 7. A: 5-HPQ; B: 5,6-DPQ; C: PQQI; D: 6OHPQQI.

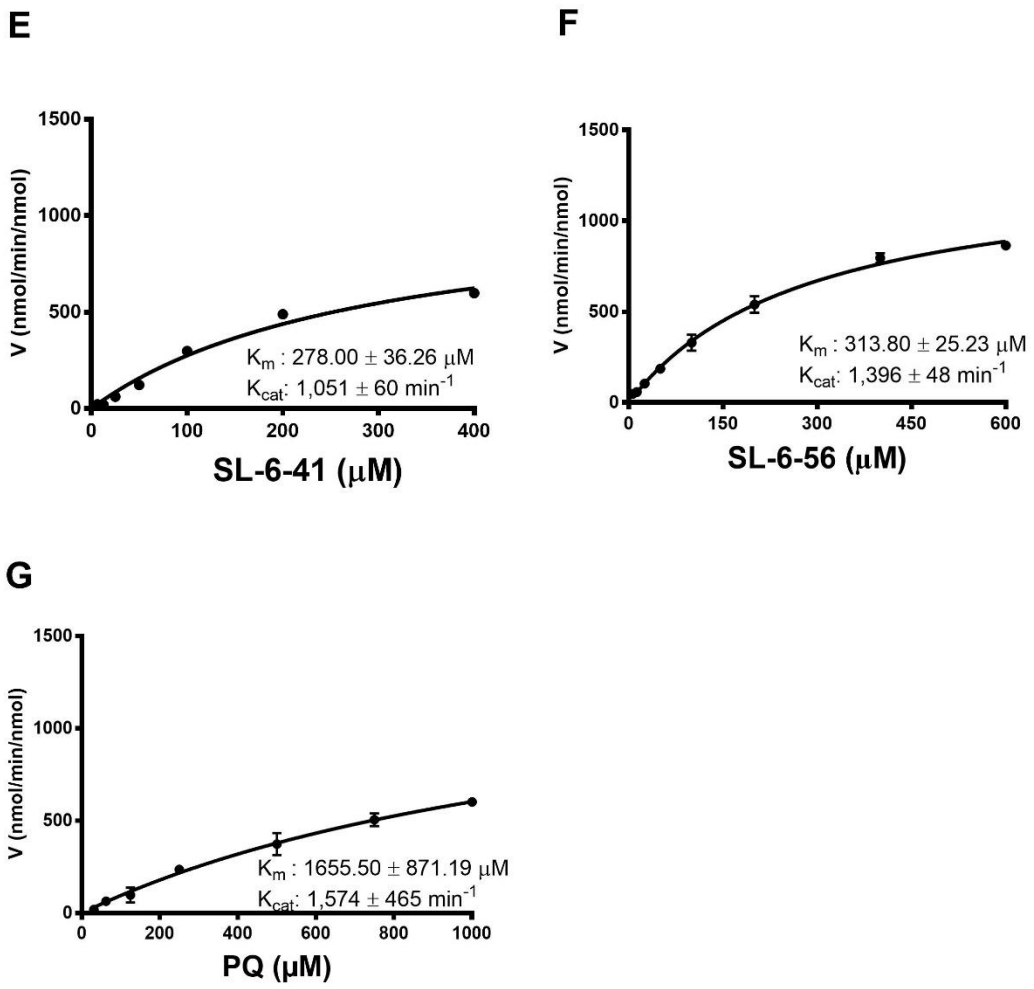

Figure 6.6 Initial reaction rates for hCPR with different PQ derivatives and 8-aminoquinolines (continue). NADPH consumption was measured at 340 nm with 25 nM hCPR, 100 μM NADPH, and various PQ derivatives. Initial reaction rates were obtained from two independent experiments with at least five determinations. The solid lines represent the Michealis-Menten curve fits using GraphPad Prism 7. E: SL-6-41; F: SL-6-56; G: PQ.

Table 6.2 Comparison of steady state kinetic parameters between PfDFR1 and hCPR for PQ derivatives and 8-aminoqionolines

Compound	K_m (µM)		k_{cat} (min^{-1})		k_{cat}/K_m ($min^{-1}µM^{-1}$)	
	PfDFR1	hCPR	PfDFR1	hCPR	PfDFR1	hCPR
5-HPQ	4.55 ±0.63	61.56 ±9.65	58 ±3	1,485 ±80	13.01 ±1.75	24.02 ±1.25
5,6-DPQ	0.71 ±0.10	19.62 ±1.43	56 ±3	1,490 ±74	80.30 ±9.37	76.22 ±2.51
6OHPQQI	0.75 ±0.12	51.40 ±18.93	58 ±3	1,402 ±204	79.89 ±7.55	29.25 ±3.56
PQQI	-	55.93 ±9.77	-	1,498 ±207	-	27.16 ±1.47
SL-6-41	123.10 ±19.78	278.00 ±36.26	72 ±6	1,051 ±60	0.60 ±0.05	3.81 ±0.29
SL-6-56	21.82 ±5.46	313.80 ±25.23	62 ±6	1,396 ±48	2.96 ±0.56	4.47 ±0.49
CPQ	383.68 ±113.75	-	49 ±6	-	0.15 ±0.04	-
PQ[a]	155.31 ±83.40	1,655.50 ±871.79	48 ±7	1,574 ±465	0.36 ±0.12	1.04 ±0.12
TQ[b]	N/A	-	N/A	-	N/A	-

[a] Due to the interfering of PQ absorbance reading at high concentrations, the estimated V_{max} and K_m from the Michealis-Menten curve fit are shown.

[b] Due to the limitation of TQ solubility, the experiments were performed at the TQ concentration below 50 µM.

6.3.2 O_2 consumption and H_2O_2 production from reactions of PQ derivatives with CPRs

To further confirm the ability of PfDFR1 and hCPR to redox cycle PQ derivatives, O_2 consumption and H_2O_2 generation was directly measured using the oxytherm system. H_2O_2 production was measured as catalase-mediated O_2 release.

6.3.2.1 PfDFR1

To monitor O_2 levels during the assay reaction, each test compound was pre-mixed with NADPH substrate. When O_2 levels were stable, PfDFR1 was added to initiate the reaction. After the O_2 consumption rate became zero, catalase was added to release O_2 from H_2O_2. An example of a full trace of O_2 monitoring from the PfDFR1 reaction with test compound is shown in Figure 6.7. The O_2 consumption and H_2O_2 production levels of each test compound were compared as shown in Figure 6.8A and 6.8B, respectively. The summary data on O_2 concentration from catalase mediated O_2 release from $H_2O_2$is shown in Figure 6.9. The results indicate that PQ derivatives and 8-aminoquinolines (with the exception of TQ) are PfDFR1 substrates. Confirming that PfDFR1 can act as a redox cycler of PQ derivatives and plays a role in the production of H_2O_2.

O_2 consumption and H_2O_2 production (determined from O_2 release) by PQ derivatives showed the compound ranking (5,6-DPQ≈6OHPQQI≥5-HPQ≈PQQI>SL-6-56>SL-6-41>SL6-46≥PQ≈CPQ≈MeOH≈ DMSO). This data is fully in line with the compound ranking from the steady-state kinetics studies. 5,6-DPQ and 6OHPQQI showed the highest O_2 consumption rate and O_2 release from H_2O_2, however they were

not significantly different from other OH-PQms (5-HPQ and PQQI) using Turkey's multiple comparison test (Appendix 6.1). The SL-6-56 was significantly more active than SL-6-41 ($P<0.05$) in line with their corresponding K_m values. The SL-6-46, CPQ and PQ are the compound demonstrating least activity.

To prove that the observed O_2 consumption was a resulted of release from H_2O_2 production, sodium pyruvate was added to the assay reaction as a H_2O_2 scavenger [286]. As shown in the inset of Figure 6.8 B, O_2 release levels in the presence of pyruvate were significantly lower than without pyruvate.

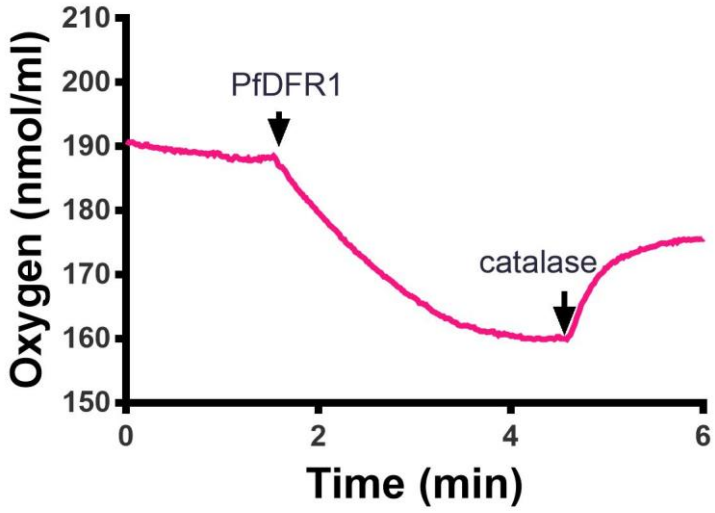

Figure 6.7 The example of full trace O_2 monitoring of PfDFR1 reaction with OH-PQm derivative. The compound and NADPH substrate were pre-incubated in the chamber with dissolved O_2 level recorded before PfDFR1 addition (arrow with PfDFR1 label). After the O_2 consumption rate became zero, catalase was added (arrow with catalase label) to release O_2 from H_2O_2.

A

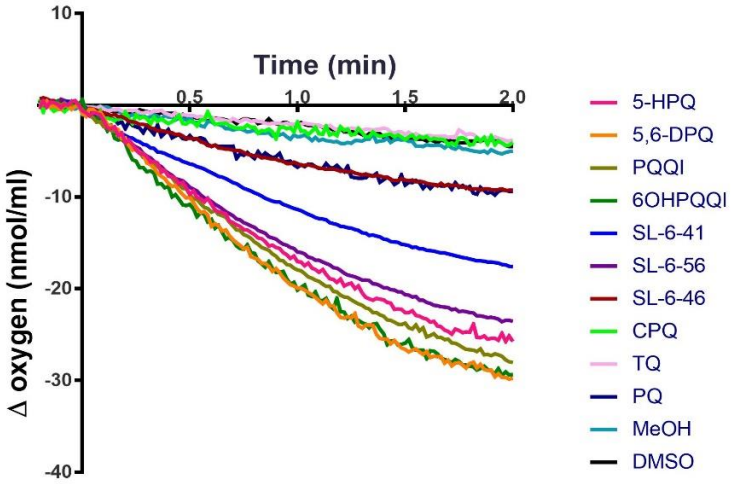

B

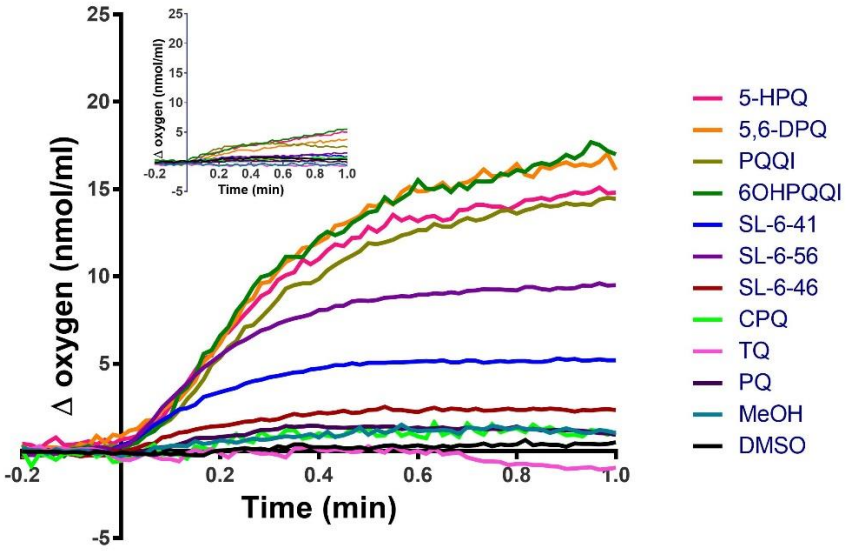

Figure 6.8 O_2 consumption and H_2O_2 generation from PfDFR1 reactions with PQ derivatives. A) Comparison of O_2 consumption from PfDFR1 reactions with different PQ derivatives. The *x* axis was adjusted by defining the addition of PfDFR1 at t=0, and the corresponding O_2 concentration in *y* axis was defined as 0 nmol/ml. B) Comparison of H_2O_2 production from PfDFR1 reactions with different PQ derivatives. The inset represents the reactions with sodium pyruvate (a H_2O_2 scavenger). The *x* axis was adjusted by defining the addition of catalase at t=0, and the corresponding O_2 concentration in *y* axis was defined as 0 nmol/ml. Solid lines were average from two independent experiments.

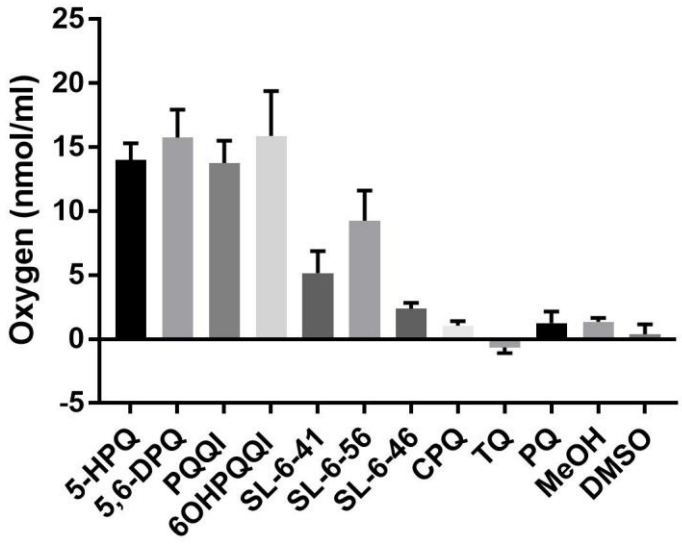

Figure 6.9 Comparison of O_2 release from H_2O_2 production from PfDFR1 reactions with PQ derivatives. O_2 release from H_2O_2 was calculated from the maximum ΔO_2 of each PQ derivative (Figure 6.8B). Average of two independent experiments are shown.

6.3.2.2 hCPR

Monitoring of dissolved O_2 was performed as described in the PfDFR1 assay reactions with minor modifications. When O_2 levels were stable, hCPR was added to initiate the reaction. To avoid the bias from O_2 exchange from air, catalase was added to release O_2 from H_2O_2 after the O_2 trace reached the plateau phase. An example of a full trace of O_2 monitoring from the hCPR reaction with test compound is shown in Figure 6.10. The O_2 consumption and H_2O_2 production levels for each test compound was compared as shown in Figure 6.11A and 6.11B, respectively. The summary of O_2 concentration data from catalase mediated O_2 release from H_2O_2 is shown in Figure 6.12. As is the case with PfDFR1, hCPR can act as a redox cycler of PQ derivatives and can play a role in H_2O_2 production.

The observed compound ranking for O_2 consumption and H_2O_2 production activities was 5,6-DPQ≥6OHPQQI≈5-HPQ≥PQQI>SL-6-41>SL-6-56>SL-6-46≥PQ≈MeOH≈DMSO, in line with the compound affinity ranking from the steady-state kinetics studies. 5,6-DPQ showed the highest O_2 coupled release from H_2O_2, but they were not significantly different from other OH-PQms (6OHPQQI, 5-HPQ and PQQ) using Turkey's multiple comparison test (Appendix 6.2). In hCPR, SL-6-56 and SL-6-41 were not significantly different in H_2O_2, production levels with comparable with their K_m values. The SL-6-46, PQ, MeOH, and DMSO are the group of compounds with less H_2O_2 production activity.

In addition, sodium pyruvate when added to the assay reaction as a H_2O_2 scavenger confirmed that the role of H_2O_2 in O_2 release in the assay reaction. Together with a modified O_2 monitoring method, the O_2 released from H_2O_2 were close to zero in all test compounds as show in the inset of Figure 6.11B.

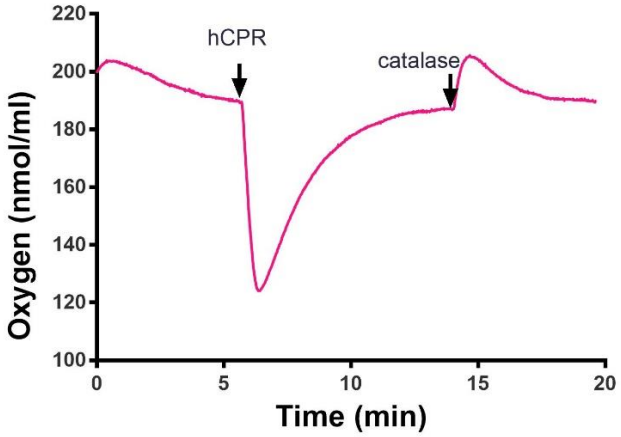

Figure 6.10 The example of full trace O_2 monitoring of hCPR reaction with OH-PQm derivatives. The compound and NADPH substrate were pre-incubated in the chamber with O_2 level record before hCPR addition (arrow with hCPR label). After the trace reached plateau for at least 1 min, catalase was added (arrow with catalase label) to release O_2 from H_2O_2.

A

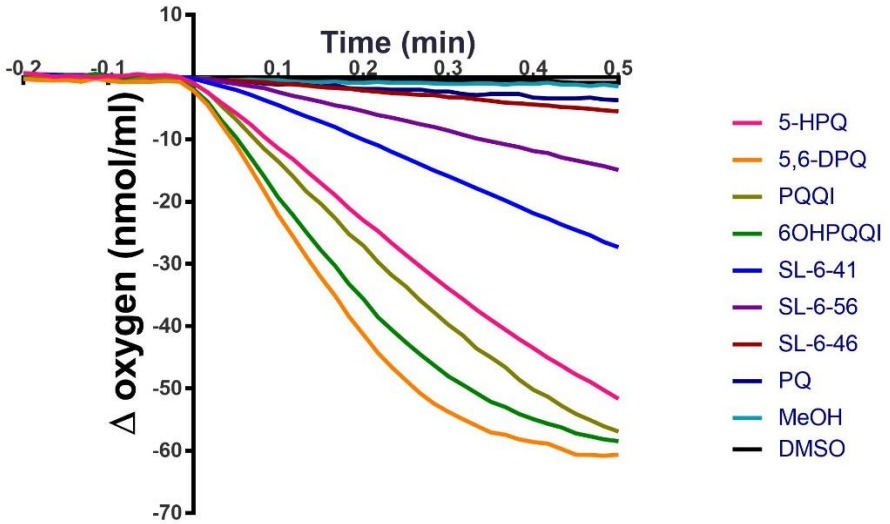

B

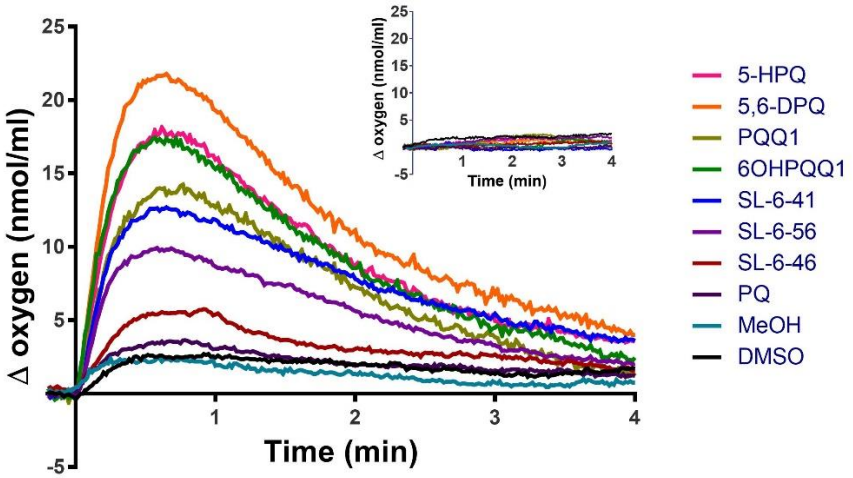

Figure 6.11 O_2 consumption and H_2O_2 generation from hCPR reactions with PQ derivatives. A) Comparison of O_2 consumption from hCPR reactions with different PQ derivatives. The *x* axis was adjusted by defining the addition of hCPR at t=0, and the corresponding O_2 concentration in *y* axis was defined as 0 nmol/ml. B) Comparison of H_2O_2 production from hCPR reactions with different PQ derivatives. The inset represents the reactions with sodium pyruvate as a H_2O_2 scavenger. The *x* axis was adjusted by defining the addition of catalase at t=0, and the corresponding O_2 concentration in *y* axis was defined as 0 nmol/ml. Solid lines were average from two independent experiments.

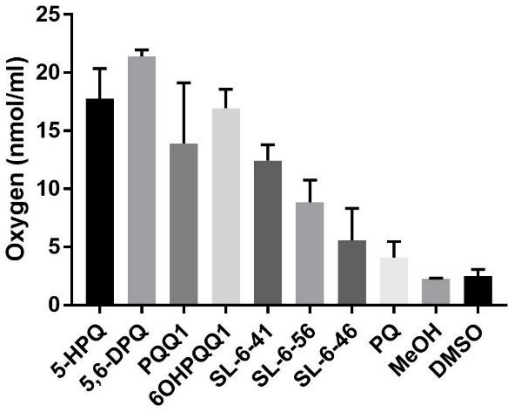

Figure 6.12 Comparison of O_2 release from H_2O_2 production from hCPR reactions with PQ derivatives. O_2 release from H_2O_2 was calculated from the maximum ΔO_2 of each PQ derivative (Figure 6.11B). Average of two independent experiments are shown.

6.3.3 O_2 consumption and H_2O_2 production from incubation of PQ derivatives with bone marrow and red blood cell extracts

Recent studies have revealed that PQ has specifically activities against parasites at gametocyte and liver stages [97]. Activity against asexual parasites is very weak and cannot be achieved therapeutically with adequate safety margins. We hypothesise that the generation reactive O_2 species by OH-PQms could be linked to the parasite localisation in the human host. To investigate this, O_2 consumption and H_2O_2 production from OH-PQms was performed using bone marrow extracts (a site of sequestered gametocytes) and red blood cell extracts (which represent the environment of circulating parasites). The O_2 consumption and H_2O_2 production from OH-PQm incubations with bone marrow extracts and red blood cell extracts are shown in Figure 6.13 and 6.14, respectively. The results demonstrate that H_2O_2 was generated from the reactions with OH-PQms incubated with bone marrow extracts (Figure 6.13). However, reactions with equivalent protein from red blood cell extract showed undetectable H_2O_2

production (Figure 6.14). These results would support the hypothesis that H_2O_2 production occurs at specific sites and corresponds with the localisation of parasites.

A

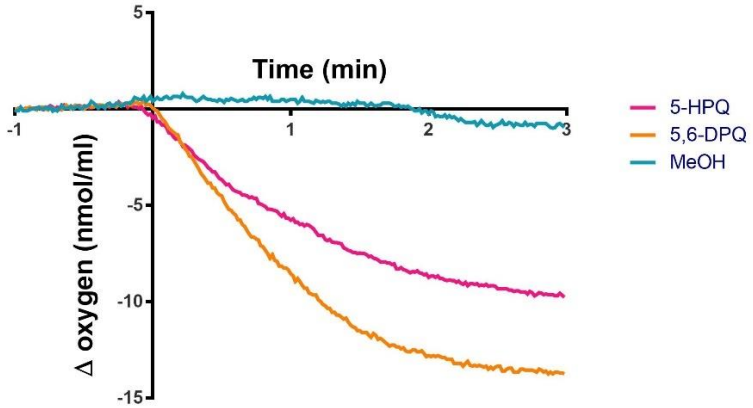

B

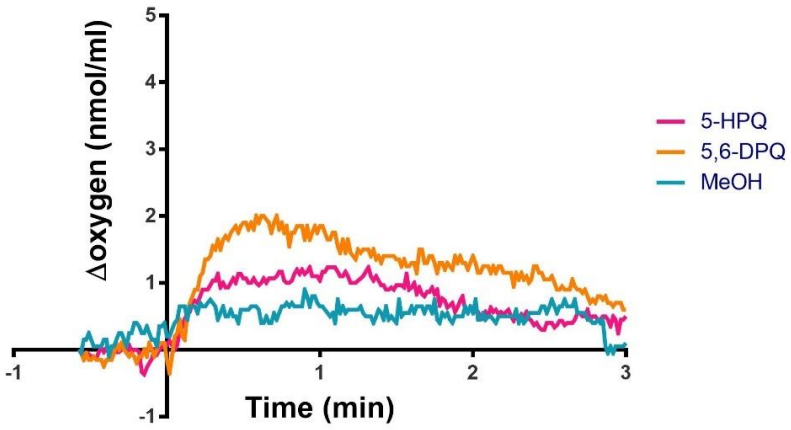

Figure 6.13 O_2 consumption and H_2O_2 generation from mice bone marrow extracts with PQ derivatives. A) Comparison of O_2 consumption from mice bone marrow reactions with 5-HPQ, 5,6-DPQ, and MeOH as a control. The *x* axis was adjusted by defining the addition of $NADP^+$ (substrate for the NADPH regeneration system) at t=0, and the corresponding O_2 concentration in *y* axis was defined as 0 nmol/ml. B) Comparison of H_2O_2 production from extracted bone marrow extracts after incubation with 5-HPQ, 5,6-DPQ, and MeOH as a control. The *x* axis was adjusted by defining the addition of catalase at t=0, and the corresponding O_2 concentration in *y* axis was defined as 0 nmol/ml. Solid lines were average from two independent experiments.

A

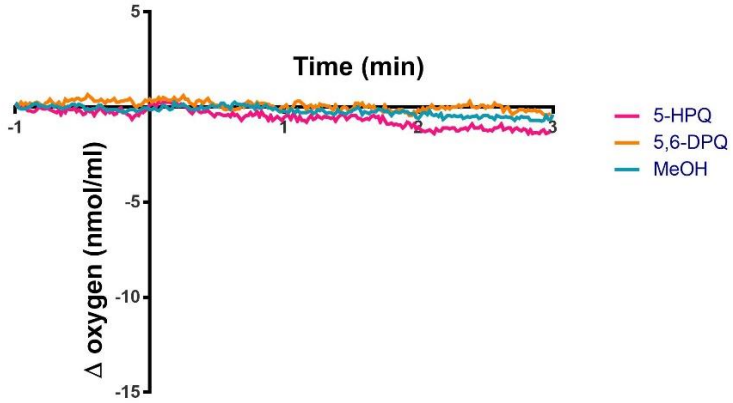

B

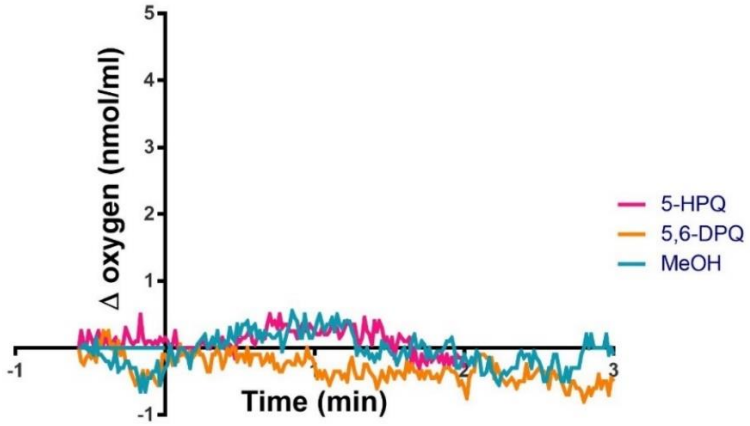

Figure 6.14 O_2 consumption and H_2O_2 generation from red blood cell extracts with PQ derivatives. A) Comparison of O_2 consumption from red blood cell reactions with 5-HPQ, 5,6-DPQ, and MeOH as a control. The *x* axis was adjusted by defining the addition of $NADP^+$ (substrate for the NADPH regeneration system) at t=0, and the corresponding O_2 concentration in *y* axis was defined as 0 nmol/ml. B) Comparison of H_2O_2 production from red blood cell extracts after incubation with 5-HPQ, 5,6-DPQ, and MeOH as a control. The *x* axis was adjusted by defining the addition of catalase at t=0, and the corresponding O_2 concentration in *y* axis was defined as 0 nmol/ml. Solid lines were average from two independent experiments.

6.3.4 Effect of O_2 on the H_2O_2 production

Based on the proposed mechanism of action of PQ (Figure 6.1), O_2 is proposed to be necessary for the production of H_2O_2. To confirm the role of O_2 on the H_2O_2 production, we performed the comparable assay reactions under normal air and O_2 limited environments. As shown in Figure 6.15, O_2 plays a role in the production of H_2O_2 production from the incubation of OH-PQm with hCPR. This result supports the role of O_2 in the proposed PQ redox dependent mechanism of action.

A **B**

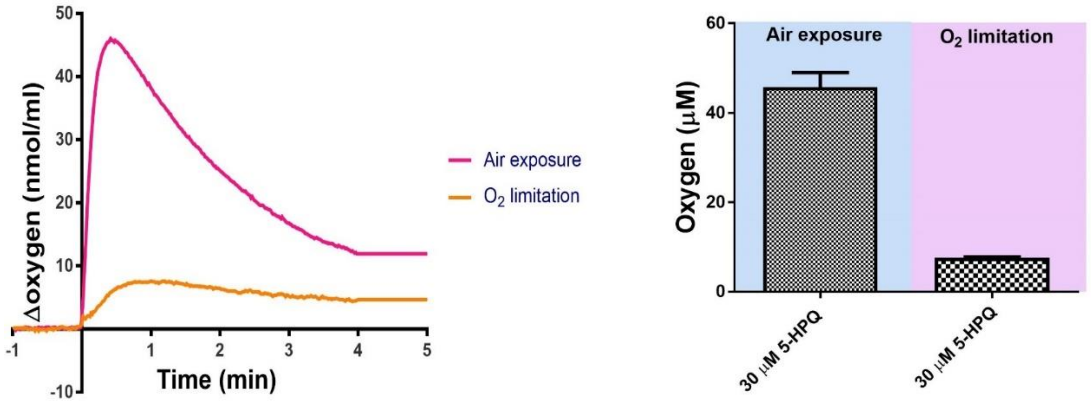

Figure 6.15 Effect of O_2 on H_2O_2 generation from CPR incubation with OH-PQm. The reactions were performed with 25 nM hCPR, 30 µM 5-HPQ and NADPH regeneration system for 30 min. A) Comparison of traces of O_2 release from H_2O_2 between reactions performed in air exposure and O_2 limitation environments. B) O_2 release from H_2O_2 was calculated from the maximum ΔO_2 of different O_2 environments. Average of two independent experiments are shown.

6.3.5 The production of pharmacologically relevant H_2O_2 concentrations from catalytic levels of OH-PQm

Recent publications show that the most abundant PQ metabolites in human plasma come from the monoamine oxidase A (MAO-A) metabolism pathway which produces PQ aldehyde species (a progenitor of carboxy PQ (CPQ) [95, 97]). OH-PQms are not the major metabolites, but as described previously and again here they are thought to be responsible for PQ antimalarial activity [101, 105]. To address the question of how relatively large (μM) concentrations of H_2O_2 can be produced from small (nM) concentrations of OH-PQm, we designed a set of experiments that attempt to mimic the intracellular environment with regard to NADPH availability using a regeneration system that does not deplete NADPH. As shown in Figure 6.16, under these conditions, high (μM) H_2O_2 concentrations could be achieved from a 30 min incubation with nM of OH-PQm.

Furthermore, OH-PQm at a concentration of 1 nM was capable of generating 1,000X the concentration of H_2O_2 over a 4 h incubation (Figure 6.17). These results support the role of redox cycling of catalytic levels of OH-PQm in the production of high pharmacologically relevant levels of H_2O_2 under conditions of unlimited reducing equivalents (NADPH).

A

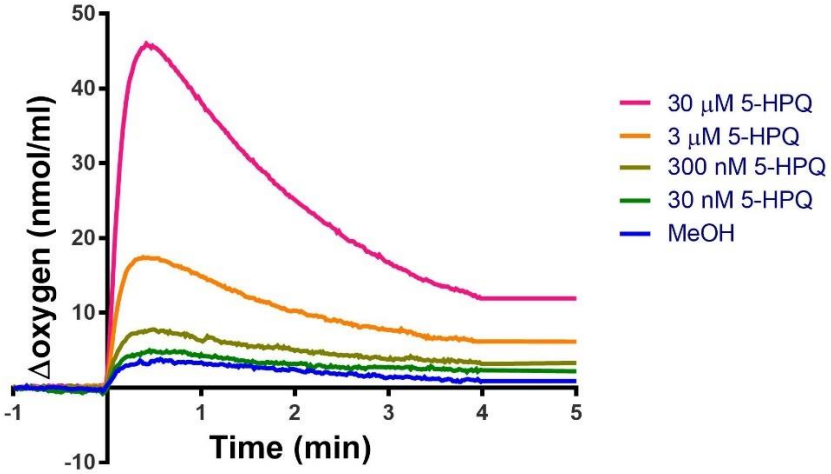

B

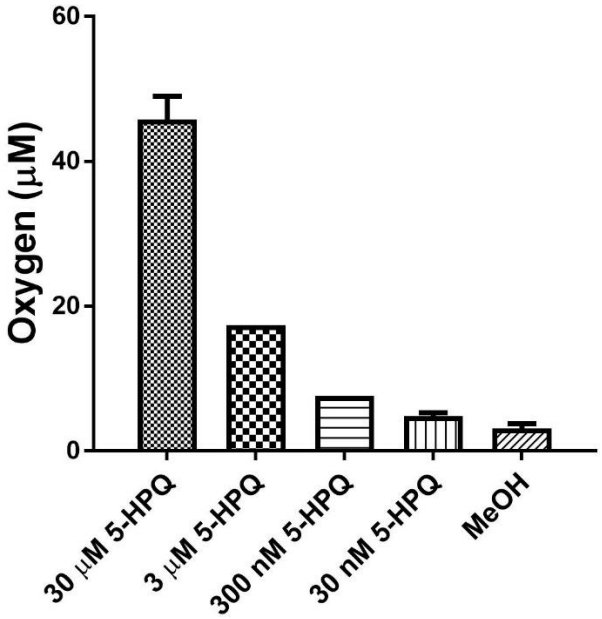

Figure 6.16 H_2O_2 generation from CPR reaction with various 5-HPQ concentrations. The reactions were performed with 200 nM hCPR, various 5-HPQ concentrations and NADPH regeneration system for 30 min. A) Comparison of traces of O_2 release from H_2O_2 from different 5-HPQ concentrations. B) O_2 release from H_2O_2 calculated from the maximum ΔO_2 of each 5-HPQ concentration. Average of two independent experiments are shown.

A

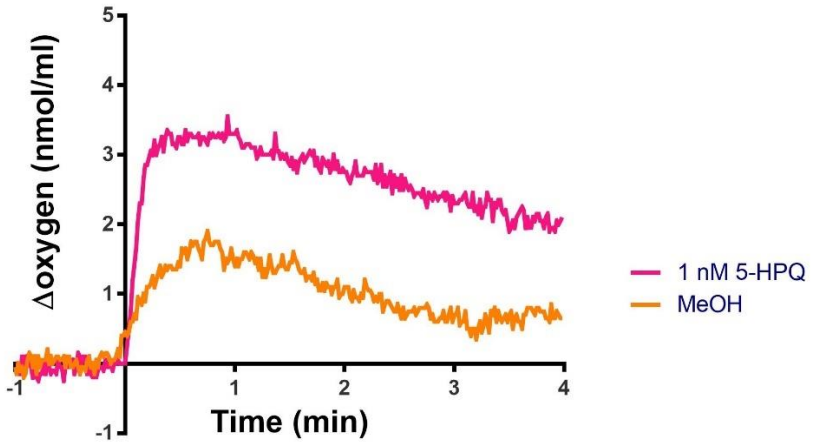

B

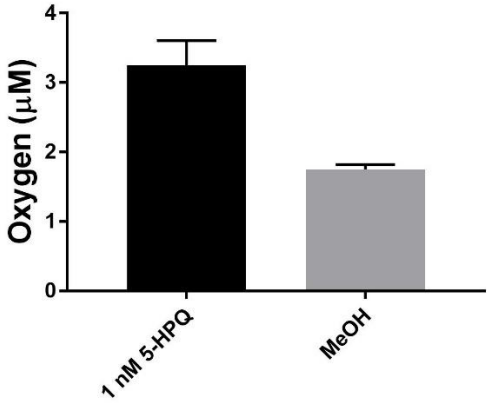

Figure 6.17 H_2O_2 generation from1 nM 5-HPQ incubation with hCPR. The reactions were performed with 200 nM hCPR, 1 nM 5-HPQ and NADPH regeneration system for 4 h. A) Comparison of traces of O_2 release from H_2O_2 from 1 nM 5-HPQ and MeOH as a control. B) O_2 release from H_2O_2 calculated from the maximum ΔO_2 of each reaction. Average of two independent experiments are shown.

6.4 Discussion

PQ is a key antimalarial drug in the global fight against malaria. It is one of only two approved drugs having activity against liver stagers (including hypnozoite of relapsing strains) and mature gametocytes [287]. Over seven decades, PQ's mechanism of action has been studied but remained poorly understood although pointing to potential mechanisms involving ROS-induced damage of the parasite mitochondrion [107, 288]. Recent studies described the dependence of PQ efficacy on CYP 2D6-mediated active metabolites [97, 101].

Here, we have demonstrated that PfDFR1 and hCPR are capable of mediating the redox cycling of a range of OH-PQm's PfDFR1 (Figure 6.3-6.6). The hCPR was shown to catalyse OH-PQm >30 times faster than PfDFR1, albeit that PfDFR1 displayed a lower K_m for OH-PQm's (Table 6.2). Further, the production of reactive H_2O_2 from the redox cycling of PQ derivatives were readily detected using the oxytherm system from reactions with both PfDFR1 and hCPR. These data support the hypothesis that H_2O_2 production occurs via CPR-mediated redox cycling of PQ derivatives. A recent report on mitomycin c (an antitumour drug) supports the ability of CPR to act as redox cycler of small molecules resulting in the production of reactive O_2 species [175, 189].

Malaria parasites are sensitive to changes in redox balance [289]. Hence, parasites maintain their redox equilibrium with a number of antioxidant defence systems, including the thioredoxin and the GSH systems [290]. PQ antimalarial activity could therefore be a result from the imbalance of redox equilibrium because of high concentrations of H_2O_2 derived from the described mechanism. Our results showed that

the parasite reductases such as PfDFR1 have ability complete the redox cycling of PQ derivatives with H_2O_2 production as shown in Figure 6.8. The idea is supported by the enrichment of this enzyme in mature gametocytes [224]. However, work from our laboratory by Dr. Grazia Camarda provided evidence that incubation of OH-PQm, even at high (10 µM) concentrations was insufficient to kill all parasites (Figure 6.18A) – thereby arguing against a mechanism of action which is exclusively based on the activity of parasite diflavin reductases. The proposed model for H_2O_2 production from the treatment of gametocytes with only OH-PQm is shown in Figure 6.19.

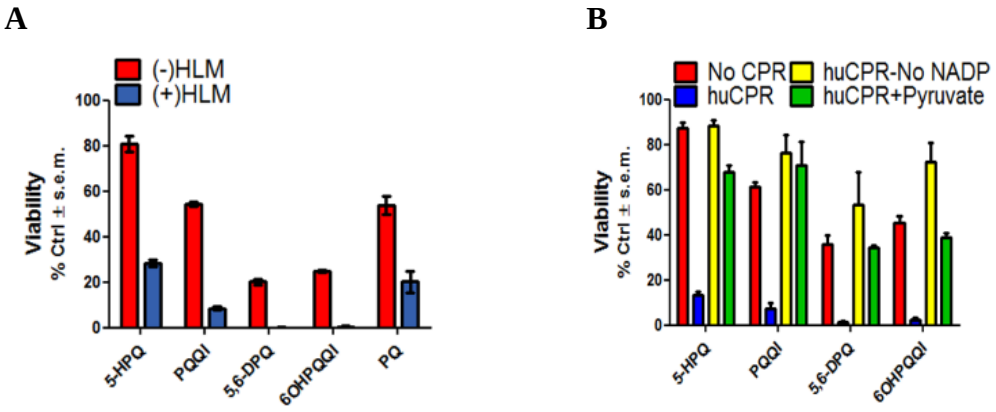

Figure 6.18 PQ derivatives and activity against gametocytes *in vitro*. A) The *in vitro* gametocyte luciferase assay. PQ derivatives ware reacted with or without human liver microsomes (HLM) prior to perform the assay with mature gametocytes. The viability of gametocytes after 72 h incubation was measured. B) The *in vitro* gametocyte luciferase assay to test PQ derivative activity against mature gametocytes: with hCPR (blue bars) or without recombinant hCPR (read bars), with hCPR without $NADP^+$ (yellow bars), with hCPR and sodium pyruvate (green bars). These works were done in our laboratory by Dr. Grazia Camarda.

Further work from our laboratory revealed that complete gametocidal activity could be shown with OH-PQm following the addition of human liver microsomes (HLM, Figure 6.18A). As we know, the CYPs and CPR, which are enzymes involved in drug and xenobiotics metabolism, are expressed in liver microsomes [291]. Hence, the enzymes in the P450 system may play an unsuspected role in promoting the PQ derivative antimalarial activity. The results in this chapter show the ability of hCPR to act as a redox cycler of PQ derivatives (Figure 6.11-6.12), supporting the findings in the gametocyte luciferase assay with additional hCPR carried out by Dr. Grazia Camarda (Figure 6.18B). The proposed model for H_2O_2 production from the treatment of gametocytes with OH-PQms and additional hCPR is shown in Figure 6.20. According to these findings, it is likely that both diflavin reductases from the human host and the parasite contribute to the OH-PQm redox cycling-mediated mechanism of action. Owing to the higher content of diflavin enzymes in the human tissues, these enzymes are more likely responsible for the parasite killing observed *in vivo.*

Indeed, liver stages and gametocytes are enriched in the human liver and the bone marrow, respectively [34, 292-294]. Both human liver cells and bone marrow cells have CYPs and CPR expression [295-297]. The incubation of bone marrow extracts with PQ derivatives presented in this chapter (Figure 6.13) supports the potential role of this site in the OH-PQm-generated of H_2O_2.

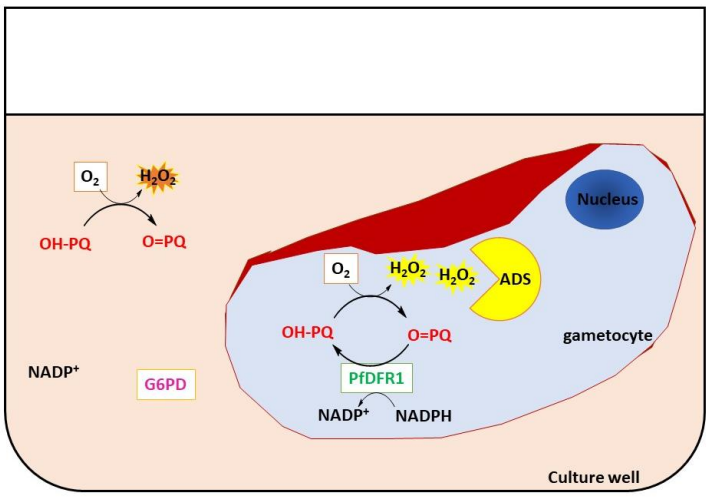

Figure 6.19 A proposed model of H_2O_2 production from the treatment of gametocytes with OH-PQms. OH-PQms (OH-PQ) are transported to gametocytes. The redox-cycling of OH-PQ is completed by parasite enzyme(s) such as PfDFR1, while the H_2O_2 are generated. The H_2O_2 equilibrium is controlled by ADS (antioxidant defence systems). If gametocytes can maintain the balance of redox equilibrium, gametocytes could survive.

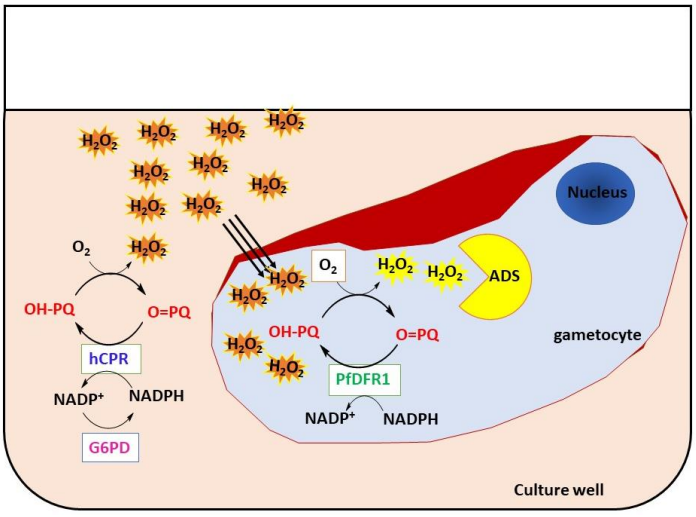

Figure 6.20 A proposed model of H_2O_2 production from the treatment of gametocytes with OH-PQms and additional hCPR. OH-PQms (OH-PQ) are stayed in the culture media as well as transported to gametocytes. The redox-cycling of OH-PQ is occurred in both inside (by parasite enzyme(s)) and outside parasite (by hCPR) with the production of H_2O_2. The combination of H_2O_2 transported from outside and produced inside parasite destroy the redox equilibrium controlled by ADS (antioxidant defence systems) leading to parasite damage and parasite death.

Alternatively, sexual blood stage parasites modify their host cells for vascular sequestration and adhesion via parasite-derived antigens (including PfEMP1, RIFIN, and STEVOR), which are involved in the cytoadhesion process of infected erythrocytes with non-infected erythrocytes and endothelial cells [298, 299]. Expression of CPR and CYPs (but not CYP 2D6) in endothelial cells has been reported [297, 300], thus endothelial cells could not support the initial steps in primaquine metabolism. Due to the tight regulation of H_2O_2 in endothelial cells [301], the requirement for aquaporins to transport H_2O_2 across cell membranes [302] and blood flow in vessels, diffusion of OH-PQm-generated H_2O_2 between endothelial cells and infected erythrocytes could be impaired. Therefore, red blood cell extracts were chosen to represent the environment of circulating asexual parasites while endothelial cells were not considered in this study. The experiments performed with red blood cell extracts, where the production of H_2O_2 was not detected (Figure 6.14), are consistent with erythrocytes not being a source of H_2O_2.

A single low dose PQ (0.25 mg/kg) has been suggested by the WHO to block malaria transmission [36]. Most of the parent drug PQ, undergoes biotransformation through the MAO-A pathway producing the precursor of the less effective end metabolite CPQ [97]. Only a small portion of parent PQ is metabolised by CYP 2D6 to the active OH-PQm's [97]. The results described in this chapter using catalytic quantities of OH-PQm to generate >1,000X H_2O_2 (Figure 6.16. and 6.17) are pharmacologically consistent with clinical data regarding the potent transmission blocking properties of PQ.

In conclusion, the results presented in this chapter support a new model for the mode of action of PQ that involves the redox cycling of OH-PQm by host and parasite diflavin reductases. The role of host enzymes (CPR) in key sites of the host, such as liver and bone marrow, provide an explanation for the observed stage specificity and potency of PQ. It is important to note that the results presented here were performed *in vitro* using recombinant CPRs. Therefore, it may not completely mimic the mechanisms occurring inside the human host and the malarial parasite, which could involve other pathway(s) or reductase(s) to support the production reactive O_2 species from PQ metabolites.

CHAPTER 7

EXPRESSION AND LOCALISATION OF PLASMODIUM FALCIPARUM NADPH-DEPENDENT DIFLAVIN REDUCTASE I

7.1 Introduction

As described in previous chapters, the *P. falciparum* NADPH-dependent diflavin reductase I (PfDFR1) is a unique and indispensable enzyme with unknown biological function that has been shown in Chapter 6 to be able to interact with primaquine hydroxylated metabolites (OH-PQms) and may in part be responsible for anti-gametocidal activity at pharmacological PQ and OH-PQm concentrations. Two *in silico* organelle localisation bioinformatic analyses were performed (Chapter 3, section 3.3.1). Both analyses indicated a high probability that PfDFR1 is localised in the mitochondria, however the analysis from the WoLF PSORT Prediction server also indicated a possibility of cytosolic or nuclear residence of PfDFR1.

To confirm PfDFR1 stage specific expression and cellular localisation, this chapter reports the expression of PfDFR1 RNA and protein levels from asexual stages, early-stage gametocytes (stage I-III) and late-stage (stage IV-V) gametocytes. Localization of PfDFR1 in malaria parasites was performed by immunofluorescent microscopy using polyclonal antibodies against the PfDFR1 FMN domain and the FAD/NADPH domains produced in mouse and rabbit, respectively.

7.2 Methods

7.2.1 Malaria parasite preparation

The *P. falciparum* strains CBG and NF54 were cultured as described in the general materials and method section 2.2.10.

For asexual parasites, the parasites were cultured until they reached 5-7% parasitemia (trophozoite and schi zont stages). To harvest asexual parasites, infected red blood cells were lysed on ice with 0.15% saponin solution (w/v) for 5 min. The mixture was centrifuged at 3,452x*g* for 5 min at 4˚C. The pellet was washed twice with PBS. Then, the pellet was solubilized in PBS containing Complete Protease Inhibitor Cocktail (Roche). The parasites were counted using a hemocytometer. Small aliquots of parasite protein were made and kept at -80 ˚C.

For gametocyte initiation, the parasites were cultured at a high parasitemia (>10% parasitemia). When young gametocytes (stage I or II) appeared in the culture, 50 mM *N*-acetylglucosamine was added to the culture for 4 days to remove asexual stage parasites. Percoll purification of gametocytes was performed to separate early and late gametocytes as already described by Carter *et al* [303]. Briefly, the Percoll step gradient consisting of 4 Percoll layers (60%, 52.5%, 45% and 30% diluted with RPMI) was prepared (Figure 7.1). The parasite solution was added on the top of the gradient. The gradient was centrifuged at 3,452x*g* for 20 min at room temperature. The desired parasite stage layers (Figure 7.1) were collected and washed twice with PBS. The parasites were counted and kept at -80˚C using the same method as for the asexual stage parasites.

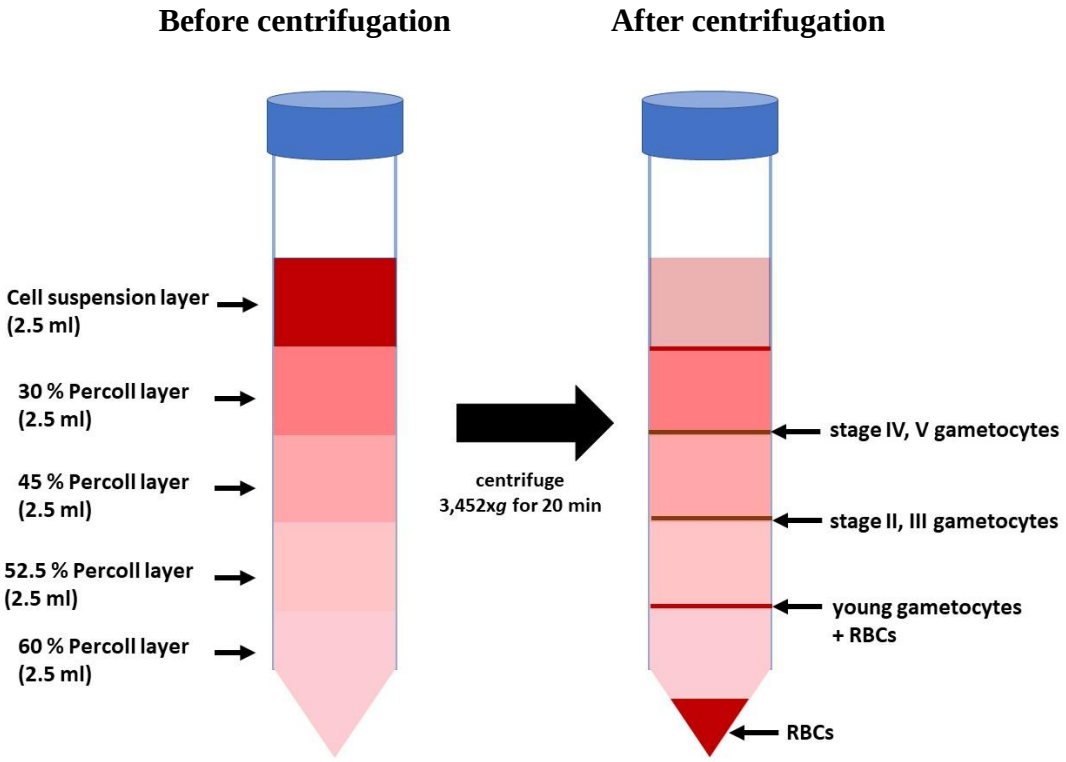

Figure 7.1 Purification of gametocytes using Percoll gradient. 4 Percoll layers were prepared and the parasite solution was added on the top of the gradient. After centrifugation at 3,542x*g*, the layer of stage IV and V gametocytes was in the interface between 30% and 45% Percoll layers. The layer of stage I and II gametocytes was in the interface between 45% and 52.5% Percoll layers.

7.2.2 RNA extraction and RT-CPR

Total RNA extraction and cDNA synthesis were performed as described in the general materials and method section 2.2.11. cDNA from each parasite stage was used as the DNA template for PCR using Phusion Hot Start II High-Fidelity DNA polymerase (Thermo Scientific) with specific primers for *PfDFR1* and control genes (Table 7.1). The PCR conditions are described in Table 7.1. The PCR products were analysed by running on 2% and 0.8% agarose gel electrophoresis.

Table 7.1 PCR primers and conditions

	PCR conditions	Primer name	Sequence
Set 1	-98˚C 30s -30 cycles, 98˚C 10s, 57˚C 30s, 72˚C 30s -72˚C 10 min	PfDFR1_F_qPCR	GGACAGCAGAAGAATTTGCC
		PfDFR1_R_qPCR	CGTTGGTTCTCCATCTCCA
		60S ribo L18 F	ATTATCACATGGCCAATCACC
		60S ribo L18 R	CAATCTCTTATCATCTGTTATT
Set 2	-98˚C 30s -30 cycles, 98˚C 10s, 58˚C 30s, 72˚C 30s -72˚C 10 min	PfDFR1 Left primer	GACATCTTGGAGAGACATGGC
		PfDFR1 Right primer	GATCCCTTAAACCATCTTCTGC
		K13 M003 F	ATGGAAGGAGAAAAAG
		K13 M003 R	TTATATATTTGCTATTAAAACGG

7.2.3 Real-time PCR

The real-time PCR samples were run using the QuantiTech SYBR Green PCR Kit (QIAGEN) according to the manufacturer's instruction as described in the general materials and methods section 2.2.12.

7.2.4 PfDFR1 polyclonal antibodies

Polyclonal antibodies against the FMN domain and the FAD/NADPH domains were generated in mouse and rabbit, respectively. In brief, recombinant proteins were produced from *E. coli* BL21 (DE3) harbouring pETM-11 PfDFR1_FMN and pETM-11 PfDFR1_FAD/NADPH. The recombinant proteins were partially purified by Ni-NTA (QIAGEN) affinity chromatography. The partial purified proteins were run on 10% SDS-PAGE gels. The expected bands of PfDFR1_FMN and

PfDFR1_FAD/NADPH were cut and sent to Davids Biotechnologie for antibody production.

7.2.5 Purification of antibody against PfDFR1

A Western blotting method was used to purify anti-PfDFR1 against the FAD/NADPH domain from rabbit antiserum. 2 mg of purified PfDFR1 (87 kDa) was run on a 10% SDS-PAGE gel. Proteins were transferred to a 0.45 µm nitrocellulose membrane. The strip containing the PfDFR1 band (87 kDa) was cut and pre-eluted with 100 mM Glycine (pH 2.5) for 10 min. The strip was blocked for 1 h in PBS containing 5% non-fat dry milk. Then, the strip was washed three times with excess PBST (PBS containing 0.05% Tween 20) for 5 min each time. 8 ml rabbit antiserum was added and incubated with the strip overnight at 4˚C. The strip was washed as described above. The antibody was eluted from the strip by incubating the membrane with 2 ml 100 mM Glycine (pH 2.5) for 2 min. The eluted antibody was neutralized by addition of 2 M Tris-HCl (pH 8.5) to the final concentration 150 mM. The purified antibody was concentrated using an Amicon Ultra-15 Centrifugal Filter Concentrator (Merck Millipore) with 3 kDa molecular weight cut-off. The concentrated antibody was aliquoted and kept at -20 ˚C.

7.2.6 Western blot analysis

The samples were prepared as follows. Parasite pellet was thawed on ice. 10 µl of parasite lysis buffer (containing 50 mM Tris-HCl pH 7.5, 150 mM NaCl, 1%

Triron X-100, 0.5% SDS, and cOmplete Protease Inhibitor Cocktail (Roche)) was added to each tube. The tube was vortexed and incubated on ice for 30 min. The tube was centrifuged at 16,200x*g* for 20 min at 4˚C, and the supernatant was collected. 10 µl of 2X Leammli was added into each parasite extracted tube and boiled for 10 min prior to loading onto an SDS-PAGE gel. Then, the Western blot was performed as described in the general materials and methods section 2.2.6. The primary antibodies (mouse anti-PfDFR1 FMN domain or purified rabbit anti-PfDFR1 FAD/NADPH domains) were prepared in dilution 1:1,000 with PBST. The secondary antibody (goat anti-mouse IgG HRP conjugated, or monkey anti-rabbit IgG HPR conjugated from Sigma and GE-healthcare, respectively) was prepared in a dilution 1: 20,000 with PBST. The signal was detected by ECL western blotting substrate (Pierce) exposed to imaging films.

7.2.7 Immunofluorescence microscopy

Thin smears of asexual and sexual parasites were prepared on microscope slides. Slides were air-dried and fixed with 4% paraformaldehyde and 0.008% glutaraldehyde in PBS for 30 min. Slides were washed with PSB. The cells were permeabilized using 0.1% Triton X-100 in PBS for 10 min. After the washing step, slides were blocked for 30 min in PBS containing 3% BSA. Then, slides were incubated in PBS containing 3% BSA and primary antibodies at room temperature for 45 min. Mouse anti-PfDFR1_FMN and purified rabbit anti-PfDFR1_FAD/NADPH domains were used at a dilution of 1: 100. Slides were further washed with PBS and incubated for 45 min in PBS containing 3% BSA, anti-rabbit IgG-Alexa flour 488 (Thermo Scientific) in a dilution of 1: 500 or anti-mouse IgG FITC conjugated (sigma) in a

dilution of 1: 200, and Hoechst in a dilution of 1: 5,000. After the final wash, images were capture using ZEISS ZEN LSM 880 confocal microscope.

Alternatively, a suspension of mixed asexual and sexual stage parasites in incomplete media was treated with 60 nM MitoTracker Deep Red FM (Thermo Scientific) for 20 min at 37˚C. Excess MitoTracker dye was removed from the mixture by washing with PBS for 3 times. The fixation step was performed in solution by incubating parasite cells in PBS containing 4% paraformaldehyde and 0.008% glutaraldehyde for 30 min. The parasite suspension was permeabilized using 0.1% Triton X-100 for 10 min followed by blocking with 3%BSA in PBS for 30 min. Then, the samples were probed with primary antibodies for 45 min. After washing with PBS, the samples were probed with secondary antibodies for 45 min. Then, the samples were washed with excess PBS and placed on a glass slide. Antibody dilutions and image processing was performed as above.

7.3 Results

7.3.1 In vitro *P. falciparum* culture

P. falciparum, both NF54 and CBG lines, were successfully cultured *in vitro* with this optimized protocol. Asexual blood stages and gametocyte stages grew well in the complete media supplemented with 10% heat-inactivated human serum and 50 μg/ml hypoxanthine. Using this procedure and optimised media, the culture typically achieved 3-5% gametocytemia.

7.3.2 Parasites grouping

Transcription information from PlasmoDB indicates that different stages in both asexual and sexual stages have different transcription levels of the *PfDFR1* gene. To compare transcription and protein levels of *PfDFR1*, we grouped parasites into three groups. The parasite groups are asexual stages (trophozoite and schizont), early gametocytes (stage II and stage III gametocytes), late gametocytes (stave IV and stage V gametocytes) as shown in Figure 7.2.

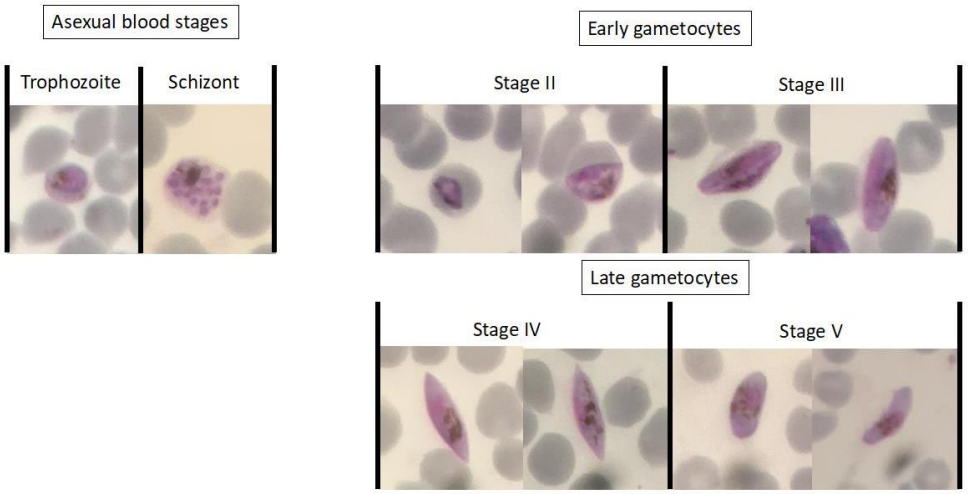

Figure 7.2 Parasite grouping based on parasite stage.

7.3.3 Expression of PfDFR1 in RNA level

To investigate the expression level of PfDFR1 in asexual blood stages and gametocytes, semi-quantitative RT-PCR analysis was performed using cDNA from asexual blood stages, early gametocytes, and late gametocytes. Total RNA was isolated, and cDNA was prepared in both the presence and absence of reverse transcriptase. Comparison of RT-PCR products from each parasite group shows an increase in PfDFR1 expression in early and late gametocytes compared with asexual blood stages (Figure 7.3A and 7.3B). Using K13 as a control gene (Figure 7.3A), early and late gametocytes show 1.62 ± 0.09-fold and 1.87 ± 0.19-fold increases in RNA expression when compared with asexual parasites. A similar trend occurred in the experiment with 60S ribo L18 control gene (Figure 7.3B). Early and late gametocytes showed an increase in RNA expression with 1.44 ± 0.03-fold and 1.66 ± 0.23-fold normalized to asexual parasite.

In order to confirm the upregulation of PfDFR1 in gametocyte stages, real-time PCR analysis was performed using cDNA with specific primers to PfDFR1 and the 60S ribosomal subunit protein 18. The C_q of each reaction was determined. $\Delta\Delta C_q$ method was used in the calculation of fold change in PfDFR1 expression level relative to asexual blood stages (Table 7.2). The expression level of PfDFR1 in early and late gametocytes were 2.13 and 3.72-fold higher than from asexual blood stages, respectively (Table 7.2).

In summary, both techniques, RT-PCR and real time quantitative PCR, indicated that the PfDFR1 RNA is highly expressed in gametocyte stages, especially in mature gametocytes.

Table 7.2 Analysis of PfDFR1 expression in different parasite stages using real time quantitative PCR and $\Delta\Delta C_q$ method

	C_q PfDFR1	C_q 60S Ribo L18	ΔC_q (C_q PfDFR1-C_q 60S Ribo L18)	$\Delta\Delta C_q$ (ΔC_q-ΔC_q Asexual)	Normalized PfDFR1 expression related to asexual stage ($2^{-\Delta\Delta Cq}$)
Asexual	28.01	29.32	-1.31		
	27.86	28.83	-0.97		
	27.71	29.06	-1.34		
		Average	-1.21±0.21	0.00±0.21	1.00 (0.86-1.14)
Early gametocyte	24.53	26.71	-2.18		
	24.42	26.62	-2.20		
	24.45	26.98	-2.52		
		Average	-2.30±0.19	-1.09±0.19	2.13 (1.86-2.43)
Late gametocyte	24.80	27.60	-2.80		
	24.46	27.40	-2.93		
	24.56	28.14	-3.58		
		Average	-3.10±0.42	-1.89±0.42	3.72 (2.78-4.96)

A

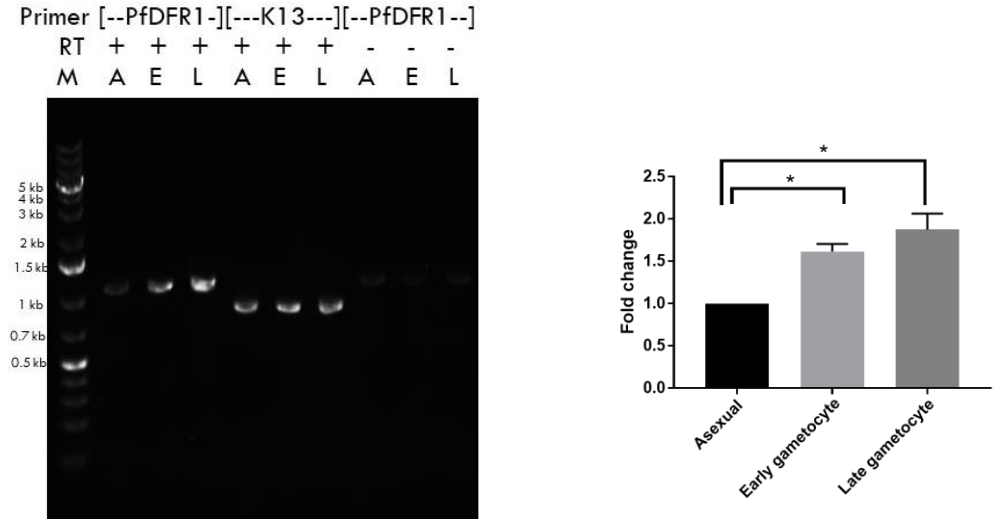

B

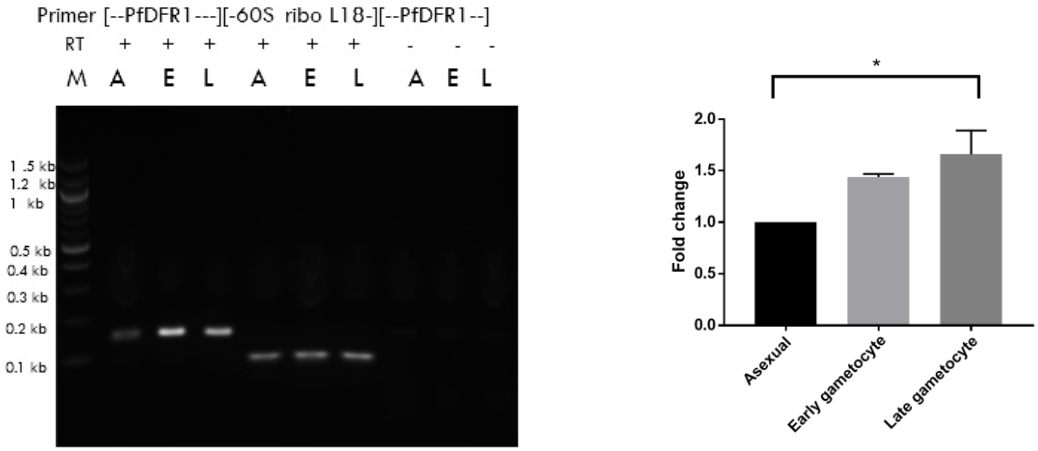

Figure 7.3 Expression of PfDFR1 at the transcription level. A) RT-PCR analysis of PfDFR1 and control K13. B) RT-PCR analysis of PfDFR1 and control 60S ribo L18. Band intensity was measured using ImageJ and fold change was calculated and normalized against intensity of control gene. A: asexual blood stages; E: early gametocytes; and L: late gametocytes. *: $P<0.05$ from Tukey's multiple comparison test. Fold changes were averaged from three independent experiments.

7.3.4 Expression of PfDFR1 at the protein level

To investigate the PfDFR1 expression, two polyclonal antibodies against PfDFR1 were raised in rabbit and mouse. The protein bands of partial purified PfDFR1 FAD/NADPH domains (68 kDa) and PfDFR1 FMN domain (30 kDa) were cut and sent to Davids Biotechnologie GmbH for antibodies production (Figure 7.4). Antibody against PfDFR1_FAD/NADPH was produced in rabbit, while antibody against PfDFR1_ FMN was produced in mouse. The antibodies were tested with parasite lysate from asexual and sexual parasites (Figure 7.5). Rabbit anti-PfDFR1_FAD/NADPH shows a low specificity for the PfDFR1 protein and non-specific protein bands were observed in the Western blot result (Fig. 7.5). However, the mouse anti-PfDFR1_FMN antibody predominantly recognized an expected PfDFR1 band and fewer non-specific bands were observed (Fig. 7.5).

A

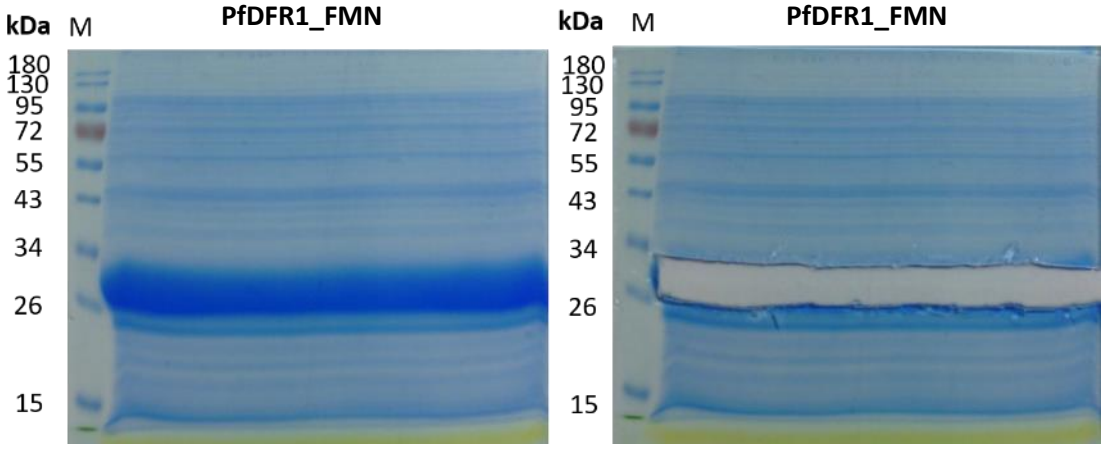

B

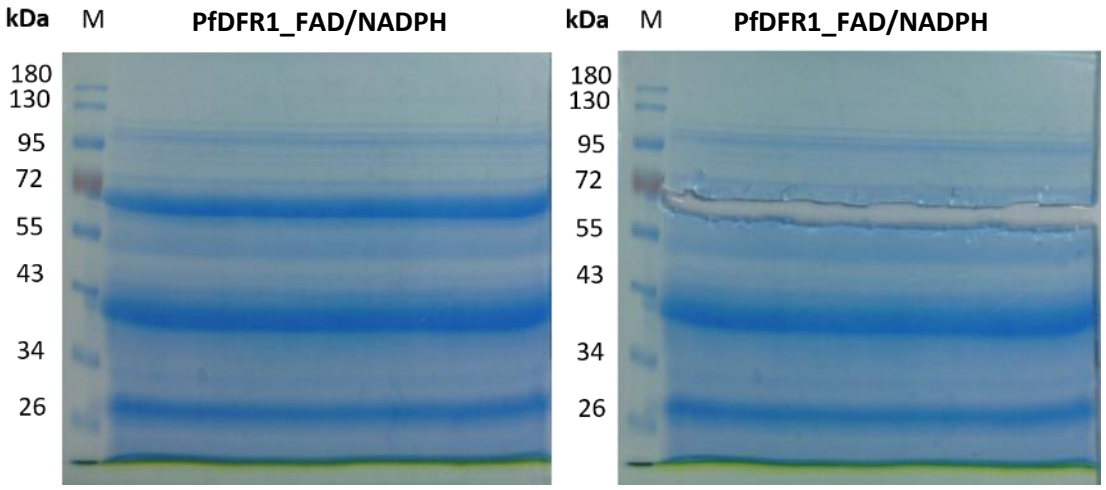

Figure 7.4 Preparation of PfDFR1 for anti-PfDFR1 antibodies production. A) SDS-polyacrylamide gel electrophoresis of PfDFR1_FMN purified by Ni-NTA affinity chromatography before and after cut a protein band. B) SDS-polyacrylamide gel electrophoresis of PfDFR1_FAD/NADPH purified by Ni-NTA affinity chromatography before and after cut a protein band.

A **B**

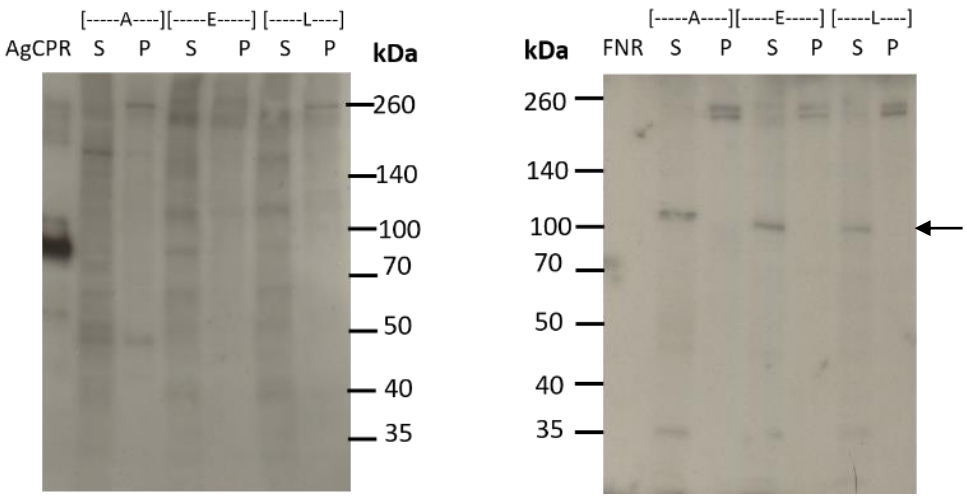

Figure 7.5 Western analysis of anti-PfDFR1 antibodies. A) Western blot result of asexual and sexual malaria parasites using rabbit anti-PfDFR1_FAD/NADPH. B) Western blot result of asexual and sexual malaria parasites using mouse anti-PfDFR1_FMN. A: asexual parasite; E: early gametocyte; L: late gametocyte; S: supernatant of parasite lysate; P: pellet of parasite lysate; AgCPR: recombinant *A. gambiae* CPR (70 kDa); Black arrow: expected PfDFR1 band.

7.3.5 Improvement of the anti-PfDFR1 antibody specificity

To improve the specificity of the rabbit anti-PfDFR1_FAD/NADPH antibody, the western blot method was used in the antibody clean up. Rabbit anti-PfDFR1_FAD/NADPH serum was probed on a nitrocellulose membrane harbouring recombinant PfDFR1. Non-specific antibodies were washed out and antibodies bound specifically to the recombinant PfDFR1 were eluted. Purified rabbit anti-PfDFR1 FAD/NADPH recognised the expected PfDFR1 in the gametocyte lysate (Figure 7.6).

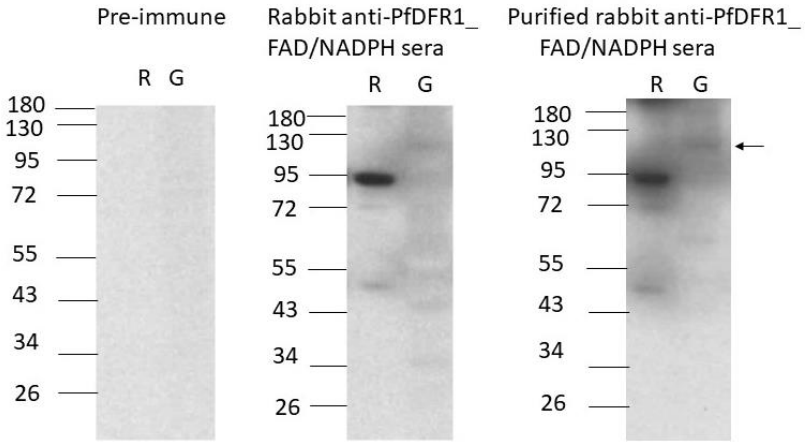

Figure 7.6 Western blot analysis of purified rabbit anti-PfDFR1_FAD/NADPH. R: truncated PfDFR1 wt (87 kDa) and G: gametocyte lysate. Molecular markers are in the left of each figure. Black arrow represents an expected band of PfDFR1.

7.3.6 Localisation of PfDFR1 in malaria parasites

To investigate the localisation of PfDFR1, an immunofluorescence assay was performed with rabbit anti-PfDFR1_FAD/NADPH. The fluorescence signal of PfDFR1 appeared across the whole gametocyte cells and in sub-population of schizonts, but the signal was not detected in trophozoites (Figure 7.7 and 7.8). In addition, a difference in fluorescent intensity between gametocytes was observed. Rabbit pre-immune sera under the same experimental conditions did not recognize any parasite cells in either asexual blood stages and gametocyte stages (Figure 7.9). Polyclonal antibodies against the PfDFR1_FMN domain raised in mouse showed a similar pattern of fluorescence signal in asexual blood stages and gametocytes (Figure 7.10).

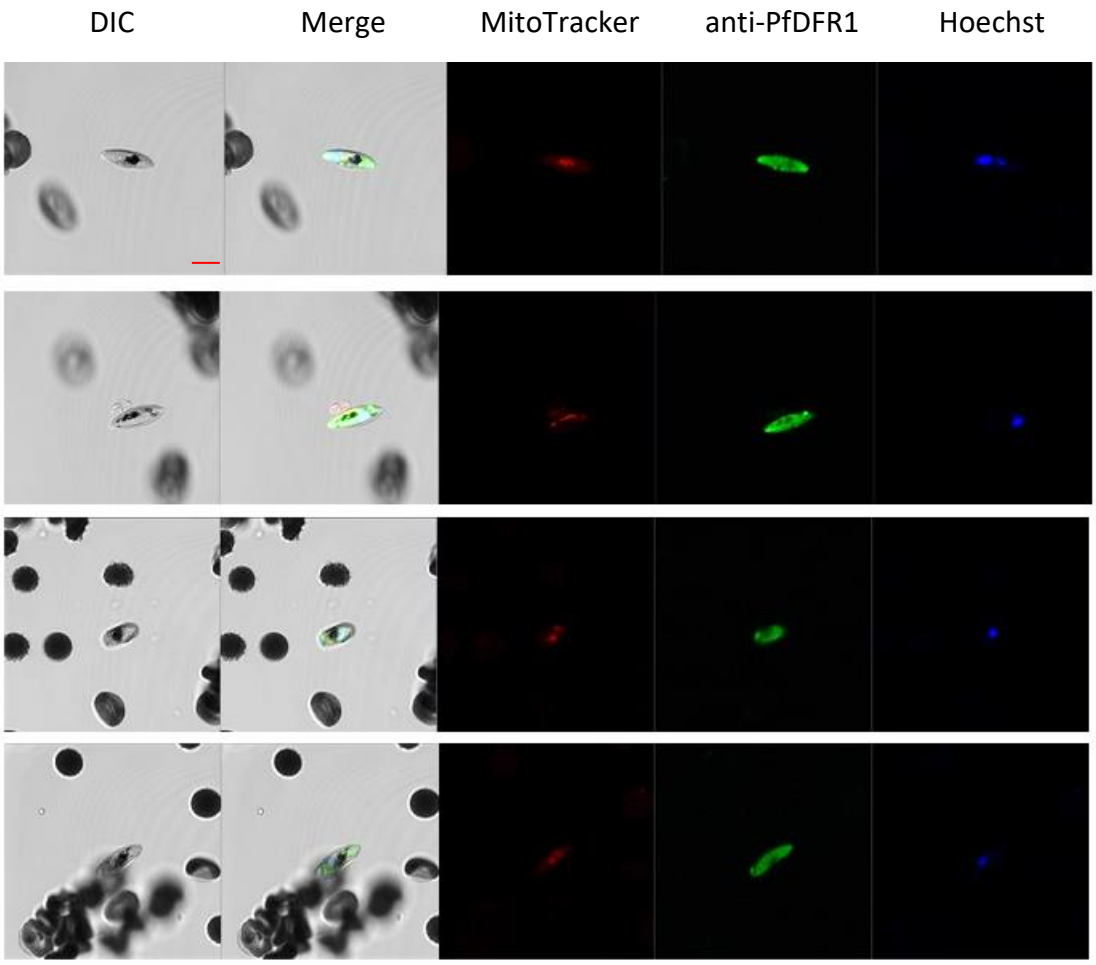

Figure 7.7 Localization of PfDFR1 and mitochondria in gametocyte stages. Immunofluorescence assay using rabbit anti-PfDFR1 FAD/NADPH antibodies and MitoTracker in gametocytes. Merge panel shows the merged image of red MitoTracker signal, green PfDFR1 signal, and blue Hoechst signal. Scale bar is 5 µm.

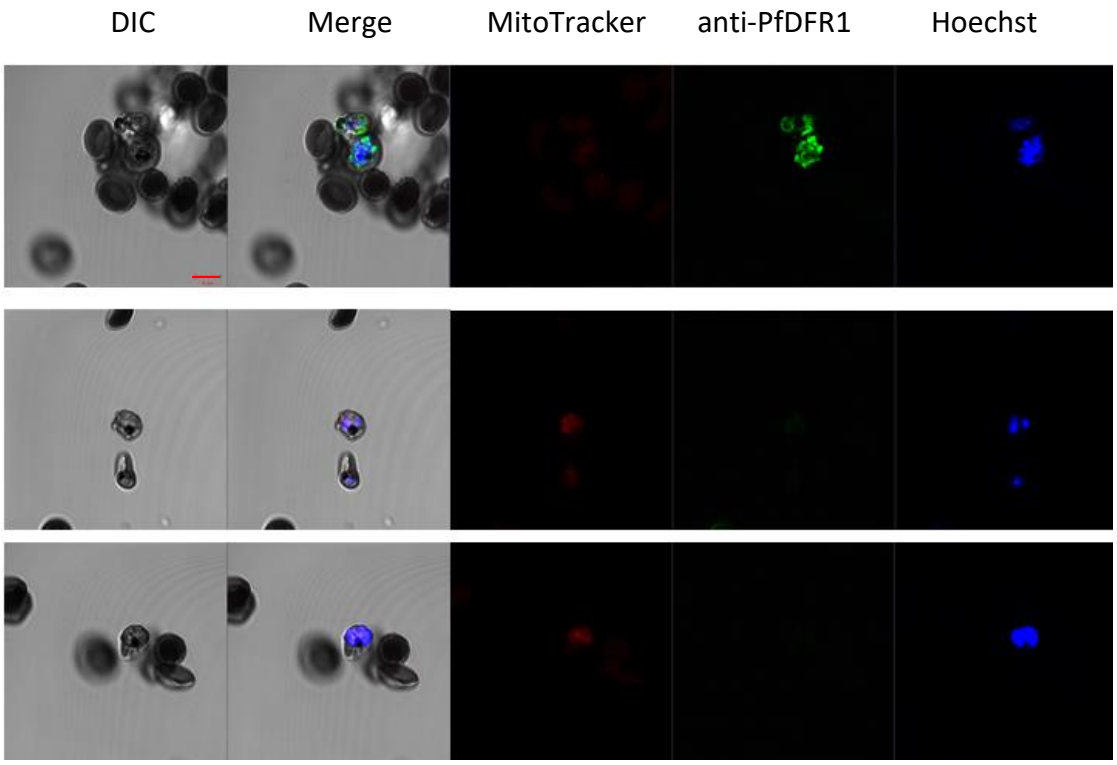

Figure 7.8 Localization of PfDFR1 and mitochondria in asexual blood stages. Immunofluorescence assay using rabbit anti-PfDFR1 FAD/NADPH antibodies and MitoTracker in asexual blood stage parasites. Merge panel shows the merged image of red MitoTracker signal, green PfDFR1 signal, and blue Hoechst signal. Scale bar is 5 µm.

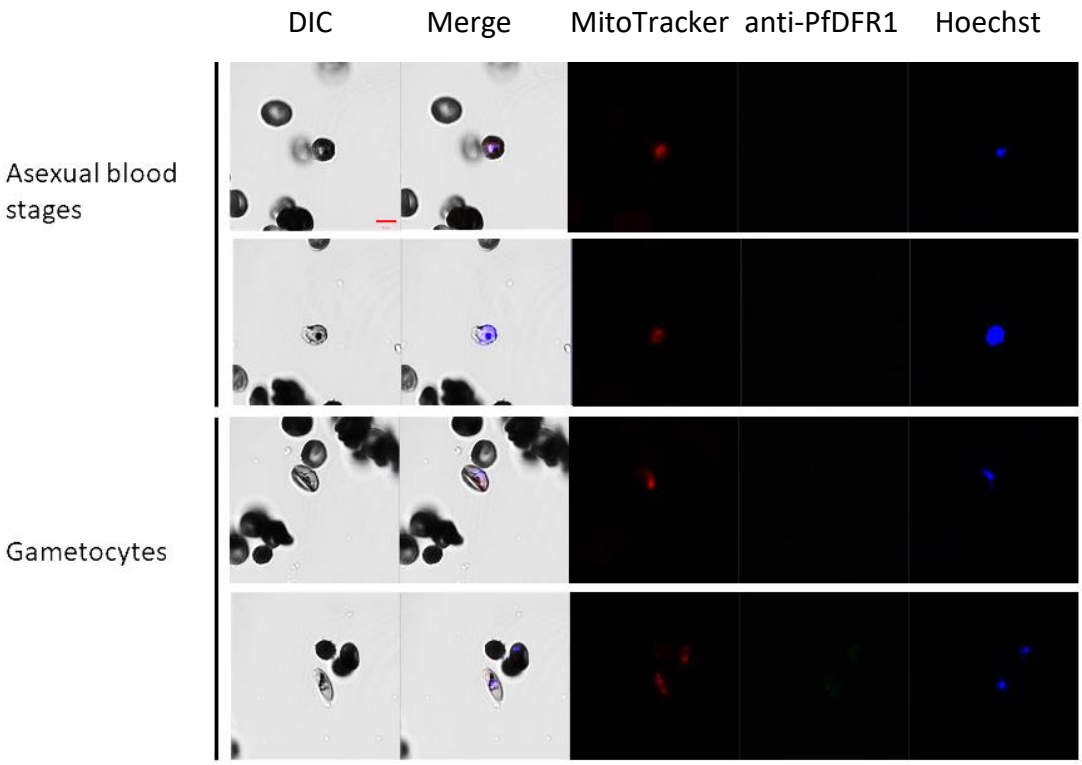

Figure 7.9 Immunofluorescence assay using rabbit pre-immune. Merge panel shows the merged image of fluorescence signals from red MitoTracker, green PfDFR1 and blue Hoechst. Scale bar is 5 µm.

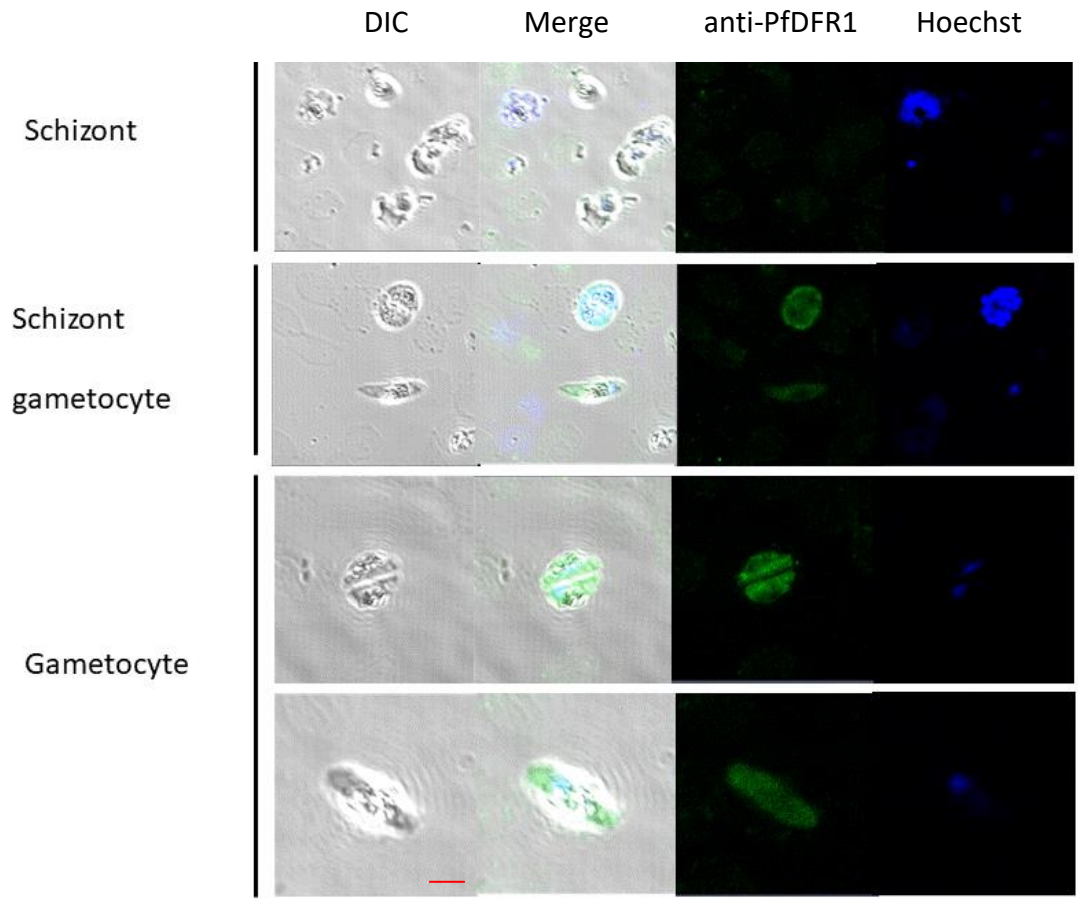

Figure 7.10 Immunofluorescence assay using mouse anti-PfDFR1_FMN antibodies. Merge panel shows the merged image from green PfDFR1 and blue Hoechst. Scale bar is 2 µm.

7.4 Discussion

The purpose of this study was to investigate the expression and localization of PfDFR1 in sexual and erythrocytic asexual stages. The RT-PCR and real time PCR data reveal that PfDFR1 transcription occurs during asexual stages but that an increase in expression is seen during gametocyte development with mature gametocytes exhibiting the highest levels of expression. These data are in agreement with the reported transcriptional profile of this gene in the *P. falciparum* 3D7 strain using RNA-Seq analysis (Figure 7.11) [304, 305].

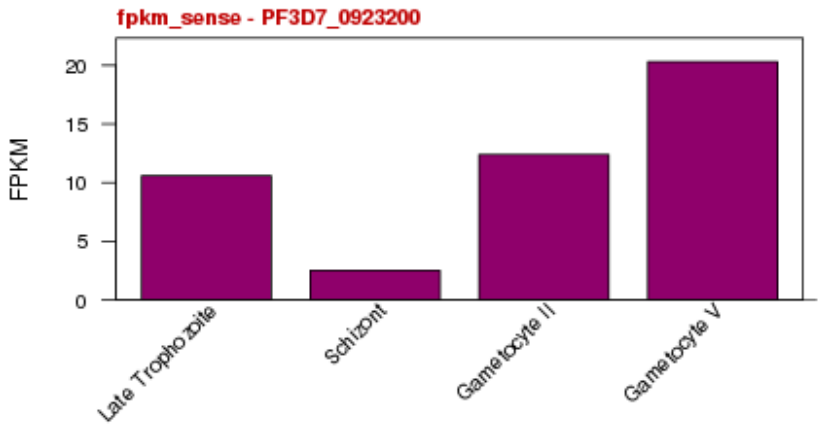

Figure 7.11 PfDFR1 transcription profile. The transcript levels of each stages are shown in fragments per kilobase of exon model per million mapped reads (FPKM). The transcription profile is available in PlasmoDB database [304, 305].

Western blot analyses were performed for PfDFR1, with PfDFR1 detected the protein in both sexual and asexual stages. However, relative protein expression levels of the various parasite stages cannot be inferred from these experiments as protein content was not normalised and therefore protein intensity from the Western blot is non-quantitative. Interestingly, the proteomics data published in PlasmoDB database shows that most of the PfDFR1 matching fragments from mass spectrometry-based expression evidence are found in gametocyte stages (Table 7.3) [304]. This is similar to the finding in the described immunofluorescence assay, whereby most of the PfDFR1 signal is found in gametocytes and some schizonts. These data are also in agreement with reported immunofluorescence experiments performed by Ostera *et al*, that did not report PfDFR1 expression in trophozoites, but did report PfDFR1 mRNA from trophozoite stages [209].

Table 7.3 Summary of PfDFR1 mass spectrometry-based data from PlasmoDB database

Transcript ID(s)	Experiment	Sample	Matching Sequences
PF3D7_0923200.1	Blood stage phospho- and total proteome (3D7)	schizont phosphopeptide-enriched	1
PF3D7_0923200.1	Gametocyte proteomics	female gametocytes	7
PF3D7_0923200.1	Gametocyte proteomics	male gametocytes	10
PF3D7_0923200.1	Gametocytogenesis: trophozoite vs early or late gametocytes (3D7, NF54)	stage V gametocytes (NF54)	11
PF3D7_0923200.1	Gametocyte proteomics	mixed gametocytes	18

The prediction of PfDFR1 localisation using the TargetP 1.1 Server online tool [225] and WoLF PSORT Prediction server [226] show that PfDFR1 has a mitochondrial targeting sequence and could locate in mitochondria. However, the immunofluorescence assay results described herein show that the PfDFR1 signal occurs throughout parasite cells. There are two possibilities that could explain the finding. First, the anti-PfDFR1 antibodies could recognize both unknown proteins located in cytoplasm and PfDFR1. As shown in the Western blot results, anti-PfDFR1 antibodies can recognise expected PfDFR1 band and few unexpected bands (Figure 7.5 and 7.6). A second explanation is that the PfDFR1 immunoassay is correct and that this protein does reside in the cytosol and that the in-silico predictions were erroneous. To confirm localisation of PfDFR1, future experiments will require a highly specific monoclonal antibody of PfDFR1 to be generated.

In immunofluorescence assay results from anti-PfDFR1 polyclonal antibodies generated from mouse and rabbit, we observed similar trends in that the PfDFR1 signal was always found in all gametocytes and sub-population of schizonts. The schizonts that react with anti-PfDFR1 antibodies could be sexually committed schizonts. The previous study from Bruce and her colleagues in 1990 shows that individual schizonts become committed to becoming gametocytes or remain asexual at this stage in development [306]. Environmental factors (i.e. host immunity, host hormones, and anti-malarial drugs) and genetic factors are hypothesized to affect the commitment of each asexual schizont stage to choose between asexual and sexual replication [307, 308]. The triggers and precise timing of the sexual commitment are unclear [309-311]. Recent works have identified the new factors such as an apicomplexa-specific transcription factor (AP2-G) as a transcriptional master switch

that initiates gametocytogenesis [24, 25]. It will be of interest to determine in future experiments whether PfDFR1 plays any role in the biochemical processes involved in gametocyte commitments and/or development.

In conclusion, the expression profiles of PfDFR1 at the RNA level was confirmed by RT-PCR and real-time PCR for both asexual and sexual *P. falciparum* parasite stages. Measured RNA levels indicate that expression occurs throughout the asexual development cycle and that it is also present during the sexual gametocyte stage development, with mature stage V gametocytes exhibiting the highest levels of PfDFR1 expression. PfDFR1 protein production for both asexual and sexual stages was confirmed by Western blot analysis. IFA revealed that PfDFR1 localisation may be in the parasite cytosol, however these results could be affected by non-specific binding and may therefore be misleading. Future experiments will be required to identify PfDFR1 cellular localisation.

CHAPTER 8

GENERAL DISCUSSION

8.1 PfDFR1 is a unique parasite NADP-dependent diflavin reductase with comparatively slow turnover kinetics

The overall aim of this PhD thesis was to characterise the novel diflavin reductase of *P. falciparum*, termed here as PfDFR1 and to investigate its potential role in the mechanism of action of primaquine (PQ). The investigations carried out in this thesis provide a new and improved understanding of this essential enzyme PfDFR1 including; a method for the optimised production of recombinant PfDFR1, insight into the stage-specific expression of PfDFR1, spectral analysis of PfDFR1, pre-steady-state kinetic studies of PfDFR1 half-reaction, steady-state kinetic and inhibition studies and comparative analyses of PfDFR1with hCPR. In addition, the thesis describes a series of experiments relating to PQ mode of action, including steady-state kinetic studies of PfDFR1 and hCPR with PQ derivatives and analogues, and analysis of redox cycling of PQ metabolites in a variety of conditions, including in the presence and absence of specific host tissues.

Before this work was undertaken in 2014, little is known about parasite diflavin reductases. Two sequences (Gene ID PF3D7_0923200 and PF3D7_1450300 from PlasmoDB and NCBI, respectively) had been identified and reported in PlasmoDB as putative CPRs. Both sequences share three predicted domains (FMN-binding, FAD-binding, and NADPH-binding) with other diflavin reductase members, suggesting that

both could be proteins in the diflavin reductase family. PF3D7_0923200 was chosen as the focus for this PhD study because it has the predicted transmembrane helix at the N-terminus (a characteristic of CPR). The PF3D7_0923200 also has a predicted mitochondrial targeting sequence and is upregulated in mature gametocytes. Hence, at the start of this work PF3D7_0923200 was the putative CPR with the greatest probability of functional relevance because it looked like it would locate in the same target organelle where PQ was thought to interact at that time based on a number of reports [107-109]. Importantly, recent genetic validation experiments also predict PF3D7_0923200 to be an indispensable gene [208].

Expression of PfDFR1 was initially very challenging and difficult. The series of codon optimised PfDFR1 constructs lacking the predicted transmembrane helices (first 27 aa) were expressed as insoluble protein products. A potential explanation for this is that the deletion of the predicted transmembrane helices may not have been adequate to cover the whole PfDFR1 transmembrane domain. Examination of the existing literature indicates that soluble recombinant CPR expression, has previously been demonstrated when a further 10 amino acids residues are truncated from the predicted transmembrane helices [118, 171, 182, 229, 230]. Several strategies (including expression temperature, inducer concentration, molecular chaperones addition, and lysis buffer) were used to solve the solubility issues. Only co-expression with chaperones improved the production of soluble PfDFR1, however this in itself generated its own issues in that using this approach the chaperones (DnaK and DnaJ) co-eluted with the PfDFR1 proteins during purification.

To overcome the difficulty in enzyme expression, the original PfDFR1 lacking the first 47 amino acids was constructed and used in the protein expression assays. Leaky expression of PfDFR1 was observed from this construct. This "leaky" expression phenomenon is known to result in low recombinant protein expression by the bacteria prior to induction has been reported in the T7 system. This is recognised to benefit membrane protein expression [240, 241]. The resultant soluble PfDFR1 with catalytic activity was successfully produced from this leaking expression strategy at low temperatures. This breakthrough, taking many months to achieve, allowed for a detailed biochemical and pharmacological characterisation of the protein.

Reassuringly, PfDFR1 showed similarities in absorption maxima peaks and spectral patterns with the reductase domains of other diflavin reductases in their oxidised and semiquinone forms [171, 179, 249, 251], confirming that PfDFR1 is a member of the diflavin reductase family. The rate constants for PfDFR1 half-reaction (2 s^{-1}) was significantly slower when compared to most reported members of the CPR family that typically show rates in the range of 20 to 55 s^{-1} [204, 247, 250, 251] including 200 s^{-1} for NOS [161]. However, PfDFR1 was comparable with human NR1 (1 s^{-1}) [253]. A similar trend was also seen in terms of enzyme kinetic studies using cytochrome *c* and ferricyanide as electron acceptors. Based on the cytochrome *c* assays, the activity of PfDFR1 is 5 to 100-fold lower than other published wild-type or N-terminus truncated CPRs. However, the PfCPR activity is close to that of the rat neuronal NOS and was comparable to the slow turnover number observed with MSR and NR1. The sequence alignment reveals that some of the residues, such as R457 and V492 in hCPR, and S457, C630 and D675 in rat CPR, are involved in cofactor and substrate binding. Mutation of these residues results in a decrease in enzyme catalytic

activity [118] and hydride transfer [250, 254]. These key residues are poorly conserved in PfDFR1 and NR1. This major difference may account for the observed reduction in rates of enzyme catalysis.

A further factor effecting enzyme catalysis is the hinge loop between the connecting domain and the FMN domain. Both lengthening and mutating the hinge loop has been shown to affect CPR and NOS activity [122, 284, 285]. The hinge loop in PfDFR1 is again poorly conserved compared with other diflavin reductases and is longer in length compared with CPRs and NOSs. However, the hinge loop of PfDFR1 is similar in length compared with hNR1. Hence, the unique hinge loop may be another factor contributing to the slow rate in the enzyme.

8.2 PfDFR1 has the potential to interact with PQ metabolites

The kinetic studies of PfDFR1 reveal that PQ derivatives are PfDFR1 substrates. The turnover rate of PfDFR1 is over 20-fold slower than seen with hCPR, but this is somewhat compensated by a lower K_m. The ability to undertake redox cycling of PQ derivatives by PfDFR1 and hCPR was confirmed. Importantly, we were able to show the formation of pharmacologically relevant H_2O_2 generation. Complementary experiments carried out concomitantly in the laboratory by Dr. Grazia Camarda showed that addition of hydroxylated PQ metabolites (OH-PQm) to gametocyte cultures resulted in incomplete killing of parasites, even at super-pharmacological concentrations (10 uM), suggesting that additional processes must be involved to explain the exquisite antimalarial and anti-gametocyte pharmacological profile of PQ when used clinically.

Subsequent experiments performed jointly in the laboratory by Dr Grazia Camarda indicated that addition of human liver microsomes to gametocytes and OH-PQm resulted in efficient gametocyte killing at pharmacologically-relevant (nM) concentrations of OH-PQm. Confirmatory experiments performed in this thesis using hCPR show that the addition of this host enzyme resulted in the generation of very high levels of H_2O_2, which consistent with a mode of action whereby parasite killing is affected by host-derived enzymes at or near the site of parasite residence. Relevant host tissues including the liver (location of liver stage parasites) and the bone marrow (a site for gametocyte maturation and cycling) are shown in Chapter 6 to be able to sustain redox cycling of OH-PQm with concomitant generation of H_2O_2.

The findings from this PhD work together with results from our laboratory and other published works allow us to postulate on the actual mechanisms by which PQ exerts its clinical effects. Then accumulated data suggests that there are three major steps that define the mechanism of action of PQ (Figure 8.1). In Step 1, PQ is metabolised to active PQ metabolites (OH-PQms) with the CYP 2D6 and CPR system being of particular importance. This reaction occurs predominantly in liver hepatocytes, bone marrow, and potentially other sites. In Step 2, unstable OH-PQms spontaneously oxidise to quinoneimines (O=PQ) in the presence of dissolved O_2 with concomitant production of H_2O_2. O=PQs are then reduced back catalytically to OH-PQms via enzyme reaction with human or parasite reductase(s), putatively hCPR and parasite reductase(s) such as PfDFR1. Importantly, this step is catalytic with nM substrate capable of generating micromolar (μM) peroxide. In Step 3, the accumulation of H_2O_2 produced from this redox cycling of catalytic concentrations of OH-PQm results in parasite damage and death as a result peroxide poisoning.

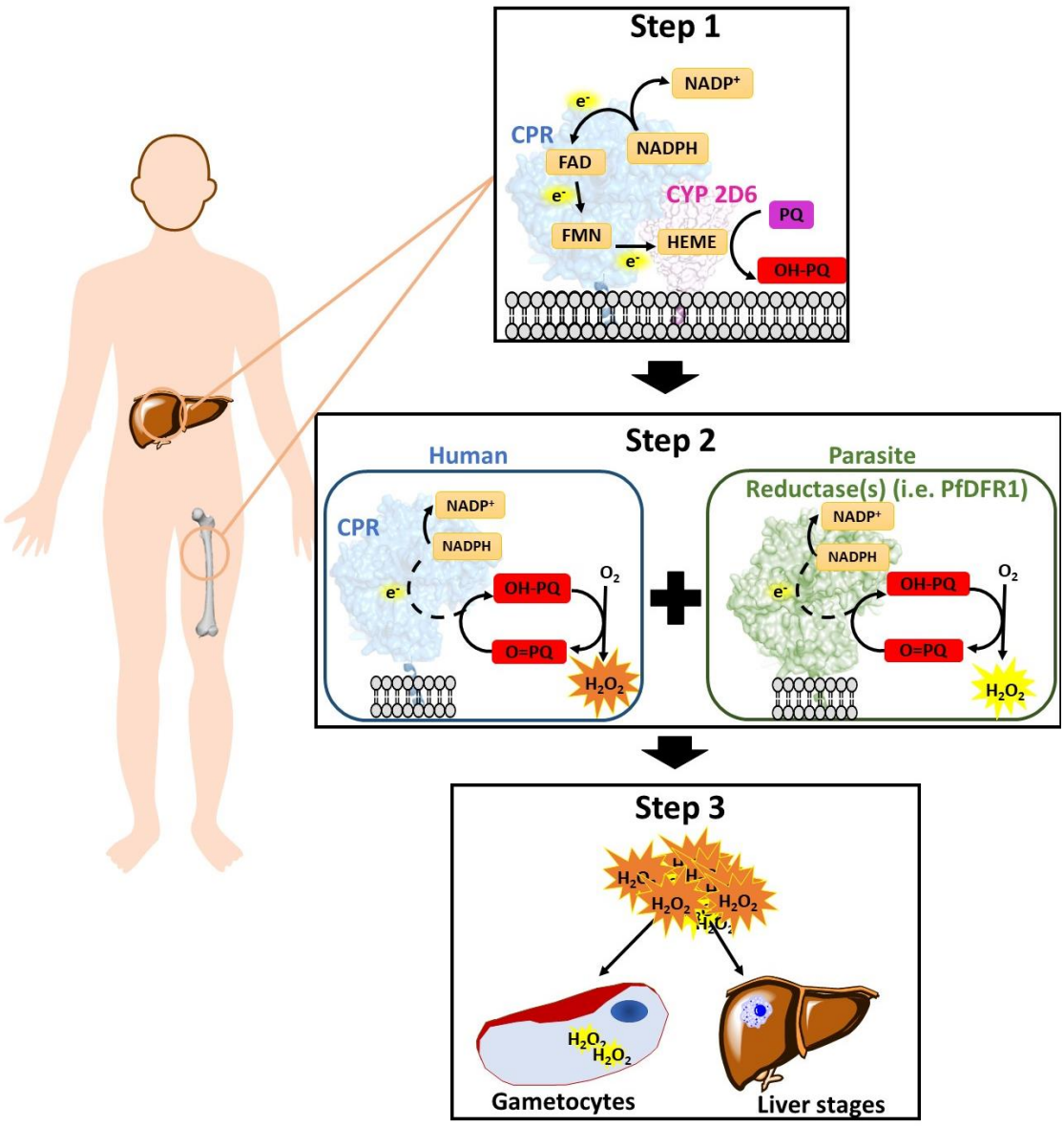

Figure 8.1 The proposed scheme of PQ mechanism of action. The results in this PhD work together with results from our laboratory and known data demonstrate the three steps PQ mechanism of action. In Step 1, PQ is biotransformation to the active PQ metabolites (OH-PQ) through CYP 2D6 and CPR system in liver and bone marrow cells. In Step 2, unstable PQ metabolites (both remained in human host cells and transported to parasites) are spontaneously oxidised to quinoneimines (O=PQ) with H_2O_2 production. Human reductase(s) such as hCPR and parasite reductase(s) such as PfDFR1 act as redox cyclers of PQ metabolites by reducing O=PQs back to PQ OH-PQ. In Step 3, the massive H_2O_2 produced from human system(s) is transported to parasites live in that location. The combination of H_2O_2 transported from outside and produced inside parasites could destroy the redox equilibrium of parasite leading to parasite damage and death

8.3 Further investigations

In this thesis we have initiated the biochemical and pharmacological characterisation of PfDFR1 from *Plasmodium falciparum*. For the complete understanding of PfDFR1 function and elucidation of its essential biological role in the life-cycle of malaria, a number of key research questions need to be addressed in future work. These questions include:

(1) What is the redox partner of PfDFR1 in malaria parasites?

(2) What is the metabolic role of PfDFR1? How is it related to the development and function of gametocytes?

(3) What are the structural factors that give rise to the observed catalytic differences between PfDFR1 and other diflavin reductases?

(4) Can differences between PfDFR1 and human homologs be exploited in terms of innovative drug discovery?

To address the first question, experiments to identify the partner protein(s) as well the localisation of PfDFR1 need to be developed. Protein identification from the general pulldown assays will not be adequate because it is not a permanent interaction between PfDFR1 and its partner(s). Hence, a method to crosslink PfDFR1 with its protein partners to generate a protein complex prior to cell lysis needs to be developed. Once the complex of PfDFR1 and partner(s) is pulled down, the partner(s) can be readily identified by mass spectrometry-based methods. The identified partner protein(s) data would allow for more detailed investigation of the catalytic properties and processes involved providing a greater understanding of the exact function of PfDFR1 in malaria parasites.

The second question relating to functional role could be looked at by introducing mutations into PfDFR1 and assessing loss of fitness/function. Fitness and function would need to be observed using a wide array of techniques such as imaging of the various parasite life cycles including blood and mosquito stages. Omics platforms such as transcriptomics and metabolomics could be used to assess whether mutations introduced into PfDFR1 result in changes in various biochemical pathways and processes.

To address the third question, possible methodology would include the generation of protein crystals to resolve the three-dimensional structure of PfDFR1, including mutagenesis studies. This information from the PfDFR1 structure would help us understand the effect of different substrate binding pockets, the hinge loop, the general structure between PfDFR1 and relatedness to other members of this enzyme family. A 3D structure would also facilitate the design of potential inhibitors exploiting structural differences of the parasite enzyme compared to human diflavin reductase homologs.

In conclusion, the work described in this thesis which has contributed to new understanding in the scientific field includes the detailed investigation of an essential parasite gene that beforehand was only an annotated putative gene in a data base. We have described its basic function, provided evidence to confirm the class of enzyme generated by the gene product and its expression in parasite life-cycle stages. Furthermore, we have provided compelling data supporting a role for this and related human reductases in the mechanisms of action of one of our most important but poorly understood antimalarial classes namely the 8-aminoquinolines as exemplified by PQ.

REFERENCES

1. Nerlich, A.G., et al., *Plasmodium falciparum in ancient Egypt.* Emerg Infect Dis, 2008. **14**(8): p. 1317-9.
2. Phillips, M.A., et al., *Malaria.* Nat Rev Dis Primers, 2017. **3**: p. 17050.
3. Baron, C. and C. Hamlin, *Malaria and the Decline of Ancient Greece: Revisiting the Jones Hypothesis in an Era of Interdisciplinarity.* Minerva, 2015. **53**(4): p. 327-358.
4. Cox-Singh, J., et al., *Plasmodium knowlesi malaria in humans is widely distributed and potentially life threatening.* Clin Infect Dis, 2008. **46**(2): p. 165-71.
5. Petersen, I., R. Eastman, and M. Lanzer, *Drug-resistant malaria: molecular mechanisms and implications for public health.* FEBS Lett, 2011. **585**(11): p. 1551-62.
6. World Health Organization, *World Malaria Report 2017*. 2017, WHO: http://www.who.int/malaria/publications/world-malaria-report-2017/en/.
7. Maitland, K., *Severe Malaria in African Children - The Need for Continuing Investment.* N Engl J Med, 2016. **375**(25): p. 2416-2417.
8. Blasco, B., D. Leroy, and D.A. Fidock, *Antimalarial drug resistance: linking Plasmodium falciparum parasite biology to the clinic.* Nat Med, 2017. **23**(8): p. 917-928.
9. Bannister, L. and G. Mitchell, *The ins, outs and roundabouts of malaria.* Trends Parasitol, 2003. **19**(5): p. 209-13.
10. Tuteja, R., *Malaria - an overview.* FEBS J, 2007. **274**(18): p. 4670-9.
11. Miller, L.H., et al., *The pathogenic basis of malaria.* Nature, 2002. **415**(6872): p. 673-9.
12. Mbengue, A., X.Y. Yam, and C. Braun-Breton, *Human erythrocyte remodelling during Plasmodium falciparum malaria parasite growth and egress.* Br J Haematol, 2012. **157**(2): p. 171-9.
13. Flannery, E.L., A.K. Chatterjee, and E.A. Winzeler, *Antimalarial drug discovery - approaches and progress towards new medicines.* Nat Rev Microbiol, 2013. **11**(12): p. 849-62.
14. Taylor, L.H. and A.F. Read, *Why so few transmission stages? Reproductive restraint by malaria parasites.* Parasitology Today, 1997. **13**(4): p. 135-140.
15. Josling, G.A. and M. Llinas, *Sexual development in Plasmodium parasites: knowing when it's time to commit.* Nature Reviews Microbiology, 2015. **13**(9): p. 573-587.
16. Bruce, M.C., et al., *Commitment of the Malaria Parasite Plasmodium-Falciparum to Sexual and Asexual Development.* Parasitology, 1990. **100**: p. 191-200.
17. Alano, P., *Plasmodium falciparum gametocytes: still many secrets of a hidden life.* Molecular Microbiology, 2007. **66**(2): p. 291-302.
18. Buckling, A., et al., *Chloroquine increases Plasmodium falciparum gametocytogenesis in vitro.* Parasitology, 1999. **118 (Pt 4)**: p. 339-46.

19. Buckling, A., L. Crooks, and A. Read, *Plasmodium chabaudi: effect of antimalarial drugs on gametocytogenesis.* Exp Parasitol, 1999. **93**(1): p. 45-54.
20. Williams, J.L., *Stimulation of Plasmodium falciparum gametocytogenesis by conditioned medium from parasite cultures.* Am J Trop Med Hyg, 1999. **60**(1): p. 7-13.
21. Dunyo, S., et al., *Gametocytaemia after drug treatment of asymptomatic Plasmodium falciparum.* Plos Clinical Trials, 2006. **1**(4).
22. Brancucci, N.M.B., et al., *Lysophosphatidylcholine Regulates Sexual Stage Differentiation in the Human Malaria Parasite Plasmodium falciparum.* Cell, 2017. **171**(7): p. 1532-1544 e15.
23. Josling, G.A., K.C. Williamson, and M. Llinas, *Regulation of Sexual Commitment and Gametocytogenesis in Malaria Parasites.* Annu Rev Microbiol, 2018. **72**: p. 501-519.
24. Kent, R.S., et al., *Inducible developmental reprogramming redefines commitment to sexual development in the malaria parasite Plasmodium berghei.* Nat Microbiol, 2018.
25. Kafsack, B.F., et al., *A transcriptional switch underlies commitment to sexual development in malaria parasites.* Nature, 2014. **507**(7491): p. 248-52.
26. Filarsky, M., et al., *GDV1 induces sexual commitment of malaria parasites by antagonizing HP1-dependent gene silencing.* Science, 2018. **359**(6381): p. 1259-1263.
27. Butterworth, A.S., et al., *Plasmodium falciparum gametocytes: with a view to a kill.* Parasitology, 2013. **140**(14): p. 1718-34.
28. Kumar, N. and H. Zheng, *Stage-specific gametocytocidal effect in vitro of the antimalaria drug qinghaosu on Plasmodium falciparum.* Parasitol Res, 1990. **76**(3): p. 214-8.
29. Adjalley, S.H., et al., *Quantitative assessment of Plasmodium falciparum sexual development reveals potent transmission-blocking activity by methylene blue.* Proc Natl Acad Sci U S A, 2011. **108**(47): p. E1214-23.
30. Buchholz, K., et al., *A high-throughput screen targeting malaria transmission stages opens new avenues for drug development.* J Infect Dis, 2011. **203**(10): p. 1445-53.
31. Fleck, S.L., M. Pudney, and R.E. Sinden, *The effect of atovaquone (566C80) on the maturation and viability of Plasmodium falciparum gametocytes in vitro.* Trans R Soc Trop Med Hyg, 1996. **90**(3): p. 309-12.
32. Bousema, T., et al., *Revisiting the circulation time of Plasmodium falciparum gametocytes: molecular detection methods to estimate the duration of gametocyte carriage and the effect of gametocytocidal drugs.* Malar J, 2010. **9**: p. 136.
33. Jeffery, G.M., M.D. Young, and D.E. Eyles, *The treatment of Plasmodium falciparum infection with chloroquine, with a note on infectivity to mosquitoes of primaquine- and pyrimethamine-treated cases.* Am J Hyg, 1956. **64**(1): p. 1-11.
34. De Niz, M., et al., *Plasmodium gametocytes display homing and vascular transmigration in the host bone marrow.* Sci Adv, 2018. **4**(5): p. eaat3775.
35. Hemingway, J., et al., *Tools and Strategies for Malaria Control and Elimination: What Do We Need to Achieve a Grand Convergence in Malaria?* PLoS Biol, 2016. **14**(3): p. e1002380.

36. World Health Organization, *Guidelines for the treatment of malaria*. 2015: http://www.who.int/malaria/publications/atoz/9789241549127/en/.
37. Coelho, C.H., et al., *Advances in malaria vaccine development: report from the 2017 malaria vaccine symposium.* NPJ Vaccines, 2017. **2**: p. 34.
38. Eisele, T.P., D. Larsen, and R.W. Steketee, *Protective efficacy of interventions for preventing malaria mortality in children in Plasmodium falciparum endemic areas.* Int J Epidemiol, 2010. **39 Suppl 1**: p. i88-101.
39. Bhatt, S., et al., *The effect of malaria control on Plasmodium falciparum in Africa between 2000 and 2015.* Nature, 2015. **526**(7572): p. 207-211.
40. Ashley, E.A., J. Recht, and N.J. White, *Primaquine: the risks and the benefits.* Malar J, 2014. **13**: p. 418.
41. D'Alessandro, S., et al., *A chemical susceptibility profile of the Plasmodium falciparum transmission stages by complementary cell-based gametocyte assays.* J Antimicrob Chemother, 2016. **71**(5): p. 1148-58.
42. Li, Y. and Y.L. Wu, *An over four millennium story behind qinghaosu (artemisinin)--a fantastic antimalarial drug from a traditional chinese herb.* Curr Med Chem, 2003. **10**(21): p. 2197-230.
43. Tu, Y., *The discovery of artemisinin (qinghaosu) and gifts from Chinese medicine.* Nat Med, 2011. **17**(10): p. 1217-20.
44. Cui, L. and X.Z. Su, *Discovery, mechanisms of action and combination therapy of artemisinin.* Expert Rev Anti Infect Ther, 2009. **7**(8): p. 999-1013.
45. Meunier, B. and A. Robert, *Heme as trigger and target for trioxane-containing antimalarial drugs.* Acc Chem Res, 2010. **43**(11): p. 1444-51.
46. Klonis, N., D.J. Creek, and L. Tilley, *Iron and heme metabolism in Plasmodium falciparum and the mechanism of action of artemisinins.* Curr Opin Microbiol, 2013. **16**(6): p. 722-7.
47. O'Neill, P.M., V.E. Barton, and S.A. Ward, *The molecular mechanism of action of artemisinin--the debate continues.* Molecules, 2010. **15**(3): p. 1705-21.
48. Li, J. and B. Zhou, *Biological actions of artemisinin: insights from medicinal chemistry studies.* Molecules, 2010. **15**(3): p. 1378-97.
49. Tilley, L., et al., *Artemisinin Action and Resistance in Plasmodium falciparum.* Trends Parasitol, 2016. **32**(9): p. 682-696.
50. Ashley, E.A., et al., *Spread of artemisinin resistance in Plasmodium falciparum malaria.* N Engl J Med, 2014. **371**(5): p. 411-23.
51. Sibley, C.H., *Infectious diseases. Understanding artemisinin resistance.* Science, 2015. **347**(6220): p. 373-4.
52. Ariey, F., et al., *A molecular marker of artemisinin-resistant Plasmodium falciparum malaria.* Nature, 2014. **505**(7481): p. 50-5.
53. Chen, P.Q., et al., *The infectivity of gametocytes of Plasmodium falciparum from patients treated with artemisinin.* Chin Med J (Engl), 1994. **107**(9): p. 709-11.
54. Skinner, T.S., et al., *In vitro stage-specific sensitivity of Plasmodium falciparum to quinine and artemisinin drugs.* Int J Parasitol, 1996. **26**(5): p. 519-25.
55. Peatey, C.L., et al., *Anti-malarial drugs: how effective are they against Plasmodium falciparum gametocytes?* Malar J, 2012. **11**: p. 34.
56. Chotivanich, K., et al., *Transmission-blocking activities of quinine, primaquine, and artesunate.* Antimicrob Agents Chemother, 2006. **50**(6): p. 1927-30.

57. Targett, G., et al., *Artesunate reduces but does not prevent posttreatment transmission of Plasmodium falciparum to Anopheles gambiae.* J Infect Dis, 2001. **183**(8): p. 1254-9.
58. Foley, M. and L. Tilley, *Quinoline antimalarials: mechanisms of action and resistance and prospects for new agents.* Pharmacol Ther, 1998. **79**(1): p. 55-87.
59. Antony, H.A. and S.C. Parija, *Antimalarial drug resistance: An overview.* Trop Parasitol, 2016. **6**(1): p. 30-41.
60. Hill, S.R. and G.K. Sharma, *Antimalarial Medications*, in *StatPearls*. 2018: Treasure Island (FL).
61. Mackerras, M.J. and Q.N. Ercole, *Observations on the action of quinine, atebrin and plasmoquine on the gametocytes of Plasmodium falciparum.* Trans R Soc Trop Med Hyg, 1949. **42**(5): p. 455-63.
62. Sowunmi, A., et al., *Effects of mefloquine and artesunate mefloquine on the emergence, clearance and sex ratio of Plasmodium falciparum gametocytes in malarious children.* Malar J, 2009. **8**: p. 297.
63. Loeb, R.F., *Activity of a new antimalarial agent, pentaquine (SN 13,276).* J Am Med Assoc, 1946. **132**: p. 321-3.
64. Najera, J.A., M. Gonzalez-Silva, and P.L. Alonso, *Some lessons for the future from the Global Malaria Eradication Programme (1955-1969).* PLoS Med, 2011. **8**(1): p. e1000412.
65. Sowunmi, A. and B.A. Fateye, *Plasmodium falciparum gametocytaemia in Nigerian children: before, during and after treatment with antimalarial drugs.* Trop Med Int Health, 2003. **8**(9): p. 783-92.
66. Sowunmi, A., et al., *Plasmodium falciparum gametocytaemia in Nigerian children: Peripheral immature gametocytaemia as an indicator of a poor response to chloroquine treatment, and its relationship to molecular determinants of chloroquine resistance.* Ann Trop Med Parasitol, 2003. **97**(5): p. 453-68.
67. Greenwood, D., *Conflicts of interest: the genesis of synthetic antimalarial agents in peace and war.* J Antimicrob Chemother, 1995. **36**(5): p. 857-72.
68. Chou, A.C. and C.D. Fitch, *Control of heme polymerase by chloroquine and other quinoline derivatives.* Biochem Biophys Res Commun, 1993. **195**(1): p. 422-7.
69. Davis, T.M., et al., *Piperaquine: a resurgent antimalarial drug.* Drugs, 2005. **65**(1): p. 75-87.
70. Slater, A.F., *Chloroquine: mechanism of drug action and resistance in Plasmodium falciparum.* Pharmacol Ther, 1993. **57**(2-3): p. 203-35.
71. Pradines, B., et al., *In vitro activity of tafenoquine against the asexual blood stages of Plasmodium falciparum isolates from Gabon, Senegal, and Djibouti.* Antimicrob Agents Chemother, 2006. **50**(9): p. 3225-6.
72. Brueckner, R.P., et al., *First-time-in-humans safety and pharmacokinetics of WR 238605, a new antimalarial.* Am J Trop Med Hyg, 1998. **58**(5): p. 645-9.
73. Edstein, M.D., et al., *Population pharmacokinetics of the new antimalarial agent tafenoquine in Thai soldiers.* Br J Clin Pharmacol, 2001. **52**(6): p. 663-70.
74. Fieser, L.F. and A.P. Richardson, *Naphthoquinone antimalarials; correlation of structure and activity against P. lophurae in ducks.* J Am Chem Soc, 1948. **70**(10): p. 3156-65.

75. Nixon, G.L., et al., *Antimalarial pharmacology and therapeutics of atovaquone.* J Antimicrob Chemother, 2013. **68**(5): p. 977-85.
76. Lalloo, D.G. and D.R. Hill, *Preventing malaria in travellers.* BMJ, 2008. **336**(7657): p. 1362-6.
77. Osei-Akoto, A., L. Orton, and S.P. Owusu-Ofori, *Atovaquone-proguanil for treating uncomplicated malaria.* Cochrane Database Syst Rev, 2005(4): p. CD004529.
78. Fry, M. and M. Pudney, *Site of action of the antimalarial hydroxynaphthoquinone, 2-[trans-4-(4'-chlorophenyl) cyclohexyl]-3-hydroxy-1,4-naphthoquinone (566C80).* Biochem Pharmacol, 1992. **43**(7): p. 1545-53.
79. Siregar, J.E., et al., *Direct evidence for the atovaquone action on the Plasmodium cytochrome bc1 complex.* Parasitol Int, 2015. **64**(3): p. 295-300.
80. Biagini, G.A., et al., *Functional characterization and target validation of alternative complex I of Plasmodium falciparum mitochondria.* Antimicrob Agents Chemother, 2006. **50**(5): p. 1841-51.
81. Srivastava, I.K., H. Rottenberg, and A.B. Vaidya, *Atovaquone, a broad spectrum antiparasitic drug, collapses mitochondrial membrane potential in a malarial parasite.* J Biol Chem, 1997. **272**(7): p. 3961-6.
82. Malmquist, N.A., et al., *Analysis of flavin oxidation and electron-transfer inhibition in Plasmodium falciparum dihydroorotate dehydrogenase.* Biochemistry, 2008. **47**(8): p. 2466-75.
83. Rawls, J., et al., *Requirements for the mitochondrial import and localization of dihydroorotate dehydrogenase.* Eur J Biochem, 2000. **267**(7): p. 2079-87.
84. Lelievre, J., et al., *Activity of clinically relevant antimalarial drugs on Plasmodium falciparum mature gametocytes in an ATP bioluminescence "transmission blocking" assay.* PLoS One, 2012. **7**(4): p. e35019.
85. Butcher, G.A., *Antimalarial drugs and the mosquito transmission of Plasmodium.* Int J Parasitol, 1997. **27**(9): p. 975-87.
86. Farber, P.M., et al., *Recombinant Plasmodium falciparum glutathione reductase is inhibited by the antimalarial dye methylene blue.* FEBS Lett, 1998. **422**(3): p. 311-4.
87. Schirmer, R.H., et al., *Methylene blue as an antimalarial agent.* Redox Rep, 2003. **8**(5): p. 272-5.
88. Arora, K. and A.K. Srivastava, *Antimalarial efficacy of methylene blue and menadione and their effect on glutathione metabolism of Plasmodium yoelii-infected albino mice.* Parasitol Res, 2005. **97**(6): p. 521-6.
89. Dicko, A., et al., *Efficacy and safety of primaquine and methylene blue for prevention of Plasmodium falciparum transmission in Mali: a phase 2, single-blind, randomised controlled trial.* Lancet Infect Dis, 2018. **18**(6): p. 627-639.
90. Wadi, I., et al., *Methylene blue induced morphological deformations in Plasmodium falciparum gametocytes: implications for transmission-blocking.* Malar J, 2018. **17**(1): p. 11.
91. Coulibaly, B., et al., *Strong gametocytocidal effect of methylene blue-based combination therapy against falciparum malaria: a randomised controlled trial.* PLoS One, 2009. **4**(5): p. e5318.
92. Ganesan, S., et al., *Understanding the mechanisms for metabolism-linked hemolytic toxicity of primaquine against glucose 6-phosphate dehydrogenase*

deficient human erythrocytes: evaluation of eryptotic pathway. Toxicology, 2012. **294**(1): p. 54-60.
93. Vasquez-Vivar, J. and O. Augusto, *Hydroxylated metabolites of the antimalarial drug primaquine. Oxidation and redox cycling.* J Biol Chem, 1992. **267**(10): p. 6848-54.
94. Bowman, Z.S., et al., *Primaquine-induced hemolytic anemia: susceptibility of normal versus glutathione-depleted rat erythrocytes to 5-hydroxyprimaquine.* J Pharmacol Exp Ther, 2004. **309**(1): p. 79-85.
95. Pybus, B.S., et al., *CYP450 phenotyping and accurate mass identification of metabolites of the 8-aminoquinoline, anti-malarial drug primaquine.* Malar J, 2012. **11**: p. 259.
96. Fasinu, P.S., et al., *Enantioselective metabolism of primaquine by human CYP2D6.* Malar J, 2014. **13**: p. 507.
97. Marcsisin, S.R., G. Reichard, and B.S. Pybus, *Primaquine pharmacology in the context of CYP 2D6 pharmacogenomics: Current state of the art.* Pharmacol Ther, 2016. **161**: p. 1-10.
98. Mihaly, G.W., et al., *Pharmacokinetics of primaquine in man: identification of the carboxylic acid derivative as a major plasma metabolite.* Br J Clin Pharmacol, 1984. **17**(4): p. 441-6.
99. Constantino, L., et al., *Metabolism of primaquine by liver homogenate fractions. Evidence for monoamine oxidase and cytochrome P450 involvement in the oxidative deamination of primaquine to carboxyprimaquine.* Exp Toxicol Pathol, 1999. **51**(4-5): p. 299-303.
100. Bennett, J.W., et al., *Primaquine failure and cytochrome P-450 2D6 in Plasmodium vivax malaria.* N Engl J Med, 2013. **369**(14): p. 1381-2.
101. Pybus, B.S., et al., *The metabolism of primaquine to its active metabolite is dependent on CYP 2D6.* Malar J, 2013. **12**: p. 212.
102. Bolchoz, L.J., et al., *Primaquine-induced hemolytic anemia: formation and hemotoxicity of the arylhydroxylamine metabolite 6-methoxy-8-hydroxylaminoquinoline.* J Pharmacol Exp Ther, 2001. **297**(2): p. 509-15.
103. Ganesan, S., et al., *Cytochrome P(450)-dependent toxic effects of primaquine on human erythrocytes.* Toxicol Appl Pharmacol, 2009. **241**(1): p. 14-22.
104. Rochford, R., et al., *Humanized mouse model of glucose 6-phosphate dehydrogenase deficiency for in vivo assessment of hemolytic toxicity.* Proc Natl Acad Sci U S A, 2013. **110**(43): p. 17486-91.
105. Potter, B.M., et al., *Differential CYP 2D6 metabolism alters primaquine pharmacokinetics.* Antimicrob Agents Chemother, 2015. **59**(4): p. 2380-7.
106. Committee, W.H.O.M.P.A. and Secretariat, *Malaria Policy Advisory Committee to the WHO: conclusions and recommendations of September 2012 meeting.* Malaria Journal, 2012. **11**(1): p. 424.
107. Lanners, H.N., *Effect of the 8-aminoquinoline primaquine on culture-derived gametocytes of the malaria parasite Plasmodium falciparum.* Parasitol Res, 1991. **77**(6): p. 478-81.
108. Aikawa, M. and R.L. Beaudoin, *Plasmodium fallax: high-resolution autoradiography of exoerythrocytic stages treated with Primaquine in vitro.* Exp Parasitol, 1970. **27**(3): p. 454-63.
109. Howells, R.E., W. Pters, and J. Fullard, *The chemotherapy of rodent malaria. 13. Fine structural changes observed in the eryhrocytic stages of Plasmodium*

berghei berghei following exposureto primaquine and menoctone. Ann Trop Med Parasitol, 1970. **64**(2): p. 203-7.
110. Zhang, J., et al., *Crystal structure of the FAD/NADPH-binding domain of rat neuronal nitric-oxide synthase. Comparisons with NADPH-cytochrome P450 oxidoreductase.* J Biol Chem, 2001. **276**(40): p. 37506-13.
111. Paine, M.J., et al., *Cloning and characterization of a novel human dual flavin reductase.* J Biol Chem, 2000. **275**(2): p. 1471-8.
112. Leclerc, D., et al., *Cloning and mapping of a cDNA for methionine synthase reductase, a flavoprotein defective in patients with homocystinuria.* Proc Natl Acad Sci U S A, 1998. **95**(6): p. 3059-64.
113. Ruettinger, R.T., L.P. Wen, and A.J. Fulco, *Coding nucleotide, 5' regulatory, and deduced amino acid sequences of P-450BM-3, a single peptide cytochrome P-450:NADPH-P-450 reductase from Bacillus megaterium.* J Biol Chem, 1989. **264**(19): p. 10987-95.
114. Ostrowski, J., et al., *Characterization of the flavoprotein moieties of NADPH-sulfite reductase from Salmonella typhimurium and Escherichia coli. Physicochemical and catalytic properties, amino acid sequence deduced from DNA sequence of cysJ, and comparison with NADPH-cytochrome P-450 reductase.* J Biol Chem, 1989. **264**(27): p. 15796-808.
115. Inui, H., et al., *Pyruvate:NADP+ oxidoreductase from Euglena gracilis: limited proteolysis of the enzyme with trypsin.* Arch Biochem Biophys, 1991. **286**(1): p. 270-6.
116. Netz, D.J., et al., *Tah18 transfers electrons to Dre2 in cytosolic iron-sulfur protein biogenesis.* Nat Chem Biol, 2010. **6**(10): p. 758-65.
117. Wang, M., et al., *Three-dimensional structure of NADPH-cytochrome P450 reductase: prototype for FMN- and FAD-containing enzymes.* Proc Natl Acad Sci U S A, 1997. **94**(16): p. 8411-6.
118. Xia, C., et al., *Structural basis for human NADPH-cytochrome P450 oxidoreductase deficiency.* Proc Natl Acad Sci U S A, 2011. **108**(33): p. 13486-91.
119. Garcin, E.D., et al., *Structural basis for isozyme-specific regulation of electron transfer in nitric-oxide synthase.* J Biol Chem, 2004. **279**(36): p. 37918-27.
120. Gruez, A., et al., *Four crystal structures of the 60 kDa flavoprotein monomer of the sulfite reductase indicate a disordered flavodoxin-like module.* J Mol Biol, 2000. **299**(1): p. 199-212.
121. Haque, M.M., et al., *Distinct conformational behaviors of four mammalian dual-flavin reductases (cytochrome P450 reductase, methionine synthase reductase, neuronal nitric oxide synthase, endothelial nitric oxide synthase) determine their unique catalytic profiles.* FEBS J, 2014. **281**(23): p. 5325-40.
122. Hamdane, D., et al., *Structure and function of an NADPH-cytochrome P450 oxidoreductase in an open conformation capable of reducing cytochrome P450.* J Biol Chem, 2009. **284**(17): p. 11374-84.
123. Xia, C., et al., *Conformational changes of NADPH-cytochrome P450 oxidoreductase are essential for catalysis and cofactor binding.* J Biol Chem, 2011. **286**(18): p. 16246-60.
124. Wada, F., et al., *Participation of the microsomal electron transport system involving cytochrome P-450 in omega-oxidation of fatty acids.* Biochim Biophys Acta, 1968. **162**(4): p. 518-24.

125. Emerson, M.R. and S.M. LeVine, *Heme oxygenase-1 and NADPH cytochrome P450 reductase expression in experimental allergic encephalomyelitis: an expanded view of the stress response.* J Neurochem, 2000. **75**(6): p. 2555-62.
126. Abu-Soud, H.M., et al., *Electron transfer in the nitric-oxide synthases. Characterization of L-arginine analogs that block heme iron reduction.* J Biol Chem, 1994. **269**(51): p. 32318-26.
127. Olteanu, H. and R. Banerjee, *Human methionine synthase reductase, a soluble P-450 reductase-like dual flavoprotein, is sufficient for NADPH-dependent methionine synthase activation.* J Biol Chem, 2001. **276**(38): p. 35558-63.
128. Yoshimoto, A. and R. Sato, *Studies on yeast sulfite reductase. 3. Further characterization.* Biochim Biophys Acta, 1970. **220**(2): p. 190-205.
129. Faeder, E.J., P.S. Davis, and L.M. Siegel, *Reduced nicotinamide adenine dinucleotide phosphate-sulfite reductase of enterobacteria. V. Studies with the Escherichia coli hemoflavoprotein depleted of flavin mononucleotide: distinct roles for the flavin adenine dinucleotide and flavin mononucleotide prosthetic groups in catalysis.* J Biol Chem, 1974. **249**(5): p. 1599-609.
130. Siegel, L.M., P.S. Davis, and H. Kamin, *Reduced nicotinamide adenine dinucleotide phosphate-sulfite reductase of enterobacteria. 3. The Escherichia coli hemoflavoprotein: catalytic parameters and the sequence of electron flow.* J Biol Chem, 1974. **249**(5): p. 1572-86.
131. Elmore, C.L. and T.D. Porter, *Modification of the nucleotide cofactor-binding site of cytochrome P-450 reductase to enhance turnover with NADH in Vivo.* J Biol Chem, 2002. **277**(50): p. 48960-4.
132. Shen, A.L., et al., *Structural analysis of the FMN binding domain of NADPH-cytochrome P-450 oxidoreductase by site-directed mutagenesis.* J Biol Chem, 1989. **264**(13): p. 7584-9.
133. Klein, M.L. and A.J. Fulco, *Critical residues involved in FMN binding and catalytic activity in cytochrome P450BM-3.* J Biol Chem, 1993. **268**(10): p. 7553-61.
134. Adak, S., et al., *Role of reductase domain cluster 1 acidic residues in neuronal nitric-oxide synthase. Characterization of the FMN-FREE enzyme.* J Biol Chem, 1999. **274**(32): p. 22313-20.
135. Iyanagi, T., C. Xia, and J.J. Kim, *NADPH-cytochrome P450 oxidoreductase: prototypic member of the diflavin reductase family.* Arch Biochem Biophys, 2012. **528**(1): p. 72-89.
136. Forstermann, U. and W.C. Sessa, *Nitric oxide synthases: regulation and function.* Eur Heart J, 2012. **33**(7): p. 829-37, 837a-837d.
137. Schuman, E.M. and D.V. Madison, *A requirement for the intercellular messenger nitric oxide in long-term potentiation.* Science, 1991. **254**(5037): p. 1503-6.
138. Izumi, Y., D.B. Clifford, and C.F. Zorumski, *Inhibition of long-term potentiation by NMDA-mediated nitric oxide release.* Science, 1992. **257**(5074): p. 1273-6.
139. Zhou, L. and D.Y. Zhu, *Neuronal nitric oxide synthase: structure, subcellular localization, regulation, and clinical implications.* Nitric Oxide, 2009. **20**(4): p. 223-30.
140. Togashi, H., et al., *A central nervous system action of nitric oxide in blood pressure regulation.* J Pharmacol Exp Ther, 1992. **262**(1): p. 343-7.

141. Kim, N., et al., *A nitric oxide-like factor mediates nonadrenergic-noncholinergic neurogenic relaxation of penile corpus cavernosum smooth muscle.* J Clin Invest, 1991. **88**(1): p. 112-8.
142. Steinert, J.R., T. Chernova, and I.D. Forsythe, *Nitric oxide signaling in brain function, dysfunction, and dementia.* Neuroscientist, 2010. **16**(4): p. 435-52.
143. Lipton, S.A., et al., *A redox-based mechanism for the neuroprotective and neurodestructive effects of nitric oxide and related nitroso-compounds.* Nature, 1993. **364**(6438): p. 626-32.
144. Wei, X.Q., et al., *Altered immune responses in mice lacking inducible nitric oxide synthase.* Nature, 1995. **375**(6530): p. 408-11.
145. Patel, T.N., M.H. Shishehbor, and D.L. Bhatt, *A review of high-dose statin therapy: targeting cholesterol and inflammation in atherosclerosis.* Eur Heart J, 2007. **28**(6): p. 664-72.
146. Nicholson, S., et al., *Inducible nitric oxide synthase in pulmonary alveolar macrophages from patients with tuberculosis.* J Exp Med, 1996. **183**(5): p. 2293-302.
147. Wong, J.M. and T.R. Billiar, *Regulation and function of inducible nitric oxide synthase during sepsis and acute inflammation.* Adv Pharmacol, 1995. **34**: p. 155-70.
148. Rafiee, P., et al., *Isolation and characterization of human esophageal microvascular endothelial cells: mechanisms of inflammatory activation.* Am J Physiol Gastrointest Liver Physiol, 2003. **285**(6): p. G1277-92.
149. Mikkelsen, R.B. and P. Wardman, *Biological chemistry of reactive oxygen and nitrogen and radiation-induced signal transduction mechanisms.* Oncogene, 2003. **22**(37): p. 5734-54.
150. Ridnour, L.A., et al., *The chemistry of nitrosative stress induced by nitric oxide and reactive nitrogen oxide species. Putting perspective on stressful biological situations.* Biol Chem, 2004. **385**(1): p. 1-10.
151. Park, C.S., et al., *Differential and constitutive expression of neuronal, inducible, and endothelial nitric oxide synthase mRNAs and proteins in pathologically normal human tissues.* Nitric Oxide, 2000. **4**(5): p. 459-71.
152. Feng, C., *Mechanism of Nitric Oxide Synthase Regulation: Electron Transfer and Interdomain Interactions.* Coord Chem Rev, 2012. **256**(3-4): p. 393-411.
153. Hedison, T.M., S. Hay, and N.S. Scrutton, *A perspective on conformational control of electron transfer in nitric oxide synthases.* Nitric Oxide, 2017. **63**: p. 61-67.
154. Lane, P. and S.S. Gross, *The autoinhibitory control element and calmodulin conspire to provide physiological modulation of endothelial and neuronal nitric oxide synthase activity.* Acta Physiol Scand, 2000. **168**(1): p. 53-63.
155. Salerno, J.C., et al., *An autoinhibitory control element defines calcium-regulated isoforms of nitric oxide synthase.* J Biol Chem, 1997. **272**(47): p. 29769-77.
156. Roman, L.J., et al., *The C terminus of mouse macrophage inducible nitric-oxide synthase attenuates electron flow through the flavin domain.* J Biol Chem, 2000. **275**(29): p. 21914-9.
157. Yokom, A.L., et al., *Architecture of the nitric-oxide synthase holoenzyme reveals large conformational changes and a calmodulin-driven release of the FMN domain.* J Biol Chem, 2014. **289**(24): p. 16855-65.

158. Campbell, M.G., et al., *Molecular architecture of mammalian nitric oxide synthases.* Proc Natl Acad Sci U S A, 2014. **111**(35): p. E3614-23.
159. Leferink, N.G., et al., *Towards the free energy landscape for catalysis in mammalian nitric oxide synthases.* FEBS J, 2015. **282**(16): p. 3016-29.
160. Tiso, M., et al., *Versatile regulation of neuronal nitric oxide synthase by specific regions of its C-terminal tail.* Biochemistry, 2007. **46**(50): p. 14418-28.
161. Knight, K. and N.S. Scrutton, *Stopped-flow kinetic studies of electron transfer in the reductase domain of neuronal nitric oxide synthase: re-evaluation of the kinetic mechanism reveals new enzyme intermediates and variation with cytochrome P450 reductase.* Biochem J, 2002. **367**(Pt 1): p. 19-30.
162. Haque, M.M., et al., *A connecting hinge represses the activity of endothelial nitric oxide synthase.* Proc Natl Acad Sci U S A, 2007. **104**(22): p. 9254-9.
163. Konas, D.W., et al., *The FAD-shielding residue Phe1395 regulates neuronal nitric-oxide synthase catalysis by controlling NADP+ affinity and a conformational equilibrium within the flavoprotein domain.* J Biol Chem, 2004. **279**(34): p. 35412-25.
164. Miller, R.T., et al., *Rapid kinetic studies of electron transfer in the three isoforms of nitric oxide synthase.* Biochem Biophys Res Commun, 1999. **265**(1): p. 184-8.
165. Martasek, P., et al., *Assay of isoforms of Escherichia coli-expressed nitric oxide synthase.* Methods Enzymol, 1999. **301**: p. 70-8.
166. Newton, D.C., H.J. Montgomery, and J.G. Guillemette, *The reductase domain of the human inducible nitric oxide synthase is fully active in the absence of bound calmodulin.* Arch Biochem Biophys, 1998. **359**(2): p. 249-57.
167. Adak, S., Q. Wang, and D.J. Stuehr, *Arginine conversion to nitroxide by tetrahydrobiopterin-free neuronal nitric-oxide synthase. Implications for mechanism.* J Biol Chem, 2000. **275**(43): p. 33554-61.
168. Adak, S., et al., *Tryptophan 409 controls the activity of neuronal nitric-oxide synthase by regulating nitric oxide feedback inhibition.* J Biol Chem, 1999. **274**(38): p. 26907-11.
169. Newman, E., et al., *Differential activation of nitric-oxide synthase isozymes by calmodulin-troponin C chimeras.* J Biol Chem, 2004. **279**(32): p. 33547-57.
170. Roman, L.J. and B.S. Masters, *Electron transfer by neuronal nitric-oxide synthase is regulated by concerted interaction of calmodulin and two intrinsic regulatory elements.* J Biol Chem, 2006. **281**(32): p. 23111-8.
171. Lian, L.Y., et al., *Biochemical comparison of Anopheles gambiae and human NADPH P450 reductases reveals different 2'-5'-ADP and FMN binding traits.* PLoS One, 2011. **6**(5): p. e20574.
172. Portal, P., et al., *Multiple NADPH-cytochrome P450 reductases from Trypanosoma cruzi suggested role on drug resistance.* Mol Biochem Parasitol, 2008. **160**(1): p. 42-51.
173. Vermilion, J.L. and M.J. Coon, *Purified liver microsomal NADPH-cytochrome P-450 reductase. Spectral characterization of oxidation-reduction states.* J Biol Chem, 1978. **253**(8): p. 2694-704.
174. Shet, M.S., et al., *Purification, characterization, and cDNA cloning of an NADPH-cytochrome P450 reductase from mung bean.* Proc Natl Acad Sci U S A, 1993. **90**(7): p. 2890-4.

175. Pandey, A.V. and C.E. Fluck, *NADPH P450 oxidoreductase: structure, function, and pathology of diseases.* Pharmacol Ther, 2013. **138**(2): p. 229-54.
176. Riddick, D.S., et al., *NADPH-cytochrome P450 oxidoreductase: roles in physiology, pharmacology, and toxicology.* Drug Metab Dispos, 2013. **41**(1): p. 12-23.
177. Porter, T.D., *New insights into the role of cytochrome P450 reductase (POR) in microsomal redox biology.* Acta Pharmaceutica Sinica B, 2012. **2**(2): p. 102-106.
178. Horecker, B.L., *Triphosphopyridine Nucleotide-Cytochrome-C Reductase in Liver.* Journal of Biological Chemistry, 1950. **183**(2): p. 593-605.
179. Vermilion, J.L. and M.J. Coon, *Identification of the high and low potential flavins of liver microsomal NADPH-cytochrome P-450 reductase.* J Biol Chem, 1978. **253**(24): p. 8812-9.
180. Madyastha, K.M. and C.J. Coscia, *Detergent-solubilized NADPH-cytochrome c(P-450) reductase from the higher plant, Catharanthus roseus. Purification and characterization.* J Biol Chem, 1979. **254**(7): p. 2419-27.
181. Smith, G.C., D.G. Tew, and C.R. Wolf, *Dissection of NADPH-cytochrome P450 oxidoreductase into distinct functional domains.* Proc Natl Acad Sci U S A, 1994. **91**(18): p. 8710-4.
182. Dohr, O., et al., *Engineering of a functional human NADH-dependent cytochrome P450 system.* Proc Natl Acad Sci U S A, 2001. **98**(1): p. 81-6.
183. Omura, T. and R. Sato, *A new cytochrome in liver microsomes.* J Biol Chem, 1962. **237**: p. 1375-6.
184. Guengerich, F.P., *Reduction of cytochrome b5 by NADPH-cytochrome P450 reductase.* Arch Biochem Biophys, 2005. **440**(2): p. 204-11.
185. Schacter, B.A., et al., *Immunochemical evidence for an association of heme oxygenase with the microsomal electron transport system.* J Biol Chem, 1972. **247**(11): p. 3601-7.
186. Ono, T., et al., *Purification of squalene epoxidase from rat liver microsomes.* Biochem Biophys Res Commun, 1980. **96**(1): p. 522-8.
187. Bartoszek, A. and C.R. Wolf, *Enhancement of doxorubicin toxicity following activation by NADPH cytochrome P450 reductase.* Biochem Pharmacol, 1992. **43**(7): p. 1449-57.
188. Bligh, H.F., et al., *Activation of mitomycin C by NADPH:cytochrome P-450 reductase.* Cancer Res, 1990. **50**(24): p. 7789-92.
189. Wang, Y., et al., *Distinct roles of cytochrome P450 reductase in mitomycin C redox cycling and cytotoxicity.* Mol Cancer Ther, 2010. **9**(6): p. 1852-63.
190. Omura, T. and O. Gotoh, *Evolutionary origin of mitochondrial cytochrome P450.* J Biochem, 2017. **161**(5): p. 399-407.
191. Omura, T., *Mitochondrial P450s.* Chem Biol Interact, 2006. **163**(1-2): p. 86-93.
192. Guengerich, F.P., M.R. Waterman, and M. Egli, *Recent Structural Insights into Cytochrome P450 Function.* Trends Pharmacol Sci, 2016. **37**(8): p. 625-640.
193. Guengerich, F.P., *Intersection of the Roles of Cytochrome P450 Enzymes with Xenobiotic and Endogenous Substrates: Relevance to Toxicity and Drug Interactions.* Chem Res Toxicol, 2017. **30**(1): p. 2-12.
194. Manikandan, P. and S. Nagini, *Cytochrome P450 Structure, Function and Clinical Significance: A Review.* Curr Drug Targets, 2018. **19**(1): p. 38-54.

195. Oshino, N., Y. Imai, and R. Sato, *A function of cytochrome b5 in fatty acid desaturation by rat liver microsomes.* J Biochem, 1971. **69**(1): p. 155-67.
196. Bhatt, M.R., et al., *Role of cytochrome b5 in the modulation of the enzymatic activities of cytochrome P450 17alpha-hydroxylase/17,20-lyase (P450 17A1).* J Steroid Biochem Mol Biol, 2017. **170**: p. 2-18.
197. Finn, R.D., et al., *Defining the in Vivo Role for cytochrome b5 in cytochrome P450 function through the conditional hepatic deletion of microsomal cytochrome b5.* J Biol Chem, 2008. **283**(46): p. 31385-93.
198. Porter, T.D., *The roles of cytochrome b5 in cytochrome P450 reactions.* J Biochem Mol Toxicol, 2002. **16**(6): p. 311-6.
199. Ono, T., et al., *Involvement of NADPH-cytochrome c reductase in the rat liver squalene epoxidase system.* Biochim Biophys Acta, 1977. **486**(3): p. 401-7.
200. Fluck, C.E., et al., *Mutant P450 oxidoreductase causes disordered steroidogenesis with and without Antley-Bixler syndrome.* Nat Genet, 2004. **36**(3): p. 228-30.
201. Sugishima, M., et al., *Structural basis for the electron transfer from an open form of NADPH-cytochrome P450 oxidoreductase to heme oxygenase.* Proc Natl Acad Sci U S A, 2014. **111**(7): p. 2524-9.
202. Aigrain, L., et al., *Structure of the open conformation of a functional chimeric NADPH cytochrome P450 reductase.* EMBO Rep, 2009. **10**(7): p. 742-7.
203. Brenner, S., et al., *Inter-flavin electron transfer in cytochrome P450 reductase - effects of solvent and pH identify hidden complexity in mechanism.* FEBS J, 2008. **275**(18): p. 4540-57.
204. Gutierrez, A., et al., *Stopped-flow kinetic studies of flavin reduction in human cytochrome P450 reductase and its component domains.* Biochemistry, 2001. **40**(7): p. 1964-75.
205. Fan, Z., et al., *Bioinformatics analysis for structure and function of CPR of Plasmodium falciparum.* Asian Pac J Trop Med, 2011. **4**(2): p. 85-7.
206. Fan, Z., et al., *Bioinformatics analysis of the structure and function of NADPH-cytochrome p450 reductase of Plasmodium vivax.* Biomed Rep, 2013. **1**(3): p. 425-427.
207. Fan, Z., et al., *Bioinformatics analysis and prediction for structure and function of nitric oxide synthase and similar proteins from Plasmodium berghei.* Asian Pac J Trop Med, 2011. **4**(1): p. 1-4.
208. Zhang, M., et al., *Uncovering the essential genes of the human malaria parasite Plasmodium falciparum by saturation mutagenesis.* Science, 2018. **360**(6388).
209. Ostera, G., et al., *Plasmodium falciparum: food vacuole localization of nitric oxide-derived species in intraerythrocytic stages of the malaria parasite.* Exp Parasitol, 2008. **120**(1): p. 29-38.
210. Baker, J., et al., *Transcription and expression of Plasmodium falciparum histidine-rich proteins in different stages and strains: implications for rapid diagnostic tests.* PLoS One, 2011. **6**(7): p. e22593.
211. Wang, P.F., et al., *Thioredoxin reductase from Plasmodium falciparum: evidence for interaction between the C-terminal cysteine residues and the active site disulfide-dithiol.* Biochemistry, 1999. **38**(10): p. 3187-96.
212. Vignais, P.V. and P.M. Vignais, *Oxidation of reduced triphosphopyridine nucleotide and associated phosphorylation.* J Biol Chem, 1957. **229**(1): p. 265-78.

213. Jick, H. and L. Shuster, *The turnover of microsomal reduced nicotinamide adenine dinucleotide phosphate-cytochrome c reductase in the livers of mice treated with phenobarbital.* J Biol Chem, 1966. **241**(22): p. 5366-9.
214. Hovemann, B.T., F. Sehlmeyer, and J. Malz, *Drosophila melanogaster NADPH-cytochrome P450 oxidoreductase: pronounced expression in antennae may be related to odorant clearance.* Gene, 1997. **189**(2): p. 213-9.
215. Mizutani, M. and D. Ohta, *Two isoforms of NADPH:cytochrome P450 reductase in Arabidopsis thaliana. Gene structure, heterologous expression in insect cells, and differential regulation.* Plant Physiol, 1998. **116**(1): p. 357-67.
216. Yabusaki, Y., H. Murakami, and H. Ohkawa, *Primary structure of Saccharomyces cerevisiae NADPH-cytochrome P450 reductase deduced from nucleotide sequence of its cloned gene.* J Biochem, 1988. **103**(6): p. 1004-10.
217. Black, S.D., G.E. Tarr, and M.J. Coon, *Structural features of isozyme 2 of liver microsomal cytochrome P-450. Identification of a highly conserved cysteine-containing peptide.* J Biol Chem, 1982. **257**(24): p. 14616-9.
218. Lu, A.Y., K.W. Junk, and M.J. Coon, *Resolution of the cytochrome P-450-containing omega-hydroxylation system of liver microsomes into three components.* J Biol Chem, 1969. **244**(13): p. 3714-21.
219. Vermilion, J.L. and M.J. Coon, *Highly purified detergent-solubilized NADPH-cytochrome P-450 reductase from phenobarbital-induced rat liver microsomes.* Biochem Biophys Res Commun, 1974. **60**(4): p. 1315-22.
220. Murakami, H., et al., *Expression of cloned yeast NADPH-cytochrome P450 reductase gene in Saccharomyces cerevisiae.* J Biochem, 1990. **108**(5): p. 859-65.
221. Porter, T.D., T.E. Wilson, and C.B. Kasper, *Expression of a functional 78,000 dalton mammalian flavoprotein, NADPH-cytochrome P-450 oxidoreductase, in Escherichia coli.* Arch Biochem Biophys, 1987. **254**(1): p. 353-67.
222. Lee, C.A., et al., *CYP3A4 expressed by insect cells infected with a recombinant baculovirus containing both CYP3A4 and human NADPH-cytochrome P450 reductase is catalytically similar to human liver microsomal CYP3A4.* Arch Biochem Biophys, 1995. **319**(1): p. 157-67.
223. Cowen, R.L., et al., *Viral delivery of P450 reductase recapitulates the ability of constitutive overexpression of reductase enzymes to potentiate the activity of mitomycin C in human breast cancer xenografts.* Mol Cancer Ther, 2003. **2**(9): p. 901-9.
224. Silvestrini, F., et al., *Protein export marks the early phase of gametocytogenesis of the human malaria parasite Plasmodium falciparum.* Mol Cell Proteomics, 2010. **9**(7): p. 1437-48.
225. Emanuelsson, O., et al., *Predicting subcellular localization of proteins based on their N-terminal amino acid sequence.* J Mol Biol, 2000. **300**(4): p. 1005-16.
226. Horton, P., et al., *WoLF PSORT: protein localization predictor.* Nucleic Acids Res, 2007. **35**(Web Server issue): p. W585-7.
227. Wittung-Stafshede, P., *Role of cofactors in protein folding.* Acc Chem Res, 2002. **35**(4): p. 201-8.
228. Apiyo, D. and P. Wittung-Stafshede, *Presence of the cofactor speeds up folding of Desulfovibrio desulfuricans flavodoxin.* Protein Sci, 2002. **11**(5): p. 1129-35.

229. Sarapusit, S., et al., *Modeling of Anopheles minimus Mosquito NADPH-cytochrome P450 oxidoreductase (CYPOR) and mutagenesis analysis.* Int J Mol Sci, 2013. **14**(1): p. 1788-801.
230. Kiefler, I., S. Bringer, and M. Bott, *SdhE-dependent formation of a functional Acetobacter pasteurianus succinate dehydrogenase in Gluconobacter oxydans--a first step toward a complete tricarboxylic acid cycle.* Appl Microbiol Biotechnol, 2015. **99**(21): p. 9147-60.
231. Hartl, F.U., A. Bracher, and M. Hayer-Hartl, *Molecular chaperones in protein folding and proteostasis.* Nature, 2011. **475**(7356): p. 324-32.
232. Hartl, F.U., *Molecular chaperones in cellular protein folding.* Nature, 1996. **381**(6583): p. 571-9.
233. Thomas, J.G., A. Ayling, and F. Baneyx, *Molecular chaperones, folding catalysts, and the recovery of active recombinant proteins from E. coli. To fold or to refold.* Appl Biochem Biotechnol, 1997. **66**(3): p. 197-238.
234. Nishihara, K., et al., *Chaperone coexpression plasmids: differential and synergistic roles of DnaK-DnaJ-GrpE and GroEL-GroES in assisting folding of an allergen of Japanese cedar pollen, Cryj2, in Escherichia coli.* Appl Environ Microbiol, 1998. **64**(5): p. 1694-9.
235. Nishihara, K., et al., *Overexpression of trigger factor prevents aggregation of recombinant proteins in Escherichia coli.* Appl Environ Microbiol, 2000. **66**(3): p. 884-9.
236. Rial, D.V. and E.A. Ceccarelli, *Removal of DnaK contamination during fusion protein purifications.* Protein Expr Purif, 2002. **25**(3): p. 503-7.
237. Birringer, M.S., et al., *High-level expression and purification of human thymidine kinase 1: quaternary structure, stability, and kinetics.* Protein Expr Purif, 2006. **47**(2): p. 506-15.
238. Agou, F., et al., *NEMO trimerizes through its coiled-coil C-terminal domain.* J Biol Chem, 2002. **277**(20): p. 17464-75.
239. Guo, L.W., et al., *One-step purification of bacterially expressed recombinant transducin alpha-subunit and isotopically labeled PDE6 gamma-subunit for NMR analysis.* Protein Expr Purif, 2007. **51**(2): p. 187-97.
240. Briand, L., et al., *A self-inducible heterologous protein expression system in Escherichia coli.* Sci Rep, 2016. **6**: p. 33037.
241. Zhang, Z., et al., *High-level production of membrane proteins in E. coli BL21(DE3) by omitting the inducer IPTG.* Microb Cell Fact, 2015. **14**: p. 142.
242. Martinez-Limon, A., et al., *Recognition of enzymes lacking bound cofactor by protein quality control.* Proc Natl Acad Sci U S A, 2016. **113**(43): p. 12156-12161.
243. Campelo, D., et al., *The Hinge Segment of Human NADPH-Cytochrome P450 Reductase in Conformational Switching: The Critical Role of Ionic Strength.* Front Pharmacol, 2017. **8**: p. 755.
244. Price, C.L., et al., *Novel Substrate Specificity and Temperature-Sensitive Activity of Mycosphaerella graminicola CYP51 Supported by the Native NADPH Cytochrome P450 Reductase.* Appl Environ Microbiol, 2015. **81**(10): p. 3379-86.
245. Malaria, G.E.N.P.f.C.P., *Genomic epidemiology of artemisinin resistant malaria.* Elife, 2016. **5**.

246. Vincent, B., et al., *The closed and compact domain organization of the 70-kDa human cytochrome P450 reductase in its oxidized state as revealed by NMR.* J Mol Biol, 2012. **420**(4-5): p. 296-309.
247. Oprian, D.D. and M.J. Coon, *Oxidation-reduction states of FMN and FAD in NADPH-cytochrome P-450 reductase during reduction by NADPH.* J Biol Chem, 1982. **257**(15): p. 8935-44.
248. Gachhui, R., et al., *Characterization of the reductase domain of rat neuronal nitric oxide synthase generated in the methylotrophic yeast Pichia pastoris. Calmodulin response is complete within the reductase domain itself.* J Biol Chem, 1996. **271**(34): p. 20594-602.
249. Olteanu, H. and R. Banerjee, *Redundancy in the pathway for redox regulation of mammalian methionine synthase: reductive activation by the dual flavoprotein, novel reductase 1.* J Biol Chem, 2003. **278**(40): p. 38310-4.
250. Shen, A.L., D.S. Sem, and C.B. Kasper, *Mechanistic studies on the reductive half-reaction of NADPH-cytochrome P450 oxidoreductase.* J Biol Chem, 1999. **274**(9): p. 5391-8.
251. Simtchouk, S., et al., *Kinetic analysis of cytochrome P450 reductase from Artemisia annua reveals accelerated rates of NADH-dependent flavin reduction.* FEBS J, 2013. **280**(24): p. 6627-42.
252. Wolthers, K.R. and N.S. Scrutton, *Electron transfer in human methionine synthase reductase studied by stopped-flow spectrophotometry.* Biochemistry, 2004. **43**(2): p. 490-500.
253. Finn, R.D., et al., *Determination of the redox potentials and electron transfer properties of the FAD- and FMN-binding domains of the human oxidoreductase NR1.* Eur J Biochem, 2003. **270**(6): p. 1164-75.
254. Hubbard, P.A., et al., *NADPH-cytochrome P450 oxidoreductase. Structural basis for hydride and electron transfer.* J Biol Chem, 2001. **276**(31): p. 29163-70.
255. Kuhn, Y., P. Rohrbach, and M. Lanzer, *Quantitative pH measurements in Plasmodium falciparum-infected erythrocytes using pHluorin.* Cell Microbiol, 2007. **9**(4): p. 1004-13.
256. Wissing, F., et al., *Illumination of the malaria parasite Plasmodium falciparum alters intracellular pH. Implications for live cell imaging.* J Biol Chem, 2002. **277**(40): p. 37747-55.
257. Porcelli, A.M., et al., *pH difference across the outer mitochondrial membrane measured with a green fluorescent protein mutant.* Biochem Biophys Res Commun, 2005. **326**(4): p. 799-804.
258. Ejezie, G.C. and E.N. Ezedinachi, *Malaria parasite density and body temperature in children under 10 years of age in Calabar, Nigeria.* Trop Geogr Med, 1992. **44**(1-2): p. 97-101.
259. Gbadegesin, R.A., et al., *Body temperature is a poor predictor of malaria parasitaemia in children with acute diarrhoea.* Ann Trop Paediatr, 1997. **17**(1): p. 89-94.
260. Ueno, T., D. Muno, and E. Kominami, *Membrane markers of endoplasmic reticulum preserved in autophagic vacuolar membranes isolated from leupeptin-administered rat liver.* J Biol Chem, 1991. **266**(28): p. 18995-9.

261. Hortsch, M. and D.I. Meyer, *Immunochemical analysis of rough and smooth microsomes from rat liver. Segregation of docking protein in rough membranes.* Eur J Biochem, 1985. **150**(3): p. 559-64.
262. Szczesna-Skorupa, E. and B. Kemper, *An N-terminal glycosylation signal on cytochrome P450 is restricted to the endoplasmic reticulum in a luminal orientation.* J Biol Chem, 1993. **268**(3): p. 1757-62.
263. Stiban, J., L. Caputo, and M. Colombini, *Ceramide synthesis in the endoplasmic reticulum can permeabilize mitochondria to proapoptotic proteins.* J Lipid Res, 2008. **49**(3): p. 625-34.
264. Vidal, M.L., A. Basseres, and J.F. Narbonne, *Seasonal variations of pollution biomarkers in two populations of Corbicula fluminea (Muller).* Comp Biochem Physiol C Toxicol Pharmacol, 2002. **131**(2): p. 133-51.
265. vanderOost, R., et al., *Biomonitoring aquatic pollution with feral eel (Anguilla anguilla) .3. Statistical analyses of relationships between contaminant exposure and biomarkers.* Aquatic Toxicology, 1997. **39**(1): p. 45-75.
266. Guengerich, F.P., et al., *Measurement of cytochrome P450 and NADPH-cytochrome P450 reductase.* Nature Protocols, 2009. **4**(9): p. 1245-1251.
267. Dignam, J.D. and H.W. Strobel, *Preparation of homogeneous NADPH-cytochrome P-450 reductase from rat liver.* Biochem Biophys Res Commun, 1975. **63**(4): p. 845-52.
268. Roerig, D.L., L. Mascaro, Jr., and S.D. Aust, *Microsomal electron transport: tetrazolium reduction by rat liver microsomal NADPH-cytochrome c reductase.* Arch Biochem Biophys, 1972. **153**(2): p. 475-9.
269. Tew, D.G., *Inhibition of cytochrome P450 reductase by the diphenyliodonium cation. Kinetic analysis and covalent modifications.* Biochemistry, 1993. **32**(38): p. 10209-15.
270. O'Donnell, V.B., G.C. Smith, and O.T. Jones, *Involvement of phenyl radicals in iodonium inhibition of flavoenzymes.* Mol Pharmacol, 1994. **46**(4): p. 778-85.
271. Feyereisen, R., *Evolution of insect P450.* Biochem Soc Trans, 2006. **34**(Pt 6): p. 1252-5.
272. Yang, Y., et al., *Constitutive overexpression of multiple cytochrome P450 genes associated with pyrethroid resistance in Helicoverpa armigera.* J Econ Entomol, 2006. **99**(5): p. 1784-9.
273. Zhu, F., et al., *RNA interference of NADPH-cytochrome P450 reductase results in reduced insecticide resistance in the bed bug, Cimex lectularius.* PLoS One, 2012. **7**(2): p. e31037.
274. Shi, L., et al., *Silencing NADPH-cytochrome P450 reductase results in reduced acaricide resistance in Tetranychus cinnabarinus (Boisduval).* Sci Rep, 2015. **5**: p. 15581.
275. Bushell, E., et al., *Functional Profiling of a Plasmodium Genome Reveals an Abundance of Essential Genes.* Cell, 2017. **170**(2): p. 260-272 e8.
276. Murataliev, M.B. and R. Feyereisen, *Interaction of NADP(H) with oxidized and reduced P450 reductase during catalysis. Studies with nucleotide analogues.* Biochemistry, 2000. **39**(17): p. 5066-74.
277. Lee, G.Y., et al., *Heterologous expression and functional characterization of the NADPH-cytochrome P450 reductase from Capsicum annuum.* Plant Physiol Biochem, 2014. **82**: p. 116-22.

278. Louerat-Oriou, B., A. Perret, and D. Pompon, *Differential redox and electron-transfer properties of purified yeast, plant and human NADPH-cytochrome P-450 reductases highly modulate cytochrome P-450 activities.* Eur J Biochem, 1998. **258**(3): p. 1040-9.
279. Zeghouf, M., et al., *The flavoprotein component of the Escherichia coli sulfite reductase: expression, purification, and spectral and catalytic properties of a monomeric form containing both the flavin adenine dinucleotide and the flavin mononucleotide cofactors.* Biochemistry, 1998. **37**(17): p. 6114-23.
280. Murataliev, M.B. and R. Feyereisen, *Functional interactions in cytochrome P450BM3. Fatty acid substrate binding alters electron-transfer properties of the flavoprotein domain.* Biochemistry, 1996. **35**(47): p. 15029-37.
281. Munro, A.W., et al., *Probing electron transfer in flavocytochrome P-450 BM3 and its component domains.* Eur J Biochem, 1996. **239**(2): p. 403-9.
282. Rafferty, S. and H.L. Malech, *High reductase activity of recombinant NOS2 flavoprotein domain lacking the calmodulin binding regulatory sequence.* Biochem Biophys Res Commun, 1996. **220**(3): p. 1002-7.
283. Gutierrez, A., et al., *Interflavin electron transfer in human cytochrome P450 reductase is enhanced by coenzyme binding. Relaxation kinetic studies with coenzyme analogues.* Eur J Biochem, 2003. **270**(12): p. 2612-21.
284. Grunau, A., et al., *Conformational dynamics and the energetics of protein--ligand interactions: role of interdomain loop in human cytochrome P450 reductase.* Biochemistry, 2007. **46**(28): p. 8244-55.
285. Haque, M.M., et al., *Control of electron transfer and catalysis in neuronal nitric-oxide synthase (nNOS) by a hinge connecting its FMN and FAD-NADPH domains.* J Biol Chem, 2012. **287**(36): p. 30105-16.
286. Giandomenico, A.R., et al., *The importance of sodium pyruvate in assessing damage produced by hydrogen peroxide.* Free Radic Biol Med, 1997. **23**(3): p. 426-34.
287. Vale, N., R. Moreira, and P. Gomes, *Primaquine revisited six decades after its discovery.* Eur J Med Chem, 2009. **44**(3): p. 937-53.
288. Rahbari, M., et al., *Hydrogen peroxide dynamics in subcellular compartments of malaria parasites using genetically encoded redox probes.* Sci Rep, 2017. **7**(1): p. 10449.
289. Becker, K., et al., *Oxidative stress in malaria parasite-infected erythrocytes: host-parasite interactions.* Int J Parasitol, 2004. **34**(2): p. 163-89.
290. Preuss, J., E. Jortzik, and K. Becker, *Glucose-6-phosphate metabolism in Plasmodium falciparum.* IUBMB Life, 2012. **64**(7): p. 603-11.
291. Rendic, S. and F.P. Guengerich, *Survey of Human Oxidoreductases and Cytochrome P450 Enzymes Involved in the Metabolism of Xenobiotic and Natural Chemicals.* Chem Res Toxicol, 2015. **28**(1): p. 38-42.
292. Aguilar, R., et al., *Molecular evidence for the localization of Plasmodium falciparum immature gametocytes in bone marrow.* Blood, 2014. **123**(7): p. 959-66.
293. Mota, M.M. and A. Rodriguez, *Invasion of mammalian host cells by Plasmodium sporozoites.* Bioessays, 2002. **24**(2): p. 149-56.
294. Sinnis, P., *The malaria sporozoite's journey into the liver.* Infect Agents Dis, 1996. **5**(3): p. 182-9.

295. Hodges, V.M., G.Y. Molloy, and S.N. Wickramasinghe, *Demonstration of mRNA for five species of cytochrome P450 in human bone marrow, bone marrow-derived macrophages and human haemopoietic cell lines.* Br J Haematol, 2000. **108**(1): p. 151-6.
296. Alonso, S., et al., *Human bone marrow niche chemoprotection mediated by cytochrome P450 enzymes.* Oncotarget, 2015. **6**(17): p. 14905-12.
297. Zanger, U.M. and M. Schwab, *Cytochrome P450 enzymes in drug metabolism: regulation of gene expression, enzyme activities, and impact of genetic variation.* Pharmacol Ther, 2013. **138**(1): p. 103-41.
298. Chan, J.A., F.J.I. Fowkes, and J.G. Beeson, *Surface antigens of Plasmodium falciparum-infected erythrocytes as immune targets and malaria vaccine candidates.* Cellular and Molecular Life Sciences, 2014. **71**(19): p. 3633-3657.
299. de Alencar, A.C., et al., *Malaria and Vascular Endothelium.* Arquivos Brasileiros De Cardiologia, 2014. **103**(2): p. 165-168.
300. Fleming, I., *Cytochrome P450 enzymes in vascular homeostasis.* Circulation Research, 2001. **89**(9): p. 753-762.
301. Breton-Romero, R. and S. Lamas, *Hydrogen peroxide signaling in vascular endothelial cells.* Redox Biology, 2014. **2**: p. 529-534.
302. Tamma, G., et al., *Aquaporin Membrane Channels in Oxidative Stress, Cell Signaling, and Aging: Recent Advances and Research Trends.* Oxidative Medicine and Cellular Longevity, 2018.
303. Carter, R., et al., *Plasmodium falciparum: an abundant stage-specific protein expressed during early gametocyte development.* Exp Parasitol, 1989. **69**(2): p. 140-9.
304. Aurrecoechea, C., et al., *PlasmoDB: a functional genomic database for malaria parasites.* Nucleic Acids Res, 2009. **37**(Database issue): p. D539-43.
305. Lopez-Barragan, M.J., et al., *Directional gene expression and antisense transcripts in sexual and asexual stages of Plasmodium falciparum.* BMC Genomics, 2011. **12**: p. 587.
306. Bruce, M.C., et al., *Commitment of the malaria parasite Plasmodium falciparum to sexual and asexual development.* Parasitology, 1990. **100 Pt 2**: p. 191-200.
307. Smith, T.G., D. Walliker, and L.C. Ranford-Cartwright, *Sexual differentiation and sex determination in the Apicomplexa.* Trends Parasitol, 2002. **18**(7): p. 315-23.
308. Dyer, M. and K.P. Day, *Commitment to gametocytogenesis in Plasmodium falciparum.* Parasitol Today, 2000. **16**(3): p. 102-7.
309. Dixon, M.W., et al., *Sex in Plasmodium: a sign of commitment.* Trends Parasitol, 2008. **24**(4): p. 168-75.
310. Alano, P., *The sound of sexual commitment breaks the silencing of malaria parasites.* Trends Parasitol, 2014. **30**(11): p. 509-10.
311. Josling, G.A. and M. Llinas, *Sexual development in Plasmodium parasites: knowing when it's time to commit.* Nat Rev Microbiol, 2015. **13**(9): p. 573-87.

APPENDICES

Appendix 3.1 The alignment results of P. falciparum NADPH-cytochrom P450 reductase candidates with known NOS proteins

P. falciparum PF3D7_1450300, *P. falciparum* PF3D7_0923200, *M. musculus* iNOS (NP_001300850.1), *R. norvegicus* eNOS (NP_068610.1), *H. sapiens* eNOS (NP_000594.2), *A. stephensi* NOS (AAC68577.1) and *D. melanogaster* NOS isoform K (NP_001027243.2). The sequences were aligned by Clustal Omega.

```
PF3D7_1450300          ------------------------------------------------------------          0
PF3D7_0923200          ------------------------------------------------------------          0
A.stephensi NOS        MADTTTVVVERREVAEGRESSKANHIGEERRGYDVSRKRCSISVHGG-GTEGGGGNMRTN          59
D.melanogaster NOS     ------------------------------------------------------------          0
M.musculus iNOS        ------------------------------------------------------------          0
H.sapiens eNOS         -------------------------MGNLKSVAQEPGPPCGLGLGLGLGLCGKQGPATPA          35
R.norvergicus eNOS     -------------------------MGNLKSVGQEPGPPCGLGLGLGLGLCGKQGPASPA          35

PF3D7_1450300          ------------------------------------------------------------          0
PF3D7_0923200          ------------------------------------------------------------          0
A.stephensi NOS        -YRELSPASLRIHRKSSHDIRNTLLGPDGEVLHLHDPSGKGGDGMGKMPAVVKPIKLKSI          118
D.melanogaster_NOS     ------------------------------------------------------------          0
M.musculus iNOS        ------------------------------------------------------------          0
H.sapiens eNOS         PEPSRAPASLLP------------PAPE------HSPP---SSPLTQPPEGPKFPRVKNW          74
R.norvergicus eNOS     PEPSQAPVPPSPTR----------PAPD------H------SPPLTRPPDGPKFPRVKNW          73

PF3D7_1450300          ------------------------------------------------------------          0
PF3D7_0923200          ------------------------------------------------------------          0
A.stephensi NOS        VTKAESYDTMHGKASDVMSCSREVCMGSVMTPHVIGTET----RKPEIVQQHAKDFLDQY          174
D.melanogaster NOS     ----------------------------MNIGNAAVEA----RKSDLILEHAKDFLEQY          27
M.musculus iNOS        ----------------------------MNPKSLTRGPRDKPTPLEELLPHAIEFINQY          31
H.sapiens eNOS         EVGSITYDTLSAQAQQDGPCTPRRCLGSLVFPRKLQGRPSPGPPAPEQLLSQARDFINQY          134
R.norvergicus eNOS     EVGSITYDTLSAQAQQDGPCTPRRCLGSLVFPRKLQSRPTQGPSPTEQLLGQARDFINQY          133

PF3D7_1450300          ------------------------------------------------------------          0
PF3D7_0923200          ------------------------------------------------------------          0
A.stephensi NOS        YSSIRRLKSPAHDSRWQQVQKEVEATGSYHLTETELIYGAKLAWRNSSRCIGRIQWSKLQ          234
D.melanogaster NOS     FTSIKRTSSTAHETRWKQVRQSIETTGHYQLTETELIYGAKLAWRNSSRCIGRIQWSKLQ          87
M.musculus iNOS        YGSFKEAKIEEHLARLEAVTKEIETTGTYQLTLDELIFATKMAWRNAPRCIGRIQWSNLQ          91
H.sapiens eNOS         YSSIKRSGSQAHEQRLQEVEAEVAATGTYQLRESELVFGAKQAWRNAPRCVGRIQWGKLQ          194
R.norvergicus eNOS     YNSIKRSGSQAHEQRLQEVEAEVVATGTYQLRESELVFGAKQAWRNAPRCVGRIQWGKLQ          193

PF3D7_1450300          ------------------------------------------------------------          0
PF3D7_0923200          ------------------------------------------------------------          0
A.stephensi NOS        VFDCRYVTTTSGMFEAICNHIKYATNKGNLRSAITIFPQRTDGKHDYRIWNNQIISYAGY          294
D.melanogaster NOS     VFDCRYVTTTSGMFEAICNHIKYATNKGNLRSAITIFPQRTDAKHDYRIWNNQLISYAGY          147
M.musculus iNOS        VFDARNCSTAQEMFQHICRHILYATNNGNIRSAITVFPQRSDGKHDFRLWNSQLIRYAGY          151
H.sapiens eNOS         VFDARDCRSAQEMFTYICNHIKYATNRGNLRSAITVFPQRCPGRGDFRIWNSQLVRYAGY          254
R.norvergicus eNOS     VFDARDCRTAQEMFTYICNHIKYATNRGNLRSAITVFPQRYAGRGDFRIWNSQLVRYAGY          253

PF3D7_1450300          ------------------------------------------------------------          0
PF3D7_0923200          ------------------------------------------------------------          0
A.stephensi NOS        KNADGKIIGDPANVEFTDFCVKLGWKSKRTEWDILPLVVSANGHDPDYFDYPPELILEVP          354
D.melanogaster NOS     KQADGKIIGDPMNVEFTEVCTKLGWKSKGSEWDILPLVVSANGHDPDYFDYPPELILEVP          207
M.musculus iNOS        QMPDGTIRGDAATLEFTQLCIDLGWKPRYGRFDVLPLVLQADGQDPEVFEIPPDLVLEVT          211
H.sapiens eNOS         RQQDGSVRGDPANVEITELCIQHGWTPGNGRFDVLPLLLQAPDDPPELFLLPPELVLEVP          314
R.norvergicus eNOS     RQQDGSVRGDPANVEITELCIQHGWTPGNGRFDVLPLLLQAPDEPPELFTLPPELVLEVP          313
```

```
PF3D7_1450300          ------------------------------------------------------------  0
PF3D7_0923200          ------------------------------------------------------------  0
A.stephensi NOS        LSHPQFKWFAELNLRWYAVPMVSSMLFDCGGIQFTATAFSGWYMSTEIGCRNLCDANRRN  414
D.melanogaster NOS     LTHPKFEWFSDLGLRWYALPAVSSMLFDVGGIQFTATTFSGWYMSTEIGSRNLCDTNRRN  267
M.musculus iNOS        MEHPKYEWFQELGLKWYALPAVANMLLEVGGLEFPACPFNGWYMGTEIGVRDFCDTQRYN  271
H.sapiens eNOS         LEHPTLEWFAALGLRWYALPAVSNMLLEIGGLEFPAAPFSGWYMSTEIGTRNLCDPHRYN  374
R.norvergicus eNOS     LEHPTLEWFAALGLRWYALPAVSNMLLEIGGLEFPAAPFSGWYMSSEIGMRDLCDPHRYN  373

PF3D7_1450300          ------------------------------------------------------------  0
PF3D7_0923200          ------------------------------------------------------------  0
A.stephensi NOS        LLEPIAIKMGLDTRNPTSLWKDKALVEINIAVLHSYQSRNITIVDHHTASESFMKHFENE  474
D.melanogaster NOS     MLETVALKMQLDTRTPTSLWKDKAVVEMNIAVLHSYQSRNVTIVDHHTASESFMKHFENE  327
M.musculus iNOS        ILEEVGRRMGLETHTLASLWKDRAVTEINVAVLHSFQKQNVTIMDHHTASESFMKHMQNE  331
H.sapiens eNOS         ILEDVAVCMDLDTRTTSSLWKDKAAVEINVAVLHSYQLAKVTIVDHHAATASFMKHLENE  434
R.norvergicus eNOS     ILEDVAVCMDLDTRTTSSLWKDKAAVEINVAVLYSYQLAKVTIVDHHAATASFMKHLENE  433

PF3D7_1450300          ------------------------------------------------------------  0
PF3D7_0923200          ----------------------------MFMRWNKISRYTLLSGMVVSFWLFYRS----  27
A.stephensi NOS        TKLRNGCPADWIWIVPPMSASVTPVFHQEMAVYYLRPSFEYQESAMKTHIWKKGRDSAKN  534
D.melanogaster NOS     SKLRNGCPADWIWIVPPLSGSITPVFHQEMALYYLKPSFEYQDPAWRTHVWKKGRGESKG  387
M.musculus iNOS        YRARGGCPADWIWLVPPVSGSITPVFHQEMLNYVLSPFYYYQIEPWKTHIWQNEKL----  387
H.sapiens eNOS         QKARGGCPADWAWIVPPISGSLTPVFHQEMVNYFLSPAFRYQPDPWKGSAAKGTGI----  490
R.norvergicus eNOS     QKARGGCPADWAWIVPPISGSLTPVFHQEMVNYFLSPAFRYQPDPWKGSAAKGTGI----  489

PF3D7_1450300          ----------------------------------MRERILLLYGSEYGTSYDCCRNIYY  25
PF3D7_0923200          ------ENFNLLRRLISKLRSLFPLFIKNNFLNNEIKNSVKIYFGSQSGTAEEFAKELKA  81
A.stephensi NOS        KKPRRKFNFKQIARAVKFTSKLF-----GRALSRR--IKATVLYATETGRSEQYARQLVE  587
D.melanogaster NOS     KKPRRKFNFKQIARAVKFTSKLF-----GRALSKR--IKATVLYATETGKSEQYAKQLCE  440
M.musculus iNOS        RPRRREIRFRVLVKVVFFASMLM-----RKVMASR--VRATVLFATETGKSEALARDLAT  440
H.sapiens eNOS         T---RKKTFKEVANAVKISASLM-----GTVMAKR--VKATILYGSETGRAQSYAQQLGR  540
R.norvergicus eNOS     T---RKKTFKEVANAVKISASLM-----GTVMAKR--VKATILYGSETGRAQSYAQQLGR  539
                                                          : :.:: * :   .:::

PF3D7_1450300          ELYTSFDIDF--FSLNEININISLYKYDNIVIIVSTTGYGCCPHNMSQFWLALHNNN----  79
PF3D7_0923200          NLNDLFHIQANIIDLEYFNKEEIKSFGIRIFIVATYGDGEPTDNAVEFFKWLKSLNN---  138
A.stephensi NOS        LLGHAFNAQI--YCMSDYDISSIEHEALLLVVASTFGNGDPPENGELFAQDLYAMKLHES  645
D.melanogaster NOS     LLGHAFNAQI--YCMSDYDISSIEHEALLIVVASTFGNGDPPENGELFSQELYAMRVQES  498
M.musculus iNOS        LFSYAFNTKV--VCMDQYKASTLEEEQLLLVVTSTFGNGDCPSNGQTLKKSLFMLR----  494
H.sapiens eNOS         LFRKAFDPRV--LCMDEYDVVSLEHETLVLVVTSTFGNGDPPENGESFAAALMEMSGPYN  598
R.norvergicus eNOS     LFRKAFDPRV--LCMDEYDVVSLEHEALVLVVTSTFGNGDPPENGESFAAALMEMSGPYN  597
                        :   *.       :.  .   :      :.:.:* * *    *   :   *

PF3D7_1450300          ------------------------------------------------------LIFY  83
PF3D7_0923200          ----------------------------------------------------DNDYF  143
A.stephensi NOS        GHHQAHSELTIAASSKSFIKANSRSDLGKFGPMGGRKIDRLDSLRGSTTDTLSEETFGPL  705
D.melanogaster NOS     SEHGLQD--SSIGSSKSFMKASSRQEFMKLPLQQVKRIDRWDSLRGSTSDTFTEETFGPL  556
M.musculus iNOS        ------------------------------------------------------ELN  497
H.sapiens eNOS         SSPRPEQH-------KSYK-----IRFNSIS-CSDPLVSSWRRKRK---ESSNTDSAGAL  642
R.norvergicus eNOS     SSPRPEQH-------KSYK-----IRFNSVS-CSDPLVSSWRRKRK---ESSNTDSAGAL  641

PF3D7_1450300          DNMKFHLFGLGDSSYDNYNQVAKKLKKKLKSLNANIVNYSLGNYQHPSMHFSNFNIWKNN  143
PF3D7_0923200          RNTKYSIMGLGSKQYKHFNKIAKKLDTFLLNFKAHQISET-IYGDDDDNIYHDFEVWKNK  202
A.stephensi NOS        SNVRFAVFALGSSAYPNFCAFGKYIDNILGELGGERLMKM-ATGDEICGQEQAFRKWAPE  764
D.melanogaster NOS     SNVRFAVFALGSSAYPNFCAFGQYVDNILGELGGERLLRV-AYGDEMCGQEQSFRKWAPE  615
M.musculus iNOS        HTFRYAVFGLGSSMYPQFCAFAHDIDQKLSHLGASQLAPT-GEGDELSGQEDAFRSWAVQ  556
H.sapiens eNOS         GTLRFCVFGLGSRAYPHFCAFARAVDTRLEELGGERLLQL-GQGDELCGQEEAFRGWAQA  701
R.norvergicus eNOS     GTLRFCVFGLGSRAYPHFCAFARAVDTRLEELGGERLLQL-GQGDELCGQEEAFRGWAQA  700
                        . :: ::.**.  * ::  ..: :.  *  : .  :       :.       *. *

PF3D7_1450300          LYTFLKKNYYNFDINTDAP--------------------LLYDVIICEDNKNENHVNSEN  183
PF3D7_0923200          FFMQLPKLLNMKNIPIYVPKEDIIELTSWRDMAEIKLDIQYYDHLIEEDNKKEKNVVTEN  262
A.stephensi NOS        VFKIACETFCLDPEETLSDAAFALQSE-LSEN-----------------------------  795
D.melanogaster NOS     VFKLACETFCLDPEESLSDASLALQNDSLTVN-----------------------------  647
M.musculus iNOS        TFRAACETFDVRSKHHIQIPKRFTSNATWEPQ-----------------------------  588
H.sapiens eNOS         AFQAACETFCVGEDAKAAARDIFSPKRSWKRQ-----------------------------  733
R.norvergicus eNOS     AFQAACETFCVGEDAKAAARDIFSPKRSWKRQ-----------------------------  732
                        :    :

PF3D7_1450300          FNKKKKNIYDKTHKEDNTNIINNNNNNNMNNMNNMKMKNTSFLLKNV-ETFNIDDHFCK  242
PF3D7_0923200          IINE-------SVTNNQQLLNHNQNNLSINN--KSNYI------STDIIGKFYFNHLTGK  307
A.stephensi NOS        ----------------TVRYAPVAEYESLDR--ALSKF----------HNKKS---MECS  824
D.melanogaster NOS     ----------------TVRLVPSANKGSLDS--SLSKY----------HNKKV---HCCK  676
M.musculus iNOS        ----------------QYRLIQSPEPLDLNR--ALSSI----------HAKNV---FTMR  617
H.sapiens eNOS         ----------------RYRLSAQAEGLQLLP--GLIHV----------HRRKM---FQAT  762
R.norvergicus eNOS     ----------------RYRLSTQAESLQLLP--GLTHV----------HRRKM---FQAT  761
                                       :  .:
```

```
PF3D7_1450300          LLNYN-K------------FVV-TKNERCTNINYERDVRYMNLITTDECSNICGLIKVHP          288
PF3D7_0923200          VISNT-KLLKNVDLSNNGDKVNHINISIEDNIIYKAAD-NLSILTKNTKEVITWWLKRLN          365
A.stephensi NOS        VKRNPINLHCEMNGTERSTILVEI---MAEGIDYEPGD-HVGIFPANRKEIVDGIIERLT          880
D.melanogaster NOS     AKAKPHNLTRLSEG-AKTTMLLEI---CAPGLEYEPGD-HVGIFPANRTELVDGLLNRLV          731
M.musculus iNOS        LKSQQ-NL--QSEKSSRTTLLVQLTFEGSRGPSYLPGE-HLGIFPGNQTALVQGILERVV          673
H.sapiens eNOS         IRSVE-NL--QSSKSTRATILVRLDTGGQEGLQYQPGD-HIGVCPPNRPGLVEALLSRVE          818
R.norvergicus eNOS     ILSVE-NL--QSSKSTRATILVRLDTGSQEGLQYQPGD-HIGVCPPNRPGLVEALLSRVE          817
                             :           :         .  *      :.:   :    :   :.

PF3D7_1450300          F---------------------LDINKTKELLKLLKINYND-------YIVI--IPNK--          316
PF3D7_0923200          IDEKEKTKKFTFVKRNKLIDNSFTMNDPKDDVKNETFNNDVNKGNNKTNIDYNSNNNGNN          425
A.stephensi NOS        G-----------------------VNDPDEMLQLQVLKEKQ-------------TQNG--          902
D.melanogaster NOS     G-----------------------VDNPDEVLQLQLLKEKQ-------------TSNG--          753
M.musculus iNOS        D-----------------------CPTPHQTVCLEVLDE-S--------------------          690
H.sapiens eNOS         D-----------------------PPAPTEPVAVEQLEK-G-------------SPGG--          839
R.norvergicus eNOS     D-----------------------PPPSTEPVAVEQLEK-G-------------SPGG--          838
                                               : :    :.

PF3D7_1450300          ------NLNNKESIYLPINKKIKVLDLFIYFLDLNKIVTPFFFTYLTTRTCSEIHRNKFY          370
PF3D7_0923200          NNNNNYNEYDDNHIYVPFPTPCSVEDALSYYCDLTTIPRLNILKKFKCFIKDIEELKMFN          485
A.stephensi NOS        ----VYK----SWEPHERLPVCTLRTLLTRFLDITTPPTRQLLTYLASCCGDKADEERLL          954
D.melanogaster NOS     ----IFK----CWEPHDKIPPDTLRNLLARFFDLTTPPSRQLLTLLAGFCEDTADKERLE          805
M.musculus iNOS        -----GS----YWVKDKRLPPCSLSQALTYFLDITTPPTQLQLHKLARFATDETDRQRLE          741
H.sapiens eNOS         ----PPP----GWVRDPRLPPCTLRQALTFFLDITSPPSPQLLRLLSTLAEEPREQQELE          891
R.norvergicus eNOS     ----PPP----GWVRDPRLPPCTLRQALTYFLDITSPPSPRLLRLLSTLAEESSEQQELE          890
                                        .:   :  : *:..      :  :     .  . : :

PF3D7_1450300          KIADTINISDYFSYVYQDKRSYFDIMFDFYNYINIDINFLINTLPNIQDRSYSILNIFTT          430
PF3D7_0923200          FILSNNQRNTFFNICKECDMTFIEFVDMFMQSAVFELSPFLQLIPRNTPKSYTISSSPKE          545
A.stephensi NOS        MLANESSVYEDWRYW--KLPHLLEVLEEFPS-CRPPAAVFVAQLNALQPRFYSISSSPRK          1011
D.melanogaster NOS     LLVNDSSAYEDWRHW--RLPHLLDVLEEFPS-CRPPAPLLLAQLTPLQPRFYSISSSPRR          862
M.musculus iNOS        ALCQ-PSEYNDWKFS--NNPTFLEVLEEFPS-LHVPAAFLLSQLPILKPRYYSISSSQDH          797
H.sapiens eNOS         ALSQDPRRYEEWKWF--RCPTLLEVLEQFPS-VALPAPLLLTQLPLLQPRYYSVSSAPST          948
R.norvergicus eNOS     ALSQDPRRYEEWKWF--RCPTLLEVLEQFPS-VALPAPLILTQLPLLQPRYYSVSSAPSA          947
                        : .       :          ::.:  * .        ::  :     : *:: .

PF3D7_1450300          YTNIDNYNFFNIYNLYVSQKFLNMLHFLKTNIISNHLLDIQNVNSVQKLQSHVPHSYGNH          490
PF3D7_0923200          SKDILSLT--------V-----------------------------KKK------QYCIH          562
A.stephensi NOS        YSNEIHLT--------V-----------------------------AIV------TYRAE          1028
D.melanogaster NOS     VSDEIHLT--------V-----------------------------AIV------KYRCE          879
M.musculus iNOS        TPSEVHLT--------V-----------------------------AVV------TYRTR          814
H.sapiens eNOS         HPGEIHLT--------V-----------------------------AVL------AYRTQ          965
R.norvergicus eNOS     HPGEIHLT--------V-----------------------------AVL------AYRTQ          964
                         .    .       *                                 *  .

PF3D7_1450300          ISNGCSENTGLTYSKILGNVYKKILKRIKGETQNKDNTNKYTYMYKQNIIELLVCLYKIE          550
PF3D7_0923200          ---------------------------SLRRALKNLKTNDMFPKLNEQK---------LRE          587
A.stephensi NOS        --------------------------DGEGAEH--------------------------          1035
D.melanogaster NOS     --------------------------DGQGDER--------------------------          886
M.musculus iNOS        --------------------------DGQGPLH--------------------------          821
H.sapiens eNOS         --------------------------DGLGPLH--------------------------          972
R.norvergicus eNOS     --------------------------DVLGPLH--------------------------          971
                                                 :

PF3D7_1450300          INKNKTLKGLCSDYLINLNPGSFVYSKIE-NSMLALNKNIFNLDYTILYISVGAAFSSLI          609
PF3D7_0923200          LCSRRWFKGSSSYYLTEELNVNDIVKFNIKPSKFVLPENIQS--SHIIMIATGAGIAPFK          645
A.stephensi NOS        -------YGVCSNYLANLQSDDKIYLFVRSAPSFHMSKD-RT--KPVILIGPGTGIAPFR          1085
D.melanogaster NOS     -------YGVCSNYLSGLRADDELFMFVRSALGFHLPSD-RS--RPIILIGPGTGIAPFR          936
M.musculus iNOS        -------HGVCSTWIRNLKPQDPVPCFVRSVSGFQLPED-PS--QPCILIGPGTGIAPFR          871
H.sapiens eNOS         -------YGVCSTWLSQLKPGDPVPCFIRGAPSFRLPPD-PS--LPCILVGPGTGIAPFR          1022
R.norvergicus eNOS     -------YGVCSTWMSQLKAGDPVPCFIRGAPSFRLPPD-PN--LPCILVGPGTGIAPFR          1021
                              * .* ::      . :         : :  :  .     : :. *:.:: :

PF3D7_1450300          QVLRHRHYLYSTKYLESNHDKNKNVKQNEHDYKNTKIKEKKDLLFLGFRQKSQDFYFKDE          669
PF3D7_0923200          AFLSEFIYY-----------D-------QQIVKDNFVRKGKRILFYGCRKREVDFLYEME          687
A.stephensi NOS        SFWQEWDHI-----------K-------TE---MVDCKIPKVWLFFGCRTKNVD-LYRDE          1123
D.melanogaster NOS     SFWQEFQVL-----------S-------DL---DPTAKLPKMWLFFGCRNRDVD-LYAEE          974
M.musculus iNOS        SFWQQRLHD-----------S-------Q----HKGLKGGRMSLVFGCRHPEEDHLYQEE          909
H.sapiens eNOS         GFWQERLHD-----------I-------E----SKGLQPTPMTLVFGCRCSQLDHLYRDE          1060
R.norvergicus eNOS     GFWQDRLHD-----------I-------E----IKGLQPAPMTLVFGCRCSQLDHLYRDE          1059
                        .  .                                :    *. * *  . *  :  *

PF3D7_1450300          MKSYL---YFSYIFLAFSQDVEDKFVYYNKLNCNDSS--RKWVEDNIISNNNNVNDNNDN          724
PF3D7_0923200          IMDALDKKHIDETYFAFSRDQE-SKIYVQDLILQKKE--LVWNL---LQKGAY-------          734
A.stephensi NOS        KEEMVQHGVLDRVFLALSREENIPKTYVQDLALKEAE-SISELI---MQEKGH-------          1172
D.melanogaster NOS     KAELQKDQILDRVFLALSREQAIPKTYVQDLIEQEFD-SLYQLI---VQERGH-------          1023
M.musculus iNOS        MQEMVRKRVLFQVHTGYSRLPGKPKVYVQDILQKQLANEVLSVL---HGEQGH-------          959
H.sapiens eNOS         VQNAQQRGVFGRVLTAFSREPDNPKTYVQDILRTELAAEVHRVL---CLERGH-------          1110
R.norvergicus eNOS     VLDAQQRGVFGQVLTAFSRDPGSPKTYVQDLLRTELAAEVHRVL---CLEQGH-------          1109
                         .      :     . *:       * :.:   .             :
```

```
PF3D7_1450300          NNNNVNDNNVNDNNVNRNNHSNNHCNNNDCSYNIYNEN-HFEEHEQNYFKMSYEQMINTL          783
PF3D7_0923200          ----------------------IYVCGNSNMSKDVNKTINSLPLHFKQ----NDKKFTKKL          769
A.stephensi NOS        ----------------------IYVCGDVTMAEHVYQTLRKILATREKRTETEMEKYMLTL          1211
D.melanogaster NOS     ----------------------IYVCGDVTMAEHVYQTIRKCIAGKEQKSEAEVETFLLTL          1062
M.musculus iNOS        ----------------------LYICGDVRMARDVATTLKKLVATKLNLSEEQVEDYFFQL          998
H.sapiens eNOS         ----------------------MFVCGDVTMATNVLQTVQRILATEGDMELDEAGDVIGVL          1149
R.norvergicus eNOS     ----------------------MFVCGDVTMATSVLQTVQRILATEGSMELDEAGDVIGVL          1148
                                             *.:   :  :           .    .       *

PF3D7_1450300          QKKKKIYVTDIILMLQNTIYDLLKEKNTIILIAGKSRPFSQNLIKT--FADIIK-NKEPN          840
PF3D7_0923200          -KKSGRYIYEIW-------------------------------------------------          780
A.stephensi NOS        -RDENRYHEDIFGITLRT-----------AEIHNKSRATARIRMASQP------------          1247
D.melanogaster NOS     -RDESRYHEDIFGITLRT-----------AEIHTKSRATARIRMASQP------------          1098
M.musculus iNOS        -KSQKRYHEDIFGAVFSY-----------GAKKGSALEEPKA---TRL------------          1031
H.sapiens eNOS         -RDQQRYHEDIFGLTLRT-----------QEVTSRIRTQSFSLQERQLRGAVPWAFDPPG          1197
R.norvergicus eNOS     -RDQQRYHEDIFGLTLRT-----------QEVTSRIRTQSFSLQERQLRGAVPWSFDPPT          1196
                        :..  *  :*

PF3D7_1450300          KNMEEINLFIKKKIDDFSIILESWY     865
PF3D7_0923200          --------------------------     780
A.stephensi NOS        --------------------------     1247
D.melanogaster NOS     --------------------------     1098
M.musculus iNOS        --------------------------     1031
H.sapiens eNOS         SDTNSP-------------------     1203
R.norvergicus eNOS     QETPGS-------------------     1202
```

Appendix 3.2 The protein identification result of PfDFR1_FMN.

The expected PfDFR1_FMN band was cut from the SDS-PAGE gel and sent to the University of York for the protein identification services. The parameters of the Mascot Search Results and the list protein hit of the PfDFR1_FMN band are shown below.

MATRIX SCIENCE **Mascot Search Results**

User : ps
Email :
Search title : UF_PID
MS data file : 13229323905446912.mgf
Database : Kings 20180921d (1110 sequences; 423335 residues)
Timestamp : 21 Sep 2018 at 09:42:05 GMT
Enzyme : Trypsin
Fixed modifications : Carbamidomethyl (C)
Variable modifications : Oxidation (M)
Mass values : Monoisotopic
Protein Mass : Unrestricted
Peptide Mass Tolerance : ± 100 ppm (# ^{13}C = 1)
Fragment Mass Tolerance: ± 0.5 Da
Max Missed Cleavages : 1
Instrument type : MALDI-TOF-TOF
Number of queries : 10

Protein hits : PF3D7_0923200

sp|P0A9K9|SLYD_ECOLI FKBP-type peptidyl-prolyl cis-trans isomerase SlyD OS=Escherichia coli (strain K12) GN=slyD PE=1 SV=1

Select Summary Report

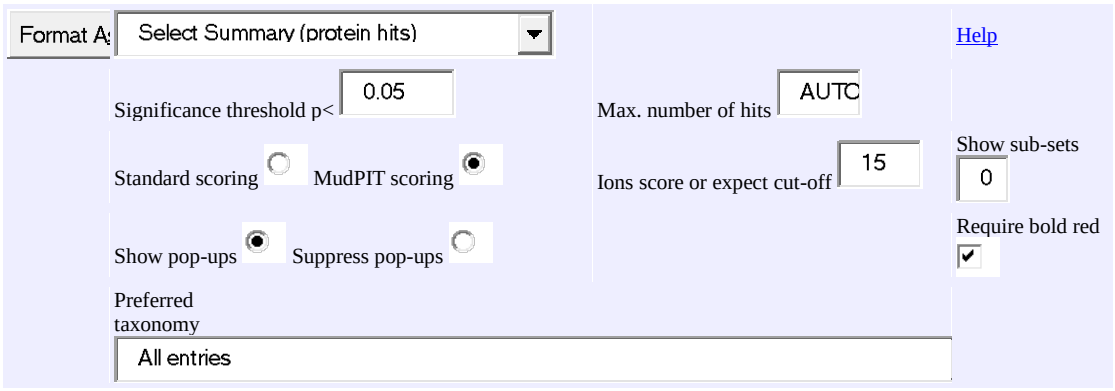

1. PF3D7_0923200 **Mass:** 92635 **Score:** 282 **Matches:** 4(4) **Sequences:** 4(4)

Query	Observed	Mr(expt)	Mr(calc)	ppm	Miss	Score	Expect	Rank	Unique	Peptide
1	1257.5857	1256.5784	1256.5422	28.9	0	48	3.7e-05	1	U	K.SLNNDNDYFR.N
3	1261.6863	1260.6790	1260.6350	34.9	0	54	1.5e-05	1	U	K.EDIIELTSWR.D
9	1634.7738	1633.7665	1633.7624	2.53	0	125	1.2e-12	1	U	K.IYFGSQSGTAEEFAK.E
10	2035.9696	2034.9623	2034.9898	-13.50	1	107	6e-11	1	U	K.LDIQYYDHLIEEDNKK.E

Matched peptides shown in ***bold red***.

1	MFMRWNKISR	YTLLSGMVVS	FWLFYRSENF	NLLRRLISKL	RSLFPLFIKN
51	NFLNNEIKNS	VK**IYFGSQSG**	**TAEEFAK**ELK	ANLNDLFHIQ	ANIIDLEYFN
101	KEEIKSFGIR	IFIVATYGDG	EPTDNAVEFF	KWLK**SLNNDN**	**DYFR**NTKYSI
151	MGLGSKQYKH	FNKIAKKLDT	FLLNFKAHQI	SETIYGDDDD	NIYHDFEVWK
201	NKFFMQLPKL	LNMKNIPIYV	PK**EDIIELTS**	**WR**DMAEIK**LD**	**IQYYDHLIEE**
251	**DNKK**EKNVVT	ENIINESVTN	NQQLLNHNQN	NLSINNKSNY	ISTDIIGKFY
301	FNHLTGKVIS	NTKLLKNVDL	SNNGDKVNHI	NISIEDNIIY	KAADNLSILT
351	KNTKEVITWW	LKRLNIDEKE	KTKKFTFVKR	NKLIDNSFTM	NDPKDDVKNE
401	TFNNDVNKGN	NKTNIDYNSN	NNGNNNNNNN	YNEYDDNHIY	VPFPTPCSVE
451	DALSYYCDLT	TIPRLNILKK	FKCFIKDIEE	LKMFNFILSN	NQRNTFFNIC
501	KECDMTFIEF	VDMFMQSAVF	ELSPFLQLIP	RNTPKSYTIS	SSPKESKDIL
551	SLTVKKKQYC	IHSLRRALKN	LKTNDMFPKL	NEQKLRELCS	RRWFKGSSSY
601	YLTEELNVND	IVKFNIKPSK	FVLPENIQSS	HIIMIATGAG	IAPFKAFLSE
651	FIYYDQQIVK	DNFVRKGKRI	LFYGCRKREV	DFLYEMEIMD	ALDKKHIDET
701	YFAFSRDQES	KIYVQDLILQ	KKELVWNLLQ	KGAYIYVCGN	SNMSKDVNKT
751	INSLPLHFKQ	NDKKFTKKLK	KSGRYIYEIW		

2. sp|P0A9K9|SLYD_ECOLI **Mass:** 21182 **Score:** 75 **Matches:** 2(2) **Sequences:** 2(2)
FKBP-type peptidyl-prolyl cis-trans isomerase SlyD OS=Escherichia coli (strain K12) GN=slyD PE=1 SV=1

Query	Observed	Mr(expt)	Mr(calc)	ppm	Miss	Score	Expect	Rank	Unique	Peptide
4	1263.7336	1262.7264	1261.7030	811	0	19	0.034	1	U	K.DLVVSLAYQVR.T
8	1595.7667	1594.7594	1594.7484	6.95	0	72	1.4e-07	1	U	K.DVFMGVDELQVGMR.F

Matched peptides shown in ***bold red***.

1	MKVAK**DLVVS**	**LAYQVR**TEDG	VLVDESPVSA	PLDYLHGHGS	LISGLETALE
51	GHEVGDKFDV	AVGANDAYGQ	YDENLVQRVP	K**DVFMGVDEL**	**QVGMR**FLAET
101	DQGPVPVEIT	AVEDDHVVVD	GNHMLAGQNL	KFNVEVVAIR	EATEEELAHG
151	HVHGAHDHHH	DHDHDGCCGG	HGHDHGHEHG	GEGCCGGKGN	GGCGCH

Appendix 3.3 The protein identification result of PfDFR1_FAD/NADPH.

The expected PfDFR1_FAD/NADPH band was cut from the SDS-PAGE gel and sent to the University of York for the protein identification services. The parameters of the Mascot Search Results and the list protein hit of the PfDFR1_FAD/NADPH band are shown below.

MATRIX SCIENCE **Mascot Search Results**

User : ps
Email :
Search title : UF_PID
MS data file : 13229323905446911.mgf
Database : Kings 20180921d (1110 sequences; 423335 residues)
Timestamp : 21 Sep 2018 at 09:41:40 GMT
Enzyme : Trypsin
Fixed modifications : Carbamidomethyl (C)
Variable modifications : Oxidation (M)
Mass values : Monoisotopic
Protein Mass : Unrestricted
Peptide Mass Tolerance : ± 100 ppm (# ^{13}C = 1)
Fragment Mass Tolerance: ± 0.5 Da
Max Missed Cleavages : 1
Instrument type : MALDI-TOF-TOF
Number of queries : 10

Protein hits : PF3D7_0923200

Select Summary Report

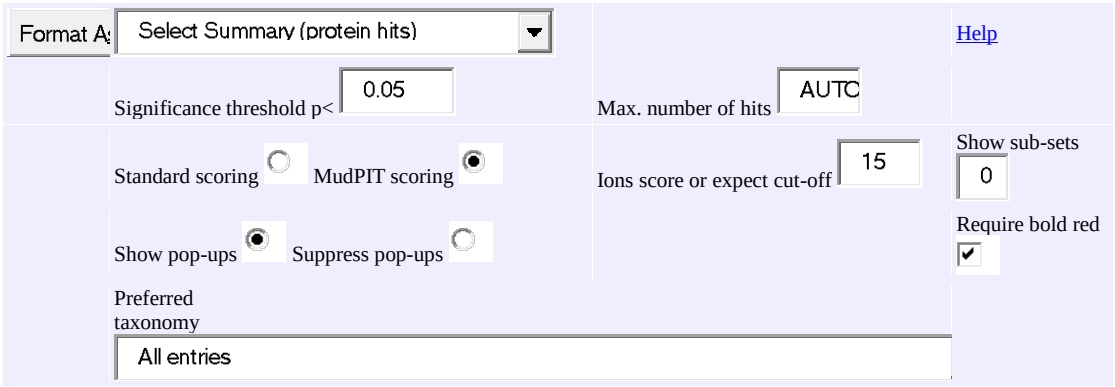

1. PF3D7_0923200 **Mass:** 92635 **Score:** 148 **Matches:** 4(4) **Sequences:** 3(3)

	Observed	Mr(expt)	Mr(calc)	ppm	Miss	Score	Expect	Rank	Unique	Peptide
1	928.4630	927.4557	927.4637	-8.60	0	43	0.00022	1	U	R.ILFYGCR.K
5	1383.7527	1382.7454	1382.6765	49.9	0	(39)	0.00043	1	U	K.MFNFILSNNQR.N
6	1385.7086	1384.7013	1384.6412	43.5	0	68	4.6e-07	1	U	K.HIDETYFAFSR.D
7	1399.7555	1398.7482	1398.6714	54.9	0	52	3.9e-05	1	U	K.MFNFILSNNQR.N

Matched peptides shown in ***bold red***.

1	MFMRWNKISR	YTLLSGMVVS	FWLFYRSENF	NLLRRLISKL	RSLFPLFIKN
51	NFLNNEIKNS	VKIYFGSQSG	TAEEFAKELK	ANLNDLFHIQ	ANIIDLEYFN
101	KEEIKSFGIR	IFIVATYGDG	EPTDNAVEFF	KWLKSLNNDN	DYFRNTKYSI
151	MGLGSKQYKH	FNKIAKKLDT	FLLNFKAHQI	SETIYGDDDD	NIYHDFEVWK
201	NKFFMQLPKL	LNMKNIPIYV	PKEDIIELTS	WRDMAEIKLD	IQYYDHLIEE
251	DNKKEKNVVT	ENIINESVTN	NQQLLNHNQN	NLSINNKSNY	ISTDIIGKFY
301	FNHLTGKVIS	NTKLLKNVDL	SNNGDKVNHI	NISIEDNIIY	KAADNLSILT
351	KNTKEVITWW	LKRLNIDEKE	KTKKFTFVKR	NKLIDNSFTM	NDPKDDVKNE
401	TFNNDVNKGN	NKTNIDYNSN	NNGNNNNNNN	YNEYDDNHIY	VPFPTPCSVE
451	DALSYYCDLT	TIPRLNILKK	FKCFIKDIEE	LK**MFNFILSN**	**NQR**NTFFNIC
501	KECDMTFIEF	VDMFMQSAVF	ELSPFLQLIP	RNTPKSYTIS	SSPKESKDIL
551	SLTVKKKQYC	IHSLRRALKN	LKTNDMFPKL	NEQKLRELCS	RRWFKGSSSY
601	YLTEELNVND	IVKFNIKPSK	FVLPENIQSS	HIIMIATGAG	IAPFKAFLSE
651	FIYYDQQIVK	DNFVRKGKR**I**	**LFYGCR**KREV	DFLYEMEIMD	ALDKK**HIDET**
701	**YFAFSR**DQES	KIYVQDLILQ	KKELVWNLLQ	KGAYIYVCGN	SNMSKDVNKT
751	INSLPLHFKQ	NDKKFTKKLK	KSGRYIYEIW		

Appendix 3.4 The protein identification result of PfDFR1 wt.

The expected PfDFR1 wt band was cut from the SDS-PAGE gel and sent to the University of York for the protein identification services. The parameters of the Mascot Search Results and the list protein hit of the PfDFR1wt band are shown below.

MATRIX SCIENCE **Mascot Search Results**

User : ps
Email :
Search title : UF_PID
MS data file : 13229323905446910.mgf
Database : Kings 20180921d (1110 sequences; 423335 residues)
Timestamp : 21 Sep 2018 at 09:41:54 GMT
Enzyme : Trypsin
Fixed modifications : Carbamidomethyl (C)
Variable modifications : Oxidation (M)
Mass values : Monoisotopic
Protein Mass : Unrestricted
Peptide Mass Tolerance : ± 100 ppm (# ^{13}C = 1)
Fragment Mass Tolerance: ± 0.5 Da
Max Missed Cleavages : 1
Instrument type : MALDI-TOF-TOF
Number of queries : 10

Protein hits : PF3D7_0923200

Select Summary Report

Format As: Select Summary (protein hits) Help

Significance threshold p< 0.05 Max. number of hits AUTO

Standard scoring MudPIT scoring Ions score or expect cut-off 15 Show sub-sets 0

Show pop-ups Suppress pop-ups Require bold red

Preferred taxonomy: All entries

Re-Search All queries Unassigned Below homology threshold Below identity threshold

1. PF3D7_0923200 **Mass:** 92635 **Score:** 253 **Matches:** 6(6) **Sequences:** 5(5)

Query	Observed	Mr(expt)	Mr(calc)	ppm	Miss	Score	Expect	Rank	Unique	Peptide
1	928.4787	927.4714	927.4637	8.38	0	38	0.0008	1	U	R.ILFYGCR.K
2	1257.5781	1256.5708	1256.5422	22.8	0	47	3.8e-05	1	U	K.SLNNDNDYFR.N
3	1261.6714	1260.6641	1260.6350	23.1	0	71	2.8e-07	1	U	K.EDIIELTSWR.D
6	1383.7720	1382.7647	1382.6765	63.8	0	(50)	3.7e-05	1	U	K.MFNFILSNNQR.N
7	1385.7281	1384.7209	1384.6412	57.6	0	66	8.9e-07	1	U	K.HIDETYFAFSR.D
8	1399.7485	1398.7413	1398.6714	49.9	0	72	3.5e-07	1	U	K.MFNFILSNNQR.N

Matched peptides shown in ***bold red***.

1	MFMRWNKISR	YTLLSGMVVS	FWLFYRSENF	NLLRRLISKL	RSLFPLFIKN
51	NFLNNEIKNS	VKIYFGSQSG	TAEEFAKELK	ANLNDLFHIQ	ANIIDLEYFN
101	KEEIKSFGIR	IFIVATYGDG	EPTDNAVEFF	KWLK**SLNNDN**	**DYFR**NTKYSI
151	MGLGSKQYKH	FNKIAKKLDT	FLLNFKAHQI	SETIYGDDDD	NIYHDFEVWK
201	NKFFMQLPKL	LNMKNIPIYV	PK**EDIIELTS**	**WR**DMAEIKLD	IQYYDHLIEE
251	DNKKEKNVVT	ENIINESVTN	NQQLLNHNQN	NLSINNKSNY	ISTDIIGKFY
301	FNHLTGKVIS	NTKLLKNVDL	SNNGDKVNHI	NISIEDNIIY	KAADNLSILT
351	KNTKEVITWW	LKRLNIDEKE	KTKKFTFVKR	NKLIDNSFTM	NDPKDDVKNE
401	TFNNDVNKGN	NKTNIDYNSN	NNGNNNNNNN	YNEYDDNHIY	VPFPTPCSVE
451	DALSYYCDLT	TIPRLNILKK	FKCFIKDIEE	LK**MFNFILSN**	**NQR**NTFFNIC
501	KECDMTFIEF	VDMFMQSAVF	ELSPFLQLIP	RNTPKSYTIS	SSPKESKDIL
551	SLTVKKKQYC	IHSLRRALKN	LKTNDMFPKL	NEQKLRELCS	RRWFKGSSSY
601	YLTEELNVND	IVKFNIKPSK	FVLPENIQSS	HIIMIATGAG	IAPFKAFLSE
651	FIYYDQQIVK	DNFVRKGKR**I**	**LFYGCR**KREV	DFLYEMEIMD	ALDKK**HIDET**
701	**YFAFSR**DQES	KIYVQDLILQ	KKELVWNLLQ	KGAYIYVCGN	SNMSKDVNKT
751	INSLPLHFKQ	NDKKFTKKLK	KSGRYIYEIW		

Appendix 3.5 Comparison of PfDFR1 wt and PfDFR1 D436G activities

A

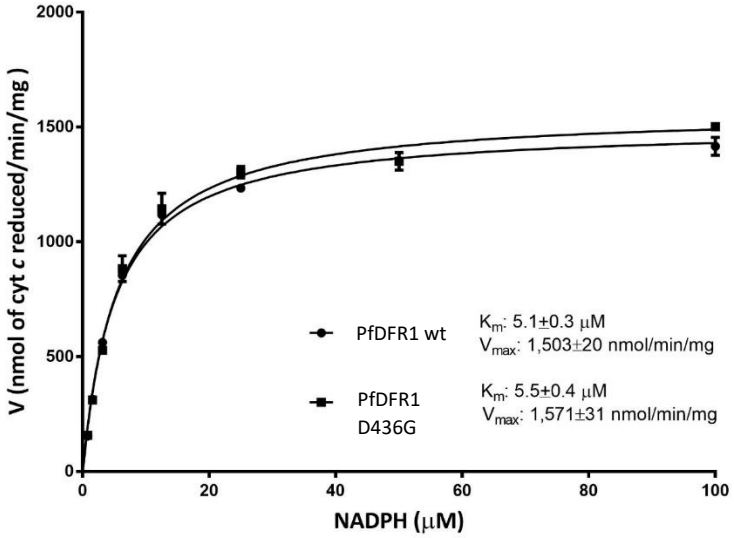

B

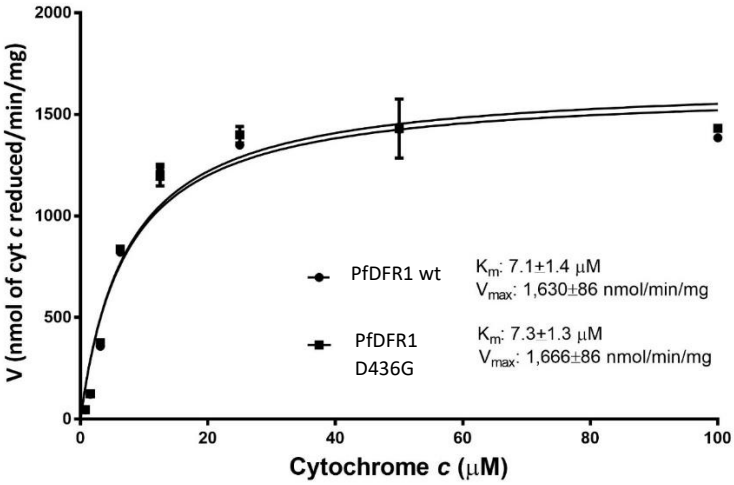

The PfDFR1 wt and PfDFR1 D436G activities were measured from partially purified recombinant proteins using cytochrome *c* as an electron acceptor. A) comparison of NADPH kinetics between both recombinant proteins. B) Comparison of cytochrom *c* kinetics between both recombinant proteins. The initial rates were obtained from three measurements. Solid lines represent curve fits of data to Michaelis-Menten equation using GraphPad Prism version 7.

Appendix 4.1 Comparison of cytochrome *c* reduction rate from PfDFR1 reactions with various pH conditions

Tukey's multiple comparisons test	Mean Diff.	95.00% CI of diff.	Significant?	Summary	Adjusted P Value
pH 5.8 vs. pH 6.2	-0.01943	-0.02026 to -0.0186	Yes	****	<0.0001
pH 5.8 vs. pH 6.6	-0.02634	-0.02717 to -0.02551	Yes	****	<0.0001
pH 5.8 vs. pH 7.0	-0.03042	-0.03125 to -0.02959	Yes	****	<0.0001
pH 5.8 vs. pH 7.4	-0.03572	-0.03655 to -0.03489	Yes	****	<0.0001
pH 5.8 vs. pH 7.8	-0.03982	-0.04065 to -0.03899	Yes	****	<0.0001
pH 5.8 vs. pH 8.2	-0.03572	-0.03655 to -0.03489	Yes	****	<0.0001
pH 6.2 vs. pH 6.6	-0.00691	-0.007743 to -0.006077	Yes	****	<0.0001
pH 6.2 vs. pH 7.0	-0.01099	-0.01182 to -0.01016	Yes	****	<0.0001
pH 6.2 vs. pH 7.4	-0.01629	-0.01712 to -0.01546	Yes	****	<0.0001
pH 6.2 vs. pH 7.8	-0.02039	-0.02122 to -0.01956	Yes	****	<0.0001
pH 6.2 vs. pH 8.2	-0.01629	-0.01712 to -0.01546	Yes	****	<0.0001
pH 6.6 vs. pH 7.0	-0.00408	-0.004913 to -0.003247	Yes	****	<0.0001
pH 6.6 vs. pH 7.4	-0.00938	-0.01021 to -0.008547	Yes	****	<0.0001
pH 6.6 vs. pH 7.8	-0.01348	-0.01431 to -0.01265	Yes	****	<0.0001
pH 6.6 vs. pH 8.2	-0.00938	-0.01021 to -0.008547	Yes	****	<0.0001
pH 7.0 vs. pH 7.4	-0.0053	-0.006133 to -0.004467	Yes	****	<0.0001
pH 7.0 vs. pH 7.8	-0.0094	-0.01023 to -0.008567	Yes	****	<0.0001
pH 7.0 vs. pH 8.2	-0.0053	-0.006133 to -0.004467	Yes	****	<0.0001
pH 7.4 vs. pH 7.8	-0.0041	-0.004933 to -0.003267	Yes	****	<0.0001
pH 7.4 vs. pH 8.2	0	-0.0008326 to 0.0008326	No	ns	>0.9999
pH 7.8 vs. pH 8.2	0.0041	0.003267 to 0.004933	Yes	****	<0.0001

Appendix 4.2 Comparison of cytochrome *c* reduction rate from PfDFR1 reactions with various assay temperatures

Tukey's multiple comparisons test	Mean Diff.	95.00% CI of diff.	Significant?	Summary	Adjusted P Value
22.5 °C vs. 25 °C	-0.01769	-0.01957 to -0.01581	Yes	****	<0.0001
22.5 °C vs. 30 °C	-0.03119	-0.03299 to -0.02939	Yes	****	<0.0001
22.5 °C vs. 32.5 °C	-0.04309	-0.04489 to -0.04129	Yes	****	<0.0001
22.5 °C vs. 35 °C	-0.05569	-0.05757 to -0.05381	Yes	****	<0.0001
22.5 °C vs. 37.5 °C	-0.05869	-0.06057 to -0.05681	Yes	****	<0.0001
22.5 °C vs. 40 °C	-0.06879	-0.07059 to -0.06699	Yes	****	<0.0001
22.5 °C vs. 42.5 °C	-0.06319	-0.06507 to -0.06131	Yes	****	<0.0001
25 °C vs. 30 °C	-0.0135	-0.01538 to -0.01162	Yes	****	<0.0001
25 °C vs. 32.5 °C	-0.0254	-0.02728 to -0.02352	Yes	****	<0.0001
25 °C vs. 35 °C	-0.038	-0.03997 to -0.03603	Yes	****	<0.0001
25 °C vs. 37.5 °C	-0.041	-0.04297 to -0.03903	Yes	****	<0.0001
25 °C vs. 40 °C	-0.0511	-0.05298 to -0.04922	Yes	****	<0.0001
25 °C vs. 42.5 °C	-0.0455	-0.04747 to -0.04353	Yes	****	<0.0001
30 °C vs. 32.5 °C	-0.0119	-0.0137 to -0.0101	Yes	****	<0.0001
30 °C vs. 35 °C	-0.0245	-0.02638 to -0.02262	Yes	****	<0.0001
30 °C vs. 37.5 °C	-0.0275	-0.02938 to -0.02562	Yes	****	<0.0001
30 °C vs. 40 °C	-0.0376	-0.0394 to -0.0358	Yes	****	<0.0001
30 °C vs. 42.5 °C	-0.032	-0.03388 to -0.03012	Yes	****	<0.0001
32.5 °C vs. 35 °C	-0.0126	-0.01448 to -0.01072	Yes	****	<0.0001
32.5 °C vs. 37.5 °C	-0.0156	-0.01748 to -0.01372	Yes	****	<0.0001
32.5 °C vs. 40 °C	-0.0257	-0.0275 to -0.0239	Yes	****	<0.0001
32.5 °C vs. 42.5 °C	-0.0201	-0.02198 to -0.01822	Yes	****	<0.0001
35 °C vs. 37.5 °C	-0.003	-0.004967 to -0.001033	Yes	***	0.0005
35 °C vs. 40 °C	-0.0131	-0.01498 to -0.01122	Yes	****	<0.0001
35 °C vs. 42.5 °C	-0.0075	-0.009467 to -0.005533	Yes	****	<0.0001
37.5 °C vs. 40 °C	-0.0101	-0.01198 to -0.008216	Yes	****	<0.0001
37.5 °C vs. 42.5 °C	-0.0045	-0.006467 to -0.002533	Yes	****	<0.0001
40 °C vs. 42.5 °C	0.0056	0.003716 to 0.007484	Yes	****	<0.0001

Appendix 6.1 Comparison of catalase-mediated O_2 release from PfDFR1 reactions with various OH-PQms and 8-aminoquinolines

Tukey's multiple comparisons test	Mean Diff.	95.00% CI of diff.	Significant?	Summary	Adjusted P Value
5-HPQ vs. 5,6-DPQ	-1.767	-6.424 to 2.89	No	ns	0.9641
5-HPQ vs. PQQI	0.25	-4.957 to 5.457	No	ns	>0.9999
5-HPQ vs. 6OHPQQI	-1.9	-6.557 to 2.757	No	ns	0.9419
5-HPQ vs. SL-6-41	8.85	4.494 to 13.21	Yes	****	<0.0001
5-HPQ vs. SL-6-56	4.75	0.3939 to 9.106	Yes	*	0.0236
5-HPQ vs. SL-6-46	11.63	7.269 to 15.98	Yes	****	<0.0001
5-HPQ vs. CPQ	12.93	8.276 to 17.59	Yes	****	<0.0001
5-HPQ vs. TQ	14.63	9.976 to 19.29	Yes	****	<0.0001
5-HPQ vs. PQ	12.75	8.394 to 17.11	Yes	****	<0.0001
5-HPQ vs. MeOH	12.63	7.976 to 17.29	Yes	****	<0.0001
5-HPQ vs. DMSO	13.63	9.269 to 17.98	Yes	****	<0.0001
5,6-DPQ vs. PQQI	2.017	-3.19 to 7.223	No	ns	0.9587
5,6-DPQ vs. 6OHPQQI	-0.1333	-4.79 to 4.524	No	ns	>0.9999
5,6-DPQ vs. SL-6-41	10.62	6.261 to 14.97	Yes	****	<0.0001
5,6-DPQ vs. SL-6-56	6.517	2.161 to 10.87	Yes	***	0.0006
5,6-DPQ vs. SL-6-46	13.39	9.036 to 17.75	Yes	****	<0.0001
5,6-DPQ vs. CPQ	14.7	10.04 to 19.36	Yes	****	<0.0001
5,6-DPQ vs. TQ	16.4	11.74 to 21.06	Yes	****	<0.0001
5,6-DPQ vs. PQ	14.52	10.16 to 18.87	Yes	****	<0.0001
5,6-DPQ vs. MeOH	14.4	9.743 to 19.06	Yes	****	<0.0001
5,6-DPQ vs. DMSO	15.39	11.04 to 19.75	Yes	****	<0.0001
PQQI vs. 6OHPQQI	-2.15	-7.357 to 3.057	No	ns	0.9373
PQQI vs. SL-6-41	8.6	3.661 to 13.54	Yes	****	<0.0001
PQQI vs. SL-6-56	4.5	-0.4394 to 9.439	No	ns	0.0996
PQQI vs. SL-6-46	11.38	6.436 to 16.31	Yes	****	<0.0001
PQQI vs. CPQ	12.68	7.477 to 17.89	Yes	****	<0.0001
PQQI vs. TQ	14.38	9.177 to 19.59	Yes	****	<0.0001
PQQI vs. PQ	12.5	7.561 to 17.44	Yes	****	<0.0001
PQQI vs. MeOH	12.38	7.177 to 17.59	Yes	****	<0.0001
PQQI vs. DMSO	13.38	8.436 to 18.31	Yes	****	<0.0001
6OHPQQI vs. SL-6-41	10.75	6.394 to 15.11	Yes	****	<0.0001
6OHPQQI vs. SL-6-56	6.65	2.294 to 11.01	Yes	***	0.0004
6OHPQQI vs. SL-6-46	13.53	9.169 to 17.88	Yes	****	<0.0001
6OHPQQI vs. CPQ	14.83	10.18 to 19.49	Yes	****	<0.0001
6OHPQQI vs. TQ	16.53	11.88 to 21.19	Yes	****	<0.0001
6OHPQQI vs. PQ	14.65	10.29 to 19.01	Yes	****	<0.0001
6OHPQQI vs. MeOH	14.53	9.876 to 19.19	Yes	****	<0.0001
6OHPQQI vs. DMSO	15.53	11.17 to 19.88	Yes	****	<0.0001
SL-6-41 vs. SL-6-56	-4.1	-8.133 to -0.06701	Yes	*	0.0437
SL-6-41 vs. SL-6-46	2.775	-1.258 to 6.808	No	ns	0.4099
SL-6-41 vs. CPQ	4.083	-0.2728 to 8.439	No	ns	0.0817
SL-6-41 vs. TQ	5.783	1.427 to 10.14	Yes	**	0.0029
SL-6-41 vs. PQ	3.9	-0.133 to 7.933	No	ns	0.0650
SL-6-41 vs. MeOH	3.783	-0.5728 to 8.139	No	ns	0.1355
SL-6-41 vs. DMSO	4.775	0.742 to 8.808	Yes	*	0.0105
SL-6-56 vs. SL-6-46	6.875	2.842 to 10.91	Yes	****	<0.0001
SL-6-56 vs. CPQ	8.183	3.827 to 12.54	Yes	****	<0.0001

SL-6-56 vs. TQ	9.883	5.527 to 14.24	Yes	****	<0.0001
SL-6-56 vs. PQ	8	3.967 to 12.03	Yes	****	<0.0001
SL-6-56 vs. MeOH	7.883	3.527 to 12.24	Yes	****	<0.0001
SL-6-56 vs. DMSO	8.875	4.842 to 12.91	Yes	****	<0.0001
SL-6-46 vs. CPQ	1.308	-3.048 to 5.664	No	ns	0.9938
SL-6-46 vs. TQ	3.008	-1.348 to 7.364	No	ns	0.4047
SL-6-46 vs. PQ	1.125	-2.908 to 5.158	No	ns	0.9967
SL-6-46 vs. MeOH	1.008	-3.348 to 5.364	No	ns	0.9994
SL-6-46 vs. DMSO	2	-2.033 to 6.033	No	ns	0.8235
CPQ vs. TQ	1.7	-2.957 to 6.357	No	ns	0.9726
CPQ vs. PQ	-0.1833	-4.539 to 4.173	No	ns	>0.9999
CPQ vs. MeOH	-0.3	-4.957 to 4.357	No	ns	>0.9999
CPQ vs. DMSO	0.6917	-3.664 to 5.048	No	ns	>0.9999
TQ vs. PQ	-1.883	-6.239 to 2.473	No	ns	0.9169
TQ vs. MeOH	-2	-6.657 to 2.657	No	ns	0.9201
TQ vs. DMSO	-1.008	-5.364 to 3.348	No	ns	0.9994
PQ vs. MeOH	-0.1167	-4.473 to 4.239	No	ns	>0.9999
PQ vs. DMSO	0.875	-3.158 to 4.908	No	ns	0.9997
MeOH vs. DMSO	0.9917	-3.364 to 5.348	No	ns	0.9995

Appendix 6.2 Comparison of catalase-mediated O_2 release from hCPR reactions with various OH-PQms and 8-aminoquinolines

Tukey's multiple comparisons test	Mean Diff.	95.00% CI of diff.	Significant?	Summary	Adjusted P Value
5-HPQ vs. 5,6-DPQ	-3.65	-12.32 to 5.019	No	ns	0.8231
5-HPQ vs. PQQ1	3.85	-4.819 to 12.52	No	ns	0.7806
5-HPQ vs. 6OHPQQ1	0.8	-7.869 to 9.469	No	ns	>0.9999
5-HPQ vs. SL-6-41	5.3	-3.369 to 13.97	No	ns	0.4333
5-HPQ vs. SL-6-56	8.9	0.2314 to 17.57	Yes	*	0.0425
5-HPQ vs. SL-6-46	12.18	4.27 to 20.1	Yes	**	0.0020
5-HPQ vs. PQ	13.65	5.737 to 21.56	Yes	***	0.0007
5-HPQ vs. MeOH	15.5	6.831 to 24.17	Yes	***	0.0005
5-HPQ vs. DMSO	15.25	6.581 to 23.92	Yes	***	0.0006
5,6-DPQ vs. PQQ1	7.5	-1.169 to 16.17	No	ns	0.1126
5,6-DPQ vs. 6OHPQQ1	4.45	-4.219 to 13.12	No	ns	0.6375
5,6-DPQ vs. SL-6-41	8.95	0.2814 to 17.62	Yes	*	0.0410
5,6-DPQ vs. SL-6-56	12.55	3.881 to 21.22	Yes	**	0.0033
5,6-DPQ vs. SL-6-46	15.83	7.92 to 23.75	Yes	***	0.0002
5,6-DPQ vs. PQ	17.3	9.387 to 25.21	Yes	****	<0.0001
5,6-DPQ vs. MeOH	19.15	10.48 to 27.82	Yes	****	<0.0001
5,6-DPQ vs. DMSO	18.9	10.23 to 27.57	Yes	****	<0.0001
PQQ1 vs. 6OHPQQ1	-3.05	-11.72 to 5.619	No	ns	0.9238
PQQ1 vs. SL-6-41	1.45	-7.219 to 10.12	No	ns	0.9995
PQQ1 vs. SL-6-56	5.05	-3.619 to 13.72	No	ns	0.4906
PQQ1 vs. SL-6-46	8.333	0.42 to 16.25	Yes	*	0.0361
PQQ1 vs. PQ	9.8	1.887 to 17.71	Yes	*	0.0116
PQQ1 vs. MeOH	11.65	2.981 to 20.32	Yes	**	0.0062
PQQ1 vs. DMSO	11.4	2.731 to 20.07	Yes	**	0.0073
6OHPQQ1 vs. SL-6-41	4.5	-4.169 to 13.17	No	ns	0.6251
6OHPQQ1 vs. SL-6-56	8.1	-0.5686 to 16.77	No	ns	0.0745
6OHPQQ1 vs. SL-6-46	11.38	3.47 to 19.3	Yes	**	0.0035
6OHPQQ1 vs. PQ	12.85	4.937 to 20.76	Yes	**	0.0012
6OHPQQ1 vs. MeOH	14.7	6.031 to 23.37	Yes	***	0.0008
6OHPQQ1 vs. DMSO	14.45	5.781 to 23.12	Yes	***	0.0010
SL-6-41 vs. SL-6-56	3.6	-5.069 to 12.27	No	ns	0.8332
SL-6-41 vs. SL-6-46	6.883	-1.03 to 14.8	No	ns	0.1096
SL-6-41 vs. PQ	8.35	0.4367 to 16.26	Yes	*	0.0356
SL-6-41 vs. MeOH	10.2	1.531 to 18.87	Yes	*	0.0169
SL-6-41 vs. DMSO	9.95	1.281 to 18.62	Yes	*	0.0202
SL-6-56 vs. SL-6-46	3.283	-4.63 to 11.2	No	ns	0.8338
SL-6-56 vs. PQ	4.75	-3.163 to 12.66	No	ns	0.4550
SL-6-56 vs. MeOH	6.6	-2.069 to 15.27	No	ns	0.2038
SL-6-56 vs. DMSO	6.35	-2.319 to 15.02	No	ns	0.2383
SL-6-46 vs. PQ	1.467	-5.611 to 8.545	No	ns	0.9974
SL-6-46 vs. MeOH	3.317	-4.597 to 11.23	No	ns	0.8265
SL-6-46 vs. DMSO	3.067	-4.847 to 10.98	No	ns	0.8775
PQ vs. MeOH	1.85	-6.063 to 9.763	No	ns	0.9937
PQ vs. DMSO	1.6	-6.313 to 9.513	No	ns	0.9978
MeOH vs. DMSO	-0.25	-8.919 to 8.419	No	ns	>0.9999

PUBLICATIONS AND PRESENTATIONS

Publications

1. Grazia Camarda, **Piyaporn Jirawatcharadech**, Richard S. Priestley, Ahmed Saif, Sandra March, Michael H.L. Wong, Suet Leung, Alex B. Miller, David A. Baker, Pietro Alano, Mark J.I. Paine, Sangeeta N. Bhatia, Paul M. O'Neill, Stephen A. Ward, Giancarlo A. Biagini. "Antimalarial activity of primaquine operates via a two-step biochemical relay", In Preparation.

2. **Piyaporn Jirawatcharadech**, Grazia Camarda, Christina Yunta-Yanes, Mark J.I. Paine, Stephen A. Ward, Giancarlo A. Biagini. "Identification and characterisation of *Plasmodium falciparum* NADPH-dependent diflavin reductase I (PfDFR1)". In Preparation.

3. **Piyaporn Jirawatcharadech**, Grazia Camarda, Christina Yunta-Yanes, Mark J.I. Paine, Stephen A. Ward, Giancarlo A. Biagini. "Role of *Plasmodium falciparum* NADPH-dependent diflavin reductase I (PfDFR1) in primaquine mechanism of action". In Preparation.

Presentations

1. **Piyaporn Jirawatcharadech**, Grazia Camarda, Christina Yunta-Yanes, Mark J.I. Paine, Giancarlo A. Biagini, Stephen A. Ward. "Expression and purification of *Plasmodium falciparum* NADPH-cytochrome P450 reductase". Liverpool School of Tropical Medicine PGR Student Conference, Liverpool, UK, 24th April 2015

2. **Piyaporn Jirawatcharadech**, Grazia Camarda, Christina Yunta-Yanes, Mark J.I. Paine, Giancarlo A. Biagini, Stephen A. Ward. "Expression, purification and characterisation of *Plasmodium falciparum* NADPH-cytochrome P450 reductase" Health and Life Sciences Poster Day 2016, Liverpool, UK, 10th June 2016

3. **Piyaporn Jirawatcharadech**, Grazia Camarda, Christina Yunta-Yanes, Mark J.I. Paine, Giancarlo A. Biagini, Stephen A. Ward. "Expression and characterisation of *Plasmodium falciparum* NADPH-cytochrome P450 reductase". BSP Spring Meeting, Dundee, UK, 2nd-5th April 2017

4. **Piyaporn Jirawatcharadech**, Grazia Camarda, Christina Yunta-Yanes, Mark J.I. Paine, Giancarlo A. Biagini, Stephen A. Ward. "Identification and characterisation of *Plasmodium falciparum* NADPH-cytochrome P450 reductase". Liverpool School of Tropical Medicine PGR Student Conference, Liverpool, UK, 4th May 2017

5. **Piyaporn Jirawatcharadech**, Grazia Camarda, Christina Yunta-Yanes, Mark J.I. Paine, Stephen A. Ward, Giancarlo A. Biagini. "Identification of *Plasmodium falc*iparum oxidoreductase involved in hydrogen peroxide production from primaquine metabolites". Liverpool School of Tropical Medicine PGR Student Conference, Liverpool, UK, 1st May 2018